UNIVERSITY OF LONDON

IMPERIAL COLLEGE OF SCIENCE, TECHNOLOGY AND MEDICINE

DEPARTMENT OF ELECTRICAL ENGINEERING

DYNAMIC ASPECTS OF A WIND/DIESEL SYSTEM WITH FLYWHEEL ENERGY STORAGE

Thesis Submitted for the Degree of Doctor of Philosophy of the University of London and for the Diploma of Membership of Imperial College.

BY

ALUN HOWARD COONICK, BSc, MSc(Lon)

JANUARY 1991

ABSTRACT

This thesis investigates the steady-state and dynamic behaviour of the various components that comprise the Rutherford Appleton Laboratory/Imperial College (RAL/ICSTM) wind/diesel/flywheel system.

The thesis begins with a review of wind/diesel projects that have been developed or are under development and their advantages/disadvantages are discussed. An overview is given of Phase I of the RAL/ICSTM wind/diesel project which examined the parallel running of the wind turbine with the diesel engine. Phase II of the project introduced a flywheel energy storage device to reduce both diesel cycling and fuel consumption.

The thesis describes the work carried out to simulate the electro-mechanical dynamics of the Phase II wind/diesel system with flywheel energy storage using numerical time stepping methods. The electro-mechanical equations are represented in state-variable form and the electrical equations are modelled using Park's "Two-Axis" method. A summary is given of the suite of computer programs developed to examine the various modes of system operation.

A discussion is given of the numerical integration methods used to time-step the simulation and the problems of modelling non-linear elements with such techniques. Linearisation and Eigenvalue analysis techniques are developed to examine small signal system stability and component interaction.

The equipment and method of interconnection are described. The individual components are then characterised using system tests and the computer models are validated against actual system runs.

Results of the simulation of the wind turbine connected to an infinite busbar are presented under both steady-state and transient conditions. Linear Analysis is used to examine the the various oscillatory modes and to provide methods of improved stability. Simulations of the autonomous operation of both the wind turbine and the diesel engine are used to demonstrate the problem of component interaction for which solutions are suggested.

The control strategies used to maintain system stability and quality of supply are tested in the simulation of the wind/diesel system with/without flywheel energy storage when subjected to wind and load variation and major system reconfiguration. Finally, these are compared with actual system results.

ACKNOWLEDGEMENTS

This research was carried out under the suprvision of Dr L L Freris whose expertise, guidance and enduring patience is gratefully acknowledged.

I am also grateful to my friends and former colleagues at the Rutherford Appleton Laboratory especially Prof N Lipman whose enthusiasm knows no bounds, Dr J Bleijs and Dr D Infield for sharing with me their invaluable knowledge of this subject.

Thanks are given to Dr A Tsitsovits, whose thesis formed the basis of my work, and also to my other friends, past and present, in the Electrical Energy Systems Group at Imperial College whose coffee resources were greatly depleted during this period.

Finally, to my long-suffering wife, Maria, may I just say "well, I could stretch it out to a couple more chapters!".

LIST OF SYMBOLS

A,B,C - System matrices

CLSTEP - admittance of each dumpload step

C_p - wind turbine coefficient of power performance

DAMP - damping torque

D_d - diesel engine frictional losses

D_{dg} - diesel generator frictional losses

D_f - flywheel frictional losses

DROOP - diesel engine droop (mechanical)

D_{wt} - wind turbine frictional losses

D_{wtg} - wind turbine generator frictional losses

E_2 - airgap voltage from the field side of the airgap

E_1 - airgap voltage from the armature side of the airgap

E_q - q-axis voltage

Excfn - function that is dependent upon the type of excitation system used in the machine.

F(i) - derivative of state variable after perturbation

F0(i) - derivative of state variable prior to perturbation

F_{nom} - nominal frequency

F_{set} - frequency setpoint

F_x - frequency measured by the transducer

$fn(X_i)$ - state matrix containing system non-linearities

G_r - ac/dc conversion factor for the triac, rectifier bridge and field resistance in the wind turbine UPF exciter

H_{dg} - diesel generator inertia constant

H_e - diesel engine inertia constant

H_f - effective flywheel inertia constant

H_{wt} - wind turbine inertia constant

H_{wtg} - wind turbine generator inertia constant

I - identity (unit) matrix

I_a - armature or load current

I_d - d-axis demagnetising component of the armature current

I_{fd} - field current

I_o - current threshold above which compounding becomes active in the Wind turbine UPF exciter

I_q - q-axis component of the armature current.

J - Jacobian matrix of the partial derivatives

J_f - flywheel inertia

J_f' - flywheel inertia referred to the main shaft

KCL - number of dumpload steps set

K_{fi} - integral gain (including the time constant)

K_{fp} - proportional gain

K_{pd} - derivative gain

K_{pi} - integral gain

K_{pp} - proportional gain

K_r, K_v, K_i - diesel generator static exciter constants

MAXSTEP - maximum number (63) of dumpload steps

MINSTEP - minimum number (0) of dumpload steps

n - number of state variables

N_p - number of generator pole-pairs

P, Q - Real and reactive electrical power at the machine terminals

P_d - diesel generator electrical power

P_{ie} - internally generated electrical power

P_{ij} - participation factor of the jth state variable, X_j, in the ith eigenvalue, λ_i.

P_{loss} - mechanical losses of friction and windage

P_m - mechanical power

P_{me} - mechanical power ouptut of the diesel engine

P_{set}' - power set point in the dumpload controller

Pw(i) - Wind turbine generator electrical power output after each state variable has been perturbed

Pw0 - Wind turbine generator electrical power output prior to perturbation

P_x - diesel electrical output power measured via the power transducer

r - radius of the wind turbine blades

R_f - field winding resistance

S - wind turbine swept area, $\pi.r^2$

Satfn - function in the form of a lookup table to provide the value of the open-circuit voltage for a given excitation current.

T_1, T_2 - Time constants of the wind turbine AVR Power System stabiliser

T_3 - equivalent mechanical torque due to the fuel flow in the diesel engine

T_d - mechanical torque delivered by the diesel engine

T_{damp} - time constant of the optional low pass filter on the wind turbine mechanical dampers

T_{dmax} - upper mechanical torque limit of the diesel engine

T_{dr} - diesel engine rated torque

T_n - time constant in the second order respresentation of the diesel governor

T_{shd} - diesel shaft torque

V - terminal voltage

$V_s(s)$ - Supplementary signal into the AVR.

V_∞ - free wind speed

W_{bus} - "speed" of the busbar at each time interval

X(t) - State state vector

X_1 - wind turbine generator q-axis reactance

X_2 - line reactance + diesel generator q-axis reactance

X_{ad} - d-axis armature reactance

X_d' - d-axis transient reactance

X_{du}, X_{qu} - unsaturated values of the d- and q-axis reactances

X_d, X_q - d- and q-axis reactances

X_f - field leakage reactance

X_i - state variable matrix

X_l - leakage reactance

$Y(t)$ - Output signal vector

YCL' - admittance actually set by the dumpload

YCL_f - total requested dumpload admittance due to frequency control in the dumpload controller

YCL_{fi} - requested dumpload admittance due to the integral term in the dumpload controller

YCL_{fp} - requested dumpload admittance due to the proportional term in the dumpload controller

α - phase shift due to the current transformer in the diesel generator static exciter

β - wind turbine blade pitch angle

β' - modified wind turbine blade pitch angle

$\Delta\theta$ - incremental gain of the effect of the reactive load current on the triac firing angle in the UPF exciter

δ_{wt} - wind turbine rotor angle wrt the reference frame

δ_{wtg} - generator angle wrt the reference frame

ζ - diesel governor damping coefficient

θ_o - no-load triac firing angle setpoint of the UPF exciter

λ - $\omega.r/V_\infty$ for the wind turbine

ρ - density of air (typically 1.25kg/m^3)

ω - rotational speed (rad/sec)

ω_d - diesel engine rotational speed

ω_f - rotational speed of the flywheel

ω_{frame} - rotational speed of the reference frame

ω_{max} - max rotational speed of the flywheel

ω_{min} - min rotational speed of the flywheel

ω_{wt} - rotational speed of the wind turbine

ω_{wtg} - rotational speed of the wind turbine generator

TABLE OF CONTENTS

CHAPTER 1

INTRODUCTION

1.0 Background

The level of a country's energy consumption is now commonly accepted as a measure of its prosperity or its degree of development. Electricity plays an ever-increasing part in the provision of this much-needed power and a wide-spread investigation is now underway to examine all the possible sources from which it can be generated.

Fossil fuels are being used at an alarming rate. The combined realisation of the finite nature of these resources and their environmental impact (eg acid rain, greenhouse effect) are causing world leaders to look towards other energy resources. Nuclear power, the great hope of the 1960's and 1970's, has in some countries (eg France) been received.as an acceptable form of power generation, but, in others, such as the United States, epecially post Three Mile Island and Chernobyl, the building programme has been halted.

The possibility of several inexhaustible sources of energy (renewable/alternative energy) such as solar, wave, tidal, geothermal and wind are now being taken seriously. In the United Kingdom on 23 March 1988, Lord Marshall of Goring [1.1], the then Chairman of the Central Electricity Generating Board, announced plans to build the UK's first

wind "parks". "We are very encouraged with the progress of this technology", Lord Marshall told the British Wind Energy Association at their Annual Conference. He went on, "The Department of Energy and ourselves, are thoroughly exploring the economic potential of wind generation in the United Kingdom. If all goes well we might hope that the wind will give us some 1000 Megawatts of economic electricity generation early next century".

Wind energy has thus matured over the last ten years to be widely accepted as the most promising renewable energy resource option for electricity generation. Since 1980 well over 10,000 wind turbines have been installed worldwide with a power production capacity in the hundreds of Megawatts. In the United Kingdom alone, more than 20 companies are now involved in the manufacture of wind turbines.

A particularly important market has emerged for lower power machines with outputs up to 100kW. These machines are ideal for small, remote locations supplying power to consumers, such as small isolated communities or remote farms, where grid connection is not possible. Wind generation is intermittent and therefore must be integrated with other systems if it is to make a significant contribution to on-demand power needs. Attention has focussed on the integration of wind generators into diesel generator supplied systems which are used extensively as sources of electrical power in remote site conditions. Such sites are attractive especially if diesel generation is expensive and

the wind regime is suitable. As in the case of connection to large systems, wind generation makes its contribution as a fuel saver with a potential to higher levels of penetration if means are found to overcome the short term shortfalls in wind.

Systems are therefore being built to interface wind power with diesel generation and energy storage to provide stand-alone electrical power systems that make best use of the available wind resource.

Whilst wind turbines have a long history of application in remote communities powering grain mills and water pumps, their ability to meet the needs of affordable, on demand electricity, provides a number of technological challenges. An examination must therefore be carried out of both the long term control strategies, needed to maximise system efficiency, and system dynamics to ensure a "steady" electrical supply.

1.1 The World Wind Resource

Before commencing an overview of the wind/diesel projects, it would be beneficial to examine the nature and scale of the world wind resource.

The circulation of air in the earth's atmosphere is caused by the non-uniform heating effect over the earth's surface by the sun. The direction of these air movements is affected by

the rotation of the earth. The net effect is a large counter-clockwise movement of air around a cyclonic (low pressure) area in the northern hemisphere and a clockwise movement in the southern.

Warm air rises at the equator and draws in cooler air from areas to the North and South. The air from the equator, having lost its heat, descends at about Latitude 30° (tropical), setting in motion a subsidiary system between 30° and 60° (temperate), and a further system between 60° and the polar regions (polar) as illustrated by Fig 1.1 [1.2]. The north and south tropical systems are separated from each other by the equatorial calm (doldrums) which is a low pressure area, and from the temperate systems by the subtropical high presssure belts. The picture is further complicated by the unequal heating of oceans and continents, and seasonal variations deforming and dividing the high and low pressure belts. There are also atmospheric disturbances created by masses of cold air ocasionally moving down from the poles towards the equator.

In general, during daytime, the air over a landmass warms up faster than over water leading to a strong onshore wind. At night-time, the air cools faster over land than water leading to an offshore wind. These winds may extend up to 50 km seaward at medium latitudes and 200 km inland in the tropics. Similar winds are noted in mountainous regions due to the summits heating quicker than the valleys in the daytime causing this air to rise and be replaced by the heavier valley air. At night, the summits cool quickest

causing a reverse airflow. Surface "roughness" leads to a drag on the wind so that over water or at height the wind blows more consistently and at greater strength.

Le Gourieres [1.2] produced maps (reprinted here as Fig 1.2) of the mean wind speeds and directions over the earth's surface for a typical January and July. They demonstrate that the wind is generally much stronger over the oceans than over land resulting in the most favourable wind regimes for wind power production to be in sites closest to the seashore. The best sites for each continent appear in Table 1.1.

Table 1.2 provides an idea of the scope of the number of major inhabited islands into which wind energy has or could be introduced.

1.2 Why Wind/Diesel?

Section 1.1 has already demonstrated that there are large portions of the world with suitable wind regimes for the introduction of wind powered electrical systems. Candidate sites would be island or isolated communities with an existing diesel supplied system or where an electricity supply is not yet available. In Canada alone there are several thousand diesel networks into which wind power could be integrated.

In isolated or island communities with existing diesel generation, equipment and fuel may have to be imported over long distances or through arduous conditions which could lead to uncertainty of delivery and maintenance problems (eg available skill, spare parts). In addition, the small diesel sets used in such systems require expensive light oils and coupled with extensive periods of partial loading, leads to poor efficiency. This may result in electricity costs being as high as five to twenty times that of a normally grid connected system.

The above points demonstrate that there are great incentives for a utility to invest in the improvement of system performance if large cost reductions can be achieved.

1.3 Composition of a Wind/Diesel System

Autonomous wind/diesel systems cover systems from the kilowatt single wind turbine single diesel generator set to multi-megawatt multi wind turbines connected to an island grid.

Typical wind turbines of the current era are principally designed for grid-connection and may not be optimally configured for autonomous wind-diesel systems. Also, the benefit of the grid's (infinite busbar) constant line voltage and frequency and its ability to meet the wind turbine's real and reactive power demand is no longer available. Additional equipment must therefore be provided

to ensure that the user is guaranteed a stable and economically efficient system.

Small wind/diesel systems of the type being considered in this thesis, may consist of one/two wind turbines/diesel generator sets. Unlike large systems, the load profile maybe extremely variable with peak loads up to five times that of the average [1.3]. In introducing wind power into an existing diesel supplied system the present diesel maybe oversized to accommodate such large peak loads and further spare capacity may be built in to allow for system expansion. Such a system will therefore produce electricity at very high cost thereby becoming not only a wind turbine integration problem, but also involving energy management.

When deciding upon the makeup of a wind/diesel system the following points must be considered:

1.3.1 The Wind Turbine

a) Wind Turbine Size

A decision must be made as to the size of the wind turbine (wind penetration) based upon system and site conditions. Lipman [1.4] suggests that for high penetration levels (eg 50%), the wind turbine should be rated at twice that of the diesel engine for a 30% wind turbine load factor.

b) Number of Wind Turbines

Some investigators [1.5] argue for a multi-wind turbine system that relies upon the local wind variation to help smooth out the stochastic nature of the wind.

c) Excess Power Shedding

A method is needed to solve the problem of shedding excess power. The question of whether to use fixed- or variable-pitch control is still being debated. Whatever method is used, some means of control has to be provided to match power supply to power demand. Several approaches are at present in use:

i) Passive/Fixed Pitch Blades

Uncontrolled (passive pitch) or fixed pitch machines have been deployed in conjunction with thyristor controlled dumploads to provide a power balance control. The excess power must either be fed to a low-priority load (eg heating, desalination plant) or must be dumped. Quite simple control strategies can be used and it also provides the means for the diesel engine to be constrained above a minimum loading. However, fixed pitch machines rely upon costly failsafe brakes to stop the turbine. Starting requires the wind turbine alternator to be motored which places a severe strain on the diesel generator set. The power limit maintained by stall-regulated, fixed pitch machines cannot

be adjusted and is susceptable to degradation by insect accumulation on the blades. They must also be able to withstand stormforce winds.

De Bonte and Costa [1.6] allow the wind turbine to overspeed and to rely upon a passive pitch control mechanism. This scheme allows the excess wind power to be stored as kinetic energy in the wind turbine rotor thereby providing a very short term energy storage facility. However, this power limiting approach requires an AC-DC-AC link at some extra cost.

ii) Variable Pitch Blades

Pitch control adds some mechanical and electrical complexity to the system. Starting can be achieved by aerodynamic torque avoiding the severe transient loading of the diesel generator. The machine can be controlled to match the desired load removing the need of a controlled dumpload. Feedback can be employed to damp undesirable modes of oscillations. Its pitch can be adjusted to alter the maximum power regulation. The machine can be brought to rest simply by feathering the blades which removes the need to design the machine to withstand stormforce blade loadings. However, blade pitch control adds greatly to the cost of a system and is therefore not frequently used in small systems.

1.3.2 Choice of Energy Storage

When deciding upon the energy storage device to be used, the structure of the wind should be taken into account. Fig 1.3 illustrates the structure of the wind as first proposed by Van der Hoven in 1957 [1.7]. The wind turbulence can be divided into two main frequency ranges. The low frequency band of between one cycle per five to two hundred hours (dependent upon the movement of weather fronts) may be controlled by longterm optimal adjustments to the system. The high frequency band of between ten to one thousand cycles/hour causes the problem of maintaining a steady electrical supply. Therefore, this is the range over which short term energy storage devices may be utilised. Longer term energy storage devices would only bring about fuel savings if they were able to bridge the gap between the short and long term turbulence fluctuations.

a) Long Term/Short Term Storage - Battery

The battery can act as both a peak load lopping device as well as an energy storage medium. If the battery is sufficiently sized it may act as a bridge across the long term windless periods. The inclusion of battery storage requires additional inversion equipment to move power in/out of the device. Although both batteries and inverters are well-proven technologies, costs are high. The inclusion of such non-linear devices in the system can lead to harmonic distortion and inversion equipment can fail catastrophically.

To date, the Lead-Acid cell, which was developed primarily to supply lighting, starting and ignition in vehicles is used in most battery storage devices. Heavy duty versions of the standard cell have been developed which can be fully charged/discharged repeatedly. The main limitation of Lead-Acid cells as a short-term energy storage medium is its poor charge/discharge rate due to its relatively high internal resistance. The cells also have a fairly limited life cycle (which is dependent upon the depth of discharge). If such a battery is to be included in a wind/diesel system, its energy storage capacity must be greatly enhanced, adding to the overall cost of the system. The cell also suffers from problems of; ageing (leading to reductions in capacity and efficiency), the requirement of watering and more seriously the problem of the build up of hydrogen gas that can lead to an explosion in a badly ventilated area.

Research into advanced battery performance has produced the long-life Zinc-Chlorine cell (operates at near ambient temperature) and the Sodium-Sulphur cell (operates at 300°C to 400°C). Both can store two to three times as much power as the equivalent Lead-Acid cell. However, neither cell has yet been perfected, whilst the operating temperature of the Sodium-Sulphur cell precludes it from use in wind/diesel systems.

b) Short Term Storage

The inclusion of a short term energy storage device enables diesel generator operation to be improved over short term windless conditions and improves the system's ability to cope with any large transient loadings. In addition to the previously discussed battery other short term devices in use include:

i) Pneumatic-Hydraulic Accumulators

Pneumatic-Hydraulic Accumulator storage is advantageous where the hydraulic pump/motor provides a favourable linkage with a mechanical system, as reported by Volvo in their study of braking energy recovery in a diesel-powered bus [1.8].

The use of commercially available equipment means that this method of storage is using a well established technology and costs are well defined. However, hydraulics can be troublesome (eg leakages) and this could lead to maintenance problems on remote sites.

ii) Coventional Flywheel

Flywheel storage is a tried and tested technology predating even the steam engine. Today it is used extensively in the automotive industry, a Swiss designed trolley bus driven by flywheel operated for several years in the 1950's. More

recently, a flywheel-electric car was built and tested in the United States [1.9].

Flywheels offer superior power charge/discharge rates, require less maintenance and have very long shelf-lives when compared to battery technology. Furthermore, they have more favourable energy to volume and energy to mass ratios.

The use of steel leads to ease of construction. However, the specific energy capacity is still quite low and is worsened if the rotor discs are pierced to recieve a shaft. The flywheel must also be mounted in a suitably robust containment vessel.

iii) Composite Flywheels

Small superfast flywheels constructed of materials that combine high tensile strength with low density such as composites of glass- or carbon- reinforced plastics can attain much greater levels of specific energy than the conventional steel flywheel. Storage losses are minimised by using high performance bearings and enclosing the entire mechanism in an evacuated casing to reduce air-drag. However, composite materials are more costly to fabricate.

1.3.3 Electrical Generator and Drivetrain

The choice of electrical generator can have a major impact on stability and power quality. For wind/diesel systems only two types of machines are in general usage ie. synchronous and induction generators.

Unlike conventional electrical generation, a wind turbine exhibits unsteady input behaviour because of the gustiness in the wind and cyclical load variation due to blade chopping which may be accentuated by wind shear, tower shadow and yaw misalignment. With a fixed speed machine and a stiff drivetrain the torque pulsations will be transmitted through the drivetrain and into the electrical system. The inclusion of some form of compliance in the system would provide the means to absorb these torque fluctuations. The induction generator can provide this compliance by allowing its rotor speed to vary (slip) and dissipate this slip energy as heat in the rotor windings. A rated slip of only 1% to 2% provides adequate compliance.

The synchronous generator, however, is a fixed speed machine whose "stiffness" is determined by its level of excitation. Therefore, the synchronous machine does not provide compliance and relies upon other means to absorb the torque pulsations. Compliance could be included in the form of a shaft with a flexible coupling, a fluid coupling or in larger systems a spring mounted gearbox [1.10].

The apparent simplicity of line connection prompted many wind turbine manufacturers to opt for the induction generator when connecting to the grid. However, the induction generator requires a separate source of reactive power to supply its magnetising current. This can be achieved by connecting shunt capacitors across the line or from a rotating synchronous compensator (an unloaded synchronous generator that maybe over/under-excited to provide leading/lagging VArs) which may have quite large spinning losses. The need for this power factor improvement and overvoltage protection adds substantially to both the complexity and the cost. Care must also be taken in the design of the machine to prevent excessive inrush currents during paralleling causing a large voltage droop.

The synchronous generator relies upon expensive synchronisation equipment (ie an alignment of voltage, angle and speed) when being paralleled to an existing electrical system. Unlike the induction machine its voltage and hence reactive power can be controlled via its excitation system. However, a dc supply is needed to power this rotor excitation. Its cost per kW is also generally higher than that of the induction machine.

Power conversion equipment between the induction generator and the system, although adding to the cost, allows the use of variable speed wind turbines, improves the power factor and transmission torque transients are reduced.

For both types of machine, protection devices have had to be included to guard against momentary outages that can lead to drive-train and gearbox damage.

1.4 Review of Other Projects

This section is not an exhaustive overview of world wind/diesel projects but is included to provide a flavour of the diversity of the work.

1.4.1 Energy Management

Harrap [1.11] in his study investigated a diesel system with/without wind power. He considered the replacement of the existing diesel (rated at ten times average power) with a diesel sized at twice the average power. An examination was made of the possibility of running the system without wind and using a battery/inverter system to help meet the load pattern and thereby improve diesel performance. The study demonstrated a 40% reduction in the cost of electricity. Commercial versions of this system with battery/inverter equipment have already been sold in Canada and Australia.

1.4.2 Load Control Schemes- Priority Loads

This was an early approach to an autonomous wind/diesel strategy pioneered by Somerville [1.12]. Three island schemes offshore of the UK and Ireland (Fair Isle, Lundy and Inis Oirr) have so far been implemented. The schemes rely upon the prioritising of loads into high, medium and low grades and a tariff system to encourage system usage when wind only is active. The medium and low grade loads are switched in/out by frequency sensing equipment sited locally. The wind turbine was sized so that its capacity would greatly exceed that of the high grade (priority) load with the excess power being taken up by the graded lower priority loads. Such a scheme meant that the diesel capacity was offline for a a great deal of the time which is reflected in reports that the wind turbine has met 75% of the load demand.

1.4.3 Load Control Schemes- Time Slots

An alternative approach to load control is the packaging of loads into time slots during a fixed period. The Dutch Company CWD have installed such a scheme on the island of Cape Verde. De Bonte and Costa [1.6] have reported their initial results which demonstrated that the scheme was more of an improvement in energy management than the successful integration of a wind turbine into the system.

The original generator set was grossly oversized at approximately four times the maximum load of 45kW. It was replaced by a 70kW set and a 30kW wind turbine as the system would not be run in wind power only mode. Nearby water pumping stations that had previously been supplied from stand-alone diesel generator sets were integrated into the grid resulting in a much improved daily load profile. The authors reported a 30% fuel saving without the improved load strategy and a 70% fuel saving when the water pumps were fed from the grid.

1.4.4 Long Term Storage

To date, long term storage exists only as battery storage. Groups active in the field include Linders et al at Chalmers University, Sweden [1.13] and Lundsager et al at the RISO test station [1.14].

The Cape Clear Scheme (Eire), as reported by Cramer and Schott [1.5 and 1.15] consists of a 72kW diesel generator set, two 30kW wind turbines with active pitch control and a 100kWh battery with a 120kW inverter. The battery acts as an energy buffer in wind turbine only mode and provides the extra power needed at peak load in diesel only mode. In wind turbine only mode, the diesel engine is decoupled and its alternator is used as a synchronous compensator.

Surprisingly for a Lead-Acid battery, storage is limited to a maximum of two hours which would greatly shorten its lifetime due to the fast charge/discharge rate.

1.4.5 Short Term Storage

i) The Hydraulic-Pneumatic Store

Musgrove et al [1.16] at Reading University have reported a scheme that uses a hydraulic-pneumatic accumulator as the energy storage device.

The accumulator consists of several vessels filled with nitrogen gas under pressure acting upon the hydraulic fluid in a separate bladder. These commercially made vessels are limited to an energy storage capacity of approximately 10 to 15kW/min but can be paralleled for larger requirements. Similarly, the hydraulic pumps are as yet only available up to 100kW but again could be run in parallel. The hydraulic pump/motor is linked to the electrical system via a synchronous alternator which may be used as a synchronous compensator when the energy storage device is decoupled from the system.

The authors report that such a store brings down the number of diesel stop/starts to an acceptable level of ten per day, whilst, fuel savings in the range of 50% to 60% may be achieved with a suitable wind regime.

ii) Flywheel Energy Storage

Both RAL/ICSTM (discussed later) and the RISO [1.17] projects utilise steel flywheels that are directly coupled to a diesel driven synchronous generator. In this configuration the diesel engine can be mechanically disengaged from the rest of the system by a clutch.

The RISO scheme has a 55kW, 15 metre diameter wind turbine coupled to 30kW turbocharged diesel set whose alternator is oversized to provide reactive power compensation for the wind turbine's induction generator. In periods of sufficient wind, the diesel engine is decoupled whilst its generator remains in the system as a synchronous compensator. If the wind drops below the load requirements, the diesel is restarted by re-engaginging the clutch. The stored energy of the flywheel is used to maintain the power supply for the 1 to 2 seconds needed to bring the diesel engine online. A dumpload is used for frequency control during periods of high winds or low consumer loading.

As will be shown later with the RAL/ICSTM scheme, such systems have the advantage that there is little increased complexity over the basic wind/diesel system and will therefore be relatively cheap with a minimal increase in maintenance.

iii) Battery and Flywheel Storage

A Danish consortium (Lundsager [1.14]) which includes the wind turbine manufacturers, BONUS, and the RISO laboratory have installed at Santa Caterina, in the Cape Verde islands, a 55kW wind turbine, 40kW diesel set, with a 66kWh battery and small flywheel. The battery typically provides 2 hours of storage whilst the small flywheel, linked to the synchronous generator, allows fast diesel starts and helps in maintaining frequency stability.

iv) Load control and Flywheel Storage

A lightweight flywheel unit, KESS, [1.18] has been developed by British Petroleum at Sunbury, UK that is quoted as operating at speeds up to 16,000rpm with a total storage capacity of 1.4MJ.

The unit has been connected into the island power system on Fair Isle. In wind powered only mode, the system consists of a 60kW wind turbine linked via a gearbox to a 100kVA alternator and a controllable dumpload is used to consume excess wind power. The diesel generator set is operated at times when a guaranteed supply is required.

During field trials, the flywheel was interfaced to the system via a synchronous alternator. The flywheel was run up to speed by a small variable speed drive and synchronised to the supply under computer control. The movement of power

in/out of the flywheel is therefore determined by the power balance and hence the frequency of the system. Constraints upon the allowable steady-state frequency variation of 45 to 53Hz therefore limit the maximum available stored energy to 300kJ. Davies reported that there was great improvement in the stability of the power output and less frequency variation when KESS was included in the wind powered system. The loss of load was therefore reduced due to the reduction in frequency variation and the number of diesel stop/start cycles was likewise reduced.

An alternative scheme under development with RISO replaces the synchronous alternator with a fully regenerative variable speed induction machine drive. The flywheel can be driven at speeds that are independent of the supply frequency and therefore the full storage capacity of the flywheel is available. An additional benefit is the removal of the small variable speed drive previously needed to run KESS up to speed. System frequency is relied upon as the signal for the control of power in/out of the drive due to its direct relationship with the power mismatch in the system.

1.5 The RAL/ICSTM Wind/Diesel Project

This thesis was undertaken as part of a Science and Engineering Research Council (SERC) industrial collaborative project. The project, which has completed its sixth year was divided into 2 phases. Its main aims were to develop:

a) A technically and economically feasible autonomous power system powered by a wind turbine (WT) and supported by a diesel generator (DG) set in the kW to 100 kW range. The integration of a single wind turbine into a single diesel generator supplied system being the worst-case problem. To achieve the highest possible fuel saving, the diesel engine would be removed from the system during favourable wind conditions.

b) A system that uses as far as possible commercially available and well-proven equipment.

c) Long-term (logistic) control strategies to ensure system efficiency via maximum fuel saving and minimum diesel wear.

d) Short-term (dynamic) models to adequately investigate modes of operation and control strategies for this and similarly constructed systems.

1.6 Project History

This SERC funded project was carried out with industrial collaboration from HAWKER SIDDELEY POWER PLANT (HSPP) and JOHN LAING (JLC). The Wind/Diesel system is sited at the RUTHERFORD APPLETON LABORATORY (RAL) where it has been developed and tested by RAL and IMPERIAL COLLEGE staff. The project was divided into two phases:

1.6.1 Phase I

Fig 1.4 shows the layout of the system used during this phase of the project. It consists of a 16kW MISTRAL MP-9 wind turbine, a 6.8kW HSPP NOVA II diesel generator set, a consumer load (resistor bank), and a controllable dumpload.

a) Continuous Wind/Diesel

Initially, the diesel set was run continuously, with the dumpload being used to maintain a minimum diesel loading. As can be seen from the graph of the diesel loading versus fuel consumption (WILLANS curve) of Fig 1.5, at no-load, the diesel is still using 30 to 40% of its full load fuel capacity [1.19]. Furthermore, manufacturers recommend a minimum diesel loading of approximately 30 to 40% to prevent bore-glazing, oiling up of the silencer etc. which would otherwise increase maintenance and shorten diesel life. Therefore only minimal fuel savings were obtained.

b) Intermittent diesel

To improve system performance, the diesel has to be run intermittently, but this produced other technical problems:

i) Wind Turbine Stand-Alone Operation

The wind turbine must be able to operate autonomously with the controllable load used to maintain the system frequency in the abscence of the diesel governor. This led to stability problems which will be addressed later in the thesis.

ii) Loss of Load

The run-up time of the diesel set (5 to 10 seconds for the NOVA II, depending on its initial temperature), is too slow to prevent the frequency of the system falling below the minimum level (under frequency) causing loss of load.

iii) Diesel Cycling

High numbers of diesel start/stop cycles occurred which led to increased wear in the engine and starter mechanism. Different control strategies such as "minimum diesel run time" and "hysteresis" were tried to reduce diesel cycling and wear, but, both led to significant fuel penalties [1.20].

1.6.2 Phase II (Energy Storage)

Logistic modelling revealed that only the use of short term energy storage (10 to 500 seconds) significantly reduced diesel cycling without a fuel penalty [1.19]. Fig 1.6 illustrates the effect of energy storage versus fuel savings and number of diesel stop/start cycles from the logistic studies.

In view of the need for system ruggedness, a "medium technology" laminated steel flywheel, designed by JLC was included into the enhanced wind/diesel system. The inclusion of the flywheel into the wind/diesel system resulted in the following investigations:

a) The optimum size of the flywheel with regard to system size , configuration and the local wind regime.

b) Methods to bring the flywheel up to speed.

c) Methods to bring the diesel rapidly online before the occurrence of loss of load and eventual system collapse.

d) Longterm control strategies to ensure maximum fuel saving with reduced diesel wear.

e) Dynamic control strategies to ensure system stability during both normal and transitional operation.

A full description of the integration of the flywheel into the enhanced wind/diesel system will be given in Chapter 2.

1.7 Longterm Logistic Modelling

Logistic models, using numerical simulation and probabilistic techniques, have been developed by the staff of the Energy Research Unit at RAL. They are used to examine longterm strategies such as optimal component sizing for a given site and conditions, annual fuel savings and diesel stop/start strategies to balance the tradeoff between fuel consumption and diesel wear.

1.7.1 Numerical Simulation [1.21]

Extensive use has been made of numerical simulations that allow the use of real 2 second wind data and the inclusion of complexities such as non-linearities into the model. The program models the flow of energy within the system, either from the diesel fuel or from the wind to the consumer load. It is a pseudo steady-state model in that all system variables are held constant within each 2 second time step. However, even though the model accurately reflects the behaviour of the system the time step discludes its use to study longterm (eg annual) runs.

1.7.2 Probabilistic Analysis [1.22]

The important problem of providing accurate descriptions of system behaviour over extended periods of time and for differing wind regimes may be tackled by the use of recently developed applied probalistic methods. Such methods can be used to represent diesel cycling in terms of the probability of the system wishing to change its state. Wind turbulence may be modelled via a Gaussian distribution within each hour and a constant site turbulence intensity. Storage can be represented provided energy flows are modelled using the Markov property.

This probabilistic method allows the user to measure the sensitivity of major properties, eg mean wind speed, site turbulence intensity, storage size, storage efficiency and load variability.

1.8 Diesel Wear Tests

As discussed in Section 1.6.1, continuous on/off cycling of the diesel engine can lead to excessive wear rates. However, before such statements can be made some means must be found to quantify this problem. The three main areas of wear in a diesel engine are the pistons, cylinders and engine bearings. Wear mechanisms have been previously studied [1.23, 1.24] and been found to be caused by both corrosion and abrasion [1.25].

To examine the rates of wear, lubricating oil samples were taken from the diesel engine at 24 hourly intervals during various longterm diesel runs. The samples were then subjected to spectrographic analysis at the department of Mechanical Engineering, University of Swansea. The analysis examines the levels of specific materials in the oil to determine the amount of component wear. Table 1.3 illustrates the materials under scrutiny, whilst Table 1.4 presents typical results of wear in a comparative study between continuous and intermittent diesel operation [1.25].

1.9 Dynamic Modelling

This thesis forms part of the study, carried out during Phase II of the project, involved in the devlopment of analysis techniques and computer models to study the electromechanical dynamics of the wind/diesel/flywheel system. Both experimental (Dr J Bleijs, Mr A Coonick) and theoretical work at RAL (Dr J Bleijs) and theoretical studies at ICSTM (Mr A Coonick) examined the following areas:

a) The development and validation of both linear (modal analysis, root locus) and non-linear (numerical time stepping) methods for the analysis both the electrical and mechanical transient/dynamic behaviour of the system.

b) An examination of the problems of wind-excited oscillations and possible methods of solution using computer simulation.

c) The use of computer models to tune the dynamic controllers to maintain system stability during 'normal' steady-state and transient conditions and during the transitional reconfiguration of the system.

d) The problem of reactive power control in an autonomous system under steady-state and transient conditions.

This thesis describes the development, validation and implementation of numerical time-stepping methods used in the solution of areas a) to d). The thesis will also address the use of linear methods such as Eigenvalue/Eigenvector analysis to help in the improvement of system stability.

1.10 Thesis Outline

Chapter 2 is a description of the equipment and its method of connection into the system, whilst chapter 3 describes the characterisation of the component parameters and models used. The electro-mechanical equations are represented in state-variable form and the electrical equations are modelled using Park's "Two-Axis" method.

Chapter 4 discusses the numerical integration methods used to time-step the simulation and the problems of modelling

non-linear elements with such techniques. Linearisation and Eigenvalue analysis techniques are developed to examine small signal system stability and component interaction. The chapter concludes with a summary of the suite of computer programs (with their associated flowcharts) developed to examine the various modes of operation.

Chapter 5 presents results of the simulation of the wind turbine connected to an infinite busbar and demonstrates the problem of wind-excited power oscillations. Simulations of the autonomous operation of both the wind turbine and the diesel engine demonstrate the problem of component interaction. Solutions are offered for all cases.

Chapter 6 presents results of the simulation of the full wind/diesel/flywheel system and demonstrates methods to maintain the electrical supply when the system is subjected to wind and load variation and major system reconfiguration.

Finally, general conclusions are drawn and a decription is given of the original elements developed in the thesis. Suggestions are also given for future work to be carried out on this subject.

CONTINENT	COUNTRIES WITH SUITABLE WIND REGIMES
Europe	Ireland: United Kingdom: France: Greece Netherlands: Scandinavia : USSSR : Portugal
Africa	Morocco: Mauritania: N W Senegal Coast: S Africa: Somalia : Madagascar
America	S E Coast of Brazil: Argentina: Chile: Canada: Coastal USA
Asia	India: Japan: Chinese Coast: Vietnamese Coast: Siberia

Table 1.1 Areas of the World with Suitable Wind Regimes

AREA	Nos of Islands
Worldwide	10,000
S Pacific	1,500
China	450 (pop. 26 Million)
Greece	45

Table 1.2 Inhabited Islands into which Wind Energy Could be Introduced

MATERIAL	SOURCE OF WEAR
Iron	Cylinder Liners:Crankshaft:Piston Rings
Chromium	Piston Rings:Cylinder Liners
Aluminium	Pistons:Bearings
Copper	Bearings
Lead	Bearings
Silicon	Ingested Dirt
Sodium	Oil Contamination (eg anti freeze)
Tin	Bearing Overlay

Table 1.3 Sources of Wear in Diesel Engines

Element	Wear rate Continuous ppm/hr	Wear Rate On/Off ppm/hr	Change %	Significant at 5% confidence
Fe	0.1024	0.1678	+64	Y
Cr	0.0140	0.0153	+9	N
Al	0.0278	0.0272	-2	N
Cu	0.0265	0.0237	-11	N
Pb	0.0262	0.0421	+61	Y
Sn	0.0172	0.0299	+73	Y

Table 1.4 Wear Rates of Diesel Engine Materials for Continuous and Intermittent Operation

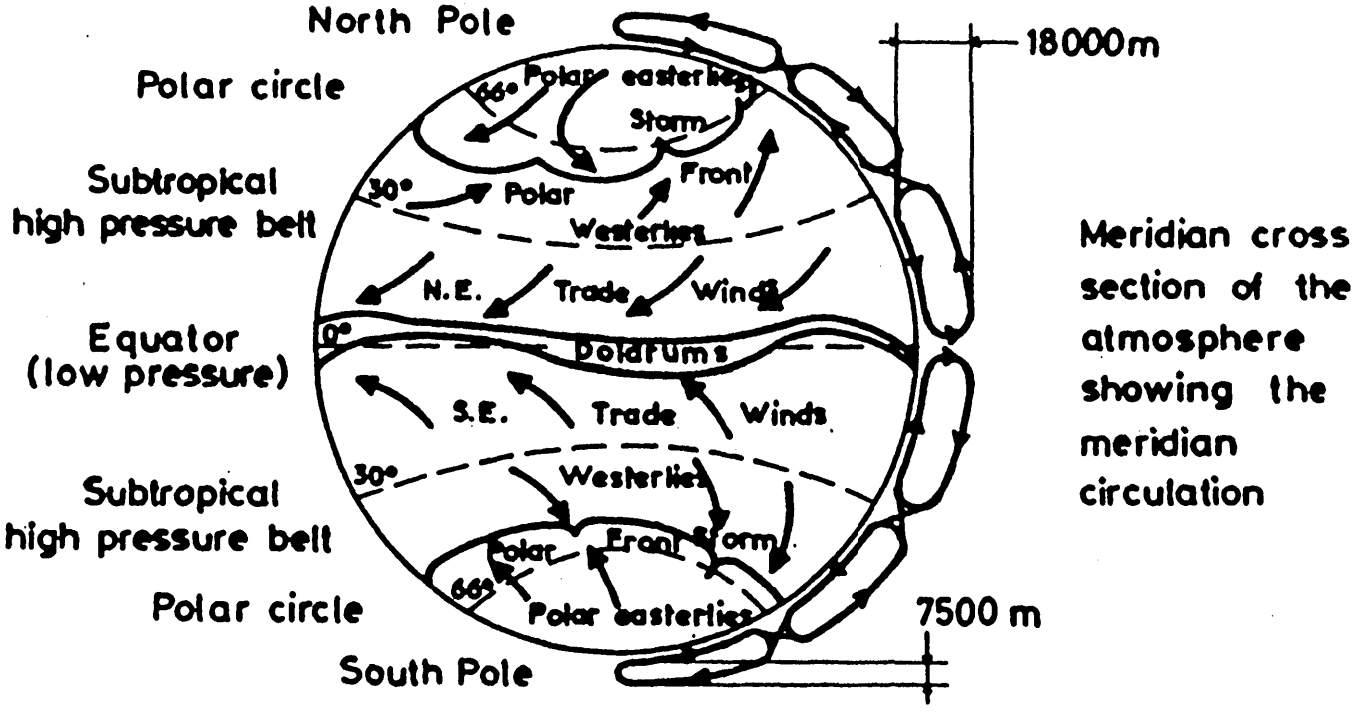

FIGURE 1.1 General World Wind Circulation [1.2]

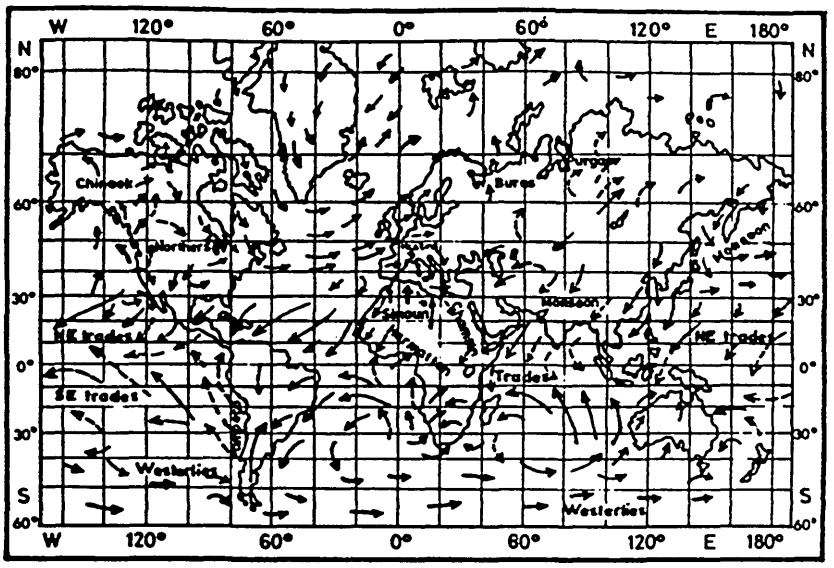

Fig. a Wind direction in January

slight wind ---→ mean ——→ violent ——→

Fig. 16a – *Wind direction in January.*

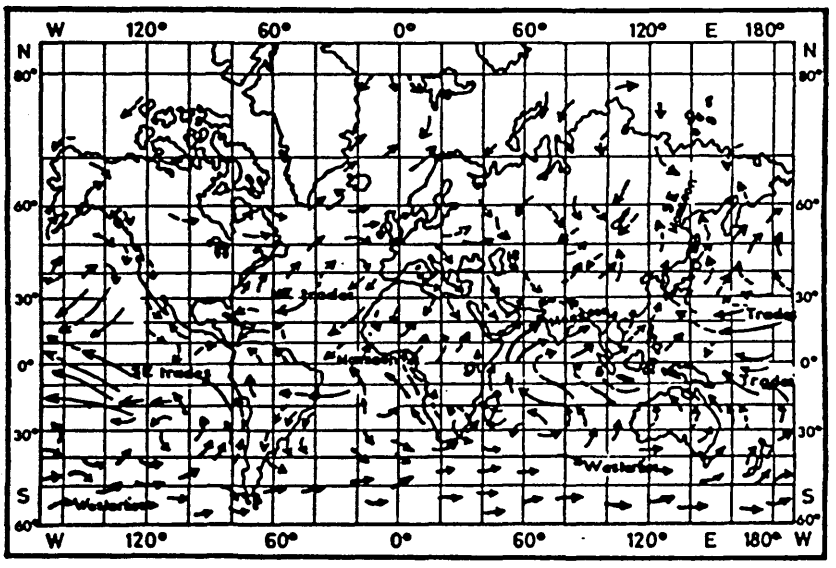

Fig. b – *Wind direction in July.*

FIGURE 1.2 Wind Direction in (a) January (b) July [1.2]

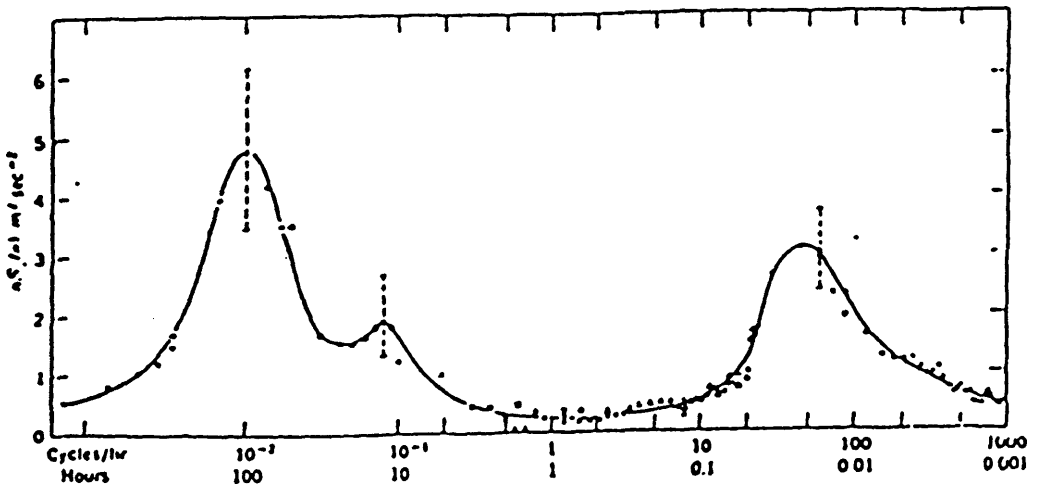

FIGURE 1.3 Power Spectrum for Wind Speed Fluctuations [1.7]

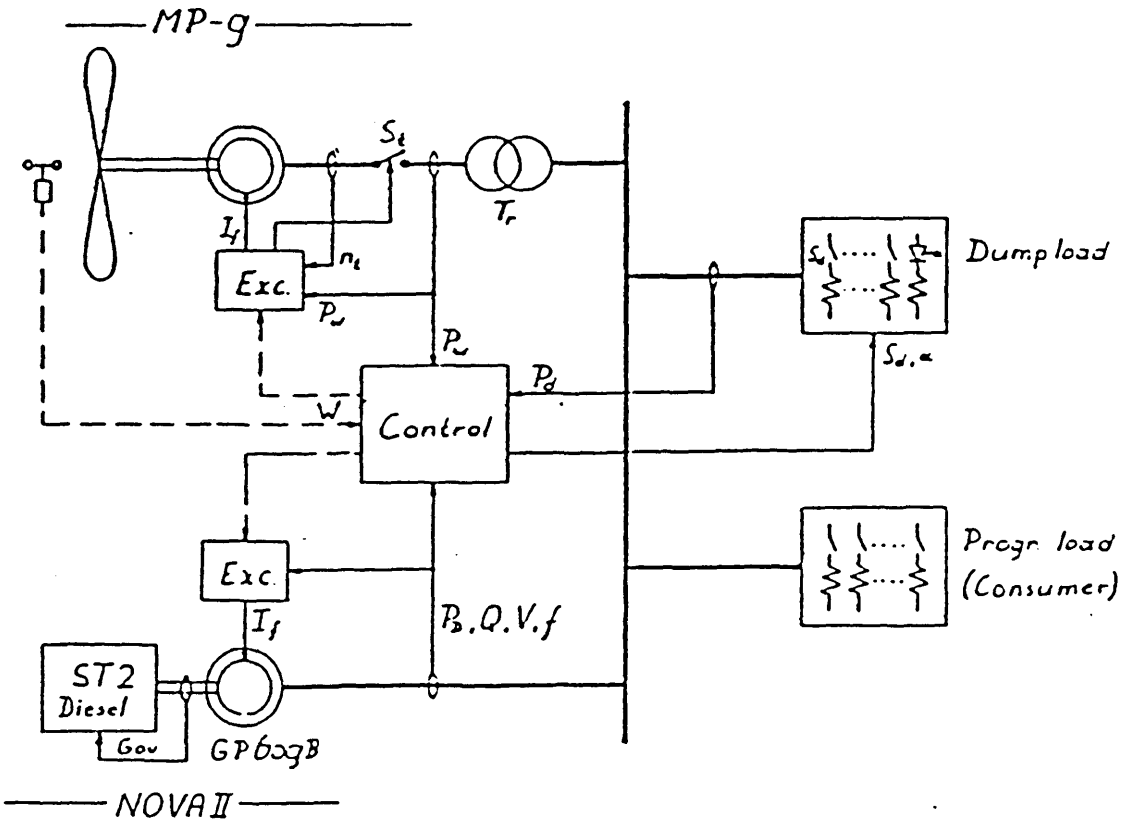

FIGURE 1.4 Schematic Layout of the Phase I RAL/ICSTM Wind/Diesel System

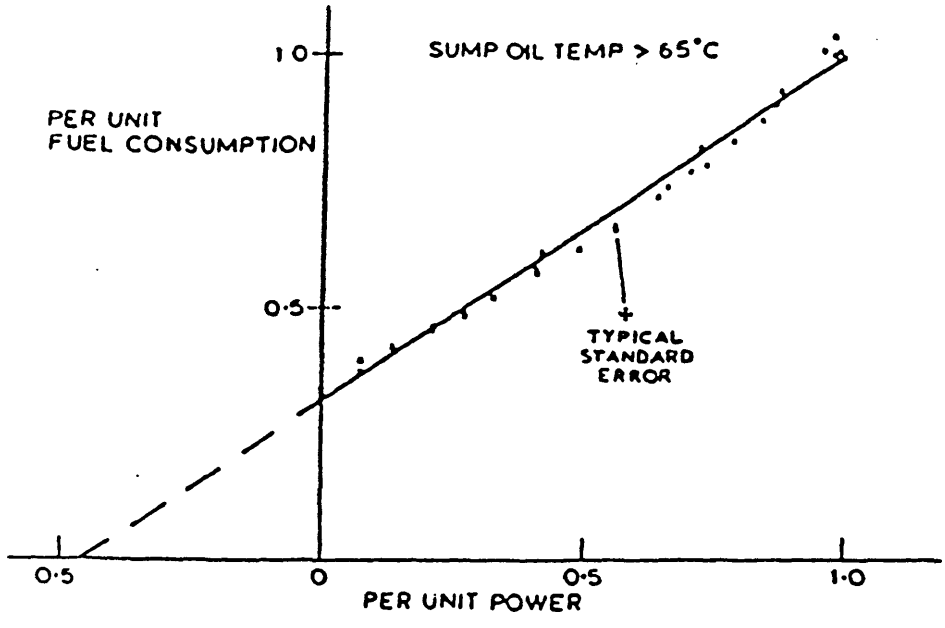

FIGURE 1.5 Diesel Loading Versus Fuel Consumption (WILLANS curve)

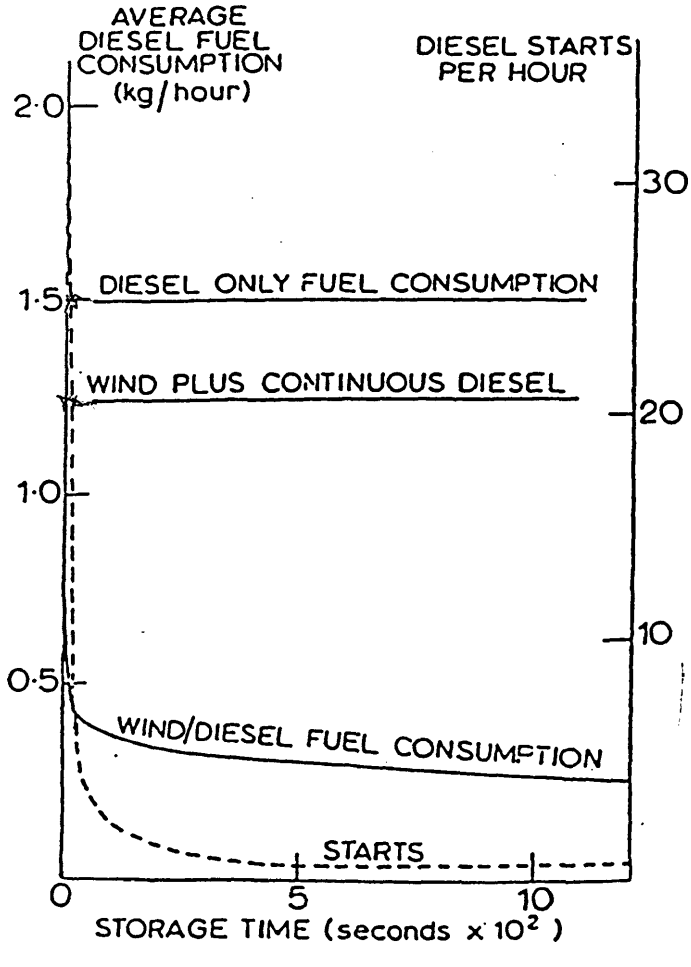

FIGURE 1.6 Impact of Storage on Fuel Consumption and Diesel Cycling

CHAPTER 2

PROJECT EQUIPMENT

2.0 Description of the Overall System

In order that an economically viable wind/diesel system could be developed a market survey was carried out by HSPP. The survey identified two preferred ranges of diesel generation; 3 to 10kW and 50kW. It was therefore decided to develop the system at the lower range due to the sales record of the HSPP NOVA II diesel generator set and to minimise costs. Both the diesel generator set and the wind turbine were provided by HSPP as part of their contribution to this SERC collaborative project.

The wind/diesel/flywheel system was developed and tested at RAL during Phase II of the project. It consisted of the Phase I system, described in Section 1.6.1, with the exception of the directly coupled diesel generator set being replaced by a diesel/flywheel rig, with modifications made to the dump load and its associated controller. Fig 2.1 illustrates the layout of the phase II system, the logistical controller for the diesel generator set is not shown.

2.1 The Wind Turbine

The Wind Turbine, shown in the photograph of Fig 2.2, was manufactured by NORTH WIND POWER CO of Vermont, USA. It was developed under a US Federal funding programme, and designated the type L916 aerogenerator. It was commercially available as the MISTRAL MP9 Wind Turbine. The machine was a prototype and as such very few detailed drawings of the design and very little test data were available.

The machine and its nacelle were assembled and erected on a 20 metre 'A' frame lattice construction tower at the RAL Wind Test Site in February 1984. The tower could be lowered via a handraulically driven winch to allow easier/safer access to the Wind Turbine and its nacelle.

The Wind Turbine had a 9.26 metre (originally believed to be 9 metre) rotor diameter. It was a horizontal axis, down wind, passive blade-pitch, free-yawing machine. The two 4.63 metre blades were of laminated birch with a modified GO797 aerofoil section. It had a cut-in wind speed of 4.5 m/s and a rated power output of 16 kW at 11.6 m/s and produced 50 Hz at 125 rpm.

The level of mechanical power developed was controlled by the passive blade-pitch control mechanism. It relied upon the aerodynamic and centrifugal forces acting upon the blades to produce a pitching torque that counterbalanced the pneumatic spring/damper mechanism. This blade-pitch control mechanism, mounted in the nacelle, utilised pneumatic rams which were

powered by compressed air (initially set to the manufacturers recommendations of 47 psi). The two pneumatic rams operated in parallel with a mechanical damper. In the event of electrical disconnection of the compressor and valve, air was vented from the system and the blades were moved safely into feather. When the control mechanism was powered, the compressor began operation and after some seconds moved the blades into the run position. Above the cut-in wind speed the machine would then achieve the desired 125 rpm. With excessive blade thrust or during excessive overspeeding the control mechanism was designed to partially feather the blades. No braking system was fitted to the main drive or yaw shaft.

2.2 Wind Turbine Drive-Train

The drive torque from the blades was transmitted via a teeter and delta 3 mechanism to the shaft as illustrated by Fig 2.3. The shaft was connected to the rotor of the synchronous generator via an overrunning (SPRAG) clutch and an elastomeric (flexible) coupling across which two mechanical (HECO) dampers were fitted.

2.3 Wind Turbine Generator

The Wind Turbine was supplied with a 21kVA (16kW) at 125 rpm, 3 phase, wound field, 48 (salient) pole synchronous alternator. Due to its design for 220/127 volt, 60Hz grid

operation, a 220/415 V stepup transformer was connected at its terminals to allow connection to the grid and the diesel generator set.

The generator had a large diameter and short axial length to accommodate the large number of poles as shown in the photograph of Fig 2.4. The 48 poles allowed the production of 50Hz from the Wind Turbine's mechanical speed of 125rpm without the aid of a gearbox. This unconventional alternator had an unusually high transient reactance, which coupled with the flexible coupling/overrunning clutch in the drive train removed the need for expensive auto-synchronisation equipment. The Wind Turbine could thus be parálleled over a speed range, determined by preset relays, of 117.5 to 132.5 rpm at any phase angle relative to the supply.

2.4 Wind Turbine Generator Exciter

Normal commercial use of this Wind Turbine was in the form of grid-connection and as such it was packaged with a "Unity Power Factor" (UPF) exciter.

Fig 2.5 is a graph of power versus power factor (PF) and illustrates the ability of the exciter to maintain unity PF in the steady-state over its load range whilst grid connected. It aimed to achieve this by the use of the static current compounding circuit illustrated by Fig 2.6.

The excitation voltage was supplied from two of the three phases via a triac and diode bridge. The excitation level was determined by the triac firing angle. This angle was obtained from the output of the current transformer in line L2 (compounding) being phase subtracted from a reference level preset by an adjustable pot. The signal was then compared with a sawtooth signal which was phase linked to the grid. The output was then used to generate a series of pulses that controlled the firing angle of the triac.

A major flaw in this device was its lack of current feedback (ie open-loop controlled), that solely relied upon a preset reference level. The device was therefore unable to respond to temperature effects changing the impedance of the field winding. Upon initial energisation of the cold grid connected wind turbine generator, reactive powers flowed of between 0.5 and +2.5kVAr (Fig 2.7), whilst for the hot wind turbine generator, the reduced excitation gave a more balanced reactive power flow of between -0.8 and +1.5 kVAr across a 12kW load range (Fig 2.8). At higher power levels, the exciter compounding is unable to provide sufficient excitation current causing excessive reactive power to be drawn from the grid.

As will be discussed in Chapter 5, the wind turbine generator could also be configured to run with an automatic voltage regulator (AVR). The CONTROLOGY AVR 15R [2.1] was a solid state automatic regulator which could be powered from the generator terminals. It used an inverse parallel thyristor bridge to provide the dc supply necessary for the rotor

winding. Sensed voltages could be inputted via single phase, two out of three phase or three phase sensing options. Adjustments could also be made to the voltage reference level, "stability" and "damping". The manufacturers claimed that its "integrating action provides close regulation". However, no information was available with regards to its characteristics or transient performance.

2.5 Diesel Engine

The diesel generator set used throughout Phase I of the project was an HSPP NOVA II set, with a continuous rating of 6.8kW (electrical). The diesel engine was a 9 kW (mechanical), 2-cylinder, 4-stroke, directly injected, naturally aspirated LISTER PETTER ST2. During Phase II of the project, the diesel engine used in the diesel/flywheel rig, as shown in the photograph of Fig 2.9, was a LISTER PETTER TS2 which was of similar design to the ST2.

2.6 Diesel Alternator

The diesel alternator was a 3 phase, 4 (salient) pole, 415V synchronous alternator packaged with a static exciter, as shown in the photograph of Fig 2.9. It was designed for commercial use as a stand-alone power generator.

The exciter was a self-exciting, self-regulating system that used the phase-compensating effect of current and voltage

transformers to supply the field via a diode bridge. The voltage ratio was such that at no-load, it produced rated voltage at the generator terminals. The current transformer produced an output voltage proportional to the load current, and phased with respect to the voltage transformer.

As will be discussed in Chapter 5, this static exciter was replaced by a CONTROLOGY AVR Type 15E [2.2]. This device was a lower power version of the Type 15R, used on the wind turbine generator, and was without "damping" adjustment. Again, little information was available regarding its characteristics and transient performance. However, the manufacturers claimed its controller to be a lead/lag network. Both devices were encapsulated in an opaque epoxy resin making internal examination of the device impossible.

2.7 Diesel/Flywheel Rig

Fig 2.10 illustrates schematically the layout of the diesel/flywheel rig. The diesel engine was no longer closely coupled to its alternator, as in Phase I. Its drivetrain was split and extended to include an electromagnetic clutch, a pulley belt system (to mechanically link the alternator to the flywheel) and torque transducer. The drivetrain was protected by flexible couplings and shearpins. Due to its length, the drivetrain was supported by Cooper Split bearings which were mounted along with the diesel engine, its alternator and the flywheel on a steel frame that was fixed to the floor. The whole structure was islanded (the concrete

floor sat upon 0.3m of gravel and was surrounded by cork) to reduce the transfer of vibration.

The flywheel consisted of several steel discs that were bolted together to provide a total inertia of 20 kgm² at 1500rpm and could be operated at speeds in excess of 6,000rpm. The discs were mounted on a shaft, supported by roller bearings and contained in a steel vessel that could be evacuated to a pressure of 1mm Hg. The steel vessel was designed to contain the flywheel if it should break up and a water injection system was available to help dissipate the heat.

Initially, the pulley belt system used a toothed belt drive with a 48 teeth pulley on the flywheel shaft and a 36 teeth pulley on the main (1500rpm) shaft to yield a nominal speed of 1125rpm (effective inertia of 11.8kgm²). An alternative ratio of the flywheel and mainshaft pulleys was also tested to yield a flywheel speed of 2,500rpm (effective inertia of 58.0kgm²).

The flywheel was therefore used as an energy store to smooth out the wind turbine fluctuations in power. Energy flow in and out of the flywheel was facilitated by allowing the speed of the mechanically linked flywheel to vary within a ±10% range maximum. The total proportion of energy, ΔE, that maybe utilised over this range maybe calculated as follows:

$$\Delta E = 1/2.J.(\omega_{max}^2 - \omega_{min}^2) \text{ Joules} \qquad (2.1)$$

where,

J - Moment of Inertia

ω_{max} - max rotational speed

ω_{min} - min rotational speed

If normalised to the rated speed of the flywheel, ie ω_{max}, 36% of the stored energy could be utilised over this speed range.

The electromagnetic clutch was included to allow the diesel engine to be disengaged during prolonged windy periods. It was also used to rapidly restart ("crash-start") the diesel to maintain the system supply during long term shortfalls in wind power. As will be discussed later, the flywheel also enabled the diesel to be crashstarted in less than a second simply by energising the diesel fuel solenoid and closing the electromagnetic clutch.

In order to commence the system supply, the diesel engine was conventionally started. The flywheel was then brought up to speed by repeatedly pulsing (on/off) the electromagnetic clutch (the clutch had to be pulsed otherwise the diesel would have stalled). The clutch could be pulsed by either manual or computer control.

2.8 Consumer Load

The consumer load was a three-phase symmetrical, resistive load which could be programmed in steps of 100 W up to 7.5kW.

The load was programmable from an 'APPLE II' computer via a parallel interface card which operated 7 reed relays. The load was configured in 6 binary (representing 100, 200, 400, 800, 1600 and 3200 Watts) and 1 non-binary (1200 Watts) steps. The resistance bank could therefore be programmed to reproduce any load pattern.

2.9 Dumpload

Due to the wind turbine having a passive blade pitch mechanism, excess power shedding was achieved via an analogue controlled dumpload. Its role was to dump surplus energy and to maintain the system frequency within certain preset limits.

2.9.1 The load

Any wind power that could not be immediately used or stored was dissipated in a resistive dumpload. The dumpload consisted of a three-phase symmetrical resistive load, switchable through triacs in 63 discrete steps from 0 to 23 kW using a binary configuration. Fig 2.11 is a photograph of the dumpload.

2.9.2 The Controller- Phase I

The wind/diesel system of Phase I of the project used a frequency based analogue Proportional plus Integral (P+I) controller. The frequency signal obtained from the system busbar was compared to a reference frequency, the error signal passed through the (P+I) loops, into an a/d convertor (8 bit successive approximation) and out to the appropriate solid-state relays.

The reference frequency was set to:

1) Maintain minimum diesel loading

As previously mentioned, manufacturers recommend that a diesel engine should not run below 30 to 40% of full load power. The governor droop characteristic provided an almost fixed power/frequency relationship so that the frequency reference was set to maintain this level.

2) Autonomous Wind Turbine Generator

With the system being totally maintained by wind power, which is stochastic in nature, any excess power over that demanded by the consumer would result in a rise in the system frequency. The reference frequency was therefore set to the desired system frequency, and hence any excess power was absorbed by the dumpload when the system frequency rose above this level.

2.9.3 The Controller- Phase II

For reasons discussed in Chapter 5, the frequency based controller was replaced by a power/frequency controller during Phase II of the project. A new controller , shown in the photograph of Fig 2.12, was also built inhouse (Mr J Bleijs) which provided the options for analogue P+I+D (proportional, integral, derivative) control. As in Phase I, two possible modes of operation existed:

1) Wind Plus Diesel (Power Control)

As in Phase I, the constraint of a minimum diesel loading had to be maintained. This was achieved by using the electrical power output of the diesel generator as the control signal which was compared with a preset value of the minimum diesel loading. If this loading was exceeded the dumpload became operational.

2) Wind Plus Flywheel (Power/Frequency Control)

When the diesel engine was disengaged, two control objectives had to met. With the diesel being motored, the diesel electrical power signal was used to limit the power flow into the diesel alternator/flywheel to the rated power of the alternator. The second objective was to maintain an upper frequency limit. This was achieved by the error signal between the frequency signal and the preset upper frequency limit being used to ramp down the power set point (eg above 55Hz the set point of 9kW (motoring) would be adjusted at 10kW/Hz).

2.10 Logistic Controller

Logistic control or supervisory control was used to monitor the wind/diesel/flywheel system to decide whether the diesel engine was required [2.3]. This it achieved via logistic control algorithms implemented on a microcomputer (RESEARCH MACHINES Nimbus PC2). Measurements of frequency, wind turbine output power and consumer load (as well as diesel on/off status) were used as control variables and were inputted to the microcomputer from a BIODATA data acquisition and control unit via an IEE488 link. The diesel status was controlled by relay outputs to the diesel engine fuel solenoid and the electromagnetic clutch.

Two separate control modes were used which were dependent upon the status of the diesel engine:

1) Diesel ON (Power Control)

Exponential smoothed/weighted values of the difference between the wind turbine (electrical) and consumer power were compared to a preset surplus power value. If this surplus power value was exceeded the diesel engine was turned off and the controller switched to the Diesel OFF mode.

2) Diesel OFF (Frequency Control)

With the diesel engine off, the algorithm switched to sampling (up to 25Hz) the system frequency and compared this

value with a preset frequency (typically 47.5Hz for the lower effective flywheel inertia) at which the diesel had to be restarted to prevent system collapse. If the sampled frequency fell below this preset value the diesel was restarted.

2.11 RAL Data Acquisition Equipment

The RAL data acquisition equipment had been designed to allow the monitoring of the wind/diesel/flywheel system for both long term testing (eg diesel wear tests, fuel consumption tests) and the short term testing of system dynamics (eg diesel crashstart, step load testing).

A range of signals were available from wind turbine yaw error angle to wind turbine alternator field current [2.4]. Both analogue (±1V) and digital (TTL compatible) signals could be logged using a combination of BIODATA and HEWLETT PACKARD equipment. The data was then sent over an IEE488 interface to a RM Nimbus PC2 microcomputer which controlled the whole logging process. Computer programs have been written by RAL staff to configure the logging process for; logging run time, scan rate and choice of signals. The signal information could either be stored to disk for future analysis or graphically displayed for hard copy.

The photograph of Fig 2.12 shows both the logistic controller and the data acquisition equipment.

2.12 "Binning" of Data

It should be stressed that with the wind as the primary source of power, it is impossible to obtain steady-state conditions directly so that data had to be "binned" to achieve pseudo steady-state results from the continually changing conditions.

Signals are captured by the data acquisition system at regular time intervals. The information is then passed to the RAL mainframe computer for processing. The signal required for the X-axis of the graph is sorted into a number of sub-ranges. The associated Y-axis values (captured during the same time slot as the X-axis signal) which fall into each of the X-axis subranges are then averaged to give a single Y-axis value for each X-axis subrange. The X-axis value is fixed at the mid-point of each X-axis sub-range.

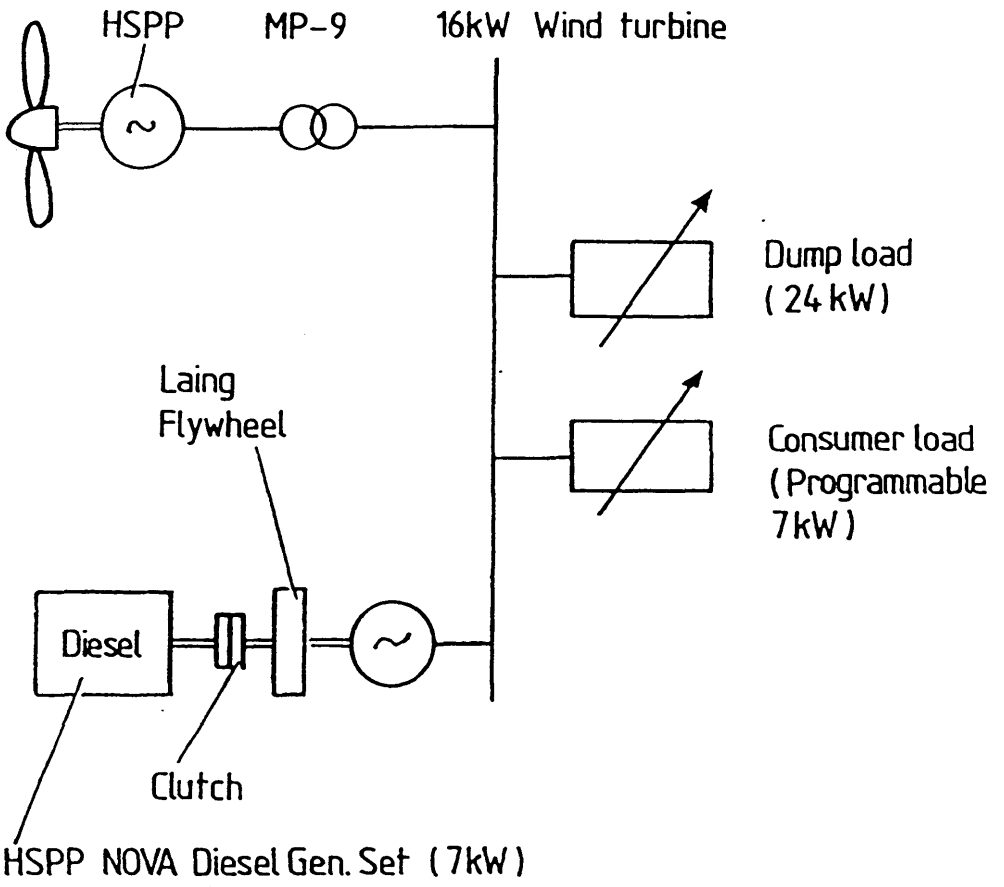

PROJECT HARDWARE

FIGURE 2.1 Schematic Layout of the Phase II Wind/Diesel/Flywheel System

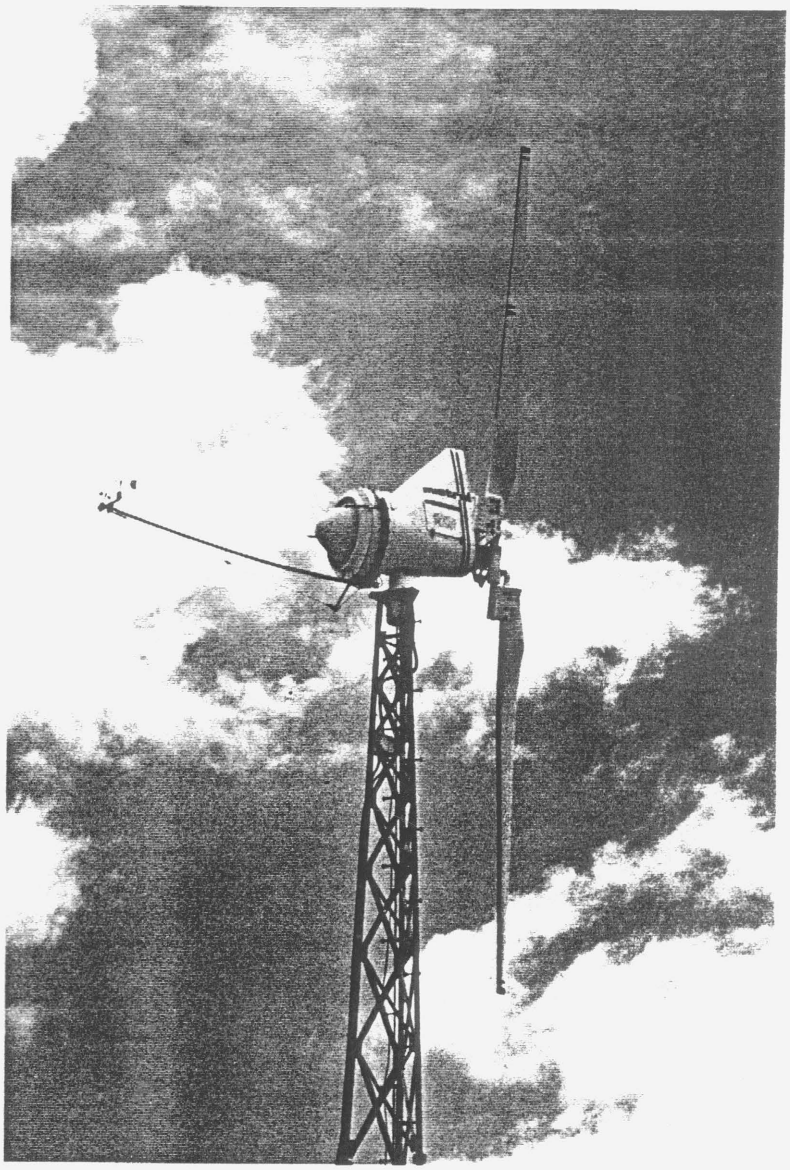

FIGURE 2.2 North Wind Power Co Mistral MP 9 Wind Turbine

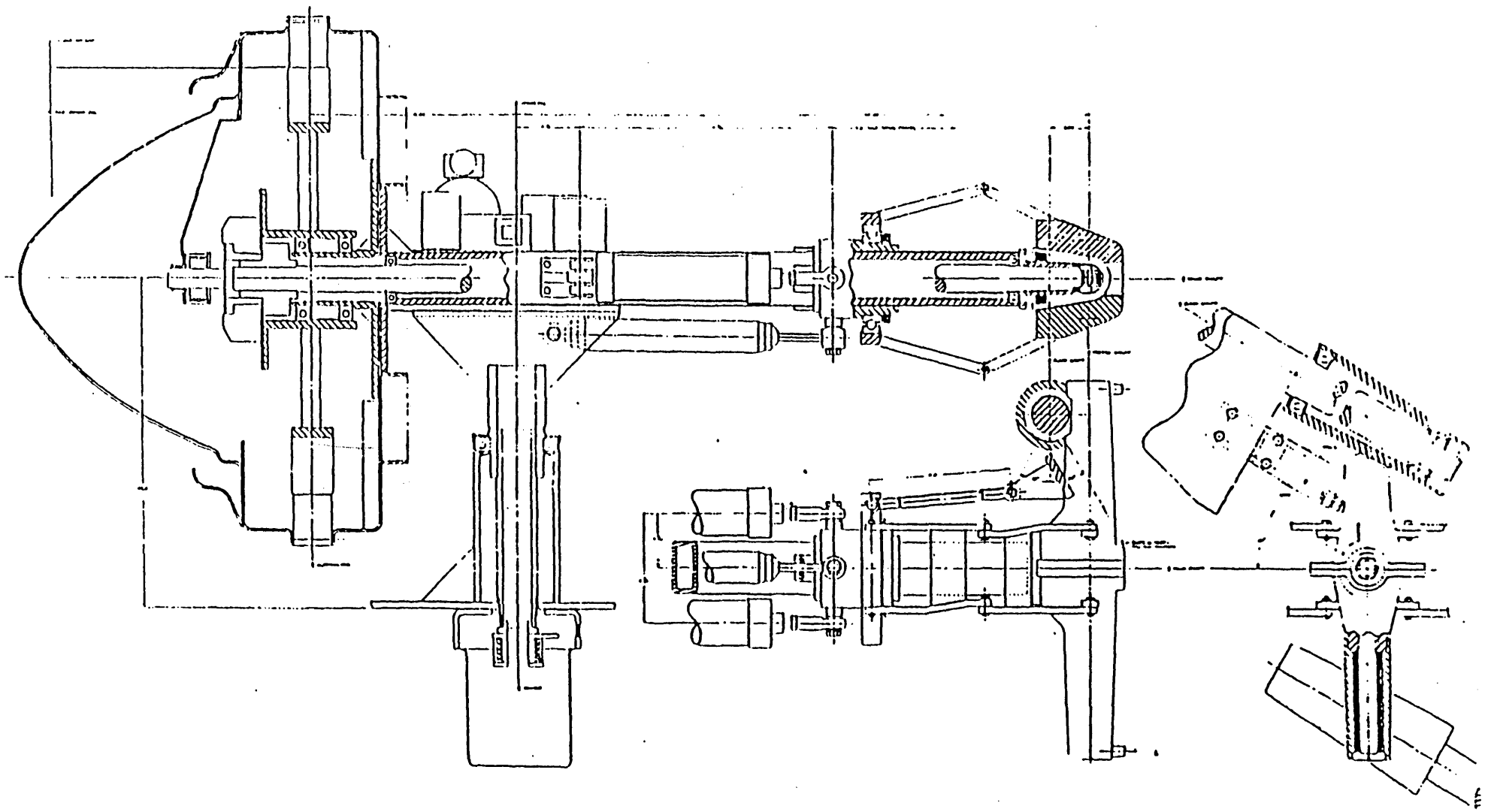

FIGURE 2.3 Teeter and Delta 3 Mechanism of the Wind Turbine

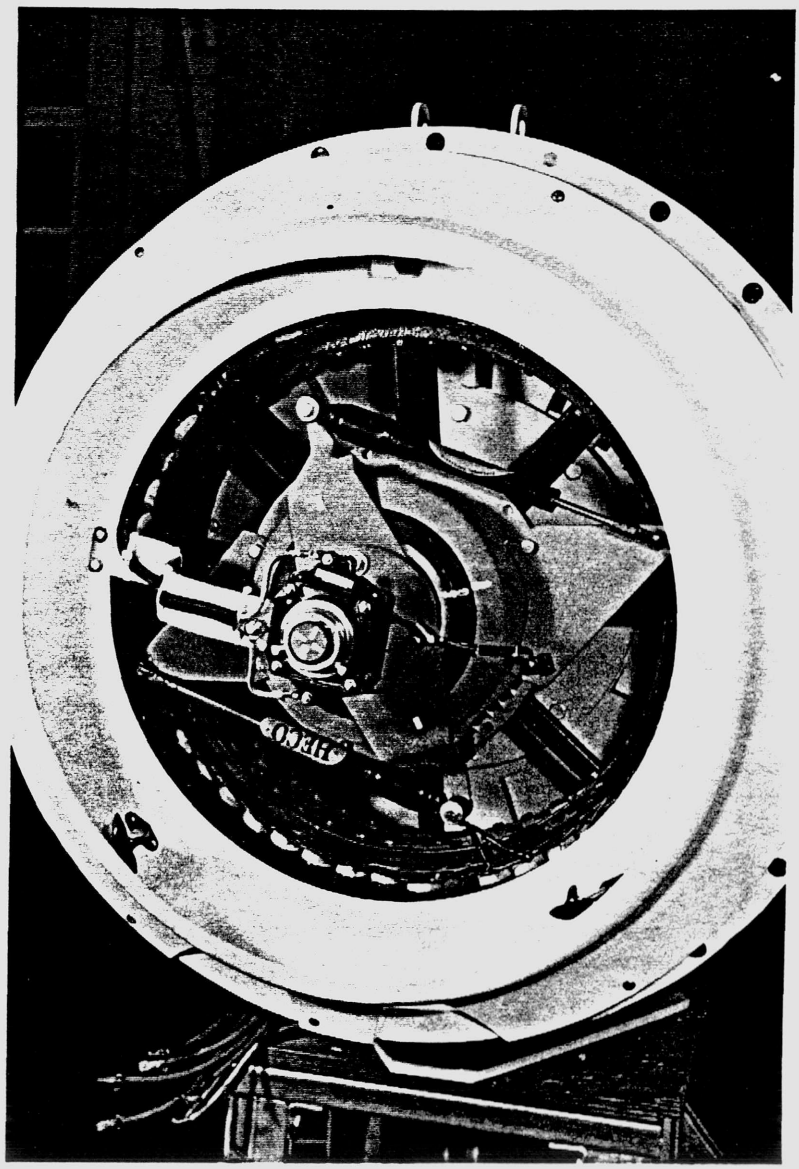

FIGURE 2.4 Wind Turbine Synchronous Generator

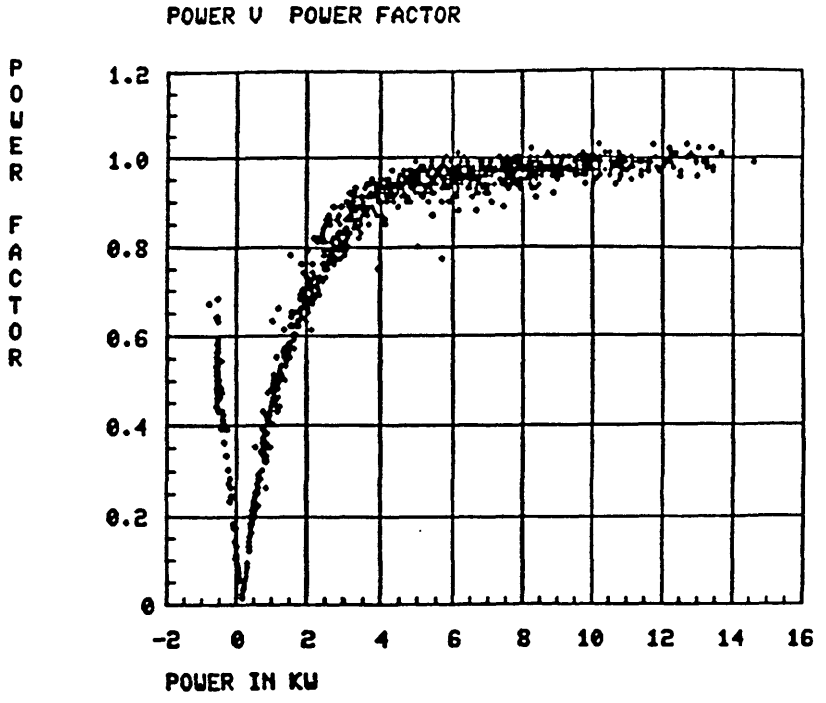

FIGURE 2.5 Graph of Power versus Power Factor for the Wind Turbine "Unity Power Factor" Exciter

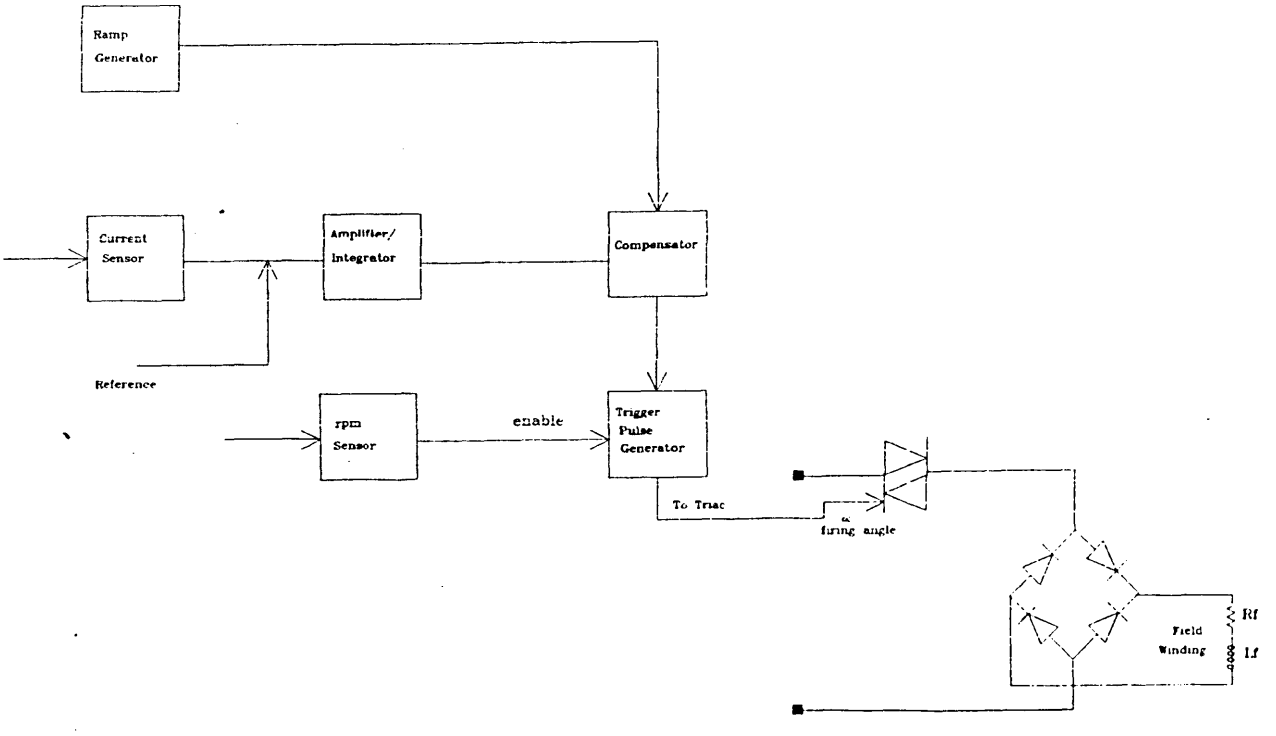

FIGURE 2.6 Static Compounding Circuit of the Wind Turbine UPF Exciter

FIGURE 2.7 Pseudo Steady-State Results of the Wind Turbine Grid Connected with the cold UPF Exciter (a) Reactive Power and (b) Excitation Current vs Real Power Output

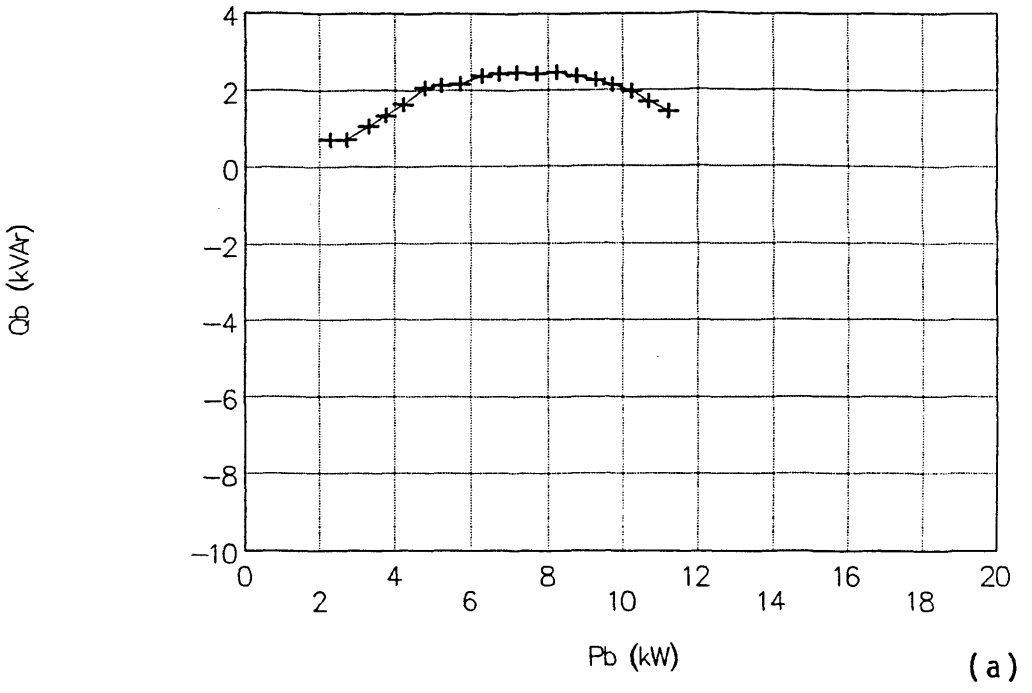

(a)

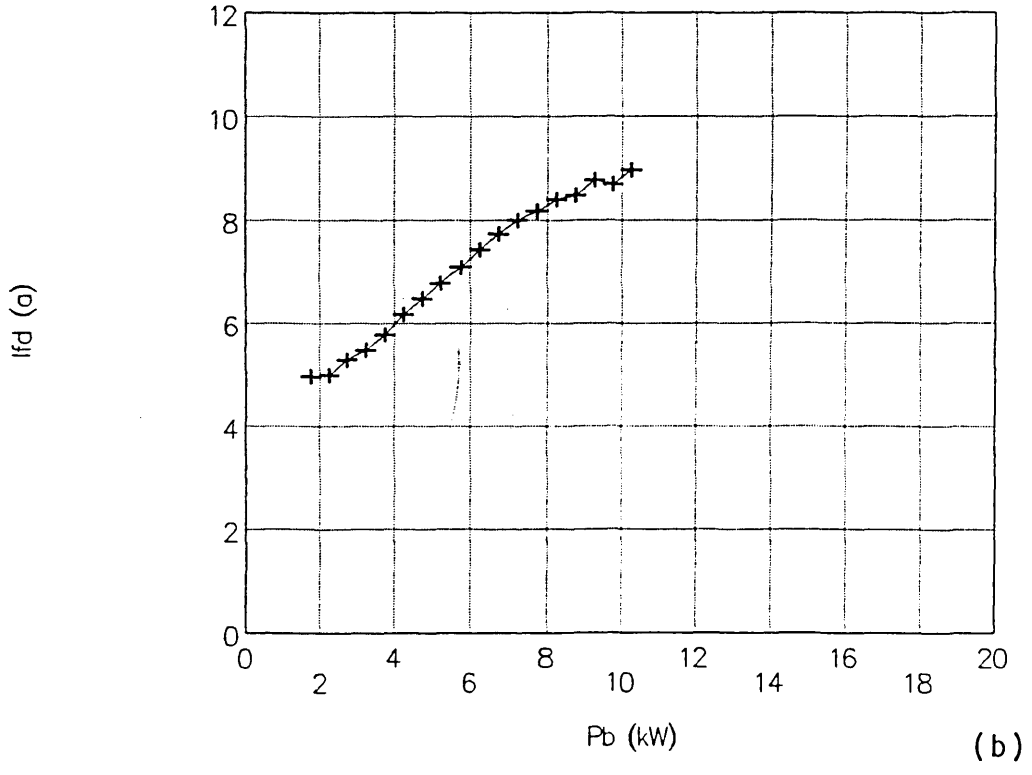

(b)

FIGURE 2.8 Pseudo Steady-State Results of the Wind Turbine Grid Connected with the hot UPF Exciter (a) Reactive Power and (b) Excitation Current vs Real Power Output

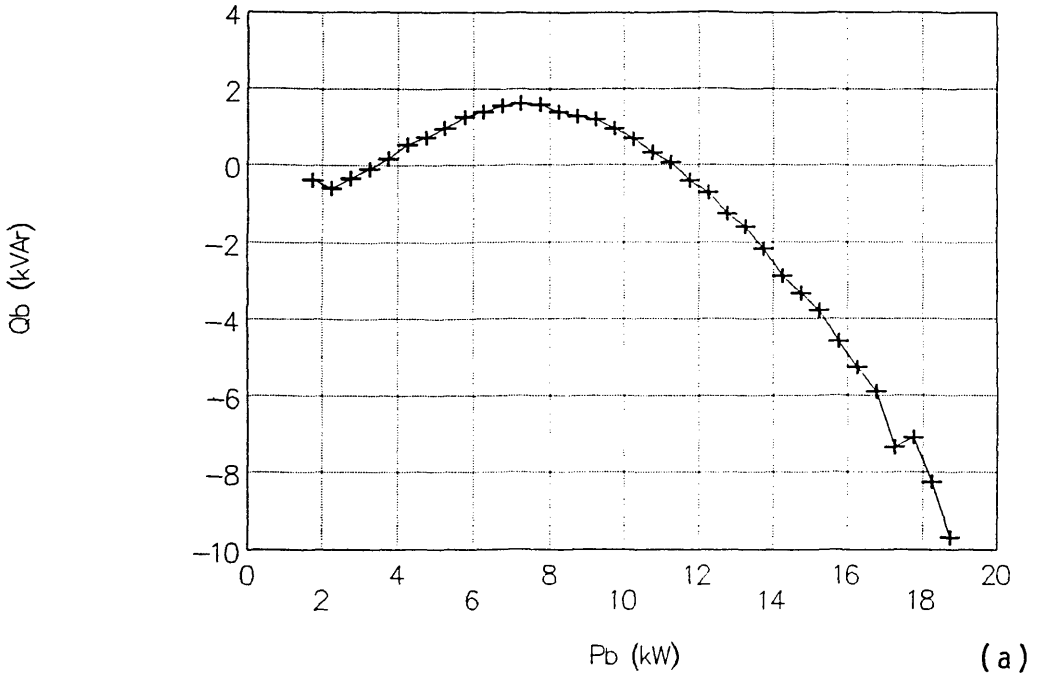

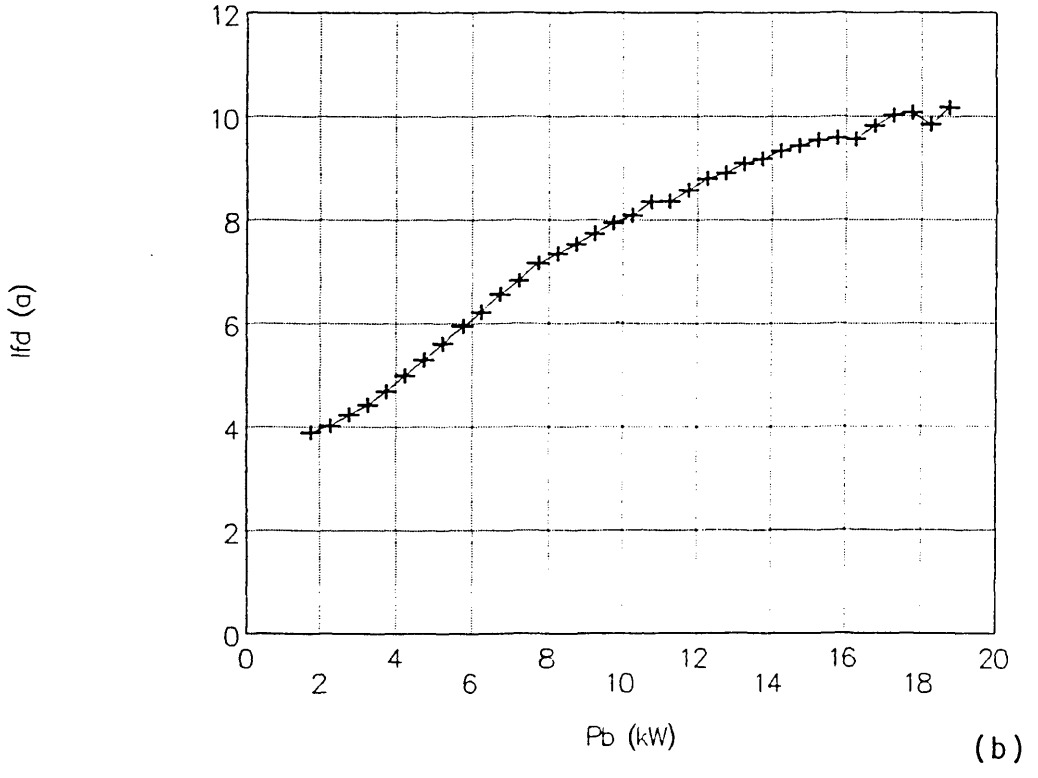

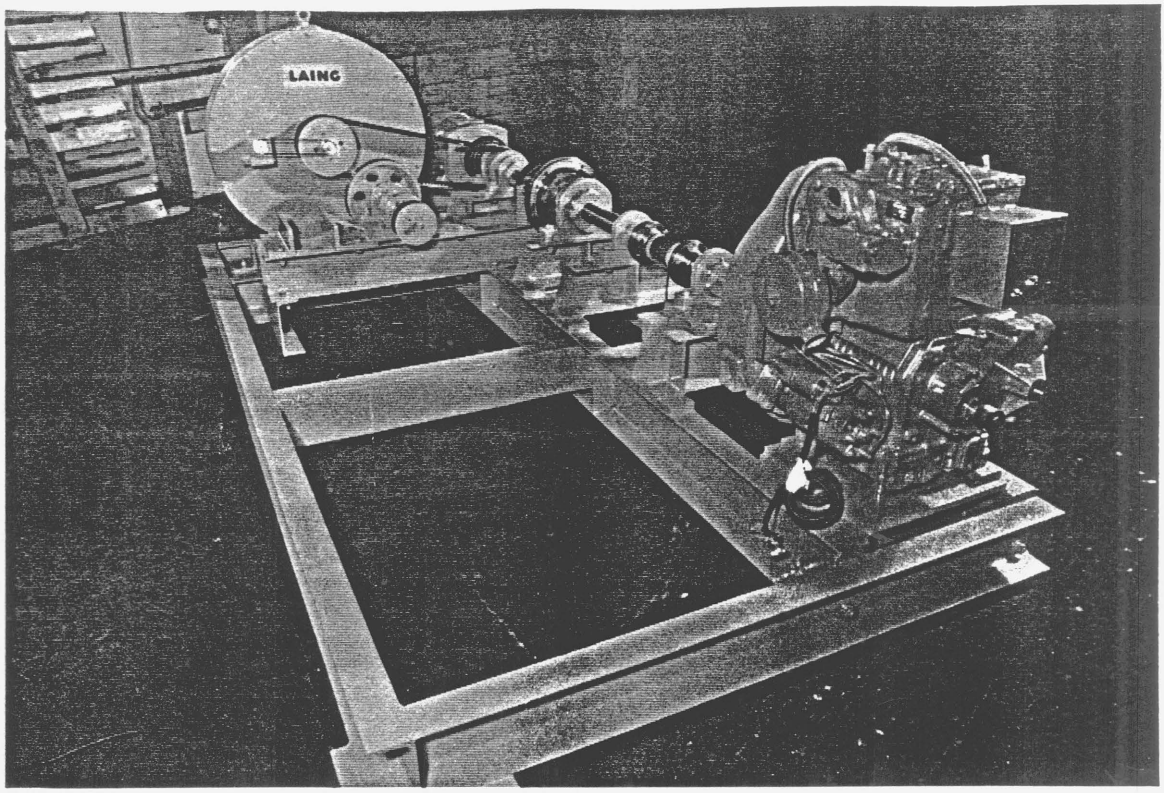

FIGURE 2.9 The Phase II Diesel/Flywheel Rig

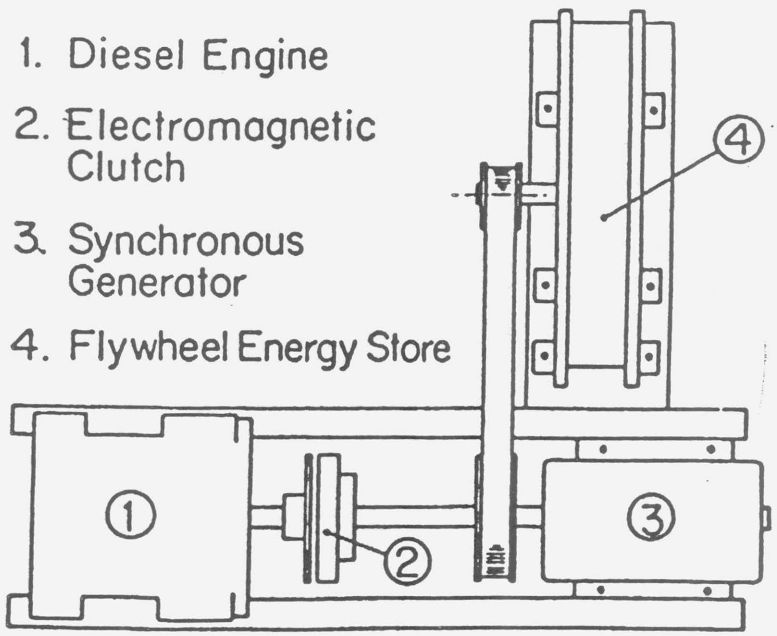

FIGURE 2.10 Schematic Layout of the Phase II Diesel/Flywheel Rig

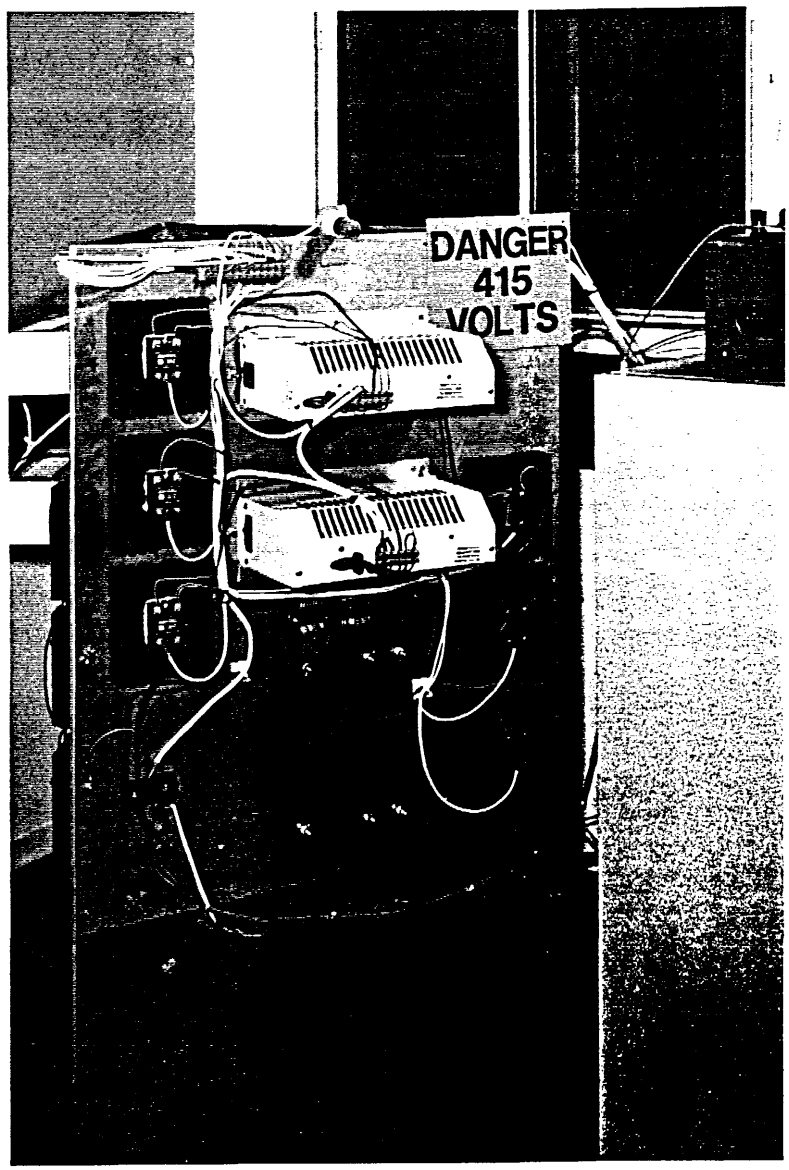

FIGURE 2.11 Phase II Dumpload

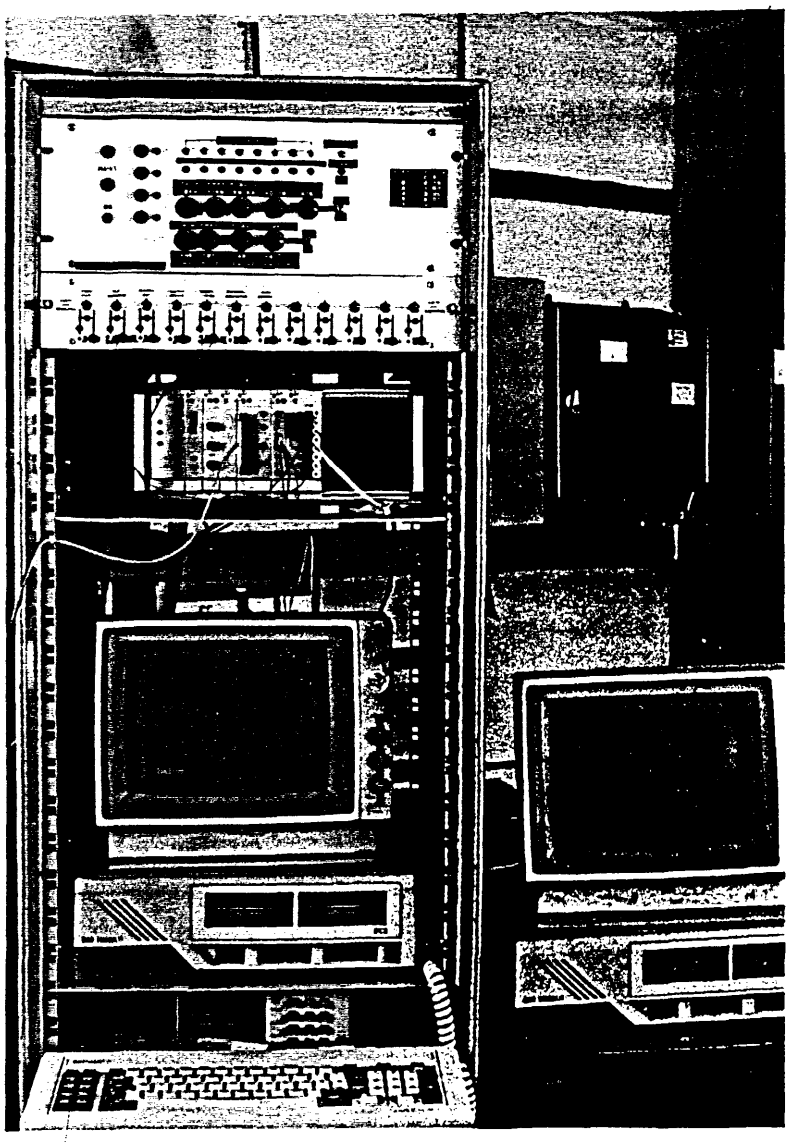

FIGURE 2.12 Phase II Dumpload Controller and Data Acquisition Equipment

CHAPTER 3

COMPONENT CHARACTERISATION

3.0 Introduction

This chapter will describe the development of the models and the site testing used to characterise each of the elements of equipment that made up the wind/diesel and the wind/diesel/flywheel systems. Certain points must be established before greater detail of the the models is given:

1) The modelling work undertaken, was not a comparison against standard ideal systems but was of a real system with all of its complexities and imperfections.

2) The wind/diesel/flywheel system did not have the benefit of an infinite busbar with a fixed voltage and frequency.

3) A large amount of time was spent trying to accurately characterise the system components. This required running the developed models against actual data (obtained from RAL) and adjusting parameter values until a reasonable fit had been obtained.

4) One of the main reasons for 3) was that manufacturers were either unable or unwilling to

provide such data and in some instances provided the wrong data (as in the case of the wind turbine).

3.1 The Wind Turbine

Certain dimensional and aerodynamic characteristics of the wind turbine must be used in order to obtain the amount of mechanical power developed from the wind turbine for a given wind speed. Standard practice has been to develop the Cp/λ characteristic of the wind turbine which forms a family of curves that includes information of; the wind speed, wind turbine rotational speed, blade pitch angle and the power coefficient, Cp.

The manufacturers of the wind turbine were unable to provide a correct C_p/λ curve and so this characteristic was developed at ICSTM. Dimensional and aerodynamic lift and drag (C_l,C_d) characteristics of the aerofoil were fed into a wind turbine analysis code developed at ICSTM [3.1]. The code used two theories to analyse the wind turbine; Axial momentum theory, which examined the movement of the air through the rotor and blade element theory, which modelled each individual blade element separately. The effects of the momentum and blade theories were brought together into one complete set of calculations which allowed an iterative solution by computer.

The wind turbine blades were of a modified GO 797 aerofoil shape, whose dimensional and aerodynamic characteristics are included as Appendix 3.A. The C_p/λ characteristic obtained from the computer solution is shown as Fig 3.1.

Due to the wind turbine having a passive blade pitching mechanism it was also necessary to obtain the relationship between the blade pitch angle and the wind speed. Tests of the wind turbine connected to the grid [3.2] monitored the movement of this angle (via a linear potentiometer) against free wind speed. The results were then binned to produce the curves of Fig 3.2(a) and (b). The former curve is the relationship when the pneumatic pressure of the blade pitch mechanism was set to the manufacturer's recommended 47psi, whilst the latter relates to a pneumatic pressure of 40psi. As will be discussed in Chapter 5, this reduction in pneumatic pressure was used as a method to derate the wind turbine.

These characteristics were used in both the steady-state and dynamic phases of the wind/diesel/flywheel simulations and were incorporated into the program as follows:

$$\lambda = \omega_{wt}.r/V_\infty \qquad (3.1)$$

$$\beta = \text{Function}(V_\infty) \qquad (3.2)$$

$$C_p = \text{Funtion}(\lambda,\beta) \qquad (3.3)$$

$$P_m = \tfrac{1}{2}.\rho.C_p.S.V_\infty^3 \qquad (3.4)$$

where,

V_∞ - free wind speed

r - radius of the wind turbine blades

ω_{wt} - rotational speed of the wind turbine

β - blade pitch angle

S - wind turbine swept area, $\pi.r^2$

ρ - density of air (typically 1.25kg/m^3)

P_m - wind turbine mechanical power

The C_p/λ characteristic was included in the wind turbine model as a look-up table.

During dynamic simulation, some account must be taken of the time needed for the blade to move to a new set angle. β was therefore modified to include a time constant that was the ratio of the pneumatic damping to the stiffness of the spring that the blade acted against.

$$\beta' = \beta/(1+pT_b) \quad (3.5)$$

$$C_p=\text{Function}(\lambda,\beta') \quad (3.6)$$

where,

T_b - Time constant=damping/stiffness, typically 200ms

β' - modified blade pitch angle

3.2 Wind Turbine Drive-Train

Fig 3.3 illustrates the model used to represent the dynamics of the wind turbine generator and its drivetrain. The wind turbine and its generator were modelled in terms of inertias and losses whilst the elasticity, SHE, represented the flexible coupling since the steel shaft was assumed stiff. The mechanical damping was modelled as a single gain, DSH, although this could be modified in the program to include a

low-pass filter to allow for a reduction in the effectiveness of the dampers at higher frequencies. The model can be written in state equation form as follows:

$$p\omega_{wt}=(-D_{wt}.\omega_{wt}-SHE.(\delta_{wt}-\delta_{wtg})-DAMP+P_m/\omega_{wt})/(2.H_{wt}) \quad (3.7)$$

$$p\omega_{wtg}=(-Dwt_g.\omega_{wtg}+SHE.(\delta_{wt}-\delta_{wtg})+DAMP-P_{ie}/\omega_{wtg})/(2.H_{wtg}) \quad (3.8)$$

$$p\delta_{wt}=(\omega_{wt}-\omega_{frame}).2.\pi.F_{nom}/N_p \quad (3.9)$$

$$p\delta_{wtg}=(\omega_{wtg}-\omega_{frame}).2.\pi.F_{nom}/N_p \quad (3.10)$$

$$DAMP=DSH.(\omega_{wt}-\omega_{wtg})/(1+pT_{damp}) \quad (3.11)$$

(the denominator providing the optional low pass filter)

where,

H_{wt} - wind turbine inertia time constant

D_{wt} - wind turbine frictional losses

δ_{wt} - wind turbine rotor angle wrt the reference frame

P_{ie} - shaft power into the generator

H_{wtg} - generator inertia time constant

D_{wtg} - generator frictional losses

δ_{wtg} - generator angle wrt the reference frame

ω_{frame} - rotational speed of the reference frame

F_{nom} - nominal frequency

N_p - number of generator pole-pairs

DAMP - damping torque

T_{damp} - time constant of the optional low pass filter on the mechanical dampers

The overrunning clutch was modelled as a logical switch, S, which decoupled the wind turbine if the rotational speed of the wind turbine fell below that of its generator (ie $\omega_t < \omega_g$). Upon re-engagement, the wind turbine rotor angle was set

to that of the generator since at this instant the torsional deflection angle would be zero.

A complete list of the wind turbine generator's mechanical parameters can be found in Appendix 3.B.

3.3 The Diesel Engine

Two possible approaches were identified as methods to model the diesel engine transient performance. One approach was based on engine cycle simulation which considered the thermo and fluid dynamics of engine operation under steady-state and transient conditions. However, such a model would be costly in computational time and would be impracticable for control system modelling or incorporation into a power system model.

The alternative approach was the use of linearised equations or transfer function models derived from small perturbations around an operating point. This method had the advantages of simplicity and short runtime, but, lost accuracy over the broader operating range of transient studies. Goyal [3.3] used the latter method to produce a model of a turbocharged diesel engine for transient analysis. A similar approach was therefore used to develop an equivalent dynamic model of the naturally aspirated diesel engine.

a) Diesel Engine Model

A block diagram of the diesel engine model is shown as Fig 3.4. It acts as a closed-loop system with the engine speed being controlled by the governor. The governor senses the difference between the actual engine speed and the set speed causing the governor rack actuator to adjust the fuel injection. The governor should therefore be modelled in terms of fuel demand and speed. Likewise, the combustion process should be a non-linear process between the fuel input and the torque output.

The whole system was modelled in terms of equivalent powers or torques and speeds (removing the non-linearity). Originally, a power/speed model was used, but this was later changed to torque/speed due to the engine having a more linear steady-state torque/speed relationship as illustrated by the diesel droop characteristics of Figs 3.5(a) and (b). The steady-state characteristics of the diesel engine can be described thus:

$$T_d = T_{dr} + T_{dr} \cdot (\omega_{ref} - \omega_d)/DROOP \qquad (3.12)$$

$$T_{shd} = T_d - D_d \cdot \omega_d^2 \qquad (3.13)$$

Where,

ω_d - diesel engine rotational speed

T_d - mechanical torque delivered by the engine

T_{dr} - diesel engine rated torque

DROOP - engine droop (mechanical)

T_{shd} - diesel shaft torque

D_d - diesel frictional losses

Under transient conditions, the dynamics of the governor and its fuel rack can be adequately represented by a second order transfer function of the form:

$$T_1=T_{dr}.(\omega_{ref}-\omega_d)/(DROOP.(1+2.\zeta.p.T_n+(p.T_n)^2)) \quad (3.14)$$

$$T_2=T_{dr}-T_1 \quad (3.15)$$

$$T_3=MIN\{T_2,T_{dmax}\} \quad (3.16)$$

$$T_3=MAX\{T_3,0\} \quad (3.17)$$

where,

T_3 - equivalent mechanical torque due to the fuel flow

ζ - damping coefficient

T_n - $1/w_n$ the natural frequency of the second order system

T_{dmax} - upper mechanical torque limit

The change in engine torque follows that of the injected fuel after a time delay, e^{-Tf}. This delay was approximated in the simulation by a three term Taylor Expansion of $1/e^x$ as follows:

$$T_d=T_3/(1+p.T_f+(p.T_f)^2/2) \quad (3.18)$$

b) Validation

The diesel engine and its alternator were subjected to electrical load application/rejection tests with power and speed being monitored. The parameters were fitted using a model of the diesel and its alternator connected to the

programmable consumer load. This was an iterative process that depended not only upon the accuracy of the tests' results but also upon the accuracy of the alternator and exciter models. Therefore, as improved alternator and exciter models were developed, the comparison between the actual and simulated responses were repeated to obtain better estimates of the diesel engine's parameters.

Fig 3.6 (a) is a graph of the typical response of the diesel generator set to a stepchange in load from 6.8 to 0 kW. Fig 3.6 (b,c) is the equivalent simulated response using the "best-fit" engine parameters listed in Apendix 3.B.

3.4 Synchronous Machine Model

Both the wind turbine and diesel alternators are salient pole synchronous machines. In this study information at the very fast subtransient level was not deemed to be required as interest centred around the system's controllability and component interaction. The equations were therefore formulated for transient and steady-state conditions using Park's d-q axis model. Early tests of the system had already revealed that small voltage differences between the two synchronous machines could lead to large reactive power flows. Therefore, it was felt necessary to include a reasonably sophisticated saturation model.

Throughout this study the computer models of the synchronous machines rely upon the per-unit convention defined in the

paper by Macdonald et al [3.4] and included as Appendix 3.C of this thesis.

3.4.1 Steady-State Equations

In order to include the effect of saliency ($X_d > X_q$) a fictitious voltage, E_q, located on the quadrature-axis (q-axis) is used as the voltage behind the q-axis reactance. This representation of the synchronous machine used in the solution of the network equations is shown as Fig 3.7 and leads to the phasor diagram of Fig 3.8(a). The full equation is as follows:

$$E_q = V + R_a.I_a + jX_q.I_a \qquad (3.19)$$

The sinusoidal flux produced by the field current acts along the d-axis. The voltage induced by the field current (also known as the airgap voltage, E_i) lags this flux by 90° and, therefore, is on the q-axis. This voltage can be determined by adding to the terminal voltage, V, the voltage drop across the armature resistance and the voltage drop representing the demagnetizing effects along the d- and q-axis. The airgap voltage, E_i, is calculated by:

$$E_i = V + R_a.I_a + jX_d.I_d + jX_q.I_q \qquad (3.20)$$

Fig 3.8(b) illustrates the associated phasor diagram. Equations (3.19) and (3.20) can be combined to produce the equation:

$$|E_q| = |E_i| - (X_d-X_q).|I_d| \qquad (3.21)$$

The effect of saturation now has to be taken into account.

3.4.2 Synchronous Machine Saturation Model

Saturation effects in synchronous machines can have an influence on loadflow, steady-state and transient stability (and electromagnetic transients). However, the rigorous modelling of saturation is difficult and time consuming and would require magnetic field calculations, eg using finite element techniques [3.4]. These techniques were impracticable for the timestep solution under study and also such detailed data for field calculation was unavailable. Therefore, an approximate solution which used data from standard test methods was used.

Data from standard "open-circuit" and "short-circuit" tests are normally made available by machine manufacturers. The open circuit curve gives a relationship between the terminal voltage and the field current for open-circuited armature windings. It thus provides an indication of the degree of saturation in the machine. Likewise, the short-circuit test gives a relationship between the armature current and the field current whilst the armature windings are short-circuited. The armature (d-axis) reactance (X_d) can then be defined in terms of the ratio between the open-circuit terminal voltage and the short-circuit armature current for a given field current.

Sugiyama et al [3.5] suggest the following approach:

1) To treat the saturation phenomena simply in terms of the variation of the mutual reactances, X_{ad} and X_{aq}, with the leakage reactances, X_l, being fixed.

2) A constant relationship, ie constant saliency, is assumed between X_d and X_q under all load conditions.

3) The values of X_d and X_q are well characterised by the value of the effective excitation current, I_e. This excitation current is calculated from the vector sum of both axis currents, thus:

$$I_e = \sqrt{((I_{fd}-I_d)^2+I_q^2)} \qquad (3.22)$$

where,

I_{fd} - field current

I_d - d-axis demagnetising component of the armature current

I_q - q-axis component of the armature current.

In discussions, Dr Bleijs [3.6] proposed a modification to the I_q component based upon the square of the ratio of the unsaturated d- and q-axis reactances, ie $(X_{du}/X_{qu})^2$, which had been demonstrated to give improved results. Dommel has also included this additional feature in his saturation model of the synchronous machine in the Electromagnetics Transients Program , EMTP [3.7]. The modified Sugiyama method was therefore adopted for this study.

3.4.3 Overall Steady-State Solution of the Synchronous Machine

The synchronous generator's steady-state performance is thus modelled with the following equations:

$$P_{ie} = P_m - P_{loss}.\omega_s^2 \quad (3.23)$$

$$P = REAL(V.CONJG(I_a) \quad (3.24)$$

$$Q = IMAG(V.CONJG(I_a) \quad (3.25)$$

$$I_d = (P.SIN(\angle E_q) + Q.COS(\angle E_q))/|V| \quad (3.26)$$

$$I_q = (P.COS(\angle E_q) - Q.SIN(\angle E_q))/|V| \quad (3.27)$$

$$I_{fd} = excfn(|V|, Ia) \quad (3.28)$$

$$I_e = \sqrt{((I_{fd} - I_d)^2 + ((X_{qu}/X_{du}).I_q)^2)} \quad (3.29)$$

$$E_{oc} = satfn(I_e) \quad (3.30)$$

$$X_{ad} = E_{oc}/I_e \quad (3.31)$$

$$X_d = X_{ad} + X_l \quad (3.32)$$

$$X_q = X_d.X_{qu}/X_{du} \quad (3.33)$$

$$|E_2| = X_{ad}.I_{fd} \quad (3.34)$$

$$|E_q| = |E_i| - (X_d - X_q).|I_d| \quad (3.21)$$

where,

V - terminal voltage

I_a - armature or load current

P_m - mechanical power

P_{ie} - internally generated electrical power

P_{loss} - mechanical losses of friction and windage

ω_s - rotational speed

P, Q - Real and reactive electrical power at the machine terminals

E_q - q-axis voltage

X_{ad} - d-axis armature reactance

X_l - leakage reactance

X_d, X_q - d- and q-axis reactances

X_{du}, X_{qu}- unsaturated values of the d- and q-axis reactances

E_1 - airgap voltage from the armature side of the airgap

E_2 - airgap voltage from the field side of the airgap

Satfn - function in the form of a lookup table to provide the value of the open-circuit voltage for a given excitation current.

Excfn - function that is dependent upon the type of excitation system used in the machine.

3.4.4 Transient Model of the Synchronous Machine

An equivalent circuit representation, similar to that used in the steady-state, is used to characterise the transient behaviour of the synchronous machine.

As its basis, the method assumes that the initial currents and flux linkages following a change of conditions can be determined solely by a group of reactances. The decay of these currents and flux linkages is achieved by time constants determined from both the reactances and resistances of these equivalent circuits.

For the d-axis transient case the equivalent circuit is as shown by Fig 3.9. The leakage reactance is in series with the parallel combination of the armature and field reactances. This total reactance is known as the transient reactance and is calculated from:

$$X_d' = X_l + X_{ad}.X_f/(X_{ad} + X_f) \quad (3.35)$$

where,

X_d' - d-axis transient reactance

X_f - field leakage reactance

The decay of this condition to the steady-state reactance, X_d $(= X_l + X_{ad})$, is determined by the time constant of the field circuit (transient open-circuit time constant), T_{do}', which is defined as:

$$T_{do}' = (X_f + X_{ad})/(\omega.R_f) \quad (3.36)$$

where,

R_f - field winding resistance

ω - rotational speed (rad/sec)

For the q-axis there is no field winding and therefore the q-axis transient reactance is the same as the q-axis synchronous reactance:

$$X_q' = X_q = X_l + X_{aq} \quad (3.37)$$

Appendix 3.D develops the equations used to represent the synchronous machine in the transient condition. A similar saturation model is used to that of the steady-state condition. The equations used in the dynamic model, in addition to Equations 3.21, 3.24 to 3.27 and 3.29 to 3.34 , are as follows:

$$E_q = E_q' + j(X_q - X_d').I_d \quad (3.38)$$

$$pE_q' = (E_2 - E_1)/T_{do}' \quad (3.39)$$

T_{do}' is recalculated in the program to take into account the effect of saturation on Xad. An equivalent phasor diagram is shown as Fig 3.10.

Functions also had to be included to represent the dynamics of the excitation system. The various functions for AVR's and static excitation systems used in the wind/diesel/flywheel system are developed later in this thesis.

3.5 Validation of the Synchronous Machine Models

Characterisation of the synchronous generators had been carried out during Phase I of the project [3.8] using Standstill Frequency Response (SSFR) tests on both machines and confirmatory open- and short- circuit tests on the diesel generator (Fig 3.11). The necessary reactance values established were as follows:

Diesel Alternator

X_d = 1.21 pu, X_q = 0.66 pu, X_d' = 0.14 pu (8.5 kVA base)

Wind Turbine Alternator

X_d = 2.21 pu, X_q = 1.87 pu, X_d' = 1.23 pu (21 kVA base)

Previous tests had attempted to confirm the values of wind turbine generator reactances, using Unity Power Factor (UPF) saturation and Zero Power Factor (ZPF) "V" tests. The "V" curve from the ZPF test was then shifted so that the zero

armature current was at zero excitation current to produce the equivalent of the short-circuit curve. However, when the equivalent open- and short-circuit curves obtained from these tests were used to calculate X_{du}, the value was only 90% of that calculated from the SSFR tests. The validity of the ZPF test was also questioned due to the amount of data scatter at the higher excitation levels. The manufacturers were therefore contacted during Phase II and two differing no-load saturation curves (but no short-circuit curves) were provided.

The lack of information necessitated the open- and short-circuit tests to be carried out on the wind-driven turbine (Bleijs, Coonick). Modifications were made to the pitching mechanism to prevent overspeeding by feathering the blades. During the open-circuit test, increasing excitation levels were set by adjusting the reference pot in the wind turbine generator exciter whilst the compounding circuit was de-activated. At very low windspeeds (3m/s), the blades were taken out of feather and the excitation was energised. At speeds of around 70rpm (approximately half-speed), one seconds worth of terminal voltage, excitation current and wind turbine speed data was captured via the data acquisition equipment (Fig 3.12). After adjustment for speed, the voltage versus excitation current was plotted. The short-circuit test adopted a similar procedure to the open-circuit test but only required a single reading. With the terminals of the wind turbine generator being shorted, one seconds worth of line current, excitation current and wind turbine speed data was collected (Fig 3.13).

The open-circuit curve obtained by the Phase II open-circuit test was found to be in good agreement with the UPF test (Fig 3.14). However, a comparison of the Phase II short-circuit curve with that of the shifted "V" curve of the ZPF test revealed that the former was only 90% of the latter. The value of Xdu calculated from the Phase II RAL tests was therefore in total agreement with that calculated from the SSFR tests.

The open- and short-circuit characteristics of both the diesel and wind turbine generators were therefore implemented in the synchronous machine saturation models of the ICSTM simulation programs.

3.6 Wind Turbine Generator Exciter

Tsitsovits [3.9] proposed that the exciter could be modelled using an equation of the form:

$$|I_{fd}| = |V|.G_r.(1 + \cos(\theta_o - \Delta\theta.I_a^2)) \quad (3.40)$$

$$P_{loss} = |I_{fd}|^2.R_f \quad (3.41)$$

Where,

G_r - ac/dc conversion factor for the triac, rectifier bridge and field resistance

θ_o - no-load triac firing angle setpoint

$\Delta\theta$ - incremental gain of the effect of the reactive load current on the triac firing angle

P_{loss} - exciter real power losses

Previous work to fit values to the parameters of this exciter model had relied upon the actual exciter being gradually loaded by a dummy resistor [3.10]. A minimisation routine was then used to adjust the parameters of the model; G_r, θ_o and $\Delta\theta$, so as to obtain a best fit between the actual and modelled field currents. During Phase II, this model and its parameters were initially used in the full wind turbine generator simulation. An investigation was then made of the steady-state operation of the wind turbine generator connected to the grid. Actual data, as illustrated by Fig 2.8, was compared with the simulated results of the wind turbine generator connected to an infinite busbar (program INFBUSS). However, large discrepancies were noted between the actual and simulated results (Fig 3.15) of the steady-state power flows and field currents at the higher power levels.

An improvement to this performance was obtained when the current compounding was remodelled such that until the current reached a set level the compounding was inactive. Above this level the effect of the compounding was approximated to a cosine function. The two conditions were represented as follows:

IF ($I_a < I_o$) THEN

$\theta = \theta_o$

ELSE

$$\theta = \theta_o + A_i.(I_o - I_a).\cos(A_j.(I_a - I_o)) \qquad (3.42)$$

where,

I_o - current threshold above which compounding becomes active

A_i, A_j - gains to obtain a best fit to the field current versus dummy load power curve of Fig 3.16

The field current was then obtained by:

$$|I_{fd}| = |V|.G_r.(1 + COS(\theta)) \quad (3.43)$$

The inherent internal time constant of the device was included in the dynamic representation as follows:

$$p\theta' = ((I_o - I_a).A_i.COS(A_j.(I_a - I_o)) - \theta')/T_{int} \quad (3.44)$$

$$\theta = \theta_o + \theta' \quad (3.45)$$

Another important factor not included in the original model was the effect of the device's reactive power losses. This loss is due to the phase shift between the supply voltage and the supply current, caused by the firing delay of the triac. Bleijs [3.11] suggested the following representation of this loss:

$$Q_{loss} = |I_{fd}|.\sqrt{(2.\sqrt{(2)}/(3.\pi).R_f.|I_{fd}|.|V| - (R_f.I_{fd})^2/3)} \quad (3.46)$$

Graphs of the simulated results of the wind turbine connected to the grid appear as Fig 3.17 and illustrate that both the power flows and field currents are in reasonably close agreement to the actual results of Fig 2.8.

As discussed in Section 2.4, the inability of the exciter to compensate for temperature affects on the field winding resistance led to reactive power flows at the lighter loadings of between 0.5 to 2.5 kVAr as opposed to the "hot" exciter's -0.8 to +1.5 kVAr. Fig 3.18 graphs the result of

the effect on the reactive power ~~by the~~ by a 10% increase in G_r (equivalent to a 10% reduction in the field winding resistance). The simulated results produced higher reactive power flows (0.4 to 2.9 kVAr). The discrepancy can be accounted for by the use of binned data from a time series of hundreds of seconds which would lead to the field winding warming up (epecially at the higher loadings) and thereby downwardly distorting the actual results of Fig 2.7. A direct comparison should not therefore be made between these results.

3.7 Diesel Generator Exciter

A model of the diesel generator exciter had also been developed at ICSTM during Phase I [3.9] which was of the form:

$$I_{fd} = K_r.(K_v.V+jK_i.I_a.e^{j.\alpha}) \qquad (3.47)$$

Where,

K_r, K_v and K_i are exciter constants

α - phase shift due to the current transformer

This model proved to be reasonably satisfactory whilst the diesel alternator was generating. However, the model was unable to match the very poor regulation of the device in the motoring mode. As can be seen from Fig 3.19, moving the alternator further into the motoring mode led to a sharp rise in the voltage. Furthermore, the exciter was therefore totally unsuited to parallel operation in this form when it would be required to both generate and motor.

Several alternative models were tested to try to simulate this sharp voltage rise when the diesel alternator was driven further into the motoring mode:

1) An empirical relationship between the voltage and power.
2) A single phase representation of the phasor diagram assuming ideal transformers .
3) A simplified single-phase model of the exciter assuming ideal transformers.

Method 3 was tried as it was hoped that an actual model of the physical system would allow changes to be made to the topology in order to improve the voltage regulation throughout the alternator's range. However, all three methods proved unsatisfactory and the investigation into the modification of the exciter's topology was not undertaken. The static exciter model was thus replaced by a P, Q, V look-up table based on the regulation characteristic of Fig 3.19.

The unsatisfactory voltage regulation of the static exciter eventually led to the decision to replace it with that of an Automatic Voltage Regulator (AVR).

3.8 Automatic Voltage Regulators

The discussion will be limited to that of the diesel generator AVR 15E, however, similar techniques were used to

develop the model of the AVR 15R on the wind turbine generator.

Previous testing of both AVR's using open-loop and frequency response tests had proved inconclusive. Closed-loop step response tests were therefore carried out with the AVR 15E in the environment and at the settings it would normally operate. The loop was closed by the terminal voltage of the diesel generator being fed back to the voltage sensing terminals of the AVR (Fig 3.20). To ensure that a sufficiently accurate model of the diesel and its alternator were being used, step response tests were carried out with a fixed level of excitation and practical results of voltage, power, current and speed were compared with simulated results (Fig 3.22(a) and (b)).

Having achieved satisfactory agreement, various models of the AVR were tried (eg lag, lead/lag, double lead/lag, lead/double lag with complex poles). For each model, a range of parameter values was tried at three stability settings. Eventually, the simulation was able to reproduce comparable responses to that of the practical tests (Figs 3.23 to 3.24) using as a basis the lead/ double lag (with complex poles) model. Fig 3.21(a) is a transfer function representation of the AVR 15E, whilst Fig 3.21(b) represents the model of the AVR 15R used throughout the study.

3.8.1 Parallel Operation of the Wind Turbine and Diesel Generators

Laboratory tests were carried out at ICSTM in order to gain an insight into the parallel operation of the wind turbine with that of the diesel generator. Special interest centred on the control of the transfer of reactive power between the two machines. Two dc machines were used to replace the prime-movers in the system of Fig 3.25.

Successful parallel operation could only be achieved with "Quadrature Droop Compensation" (QDC) on the AVR's, by the external circuitry illustrated in Fig 3.26. The quadrature droop connection in the sensing phase allowed a voltage to be injected into the sensing circuit from the secondary of the current transformer. The transformer was connected to the AVR so as to inject a voltage which added/subtracted directly to the sensed voltage when the line current carried a reactive lagging/leading current. The voltage fed into the AVR was thus dependent on the level of reactive power flow but was still independent of any resistive load due to it producing an injected voltage that was 90° out of phase with the sensed voltage.

It was therefore decided that if AVR's were to be used in the actual system then QDC's would also have to be included to control the transfer of reactive power between the two machines. The effect of QDC compensation is further investigated in Chapter 5.

3.9 Diesel/Flywheel Rig

a) Flywheel

The flywheel has been modelled throughout the study as an inertia plus losses. The pulley belt system was modelled as a perfect gearbox ie the effective inertia of the flywheel was therefore:

$$J_f' = J_f.(\omega_f/\omega_s)^2 \qquad (3.48)$$

where,

J_f - flywheel inertia

J_f' - flywheel inertia referred to the main shaft

ω_f - rotational speed of the flywheel

ω_s - rotational speed of the main shaft

Both the flywheel effective inertia and its losses were then included in the calculation of the derivative of the diesel alternator speed equation as follows:

$$p\omega_s = (-(D_{dg} + D_f).\omega_s + TORQ_d - P_d/\omega_s)/(2.(H_{dg}+H_f)) \qquad (3.49)$$

where,

H_f - effective flywheel inertia constant

H_{dg} - diesel generator inertia constant

P_d - diesel generator electrical power

$TORQ_d$ - shaft torque from the diesel engine

D_f - flywheel frictional losses

D_{dg} - diesel generator frictional losses

The speed equation of the diesel engine was represented thus:

$$p\omega_e = (-D_e.\omega_e - TORQ_d + P_{me}/\omega_e)/(2.H_e) \qquad (3.50)$$

where,

H_e - diesel engine inertia constant

ω_e - diesel engine rotational speed

D_e - diesel engine frictional losses

P_{me} - mechanical power ouptut of the diesel engine

b) Drive-Train

The drive-train of the diesel/flywheel rig was modelled as a rigid shaft with the electromagnetic clutch, used to decouple the diesel engine, controlled via a logical switch ICLUTCH. The action of the clutch on the diesel/flywheel rig had to be considered during two processes; disengagement and re-engagement of the diesel engine.

i) Disengagement

In order that the diesel engine was decoupled from the rest of the system the logical switch ICLUTCH was set to 0. The program then immediately set both TORQd and the demanded speed of the diesel engine to zero (equivalent to turning off the fuel).

ii) Re-engagement

Tests carried out on the torque transfer response of the clutch to the signal for closure, revealed that it could be

adequately represented by a first order time constant with an upper torque transfer limit, as illustrated by:

$$pTORQ_d = (TORQ_d - TORQ_{ec})/T_{ec} \quad (3.51)$$

$$TORQ_d = MIN(TORQ_d, MAXTORQ_d) \quad (3.52)$$

A study of the diesel engine's response during startup revealed that the engine was motored until a speed of approximately 250 rpm was exceeded. Above this speed, the fuel was turned on and the engine began to fire. Fig 3.27 is a flowchart of the clutch and diesel engine status during re-engagement used in the simulation.

3.10 Consumer Load

The consumer load was represented in terms of the admittance (G - jB). In order that different load patterns (eg stepchange, cyclic variation) could be applied to the system, a time series of these admittances was stored in an array. Each element of the array represented the state of the load at each timestep. Linear interpolation was used to adjust the value of the load at the smaller numerical integration timesteps.

3.11 The Dumpload Controller

a) Phase I (Frequency Control)

Fig 3.28(a) is a block diagram of the frequency based dumpload controller used during Phase I of the project. The state equations used to represent this P + I controller were:

$$YCL_{fp} = (F_x - F_{set}).K_{fp} \quad (3.53)$$

$$pYCL_{fi} = (F_x - F_{set}).K_{fi} \quad (3.54)$$

$$YCL_f = YCL_{fp} + YCL_{fi} \quad (3.54)$$

where,

F_{set} - frequency setpoint

F_x - frequency measured by the transducer

K_{fp} - proportional gain

YCL_{fp} - requested dumpload admittance due to the proportional term

K_{fi} - integral gain (including the time constant)

YCL_{fi} - requested dumpload admittance due to the integral term

YCL_f - total requested dumpload admittance due to frequency control

b) Phase II (Power/Frequency Control)

Fig 3.28(b) is the block diagram representation of the dumpload's power/frequency controller used during Phase II. Power control was the main mode of operation, however, if the system frequency rose above a frequency setpoint the frequency loop was enabled. The P + I + D controller was represented in state equation form as follows:

$$YCL_p = (P_x - P_{set}').K_{pp} \quad (3.56)$$

$$pYCL_i = (P_x - P_{set}').K_{pi} \quad (3.57)$$

$$YCL_d = p(P_x - P_{set}).K_{pd} \quad (3.58)$$

$$YCL = YCL_p + YCL_i + YCL_d \quad (3.59)$$

where,

K_{pp} - proportional gain

K_{pi} - integral gain

K_{pd} - derivative gain

P_x - diesel electrical output power measured via the power transducer

P_{set}' - power set point = P_{set}, for the conditions:

a) minimum diesel loading during diesel online

b) rated diesel power during diesel offline

If the frequency set point was exceeded the power set point ,P_{set}', was adjusted using the equations of (3.53) to (3.55) plus:

$$P_{set}' = P_{set} + YCL_f \quad (3.60)$$

Before the controller signal passed to the dumpload, an analogue to digital (a/d) conversion took place. The a/d conversion in the dumpload required the representation of deadtime (T_{dead}), ie periods of time in which the device took to process the signal information. Deadtime was therefore modelled by sampling the information at a given timestep (T_{step}) and using an array as a FIFO (first-in, first-out) list, illustrated by Fig 3.29. The number of storage locations (N_{sl}) was calculated from:

$$N_{sl} = INT(T_{dead}/T_{step}) \quad (3.61)$$

3.12 The Dumpload

The dumpload was modelled as a purely resistive load that was divided into 63 * 375ohm steps to represent its non-continuous nature. The level of loading requested by the controller was therefore modified as follows:

KCL = INT(YCL/CLSTEP)

KCL = MIN(KCL,MAXSTEP)

KCL = MAX(KCL,MINSTEP) (3.62)

YCL' = KCL.CLSTEP (3.63)

where,

CLSTEP - admittance of each dumpload step

KCL - number of dumpload steps required

MAXSTEP- maximum number (63) of dumpload steps

MINSTEP- minimum number (0) of dumpload steps

YCL' - admittance actually set by the dumpload

3.13 The Wind Turbine Generator Stepup Transformer

Fig 3.30 is a schematic representation of the stepup transformer as characterised by Jenkins [3.10] and used in this study.

3.14 Line Representation

The short-line representation of (R + jX) was used as the equivalent circuit of connection cabling in the wind/diesel/flywheel system. Values used in the model appear in Appendix 3.B.

3.15 The Wind/Diesel/Flywheel System Network Topology

Fig 3.31 illustrates the network topolgy used in both the normal and pseudo steady-state phases of the wind/diesel/flywheel dynamic simulation program.

3.16 Frequency

Unlike large power system models, the wind/diesel/flywheel system did not operate at a fixed frequency. Also, the network equations were not represented as differential equations, therefore, some means had to be found to evaluate this variable. Elgerd [3.12] proposed the use of an equation that defined the frequency in terms of an inertia centre. However, this method relied upon the drivetrain between the prime-mover and its alternator being approximated as stiff, which would be inappropriate for the wind turbine generator model. An alternative approach that was tested on the ICSTM simulation involved the numerical differentiation of the busbar load angle (calculated from the steady-state network equations) to produce the new busbar "frequency". However,

this method proved very susceptible to spikes due to any sudden system changes.

An heuristic approach was therefore used that took into account the electrical stiffnesses of the two alternators plus any associated line. The equation is as follows:

$$\omega_{bus} = (\omega_{wtg}.X_2 + \omega_{dg}.X_1)/(X_1+X_2) \qquad (3.64)$$

where,

ω_{bus} - "speed" of the busbar at each time interval

ω_{wtg} - wind turbine generator speed

ω_{dg} - diesel generator speed

X_1 - wind turbine generator q-axis reactance

X_2 - line reactance + diesel generator q-axis reactance

3.17 Transducers

Due to the large number of signal transducers and hence the increased burden upon computation only the characteristics of three devices were included in the simulation; the busbar voltage, diesel electrical power output and frequency transducers.

The characteristic of the voltage transducer was approximated to that of a first order low-pass device with an 80msecs time constant. Frequency response tests on the power transducer revealed it to be a second order low pass device with a double time constant of 16.8msecs. The characteristics of the frequency transducer will be discussed in Chapter 5.

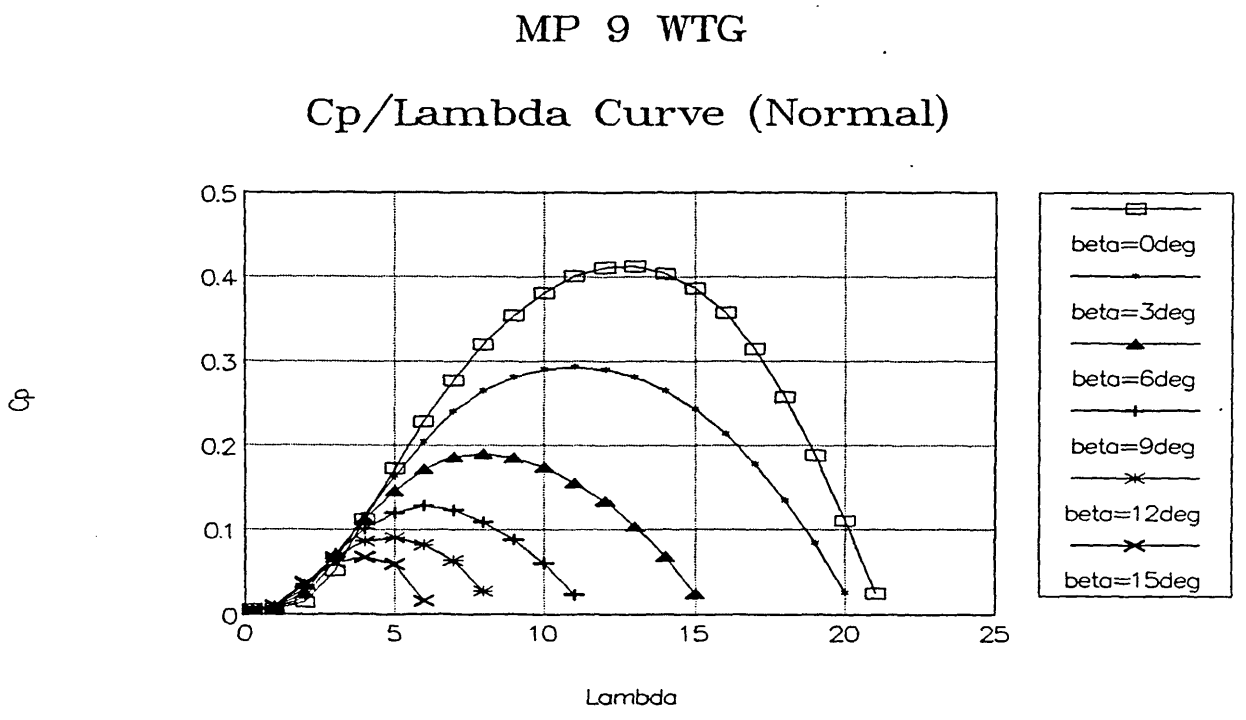

FIGURE 3.1 Computed Cp/lambda characteristic of the MP 9 Wind Turbine

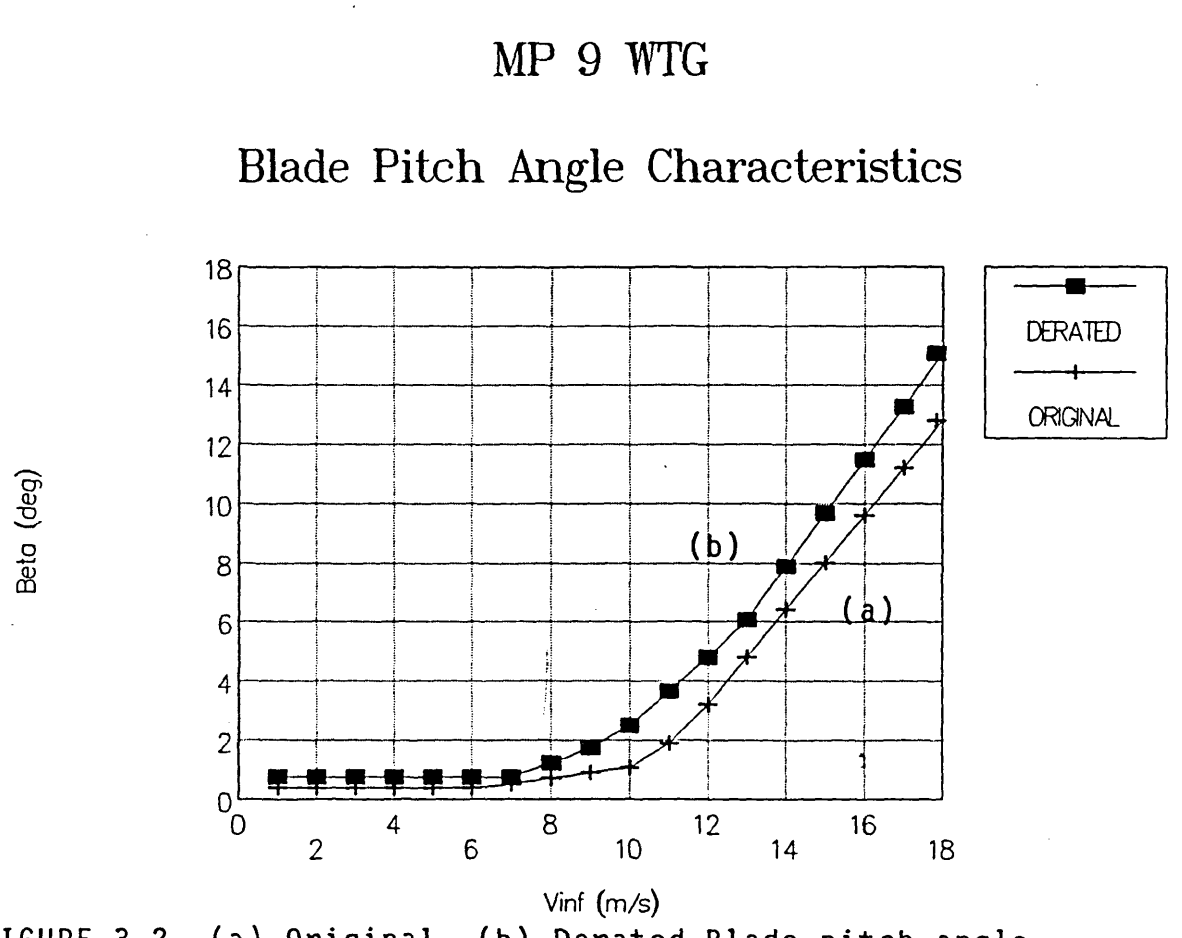

FIGURE 3.2 (a) Original (b) Derated Blade pitch angle characteristics for the MP 9 Wind Turbine

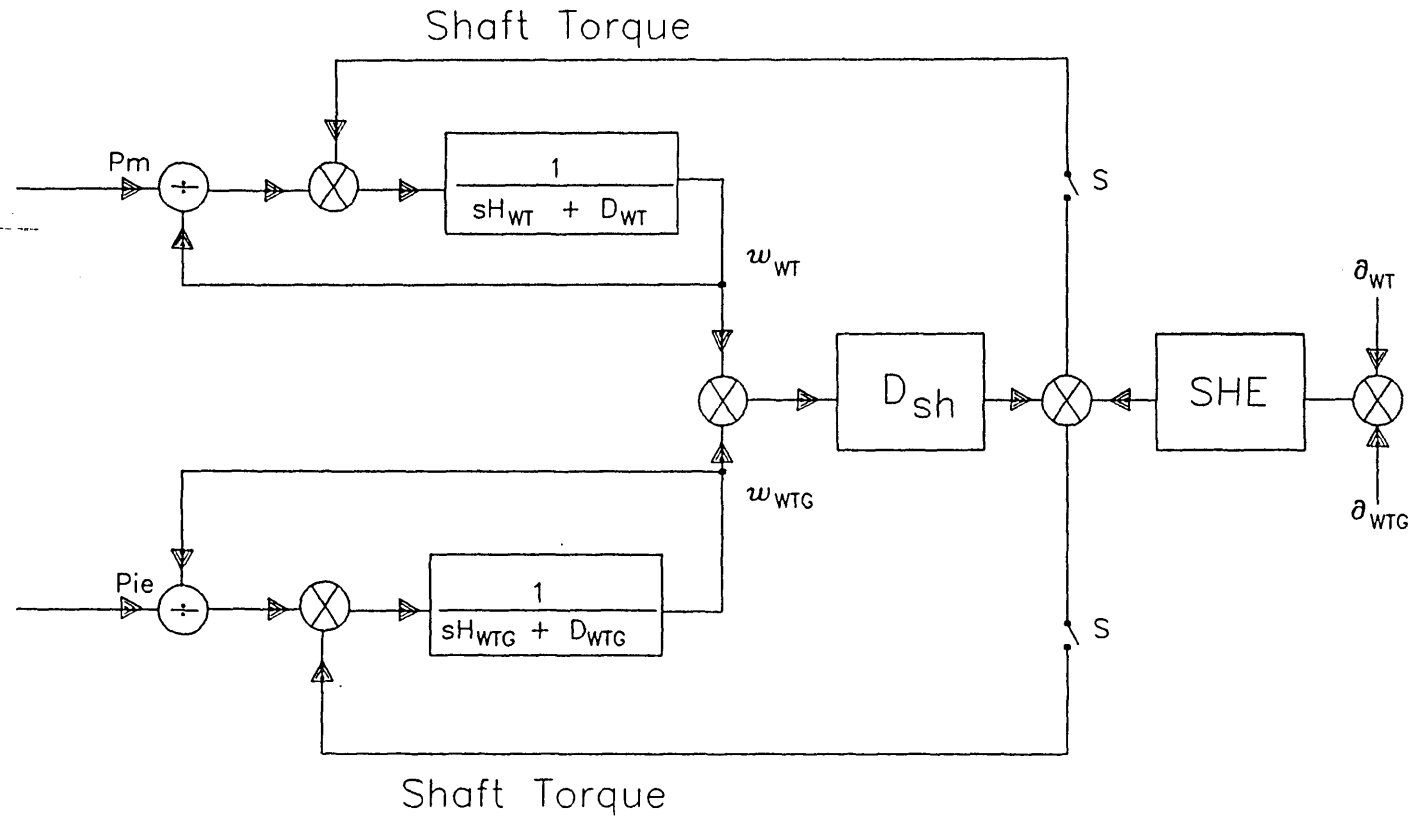

FIGURE 3.3 Model used to represent the dynamics of the Wind Turbine Generator and its drivetrain

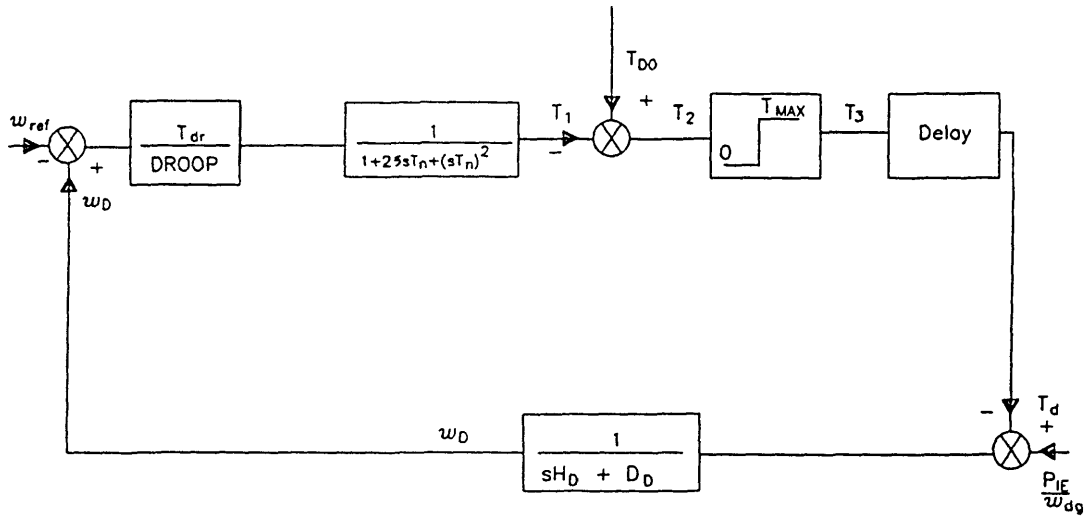

FIGURE 3.4 Block diagram of the diesel engine model based on the torque speed relationship

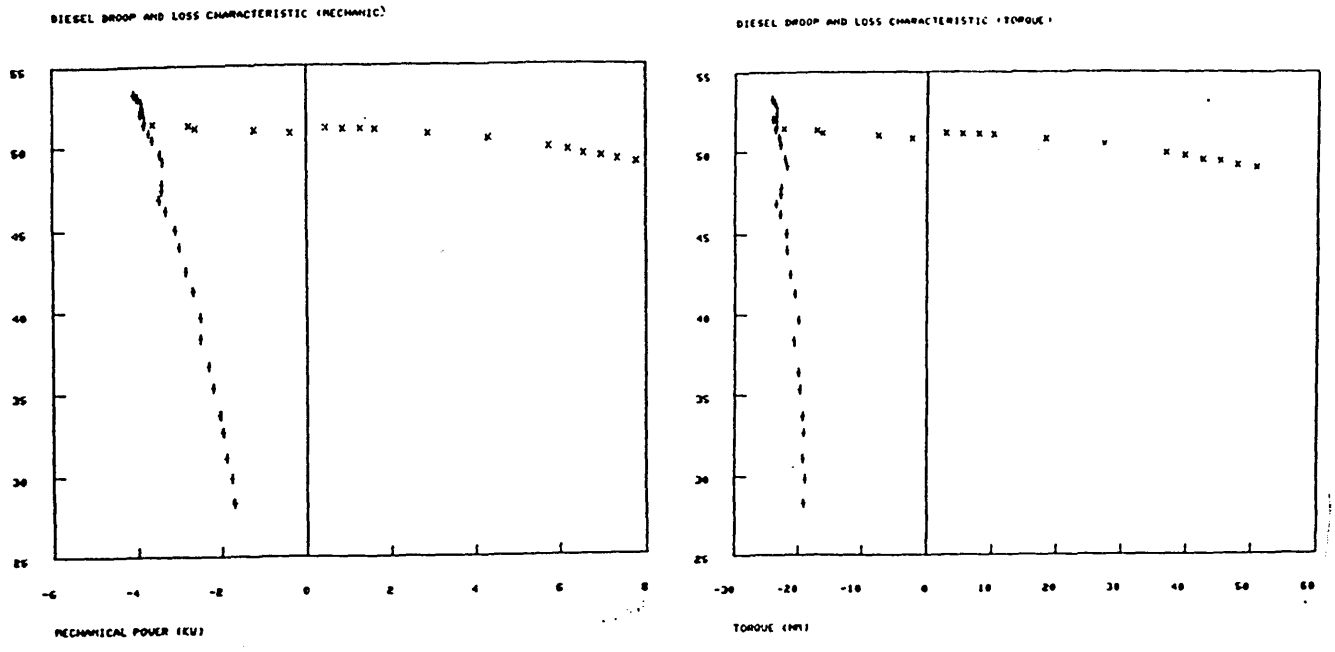

FIGURE 3.5 (a) Power/speed (b) Torque/speed characteristic of the diesel engine

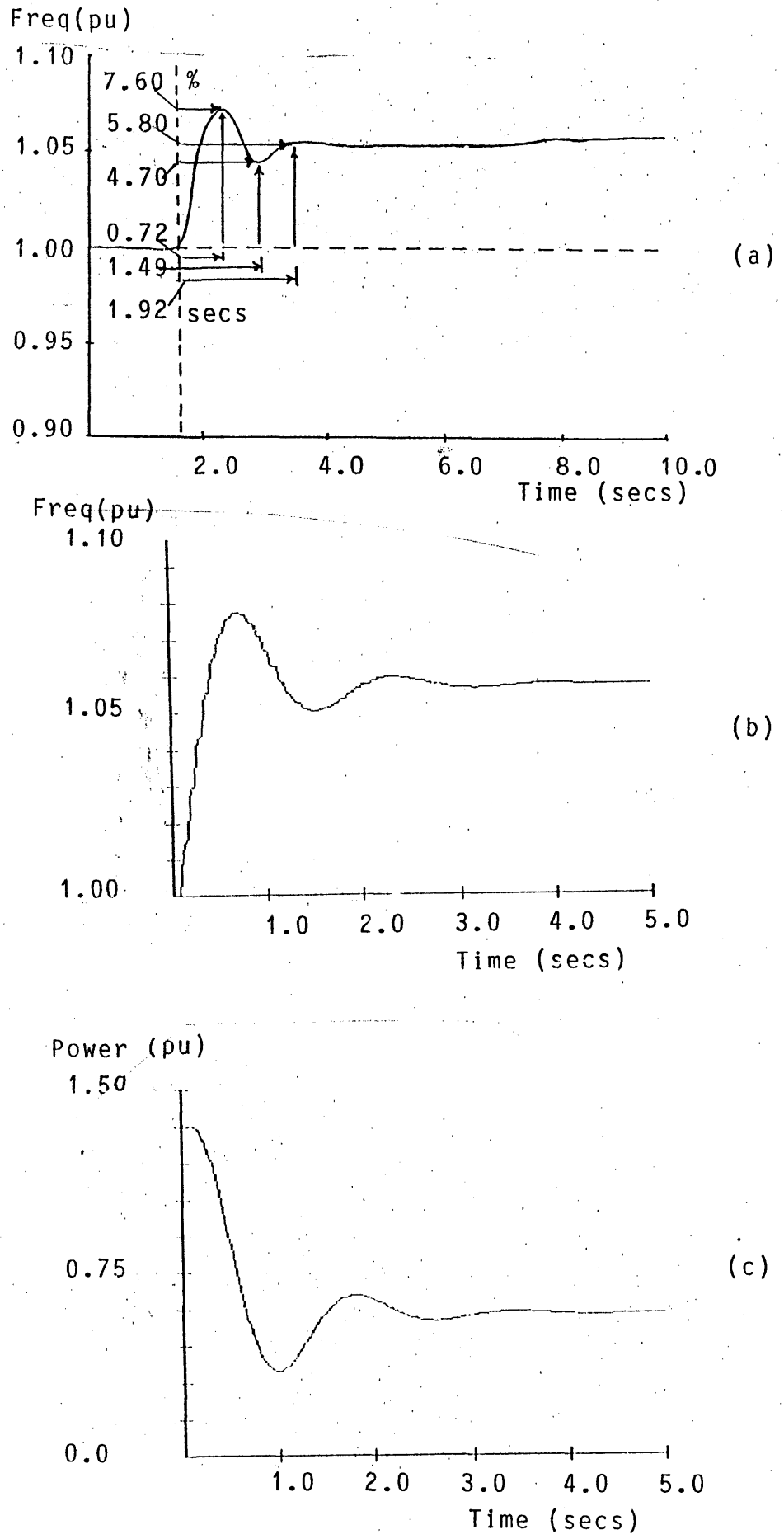

FIGURE 3.6 Diesel engine response to load rejection
(a) actual (b) (c) simulated

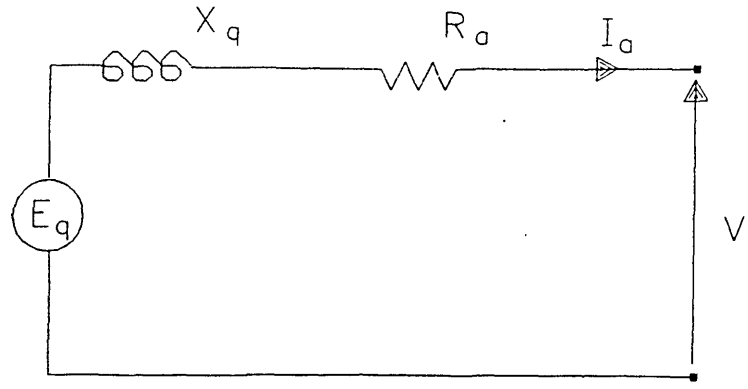

FIGURE 3.7 Steady-state model of the synchronous machine

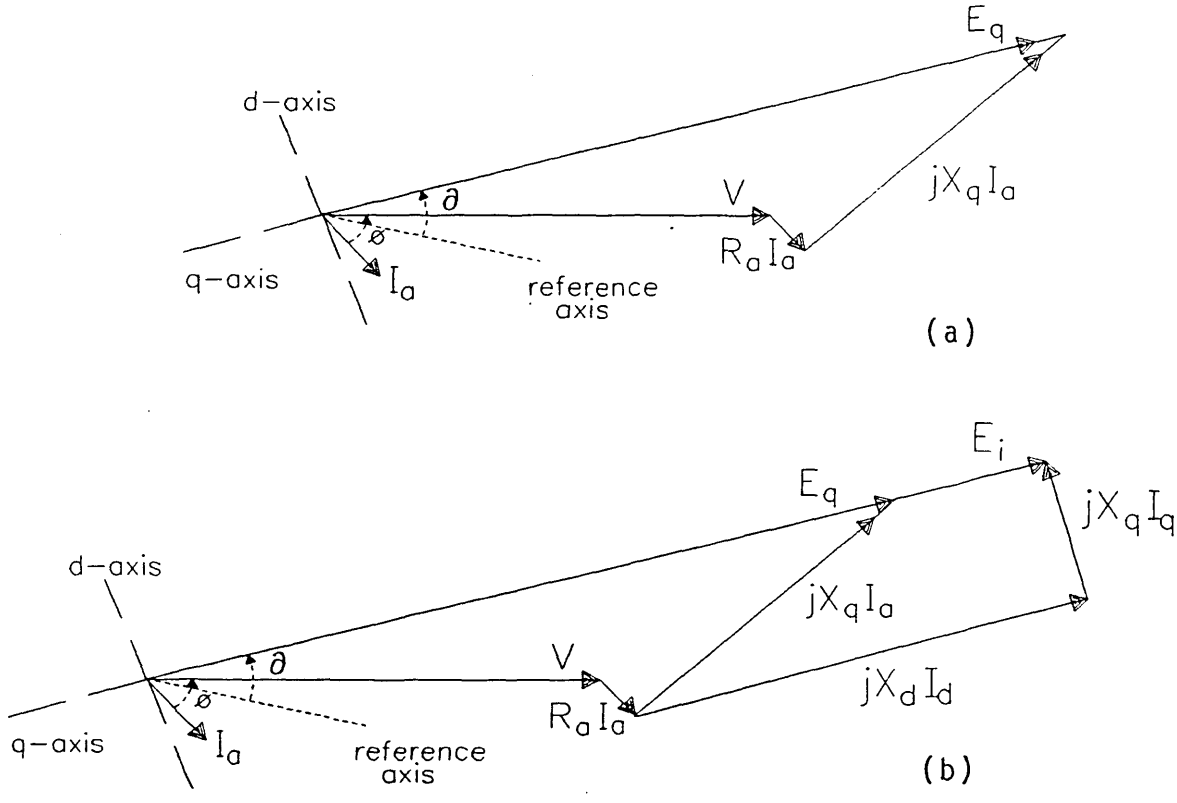

FIGURE 3.8 Steady-state phasor diagram of the synchronous machine

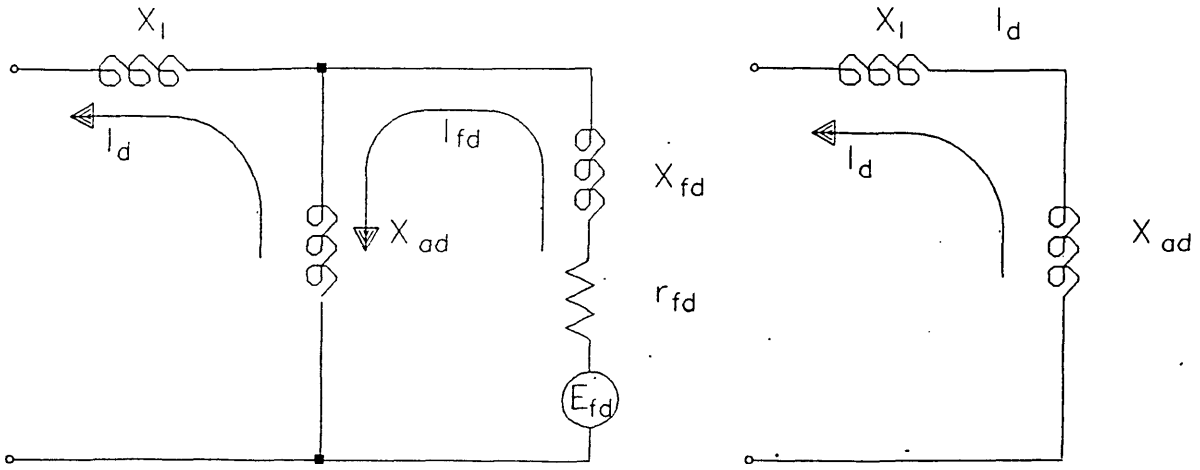

FIGURE 3.9 The equivalent (i) transient (ii) steady-state d-axis model of the synchronous machine

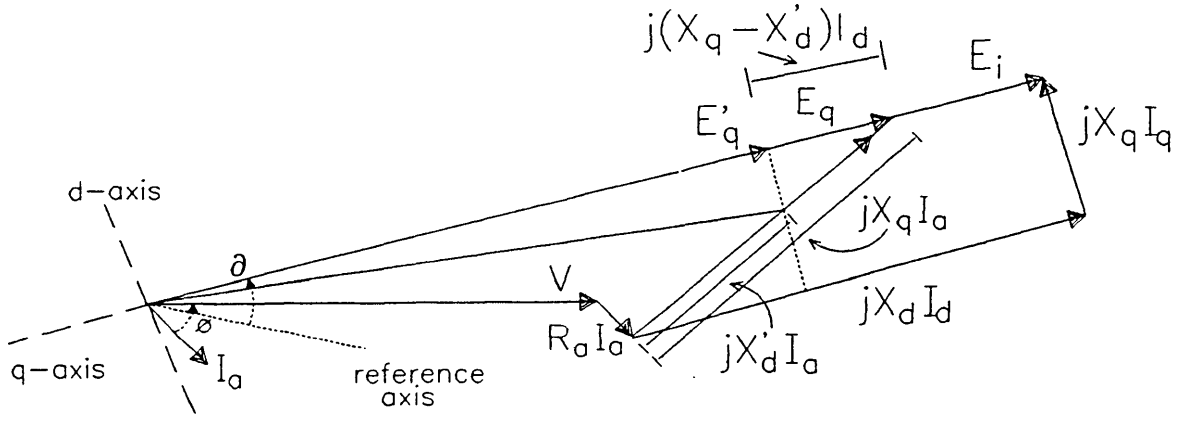

FIGURE 3.10 Transient phasor diagram of the synchronous machine

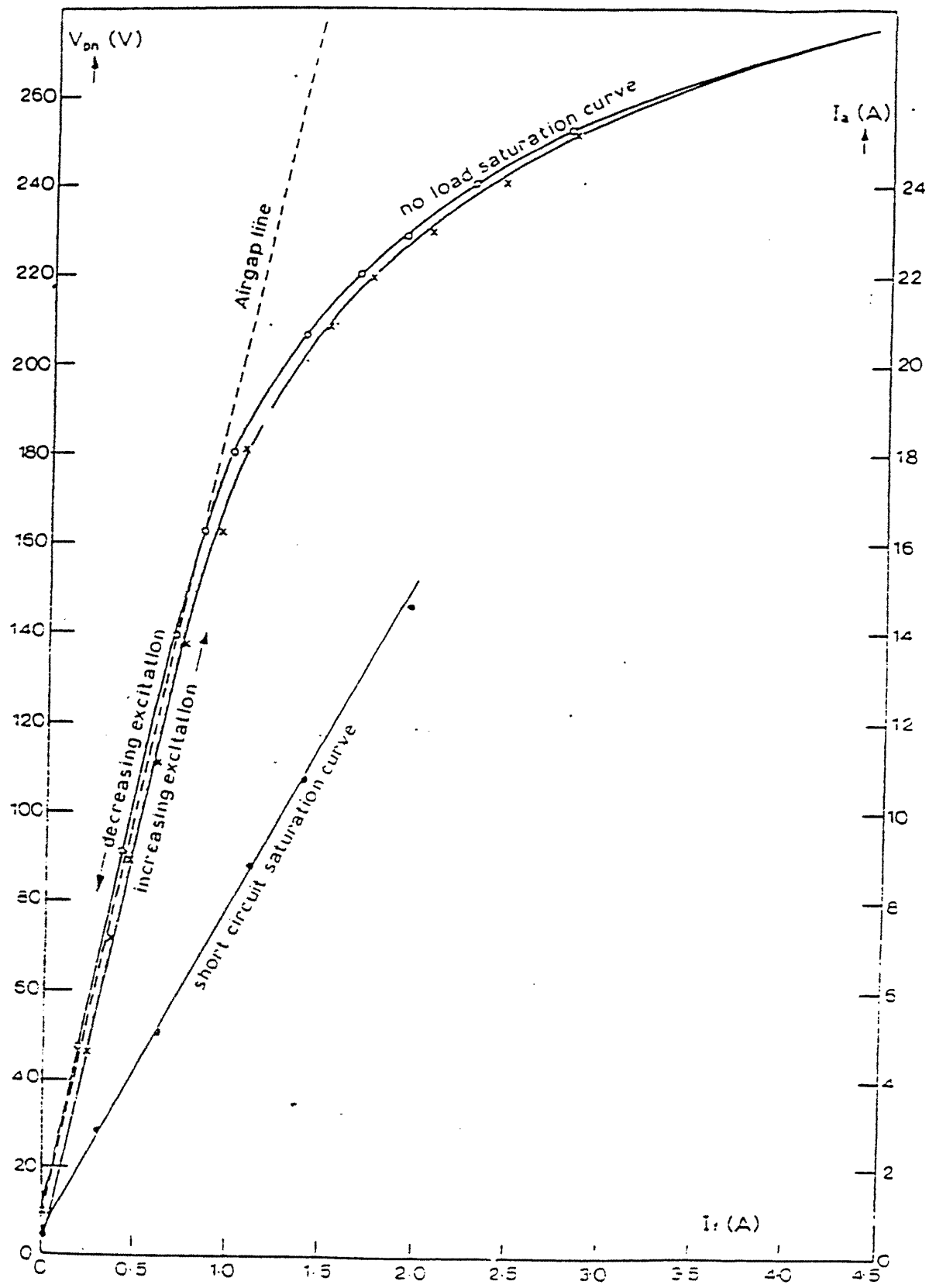

FIGURE 3.11 Open-and short-circuit characteristics of the BKB diesel generator

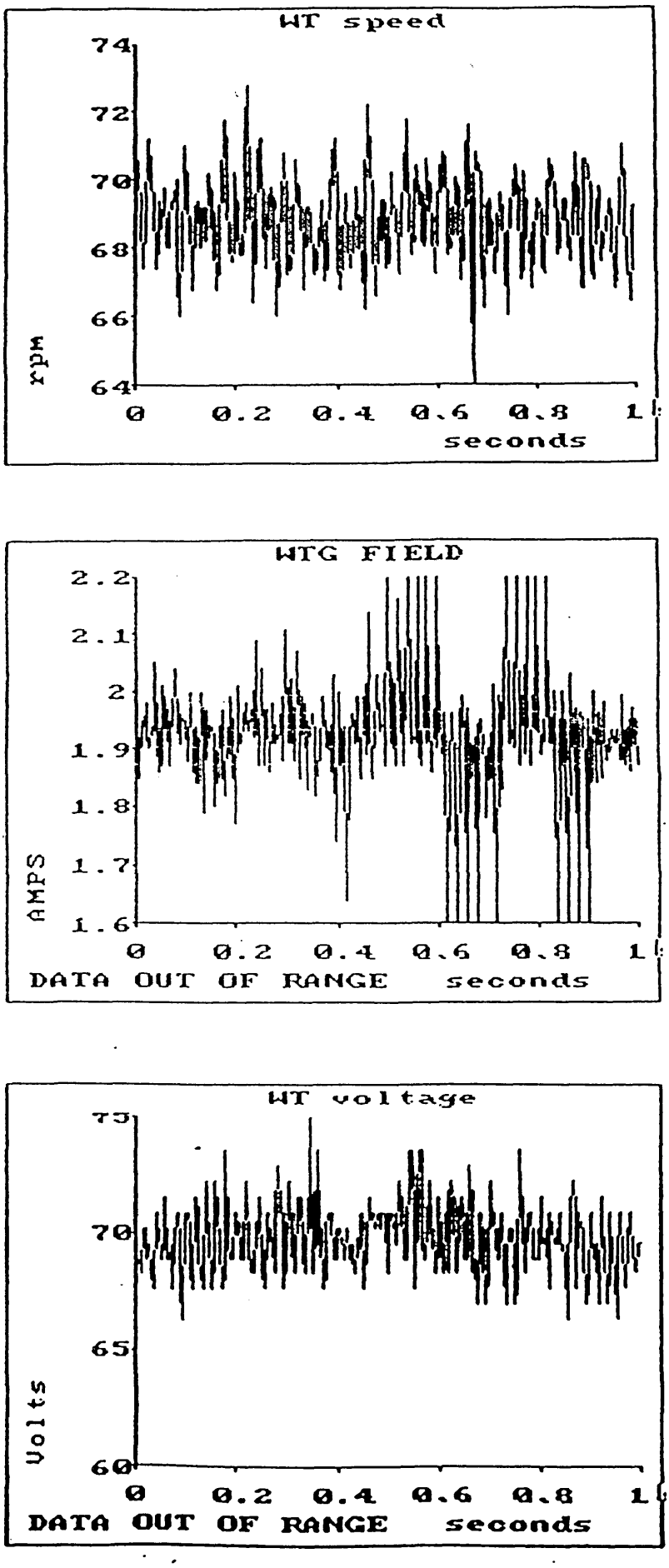

FIGURE 3.12 Actual data recorded during the open circuit test on the Wind Turbine Generator

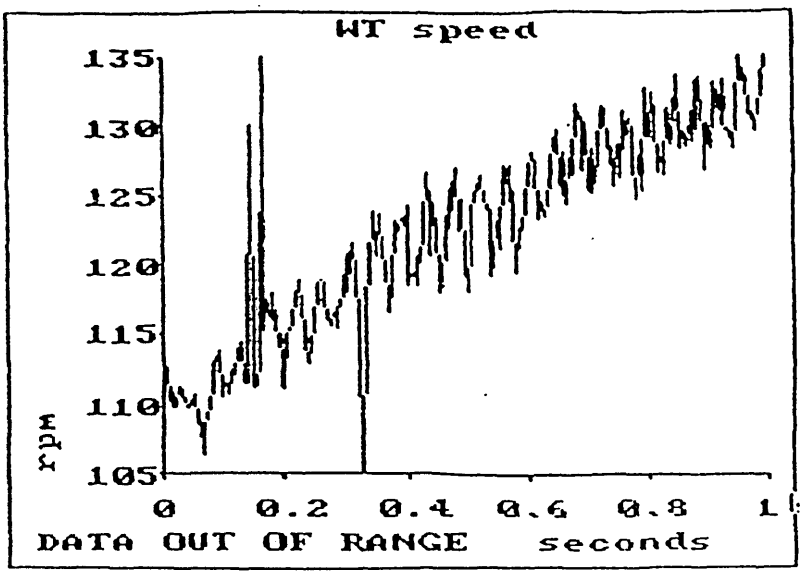

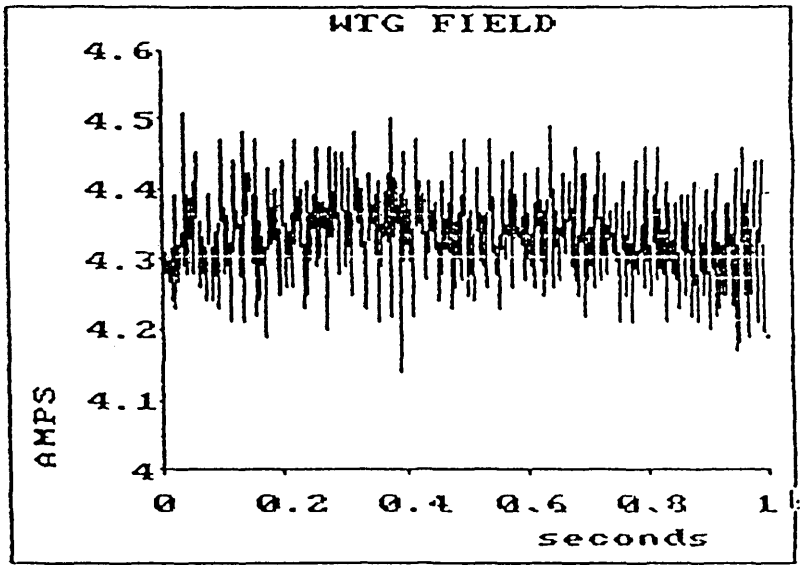

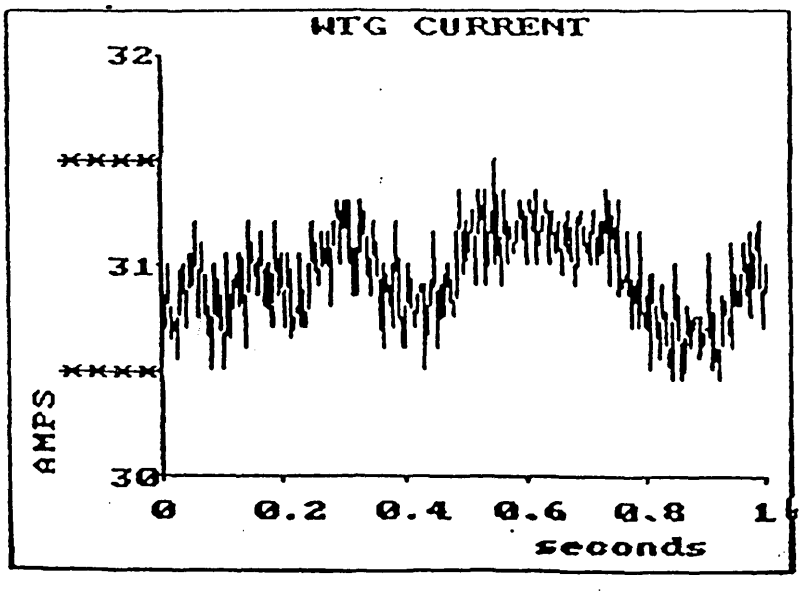

FIGURE 3.13 Actual data recorded during the short circuit test on the Wind Turbine Generator

FIGURE 3.14 Open-and short-circuit characteristics of the Wind Turbine Generator

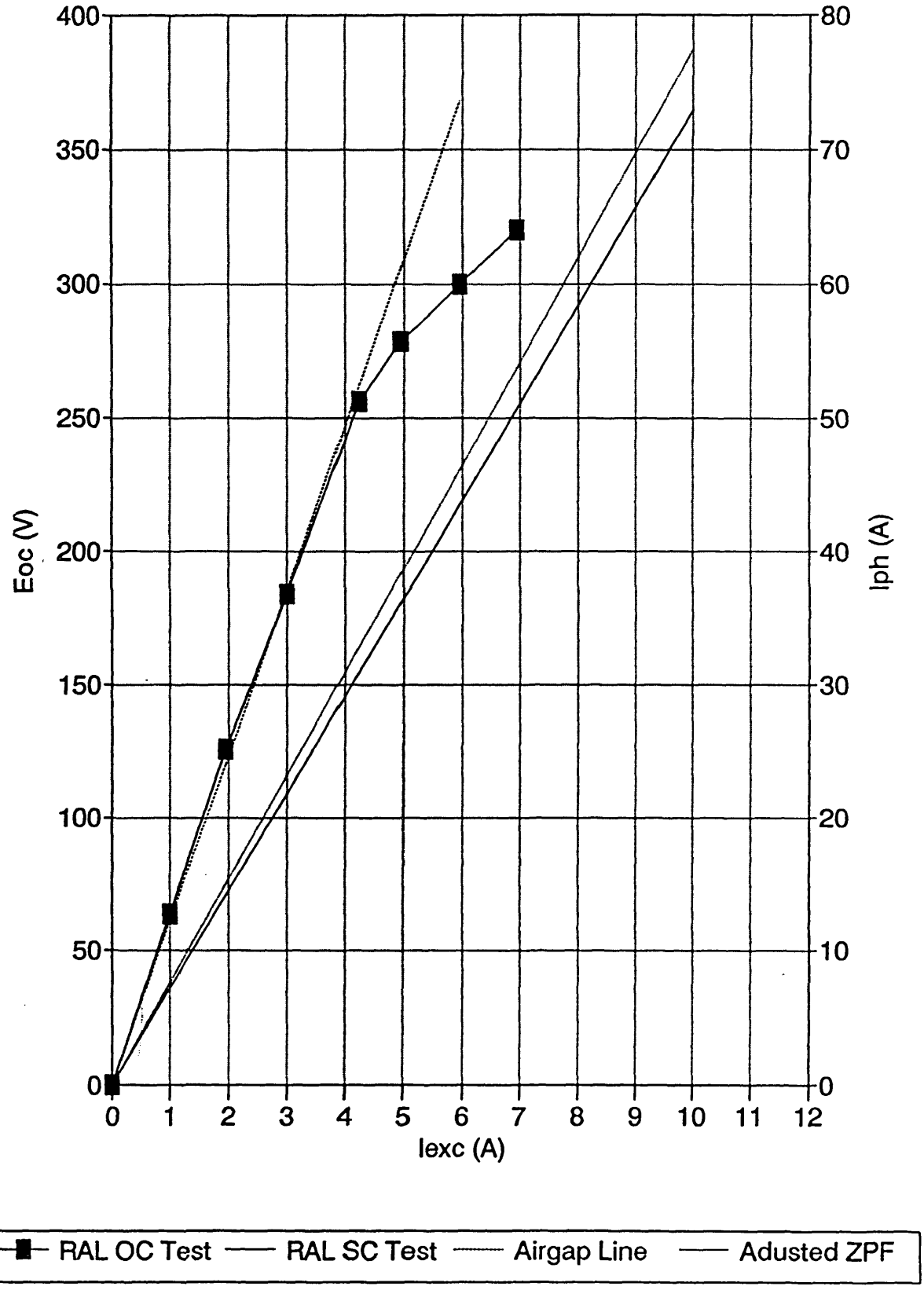

WTG CONNECTED TO GRID

STATIC EXCITER (HOT)

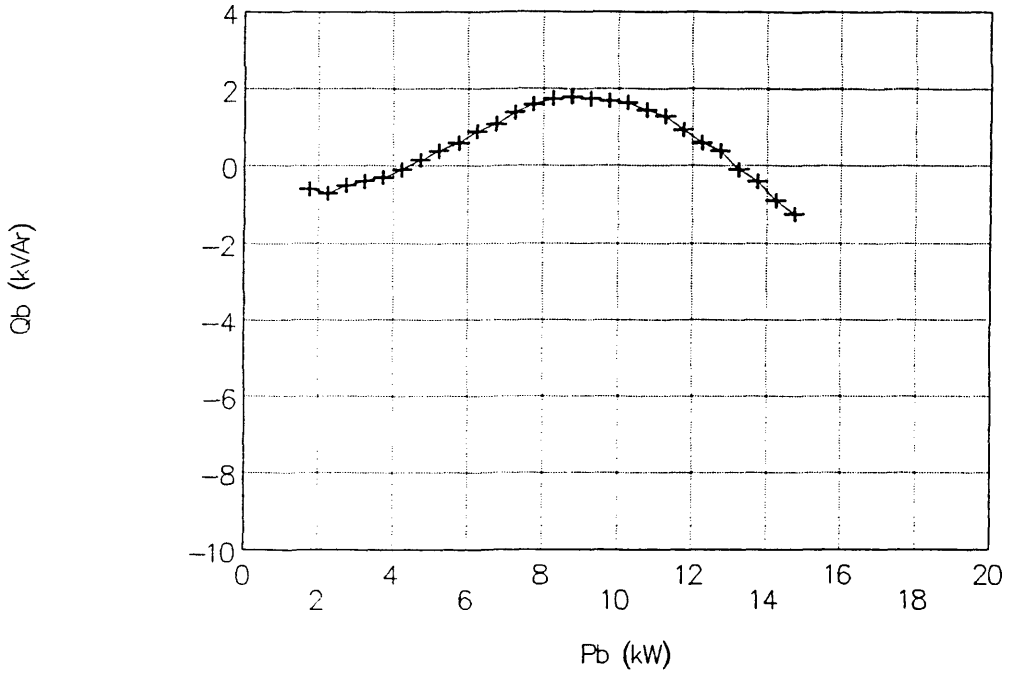

FIGURE 3.15 Simulated results of the steady-state power flow and field currents of the WTG connected to the Grid (exciter current compounding using linear function)

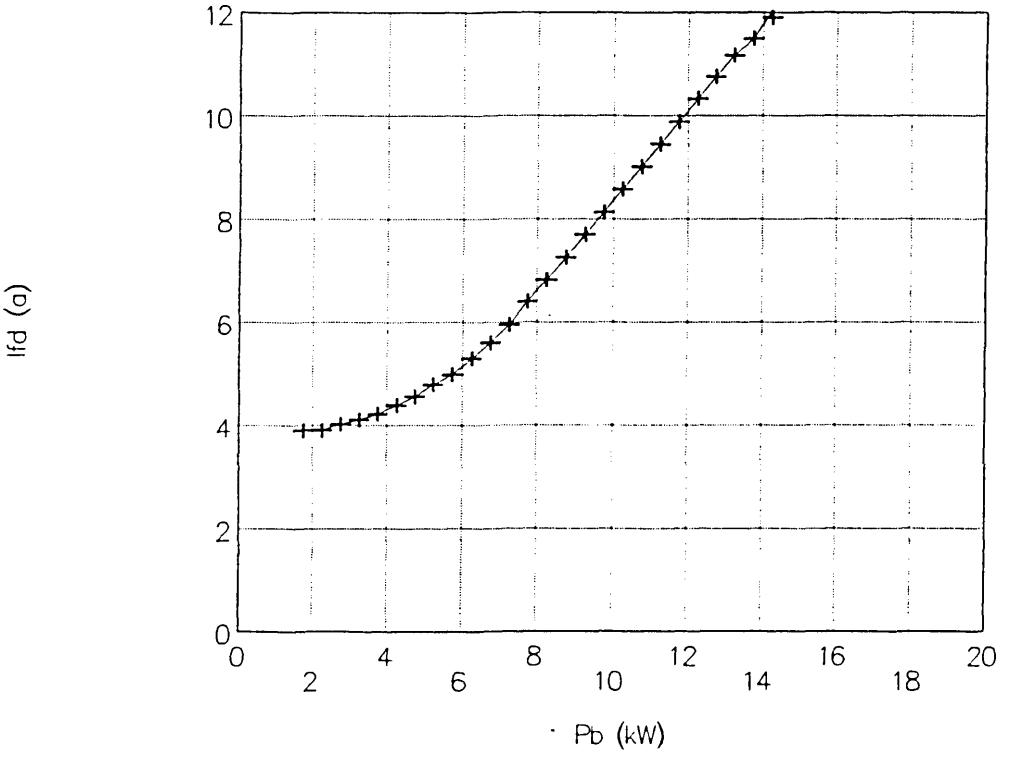

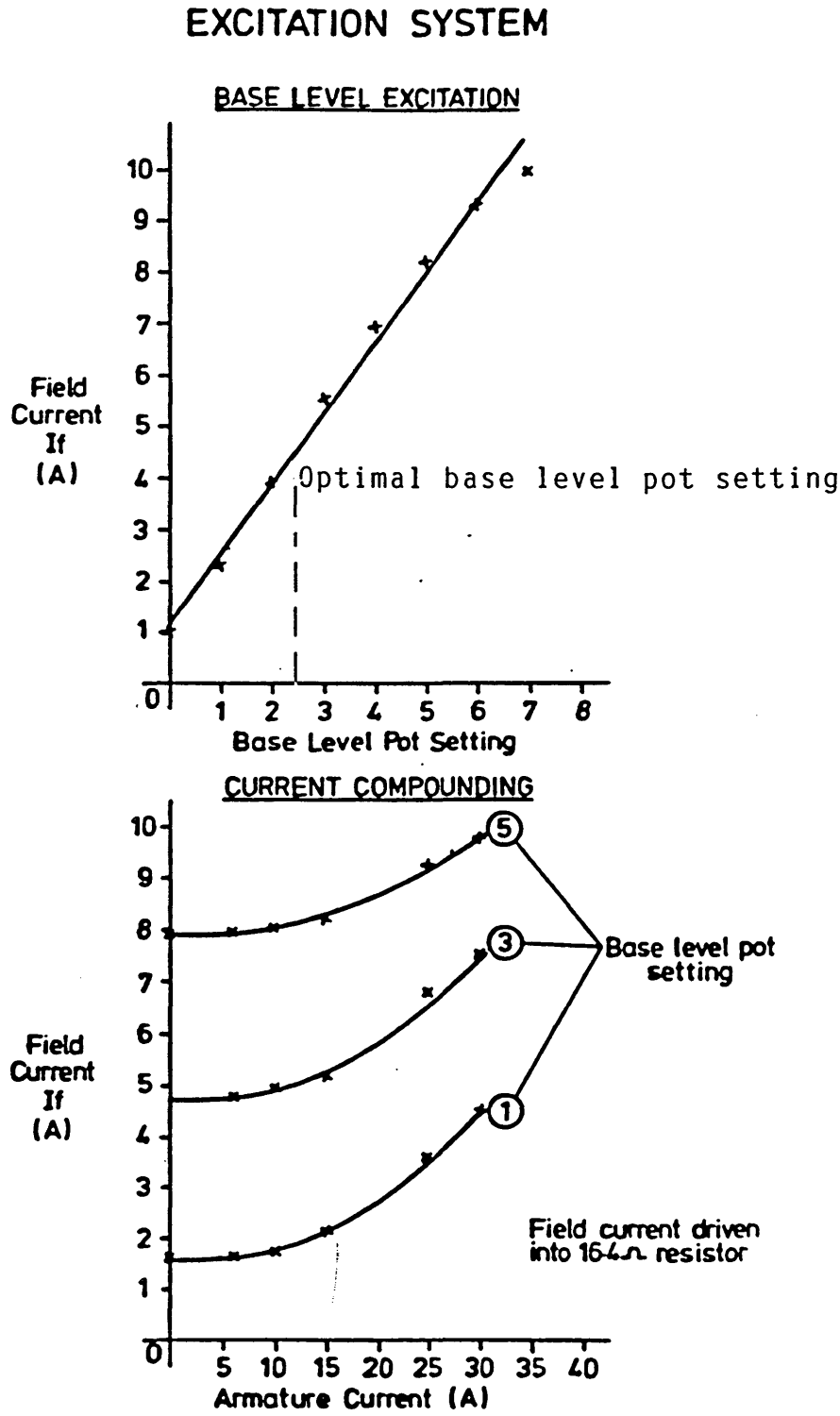

FIGURE 3.16 Experimental results to obtain the relationship of the WTG field current versus load current for the UPF exciter (exciter loaded by a 16 ohm dummy load)

WTG CONNECTED TO GRID

STATIC EXCITER (HOT)

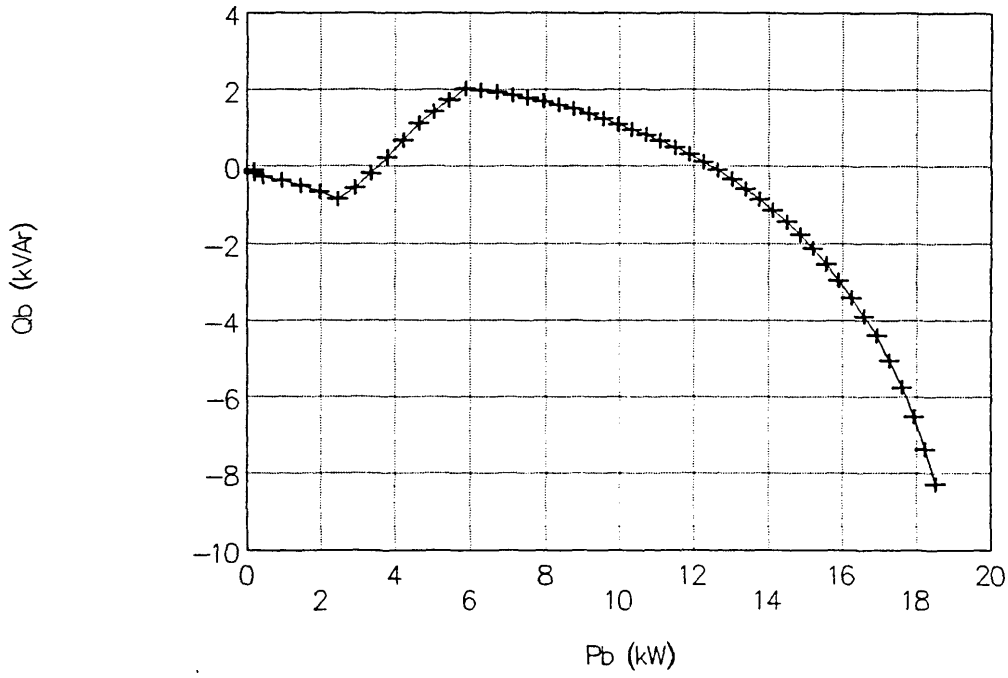

FIGURE 3.17 Simulated results of the steady-state power flow and field currents of the WTG connected to the Grid (exciter current compounding using cosine function)

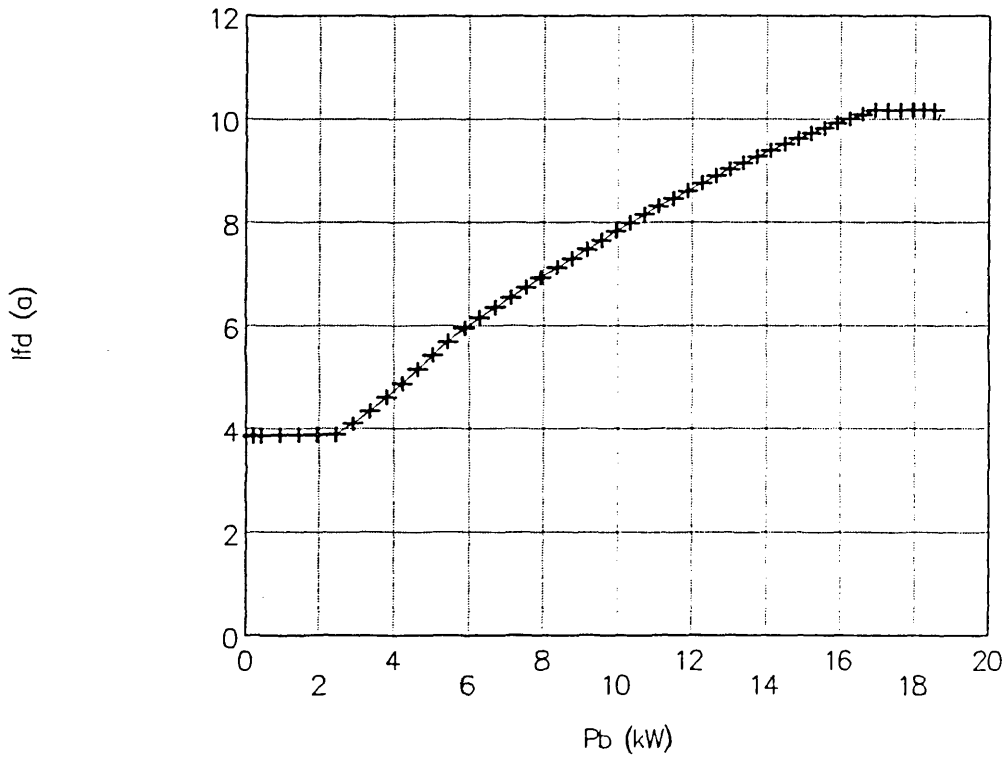

WTG CONNECTED TO GRID

STATIC EXCITER (COLD)

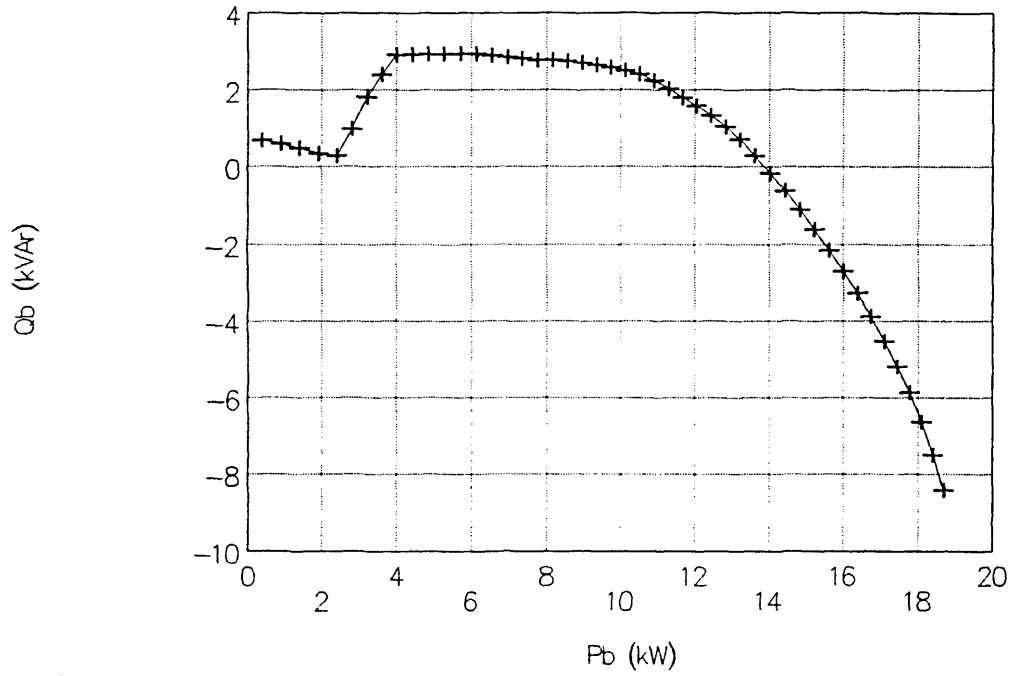

FIGURE 3.18 Simulated results of the steady-state power flow and field currents of the WTG connected to the Grid - "cold" exciter represented by a 10% increase in Gr (exciter current compounding using cosine function)

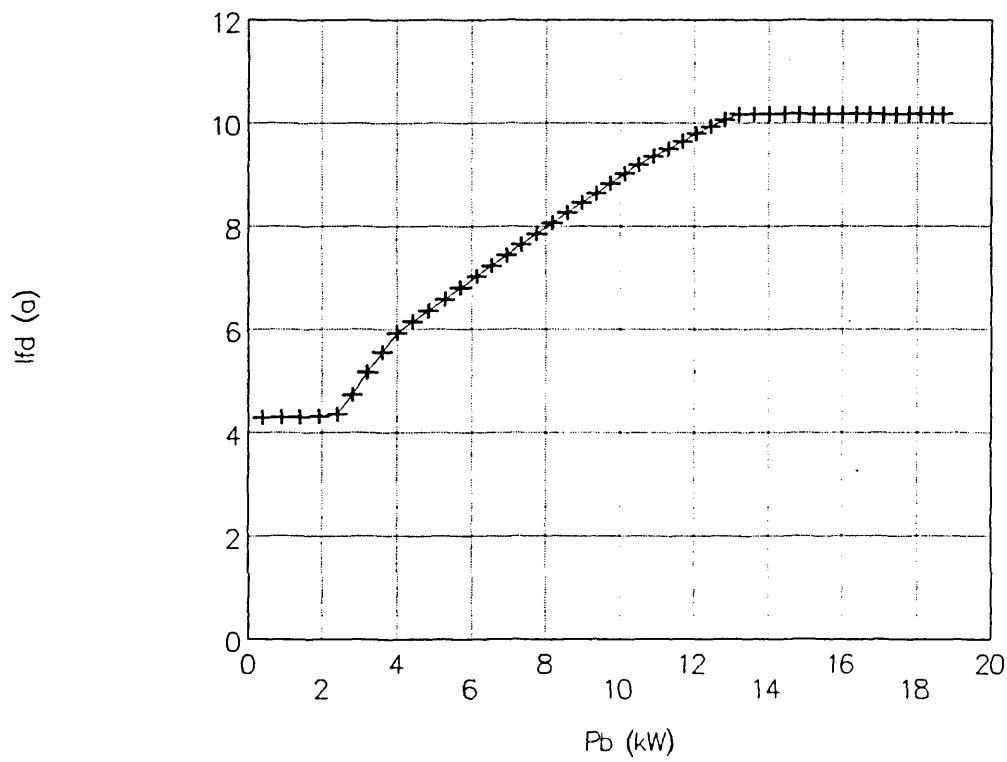

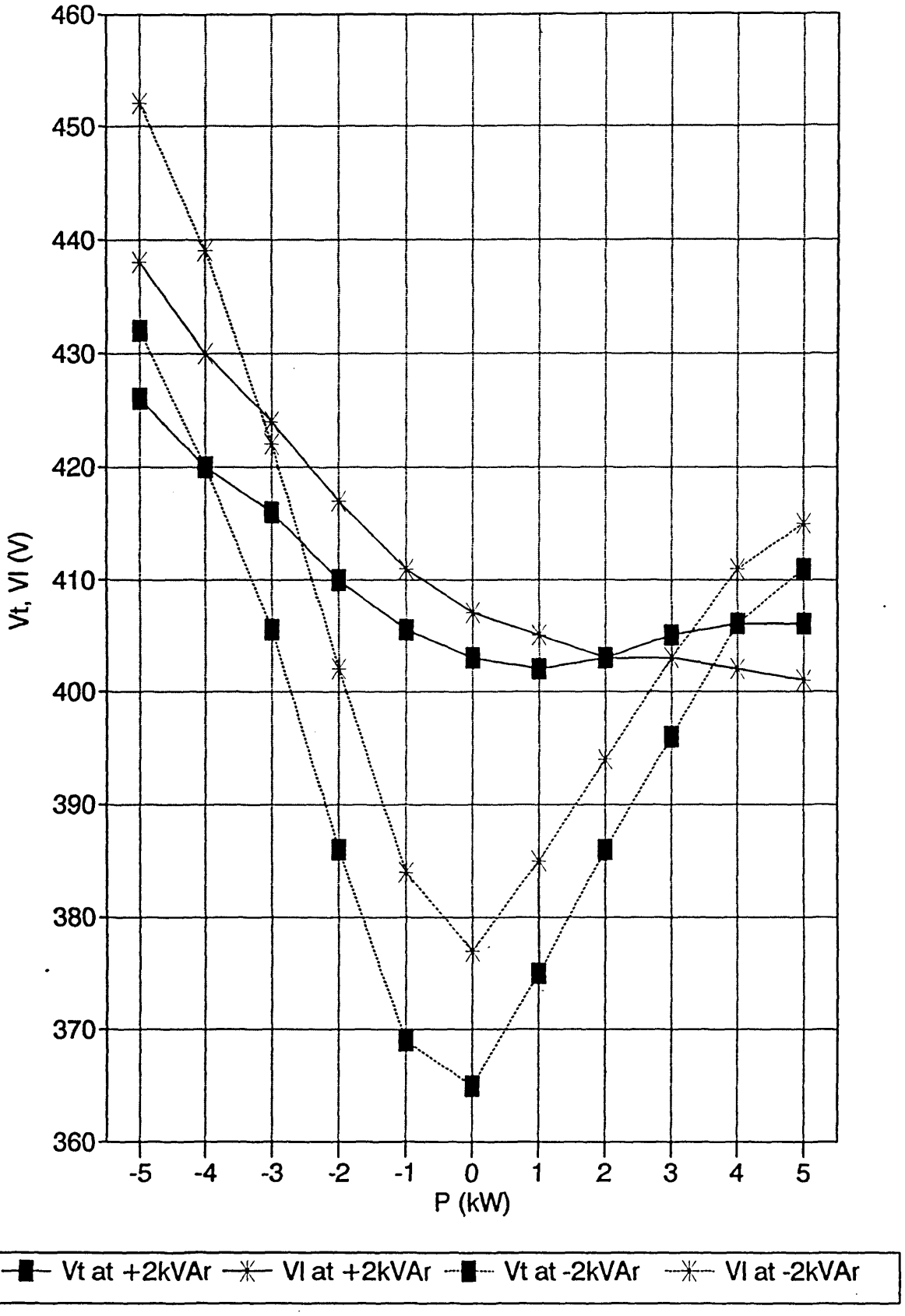

FIGURE 3.19 Voltage regulation of the diesel generator with the static exciter for both its generating and motoring modes

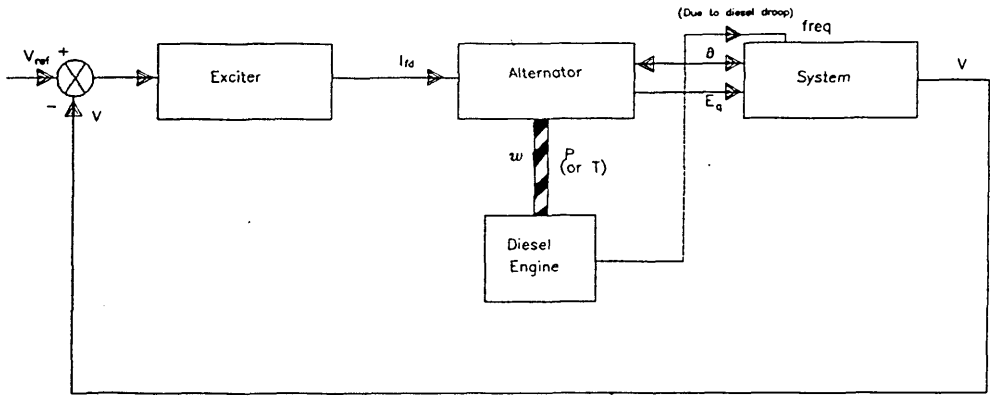

EXCITER	SYSTEM
a) Constant Current	Consumer Load
b) Automatic Voltage Regulator	Subjected to load
Models investigated of the form:	rejection tests
i) Double Lead/Lag	
ii) Lead/Lag	
iii) Lead/double Lag	
. Real Poles	
. Complex Poles	

FIGURE 3.20 Schematic representation of the closed loop test used to investigate the AVR

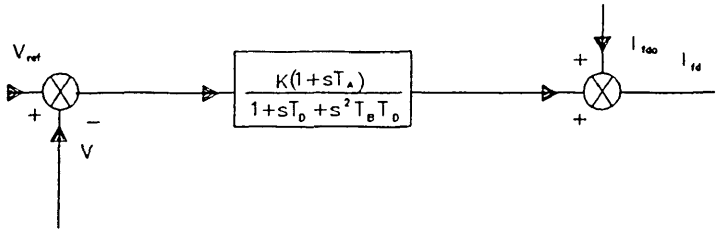

(a) AVR 15E

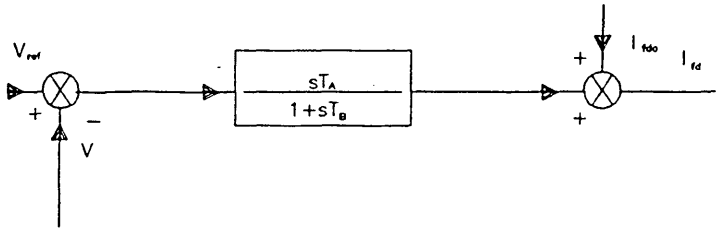

(b) AVR 15R

FIGURE 3.21 Transfer functions of (a) diesel generator AVR (b) WTG AVR used in the computer simulations

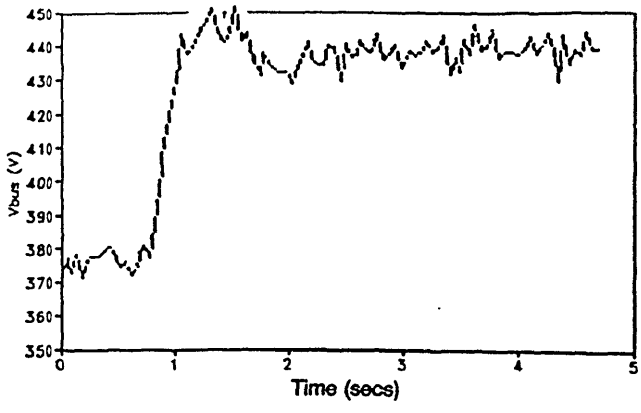

(a) actual

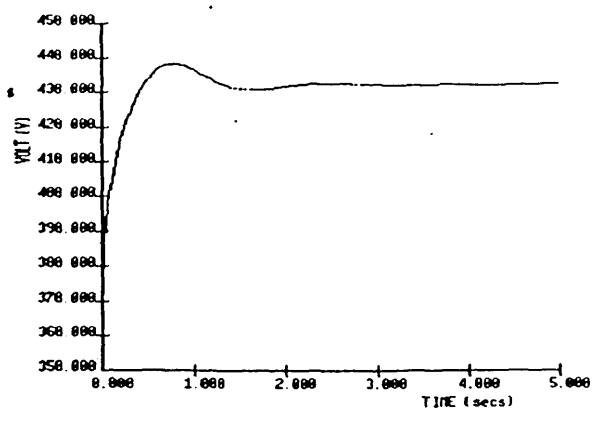

(b) simulated

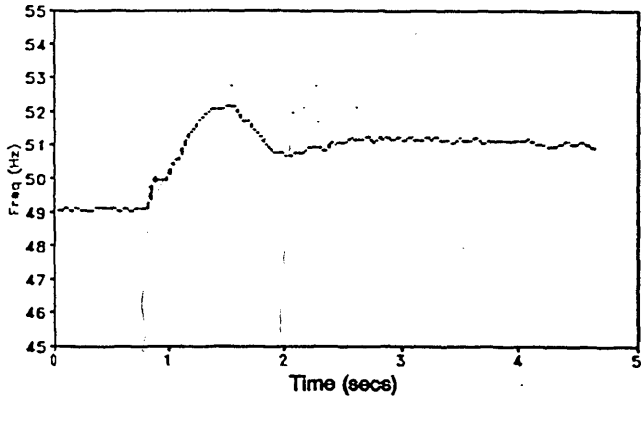

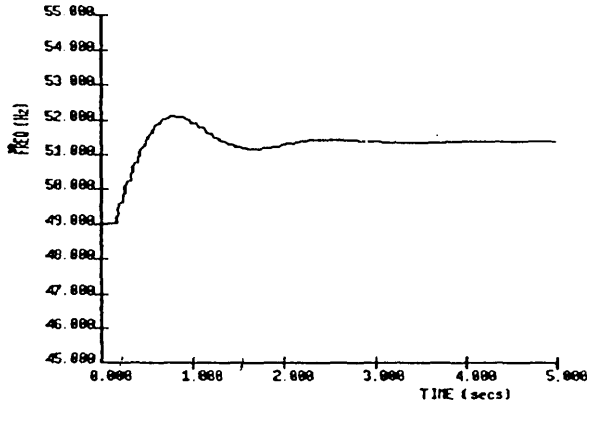

FIGURE 3.22 Step load rejection test of the diesel generator at a fixed excitation of 2.5A

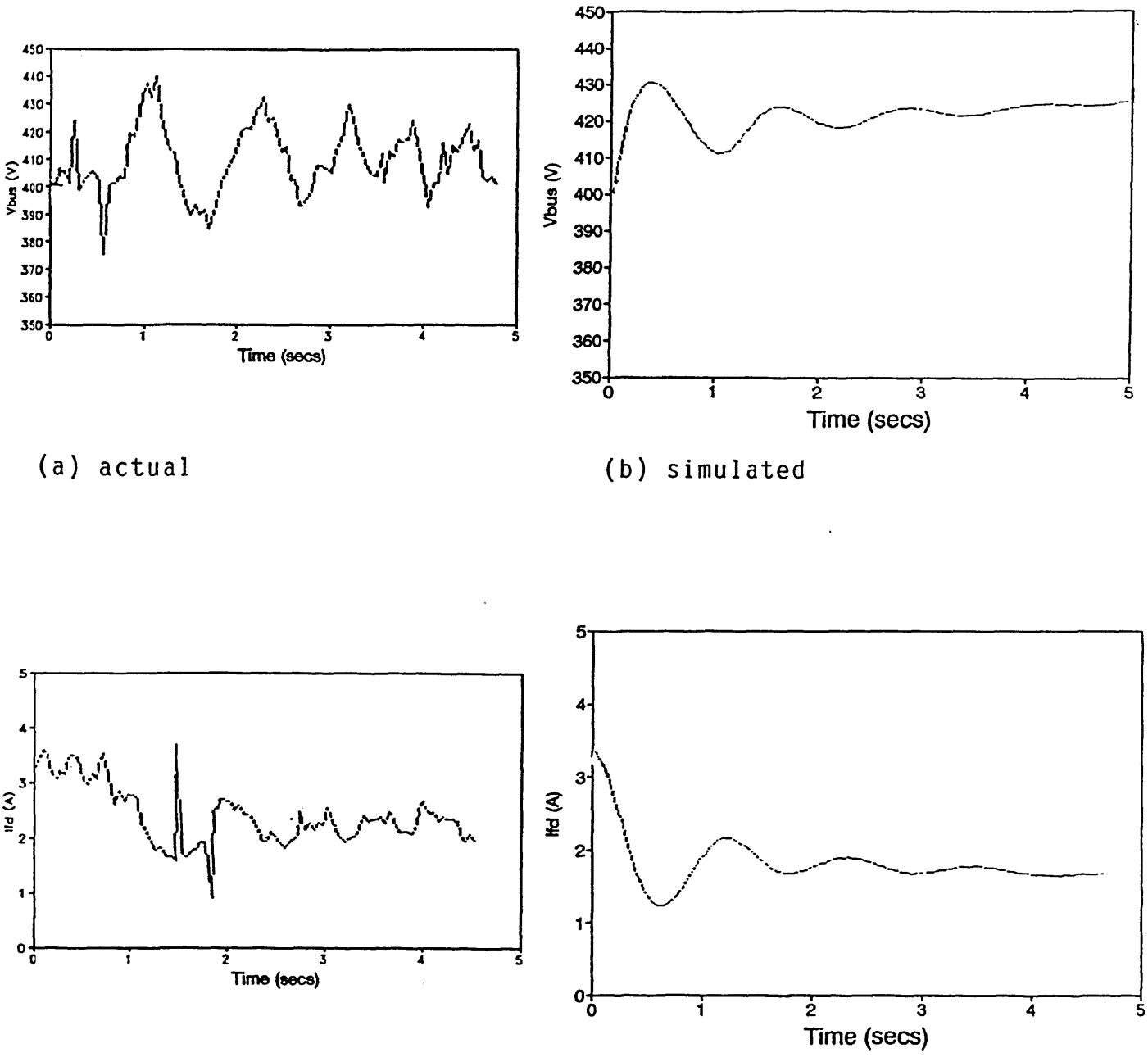

(a) actual

(b) simulated

FIGURE 3.23 Step load rejection test of the diesel generator plus AVR 15E at its least stable setting

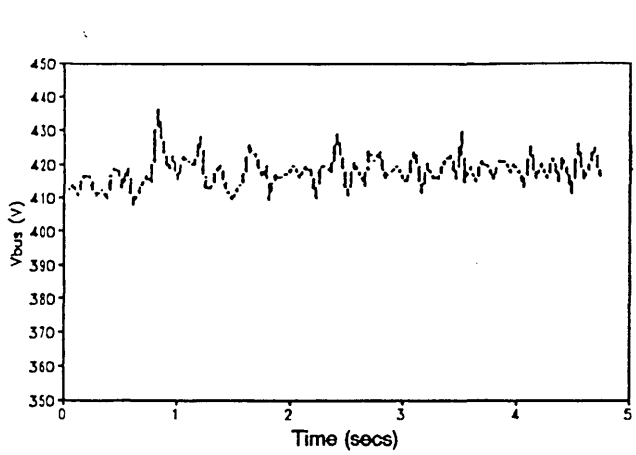

(a) actual

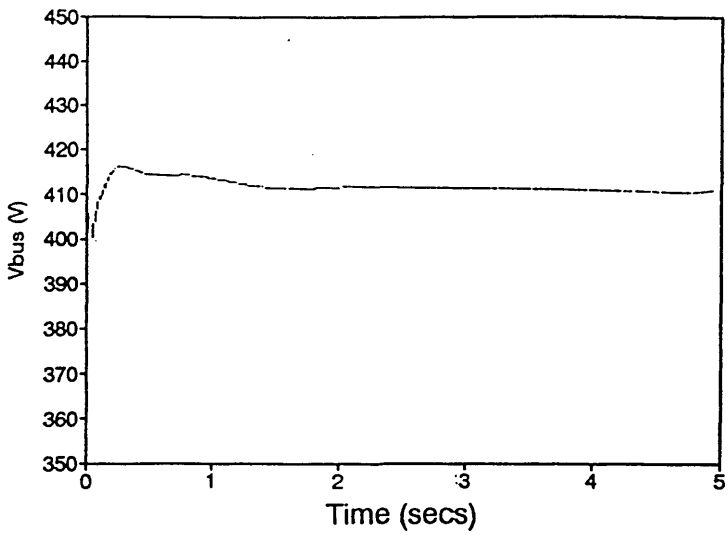

(b) simulated

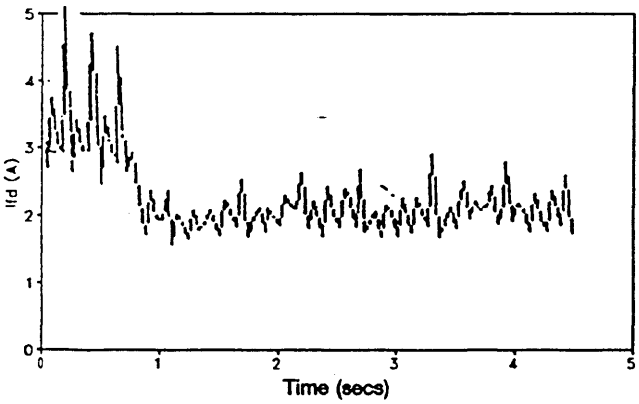

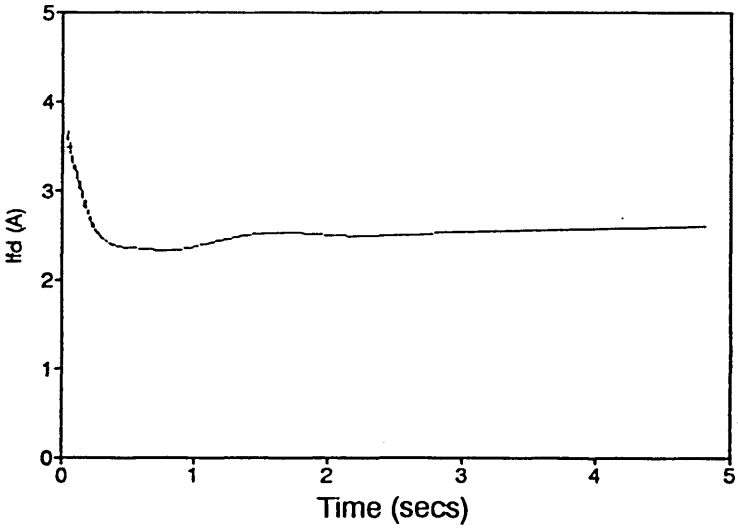

FIGURE 3.24 Step load rejection test of the diesel generator plus AVR 15E at its most stable setting

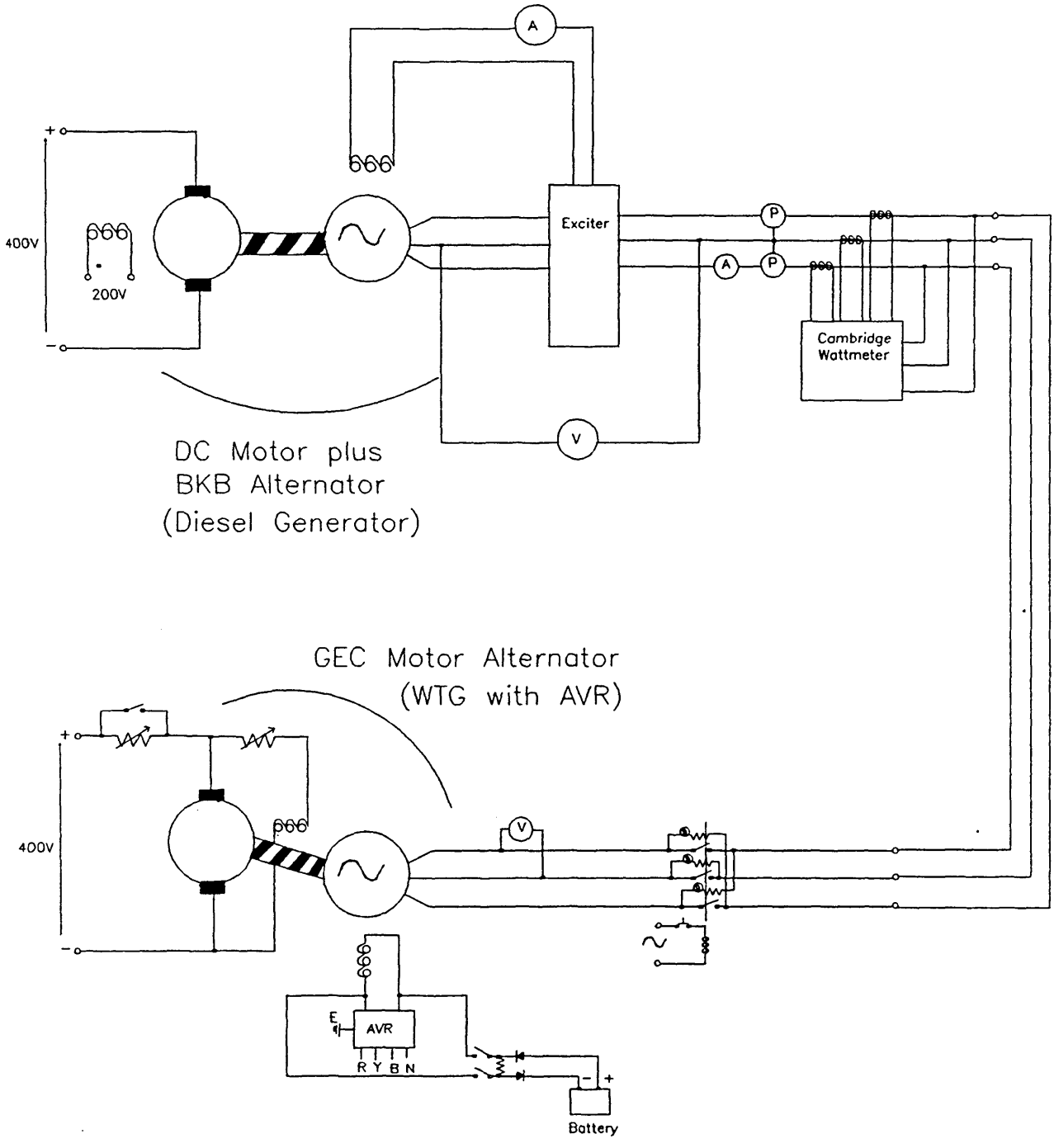

FIGURE 3.25 Laboratory test arrangement of the parallel operation of the Wind Turbine and Diesel Generators - prime-movers replaced by dc machines

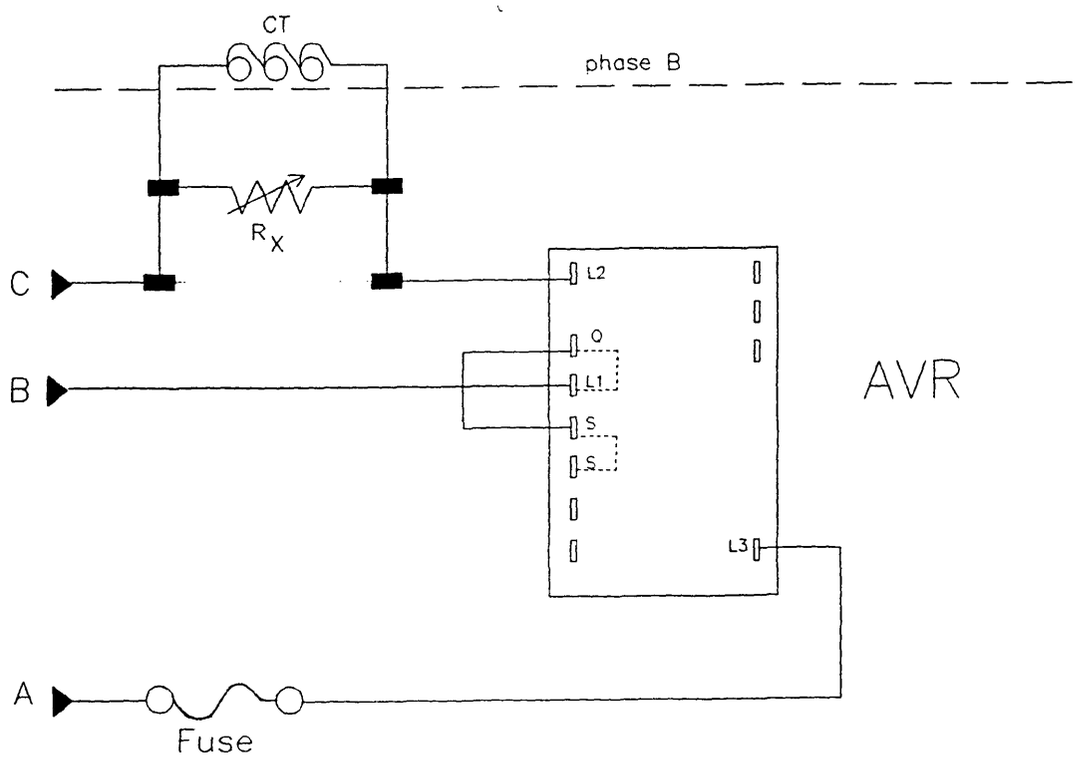

(a)

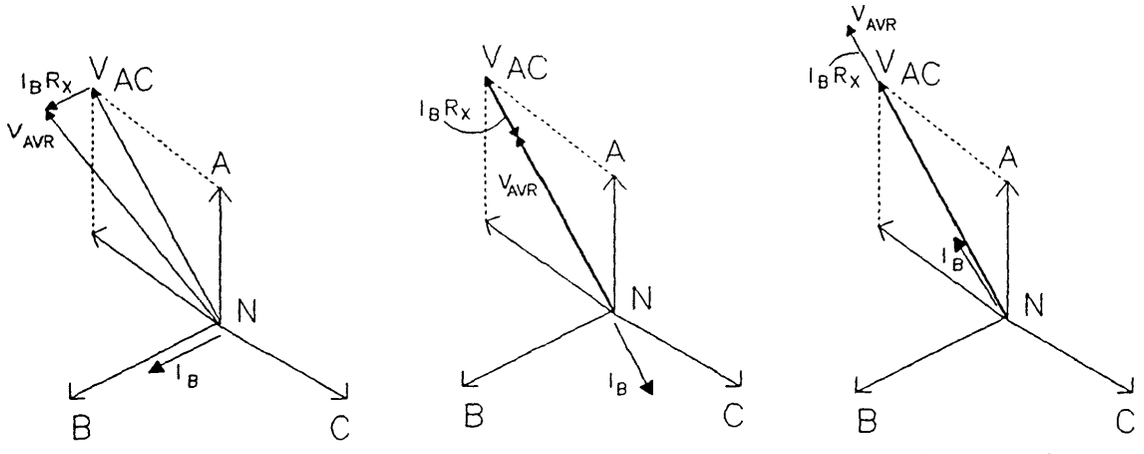

(b)

FIGURE 3.26 (a) External circuitry and
(b) Phasor representation of "quadrature droop compensation" used with the AVR

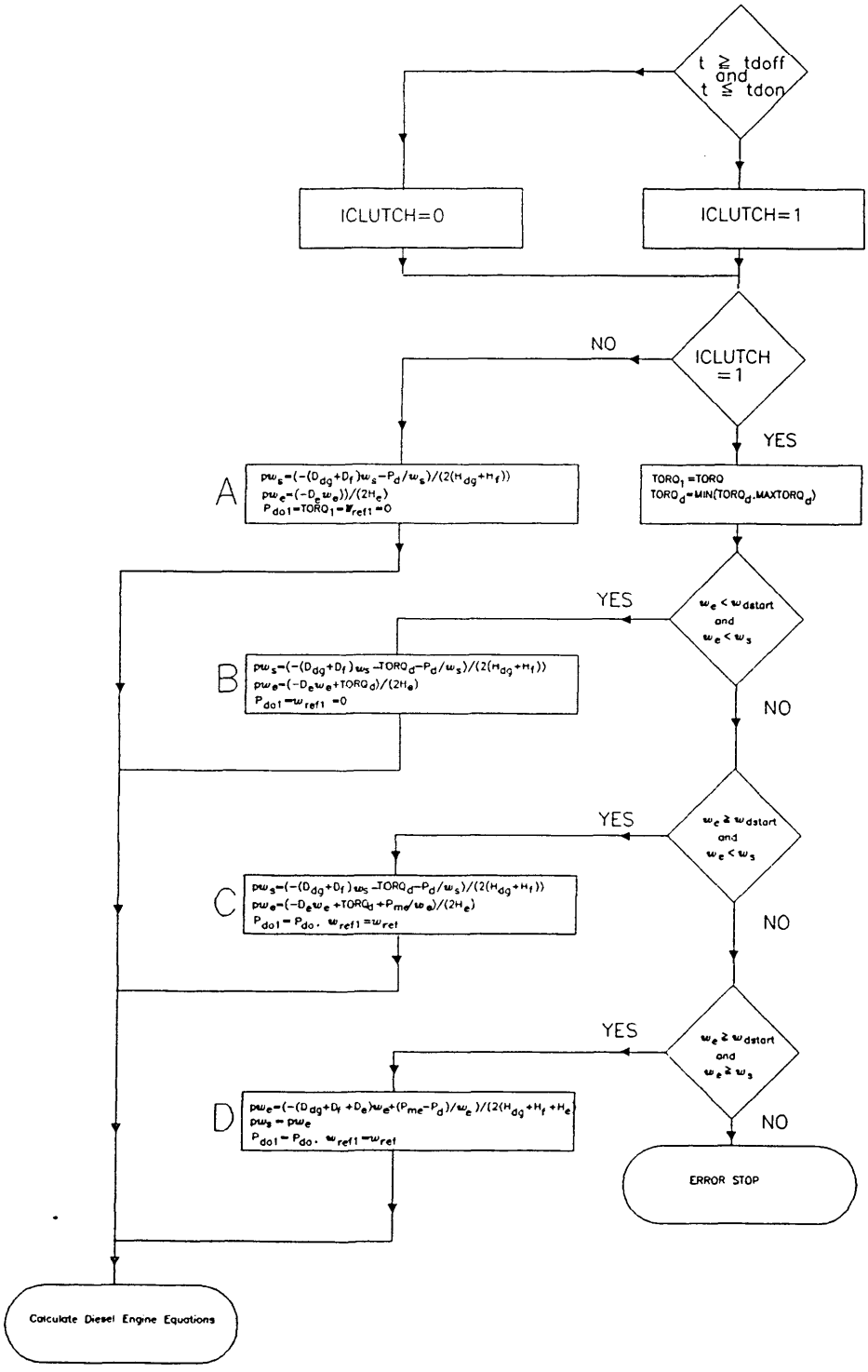

KEY

A – Clutch open

B – Clutch closed diesel not firing

C – Clutch closed diesel firing (clutch slip)

D – Clutch closed diesel firing (clutch locked)

FIGURE 3.27 Flow chart of the clutch and diesel engine status during re-engagement

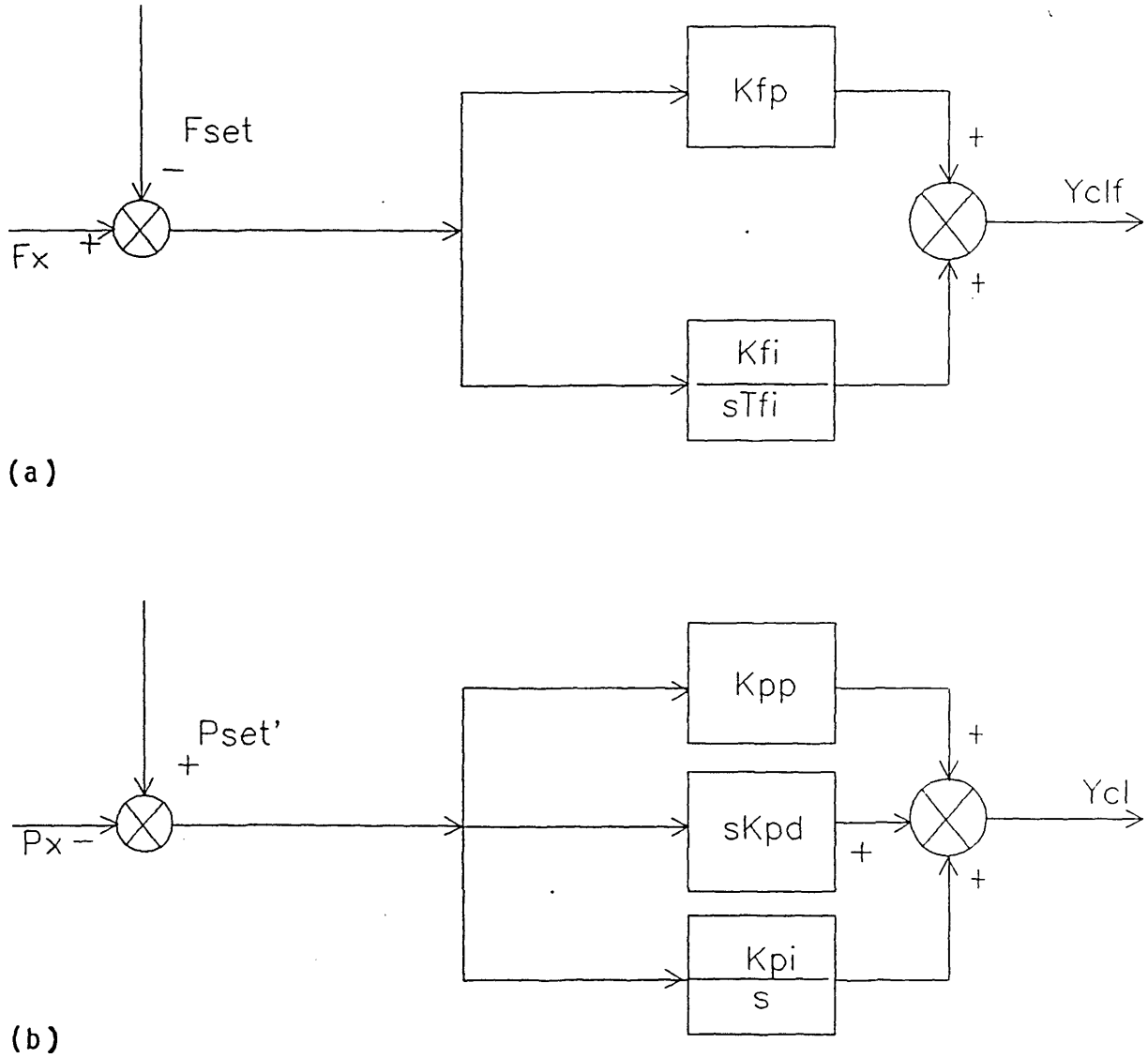

FIGURE 3.28 Block diagram of (a) Phase I frequency based dump load controller
(b) Phase II power/frequency based dump load controller

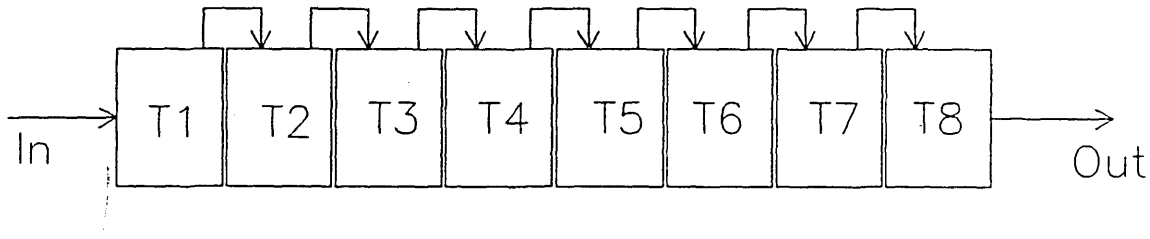

FIGURE 3.29 FIFO representation of dead time in the dump load a/d convertor

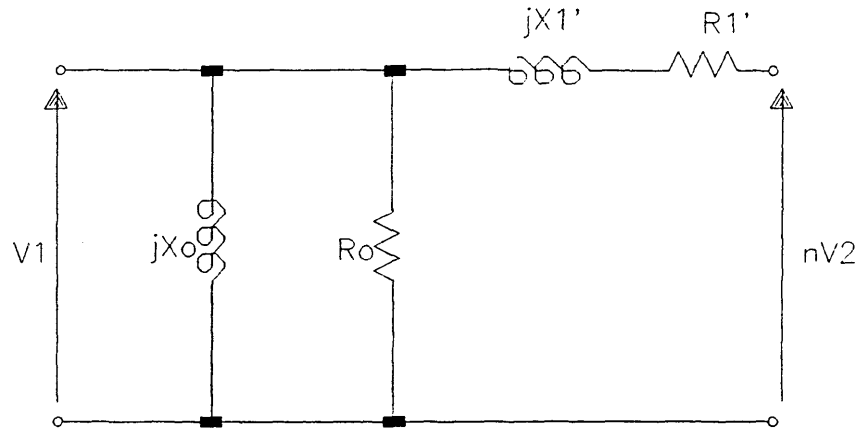

FIGURE 3.30 Schematic representation of the WTG Stepup Transformer

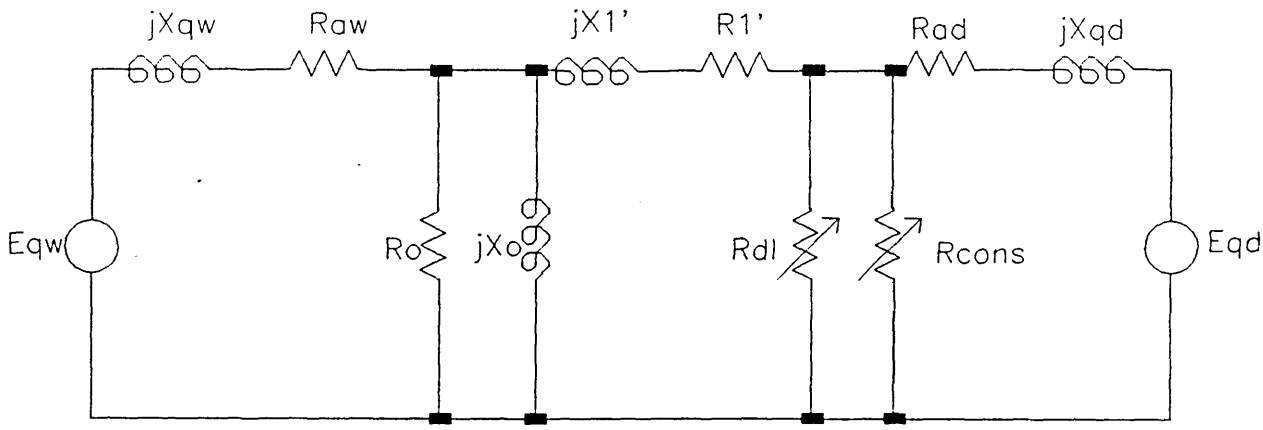

FIGURE 3.31 Network topology used in both the normal and pseudo steady-state segments of the wind/diesel/flywheel dynamic simulation program

CHAPTER 4

COMPUTER TOOLS

4.0 Introduction

This chapter examines the typical structure of the program used in the modelling of the wind/diesel/flywheel system and the various sub-programs. The method of loadflow solution and the two numerical methods used in the study will be discussed.

Besides the time stepping methods, which were the main form of investigative tool, linearisation techniques were also used to provide information with regards to the stability of the system and to the root cause of any instabilities. The final sections of this chapter will therefore be devoted to the development of such techniques.

4.1 The Suite of Programs

Due to the number of modes of operation that the wind/diesel/flywheel system could be configured to and due to project time-constraints, it was decided to develop several simulation programs instead of just one all-purpose program. Fig 4.1 illustrates the six steady-state and dynamic programs. The programs are written in FORTRAN 77 and can be run on the Electrical Power System's Group (EPSG) DEC Microvax minicomputer or can be configured to run on an IBM

PC or compatible (preferably with a maths co-processor). The programs are as follows:

1. INFBUSS

A steady-state program used to analyse the effect of the wind turbine generator connected to an infinite busbar. The program was used to; estimate the electrical output power of the wind turbine generator across the full range of wind speeds, characterise the wind turbine generator's unity power factor exciter.

2. INFSYN

A dynamic program that simulates the synchronisation of the wind turbine generator onto an infinite busbar. The speed of the wind turbine and its load angle with respect to the bus are controlled so as to examine their effect upon the synchronisation transient.

3. WTDL

A dynamic simulation of a system consisting of the wind turbine generator, consumer load and controllable dumpload. It has been used to study the autonomous operation of the wind turbine generator and has aided in the characterisation of the wind turbine generator model and dumpload controller.

4. DGTRY

A dynamic simulation of the system consisting of the diesel generator set, consumer load and controllable dumpload. It

has been used to study the autonomous operation of the diesel generator set and has been used to investigate suitable diesel engine models, the saturation and exciter models of the alternator and has aided in the characterisation of the dumpload controller.

5. **PARDYN**

A dynamic simulation of the full wind/continuous diesel system of Phase I of the project. It has been used to study component interaction and system instabilies. It has also been used as a simple version of the wind/diesel/flywheel system of Phase II by lumping the flywheel's inertia and losses onto that of the diesel alternator.

6. **WDF**

A modified version of PARDYN used to simulate the effect of the diesel engine's disengagement/re-engagement to the wind/diesel/flywheel system of Phase II.

Both WDF and PARDYN were used to investigate the effects of power/frequency as opposed to frequency control of the dumpload.

4.2 General Structure of the Programs

It would not be appropriate to include a full description of each of the six programs in this thesis. However, an overview of program PARDYN will be given as this encapsulates the

majority of the modelling techniques used in the study. Appendix 4.A contains a flowchart of the program structure used in the dynamic simulation of the wind/diesel system (PARDYN).

4.2.1 Solution of the Steady-State Conditions

Initially, the system parameters are inputted in SI form. They are then converted to the per-unit base of the diesel generator set (ie 415V, 8.5kVA and 50Hz). The steady-state solution relies upon the linear torque/speed relationship of the diesel governor to adjust the system frequency. The steady-state machine equations of the wind turbine generator (STWGEN) are solved for the given wind turbine mechanical power, consumer load and dumpload. This routine provides new estimates for the diesel generator electrical loading which is then used to calculate the dumpload power and network conditions (PARAST). The diesel generator machine equations (SYNGDSS) are then used to calculate new estimates of the busbar voltage whilst the system frequency is recalculated from the diesel engine's mechanical torque. The process is then repeated by the program returning to the routine used to calculate the wind turbine generator machine eqautions. Continuous checks are made on the tolerances of the new and old; currents, voltages and frequency. When all tolerances are met the program passes to the dynamic solution.

4.2.2 Initialisation of the State Variables

Before the time-stepping process can begin, the state variables must be initialised (INPAR). This is achieved by the rearrangement of the state variable equations so as to solve for each state variable with the derivative terms set to zero.

4.2.3 Dynamic Solution

The method of solution revolves upon the ability of the program to take "snapshots" of the system conditions at a given time interval. The program therefore requires not only the equations to adequately represent the mecahnical and electrical dynamics of the machines, but also, equations to solve the pseudo steady-state conditions of the machines and network. The machine equations are solved in terms of local reference frames which are then referred to a common reference frame (in this system the speed of the diesel alternator) in order that the network equations maybe solved. At each snapshot, the steady-state equations are solved using similar routines to the wind turbine and diesel generator routines of Section 4.2.1. Upon successful convergence of the machines' voltages and currents, the derivatives of the state variables are solved and then passed to the numerical integration routine. The time-step is then incremented.

4.3 Numerical Methods

The electrical and mechanical dynamic equations can be represented in state variable form as:

$$pX_i = fn(X_i) \qquad (4.1)$$

where,

X_i- state variable matrix

$fn(X_i)$- state matrix containing system non-linearities

$fn(X_i)$ is a matrix that is indirectly a function of the unknown, pX. Therefore, equation 4.1 is a set of non-linear equations that can only be solved numerically.

Any numerical integration method is only approximate, because the curve is approximated by a series of short straight lines and the accuracy obviously depends on the number of discrete steps - the steplength, Δt. It is therefore advantageous to use a steplength that is just large enough to give the necessary accuracy, but at the same time minimises computer time. If the system is represented by a stiff set of equations, ie the range of time constants is wide, the simulation will be highly sensitive to errors. Errors can be propogated from step to step (roundoff) and can depend on the choice of steplength or on the integration method used.

4.3.1 Gear's Method

Due to the wide range of time constants, 2msec to 2sec (ie a range of 10^3) inherent in the wind/diesel/flywheel system, Gear's method of numerical integration [4.1] was initially used. This is a variable order (adjusted to meet the error tolerance) variable steplength method that is ideally suited to the numerical integration of stiff systems. A Gear routine from the Numerical Algorithms (NAG) Library [4.2] was therefore included in the simulation.

However, the Gear method was eventually replaced by a fourth order Runge Kutta algorithm due to:

i) The desire to create transportable code.
ii) Difficulties in controlling the flow of information through the deadtime devices (eg frequency transducer, dumpload a/d converter) due to the variable timestep hunting both forwards and backwards in time around a solution point.

4.3.2 Runge Kutta

The Fourth Order Runge Kutta method is one in which four evaluations of the slope are made within the duration of the timestep, and from these a mean weighted slope is computed.

The algorithm stems from the truncated infinite series expansion of X over the interval Δt.

$$\underline{X}_{n+1} = \underline{X}_n + \frac{\underline{K}_0}{6} + \frac{\underline{K}_1}{3} + \frac{\underline{K}_2}{3} + \frac{\underline{K}_3}{6} \qquad (4.2)$$

where,

$$\underline{K}_0 = \Delta t.fn(t_n, \underline{X}_n, \underline{Y}_n)$$

$$\underline{K}_1 = \Delta t.fn(t + \frac{\Delta t}{2}, \underline{X}_n + \frac{\underline{K}_0}{2}, \underline{Y}_n\ (t + \frac{\Delta t}{2}))$$

$$\underline{K}_2 = \Delta t.fn(t + \frac{\Delta t}{2}, \underline{X}_n + \frac{\underline{K}_1}{2}, \underline{Y}_n\ (t + \frac{\Delta t}{2}))$$

$$\underline{K}_3 = \Delta t.fn(t + \Delta t, \underline{X}_n + \underline{K}_2, \underline{Y}_n\ (t + \Delta t))$$

Before the Runge Kutta algorithm was used on the full wind/diesel/flywheel model a comparative study was carried out with Gear's method using program DGTRY. A 1msec timestep in the Runge Kutta method produced sufficiently similar diesel generator step response characteristics to that of Gear's method as to justify its use.

4.4 Linearised Models

Thusfar, non-linear system models have been developed, however, considerable insight can be gained by examining their small signal behaviour. Several techniques are available to develop such models:

4.4.1 Simple Mass/Spring/Damper Model

Bleijs [4.3] has adopted an approach that uses a simple mass/spring/damper analogy to examine the natural oscillations and their associated mode shapes in the system.

This simple method produces results very quickly and results in equations that can be solved with a calculator. However, the method solely represents each electrical machine in terms of a single equivalent electrical stiffness with no account being taken of its controllability.

4.4.2 Linearisation of the System Eqations

The small signal behavior of the system can be developed from the linearisation of the system equations about an operating point. The resulting set of linear differential equations describes the dynamic behaviour of small disturbances about this operating point.

Anderson and Fouad [4.4], Yu [4.5] develop the linearised equations of a synchronous machine connected to an infinite busbar. Each machine variable, X_{io}, is displaced dX_i about the fixed operating point resulting in:

$$X_i = X_{io} + dX_i \qquad (4.3)$$

This new value ($X_{io} + dX_i$) replaces X_i in the machine equations. All multiplications are then performed, the steady-state expressions are cancelled from both sides of the equations and all products of the small displacements, ie ($dX_1.dX_2$), are neglected. The resulting equations are the small signal linearised equations. Fig 4.2 is the schematic representation of the linearised equations of the wind turbine generator (including drivetrain) connected to an

infinite busbar. Although this method was initially used in the study of the stability of the wind turbine connected to the grid (refer to Chapter 5), the method is limited:

i) Some means has to be found to estimate the state of the variables at each operating point.

ii) The wind/diesel/flywheel system operates in a number of configurations which would mean the development of a set of linearised equations for each condition.

4.4.3 Small Perturbation Method

A more direct approach involves the use of numerical perturbation techniques upon the actual ICSTM dynamic models. Consider equation 4.1:

$$pX_i = fn(X_i) \qquad (4.1)$$

To linearise $fn(X_i)$, expand it about a nominal operating point, X_{io}, using a Taylor series expansion:

$$fn(X_i) = fn(X_{io} + dX_i) = fn(X_{io}) + J.dX_i + (\text{higher terms}) \qquad (4.4)$$

where,

J- Jacobian matrix of the partial derivatives

Ignoring the higher terms, the remaining equation can be applied to the actual machine equations as an alternative

means of forming the linearised equations, or, can be manipulated to produce a computational method of forming the Jacobian matrix:

$$J = (fn(X_i) - fn(X_{io}))/dX_i \qquad (4.5)$$

From eqn 4.1, $fn(X_i) = pX_i$, likewise, $fn(X_{io}) = pX_{io}$

$$J = (fn(X_i) - fn(X_{io}))/dX_i = (pX_i - pX_{io})/dX_i \qquad (4.6)$$

Eqn 4.4 can be rewritten:

$$pX_i = pX_{io} + pdX_i = fn(X_{io} + dX_i) \qquad (4.7)$$
$$= fn(X_{io}) + J.dX_i$$

Equating terms in pdX_i:

$$pdX_i = J.dX_i \qquad (4.8)$$

This is the small signal form of the linearised equations which maybe obtained by forming the Jacobian matrix from eqn 4.6. This equation replaces the numerical integration routine in each of the simulation programs as follows:

i) Solve the steady-state conditions of the system.

ii) Initialise the state variables.

iii) Calculate the derivatives of the state variables for the initial conditions.

iv) Perturb each of the state variables in turn and recalculate all of the derivatives of the state variables.

v) Calculate the small signal linearised matrix from eqn 4.8.

Before this technique can be successfully used, all non-continuous activities have either to be removed or approximated to a continuous function. Also, flags are included in the programs to inform the user if any hard limits are reached.

4.5 Eigenvalue Analysis

The linearisation of the system equations means that they are in a suitable form for the study of the natural modes of oscillations and their sources in the system using eigenvalue techniques. They also provide a form that is suitable for the design of additional control. From eqn 4.8 the eigenvalues, or roots of the characteristic equation, can be formed with the knowledge that:

$$DET[A - \lambda.I] = 0 \qquad (4.9)$$

where,

A- the small signal (linearised) state matrix (the Jacobian matrix, J)

λ- vector of eigenvalues

I- identity (unit) matrix

Each eigenvalue corresponds to a system response in the form:

$$fn(t) = k.e^{\lambda.t} \qquad (4.10)$$

These eigenvalues are usually in complex pairs of the form:

$$\lambda_{i,i+1} = \alpha +/- jw \qquad (4.11)$$

which results in the response:

$$fn(t) = k.e^{(\alpha +/- jw)t} = (k/2).e^{\alpha.t}.COS(wt) \qquad (4.12)$$

Therefore, if the system is to be stable each eigenvalue must have a negative real part and its closeness to the imaginary axis indicates the degree of damping. The imaginary term is the frequency of this mode in rad/sec.

In order to obtain the system eigenvalues, two methods of determination have been used:

i) An eigenvalue estimation routine, F02AGF, from the NAG library on the EPSG Microvax minicomputer. The user only has to prepare the data in the desired form for passing the information to the routine and outputting the eigenvalue information to the desired output device.

ii) The MATLAB matrix manipulation language [4.6], available on the IBM PC, that uses as its driving routines part of the EISPACK library [4.7]. The processing of the A matrix is as follows:

```
LOAD('A');
E = EIG(A);
SAVE('E');
```

A comparative study between the two methods revealed that as long as the pertubation step in the linearising program was smaller than $1*10^{-6}$ and tolerances were smaller than $1*10^{-9}$, then the two methods were in good agreement.

4.5.1 Eigenvectors

Further information can be gleaned from the right and left eigenvectors, r_i and l_i, which are defined from:

$$A.r_i = \lambda_i.r_i \qquad i = 1,2...n \tag{4.13}$$

$$l_i.A = \lambda_i.l_i \qquad i = 1,2...n \tag{4.14}$$

and normalised such that:

$$l_i.r_i = 1 \tag{4.15}$$

The right eigenvector provide details of the mode shapes, ie the amplitude and phase relationship of a state variable to a particular excitation frequency. The left eigenvector provides information with reagards to the weighting of the state varaibles to construct these modes. Right eigenvector analysis is useful when comparing like with like, ie the mode shapes of the angles along a drivetrain. However, if several different physical variables (eg angle, anngular

velocity, current) are under study, the magnitudes of the entries of r_i (and l_i) will change as the units in the state variables are changed.

4.5.2 The Participation Matrix

An alternative approach is to define the dimensionless matrix, P (the Participation matrix), which is invariable with the change of scale of the state variables as:

$$P_{ij} = l_{ij}.r_{ij} \qquad (4.16)$$

where,

P_{ij}- participation factor of the jth state variable, X_j, in the ith eigenvalue, λ_i.

The participation factor, P_{ij}, can also be interpreted as the sensitivity of the eigenvalue, λ_i, with respect to a particular state variable, X_{ij}.

The Participation matrix has thus been used throughout the study and has been estimated using MATLAB on an IBM PC as follows:

```
LOAD('A');
<R,E> = EIG(A);
L = INV(CONJ(R'));
P = L.*R;
SAVE('P');
```

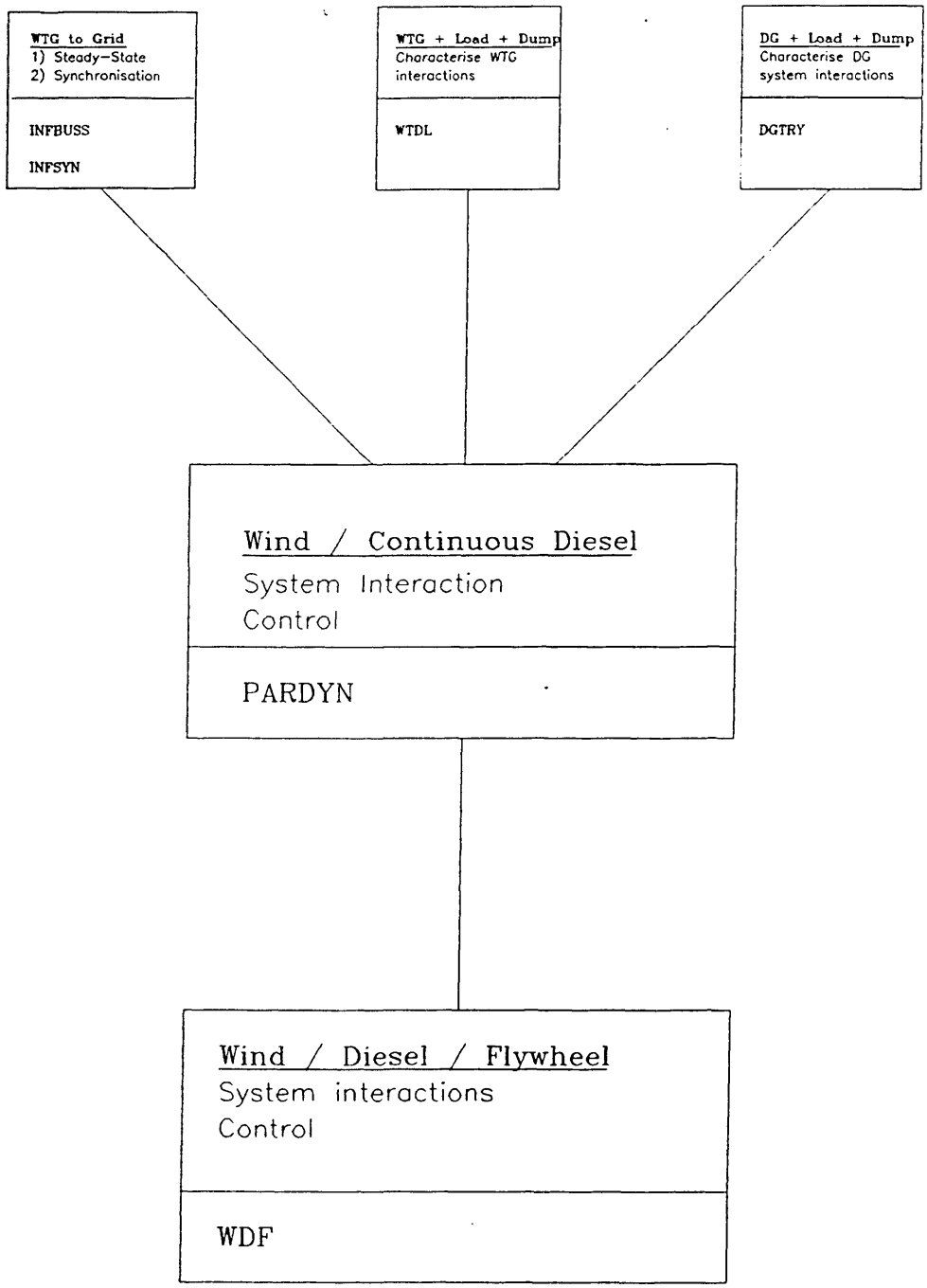

Fig 4.1 ICSTM Steady-State and Dynamic Computer Simulation Programs

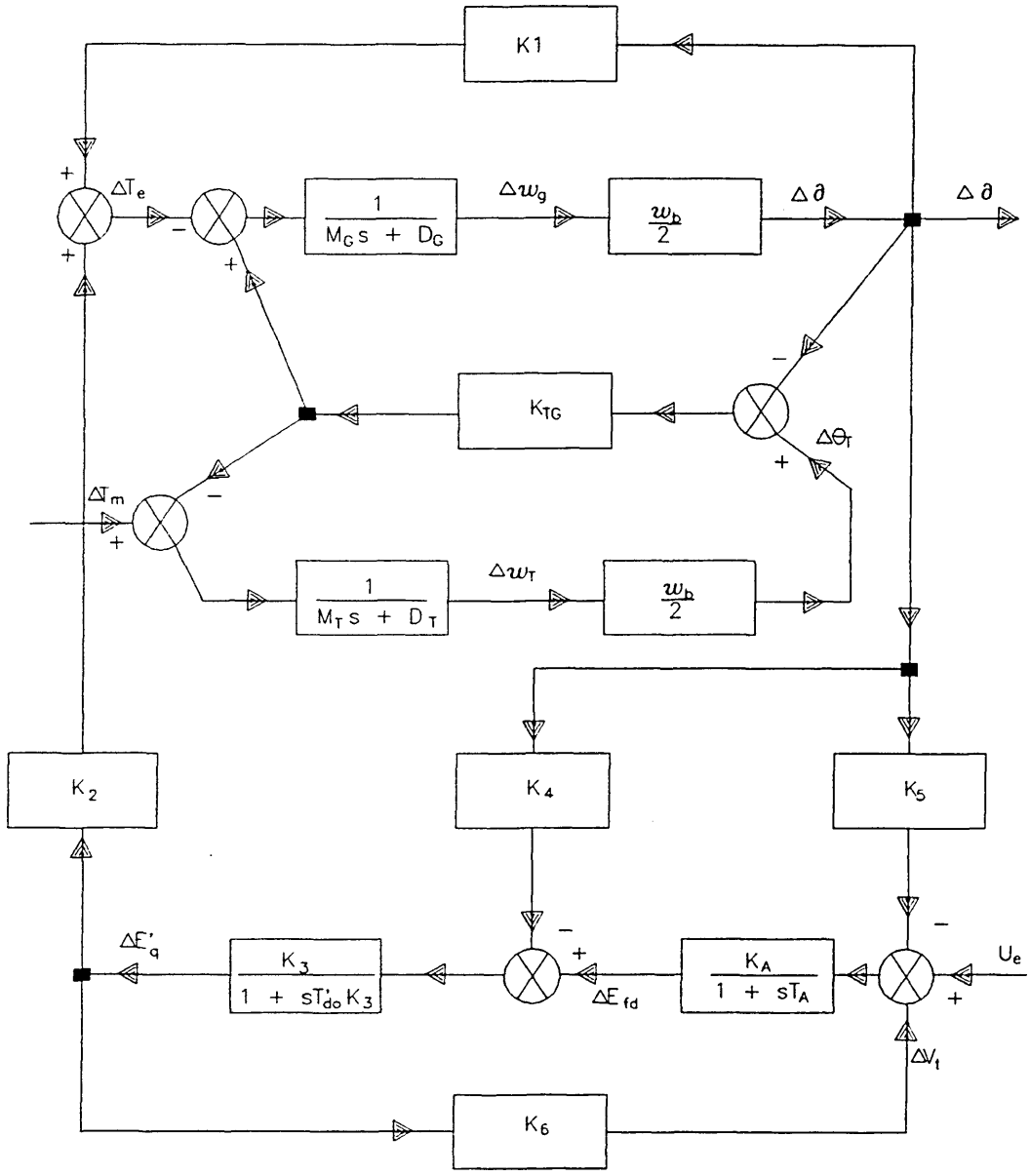

FIGURE 4.2 Schematic representation of the linearised equations of the Wind Turbine Generator including drivetrain connected to an infinite busbar.

CHAPTER 5

Single Prime Mover Simulations

5.0 Introduction

In order to gain a fuller insight into the steady-state and dynamic behaviour of the individual components that make up the wind/diesel/flywheel system the following subsystems were tested/simulated:

1) Wind Turbine connected to an infinite busbar
2) Wind Turbine autonomously supporting the consumer load under frequency or power based dumpload control.
3) Diesel generator autonomously supporting the consumer load under frequency or power based dumpload control.

5.1 Wind Turbine Generator Connected to the Grid - Steady State

5.1.1 Power Performance

Section 3.1 discussed the determination of the Cp/λ characteristic of the wind turbine whilst Section 3.6 compared the measured and simulated results of the wind turbine generator with its static exciter connected to the grid. A version of program INFBUSS was used to bring together both aspects to determine the machine's electrical power

output at a given wind speed (ie the power performance curve).

Originally, the wind turbine was rated at 16 kW, and was characterised by the Cp/λ characteristic of Fig 3.1 and the "original" blade pitch characteristic of Fig 3.2(a). Fig 5.1 illustrates the results for the measured (binned 2 second data) and simulated power versus free wind speed for the grid connected machine. At lower wind speeds the two curves are in reasonable agreement. However, at higher wind speeds the error between the two curves is growing. A possible source of the error difference maybe explained as follows. At high wind speeds, the stability of the system worsens leading to sustained 1Hz oscillations. The passive blade pitching mechanism of the wind turbine is unable to respond "instantaneously" to such changes leading to the measured power being either significantly above or below the average value given by the power curve. Infield [5.1] has also examined the time series structure and concluded that there was no consistent response. It is further suggested [5.2] that this could be due to the varying inherent friction in the pitching mechanism.

Due to the decrease in system stability at the higher power levels, the wind turbine was derated by reducing the pressure of the blade pitching mechanism characterised by the "derated" blade pitching curve of Fig 3.2(b). Although this produced an improvement in system stability, Infield suggests that the response of the blade pitching mechanism is worsened leading to a further deterioration in the accuracy of the

binned 2 second data. To accommodate this effect, the measured power performance curve is split into an upper and lower limit at the higher wind speeds. Fig 5.2 shows that the measured and simulated performances are in good agreement and demonstrates that the machine has been derated to approximately 10kW.

Due to the large degree of uncertainty with the blade pitching dynamics, unless otherwise stated, wind turbine mechanical power and not free wind speed will be used as the input source of the wind turbine.

5.1.2 Wind Turbine Generator with AVR

Because of limitations with the unity power factor exciter of the wind turbine generator it was replaced by the CONTROLOGY AVR 15R. Manufacturers literature and previous testing confirmed its integrating action (ie no voltage error in the steady-state). Program INFBUSS was therefore rewritten to accommodate this device. Fig 5.3 illustrates the simulated reactive power flows of the wind turbine generator with the AVR whilst grid connected. The curve demonstrates that some form of reactive power compensation must be included before its performance could compete with that of the unity power factor exciter. As discussed in Section 3.8.1, Quadrature Droop Compensation (QDC) was identifed and tested as a means of overcoming this problem.

Fig 5.4 graphs the simulated effects of the level of QDC on the reactive power flow. For ease of comparison, the voltage reference of the AVR has been adjusted to produce a reactive power of 2kVAr at zero mechanical load for each level of QDC. The graphs demonstrate that unlike the unity power factor exciter, reactive power decreases almost linearly with increasing real power. However, quite high levels of QDC (> 25%) are needed to provide satisfactory reactive power flows across the full load range. It can therefore be concluded from Fig 5.4 that a 37.5% QDC appears to be an optimal level for this steady-state study (the effects of QDC on system stability will be addressed later in this thesis).

A comparative study of measured and simulated results of the wind turbine generator with the CONTROLOGY AVR 15R and 25% QDC initially produced curves that were vastly in error at the higher power levels. However, unlike during the study of the wind turbine plus unity power factor exciter it was noticed that the busbar voltage did not remain constant at 415V but steadily rose (almost linearly) with increased loading. With this adjustment to the voltage profile, the errors at the higher power levels are greatly improved. However, Fig 5.5 demonstrates that a 0.7kVAr error is still apparent at wind turbine generator electrical power output of 12kW.

Adjustment of the measured value of busbar voltage by 0.3% (well within experimental error) was found to produce a change in the simulated reactive power output of 0.7kVAr. The sensitivity of the reactive power to small voltage changes

could therefore provide an explanation for the errors between the measured and simulated reactive power flows at the higher load levels.

5.2 Wind Turbine Connected to the Grid-Dynamic

5.2.1 Synchronisation

Initially, the wind turbine generator must be synchronised onto the diesel fed system. To examine this condition, both measured and simulated tests were carried out with the wind turbine generator being synchronised onto the grid. Figs 5.6 and 5.7 show the measured synchronisation reponse of the wind turbine power and current at load angles wrt the grid of 0° and 270 °. Figs 5.8 to 5.11 illustrate the simulated synchronisation of the wind turbine onto the grid at load angles wrt the grid of 0°, 90°, 180° and 270° at a synchronisation speed of 0.94 pu. Table 5.1 contains the magnitudes of the maximum transient powers, currents and angular difference.

From the simulation, maximum transient real power occurs at synchronising angle of 270° whilst a relative synchronising angle of 180° produces the largest transient current and the largest angular difference. The simulated maximum power and current for the in-phase synchronisation appears optimistically low (due to the simulated results being outputted at 20msec intervals and not instantaneously).

However, the worst case synchronisation (270°) is in reasonable agreement with the measured values. Both the measured and simulated results demonstrate that the transient current and power flow oscillations are limited in both magnitude and duration. This is due to the high transient reactance of the wind turbine generator in combination with the overrunning clutch and flexible coupling in the drivetrain (the system does not use autosynchronisation equipment). Figs 5.12 and 5.13 demonstrate the simulated effect of a locked overrunning clutch on the synchronisation at the two worst case conditions of 180° and 270° at a speed of 0.94pu. For both cases, even though the initial transient power and current are similar to that with the unlocked clutch, the subsequent 1Hz oscillations are much more severe.

5.2.2 Wind Excited Oscillations

Whilst the wind turbine generator was grid connected, it was noticed that the system suffered from a sustained 1Hz power oscillation (natural mode) which became more pronounced at the higher power levels as illustrated by Fig 5.14. Since actual wind data could not be inputted into the simulation model, initially, random (Gaussian) wind power was used in its place. As in the actual sytem, the simulated response of Fig 5.15 exhibits the sustained 1Hz oscillation.

The inclusion of the aerodynamic characteristics in the wind turbine model allowed the replacement of the wind turbine

mechanical power with that of gaussian wind speed. Figs 5.16 (a) and (b) are the simulated responses of the wind turbine connected to the grid using the Cp/λ characteristic of the wind turbine for mean wind speeds of 4.5 and 10m/s. The more pronounced oscillations at the higher power levels were found to be due to the aerodynamic characteristics of the wind turbine. At wind speeds in excess of 6m/s the Cp/λ characteristic is on the positive part of the slope. Therefore, for a fixed wind speed, as the rotational speed of the wind turbine increases (decreases) the effective mechanical power output inreases (decreases) producing a positive feedback effect (negative damping) as illustrated by the schematic diagram of Fig 5.17.

A Root Locus analysis on a simplified linear model (carried out by Mr Bleijs) had identified that a tenfold increase in the mechanical damping would bring about a much reduced oscillation [5.3].

Fig 5.18 is the root locus of the effect of the mechanical damping using the small perturbation techniques described in Chapter 4. Two natural modes of oscillation were identified, ie 1 Hz and 7 Hz (approx).

From the participation matrix, the low frequency mode was found to be due to the wind turbine rotor swinging against the grid, whilst, the high frequency mode was due to the wind turbine alternator swinging against the grid. As can be seen from the root locus of the lower frequency mode, the original damping of 220Nm/rad (1.75pu) is inadequate (ie zeta = 0.1),

whilst a tenfold increase (17.5pu) greatly improves the stability of this mode (zeta = 0.52). At this higher level of mechanical damping, the already well damped complex poles of the high frequency mode becomes two real poles. However, confirmation that this would be the case and that this increase would not seriously worsen the synchronisation operation was sought from the ICSTM models.

Fig 5.19 (a) and (b) illustrate that the 1Hz power oscillation is indeed reduced with this tenfold increase in the wind turbine mechanical damping when subjected to random wind speeds around 4.5 and 10m/s. Figs 5.20 and 5.21 illustrate the worst case synchronising conditions (delta = 180°, 270 °) for the increased mechanical damping. Due to this increased damping the sustained 1Hz oscillation is quickly damped, but the 6Hz mode is increased. There appears to be little change in the magnitudes of the maximum transient power and current.

However, simulation of the wind turbine synchronised onto the grid with a twentyfold increase in the mechanical damping was found to result in pole-slipping. The tenfold increase in mechanical damping was therefore implemented in the real system.

5.3 Small Perturbation Studies

5.3.1 Fixed excitation

The previous section of work prompted a study into the reasons why the wind turbine generator demonstrated such poor stability. Bleijs, using the simple mass/spring analysis of the wind turbine connected to the grid (and therefore fixed component values) suggested that the stability of the system at the increased level of mechanical damping was far worse than that found in the previous section for the low frequency mode (ζ=0.48 instead of ζ=0.58).

To more fully understand this phenomenon, an eigenvalue analysis was carried out with the unity power factor exciter replaced by a constant current source (ie fixed excitation). Comparison of Fig 5.18 with Fig 5.22 demonstrates that the low frequency mode stability is improved by the use of the UPF exciter at the higher levels of mechanical damping over that of fixed excitation. However, at reduced levels of mechanical damping (eg 220Nm/rad/s) the stability of both the low and high frequency modes is worsened.

5.3.2 Faster Response UPF Exciter

Fig 5.23 is the root locus plot of increased mechanical damping with a hundredfold reduction in the magnitude of the UPF exciter time constant. It suggests that a reduction in the internal time constant (due to the smoothing circuit) of

the UPF exciter would further improve the stability of the system at the increased level of mechanical damping. However, if the mechanical damping was returned to its original value, system stability would further suffer.

5.3.3 Synchronous Generator

It was noted that throughout this eigenvalue study, at zero levels of mechanical damping the high frequency oscillation (due to the generator swinging against the grid) was unstable. An eigenvalue analysyis of the system at zero mechanical damping with X_d', X_l and T_{do}' reduced by a factor of ten produced stable low and high frequency modes as illustrated by Table 5.2.

It can therefore be concluded that the synchronous generator is inherently unstable due to its large transient reactance.

5.3.4 Decoupled Wind Turbine

In order to understand the effect of opening the overrunning clutch on the grid connected wind turbine generator the perturbation model was run with the wind turbine decoupled from the system. As expected the 1Hz mode was no longer present whilst the system was dominated by a 6Hz mode (ie σ=-0.52+/-j39.2) having a damping factor of 0.014. The system is therefore only lightly damped when the overrunning clutch is open.

5.3.5 Effect of Quadrature Droop Compensation

Section 5.1.2 discussed the effect of the CONTROLOGY AVR 15R plus QDC on the steady-state performance and concluded that a QDC of 37.5% was optimal for the minimisation of reactive power flow over the full load range.

The results of an eigenvalue analysis study of the wind turbine generator with the AVR at various levels of QDC is summarised as Table 5.3. The Table demonstrates that there is only a slight reduction in stability for both modes of oscillation with increased QDC. It therefore seems plausible to increase the present level of QDC in the actual system from 25.0 to 37.5%.

A comparison between the stability levels of the above table with that of the UPF exciter reveals that although the AVR gives improved stability for both modes at the original level of damping, at the higher damping level its stability is slightly worse.

5.4 Improved Stability Via a Power System Stabiliser (PSS)

With the replacement of the UPF exciter by an AVR it became possible to feedback supplementary signals (eg speed, power) into the excitation to improve system stability as an alternative to the increased mechanical damping.

The use of the wind turbine speed as the additional signal was dismissed due to the tachogenerator being sited on the wind turbine side of the overrunning clutch in the actual system thereby providing an incorrect signal when the wind turbine was decoupled. The design of the wind turbine prevented its repositioning to the other side of the clutch.

The wind turbine generator electrical power was therefore used as the feedback signal to provide increased damping torque. A simple controller of the form:

$$H(s) = \frac{s.T_1}{1+s.T_2} \qquad (5.1)$$

$$V_s(s) = H(s).P_w \qquad (5.2)$$

$$V_{err} = V_{ref} - V_w + V_s(s) \qquad (5.3)$$

where,

T_1 - Gain term whereby the derivative term ensures response only to changes in power.

T_2 - Time constant to provide phase shift.

$V_s(s)$ - Supplementary signal into the AVR.

was used to demonstrate that a PSS could be made to improve system stability.

Appendix 5.A describes the "Pole Placement" technique, as proposed by Hsu and Chen [5.4], used to improve the stability of the low frequency (1Hz) mode. T_1 and T_2 were assigned by this method which allowed the placement of a pair of complex poles without affecting the rest of the system.

To validate the results of the pole placement techinique, dynamic simulations of the wind turbine generator connected to the grid with and without the PSS were carried out. With the original level of mechanical damping (ie 220Nm/rad/s), the system was subjected to a wind turbine mechanical power of i) approximately 4kW gaussian (mean = 4kW, standard deviation = 0.6kW) and ii) a step change of 4 to 5kW (at t = 0secs):

1) No PSS (σ_{1o} = -0.53 + j5.97)

Fig 5.24 illustrates that both the wind turbine speed and generator real power exhibit a large sustained 1Hz oscillation. The step load case (Fig 5.25) demonstrates the poor system stability in that the wind turbine speed oscillations have not totally died away within 10 seconds. In both cases, the excitation system appears to show little response to the 1Hz mode.

2) With PSS (σ_{1o} = -1.0 + j6.0, T_1 = -3.626, T_2 = 0.2257)

Fig 5.26 shows that there is quite a large reduction in the 1Hz oscillation for the random wind speed input. The step load case (Fig 5.27) demonstrates that there is very little change in the magnitude of the first oscillation (transient condition), but the wind speed oscillation dies down within 3 seconds. In both cases, it can be clearly seen that the exciter is now responding to the 1Hz mode and this effect is reflected in both the generator voltage and reactive power responses.

3) With PSS (σ_{1o} = -2.0 + j6.0, T_1 = -7.99, T_2 = 0.178)

Fig 5.28 demonstrates the very large reduction in the low frequency mode for the wind turbine speed and electrical power output. However, the excitation system has become very active leading to reactive power flows that would be unacceptable in the autonomous wind/diesel system. Fig 5.29 shows that although the initial transient response is little improved, the system's response is very well damped and settles within 2.5 seconds. However, due to the PSS, the reactive power flows again reach unacceptable levels.

The conditions of section 2 (ie σ_{1o} = -1.0 + j6.0) therefore provide an ideal compromise between improved system damping and worsening reactive power flow. To date, however, this method of improved stability has not been tried in the actual system and so a comparison with measured results cannot be demonstrated. In Chapter 6, the PSS along with the pole placement technique will again be used on the full wind/diesel/flywheel system.

The time responses of the dynamic simulation demonstrates that the pole placement technique can be used to improve the damping of a particular oscillatory mode for a particular set of conditions . If it is desired to improve the damping of more than one pole-pair, the technique can be extended to more complicated controllers (eg P + I + D with washout filters).

5.5 Autonomous Wind Turbine operation

During initial testing of the wind turbine autonomously supporting the system, with frequency-based proportional control of the dumpload, P gains in excess of 4kW/Hz brought about a sustained 3.4 Hz oscillation of the form shown in Fig 5.30 (a) whenever the dumpload was active (larger gains were needed in order to limit the system frequency to 50+/- 5Hz).

Initially, the sustained 3.4 Hz oscillation could not be reproduced using the dynamic model. Attention turned to the wind turbine drivetrain shaft elasticity which was suspected of being incorrectly modelled, however, parameter range adjustments proved fruitless.

Testing of the frequency transducer model under different configurations using the simulation was therefore carried out. Initially, the frequency transducer was modelled as a single lag. This model was then changed to that of an 80msec delay but although the system could be made to go unstable, the shape of the frequency waveform bore little resemblance to that of Fig 5.30 (a). The model was then changed to that of an 80msec sample and hold with a single 15msec lag at its output. The sample and hold was modelled by grabbing the value of the frequency signal every 80msec, storing the information in a dummy variable for a further 80msec and finally passing this information to another dummy variable which was used as the input to the 15msec lag.

Upon using this model, the waveform of Fig 5.30 (b) was obtained which bears a striking resemblance to the actual waveform. The model was therefore able to confirm that the sustained oscillation was excited by the action of the dumpload controller causing the alternator to swing against the rotor due to the flexibility of the drivetrain. Note, the shapes of the measured and simulated dump load power differ because the actual waveform has been passed through a power transducer with an 80msec time constant.

Using this model of the frequency transducer, the stability limit with I control was also found. Figs 5.31 (a) and (b) demonstrate that the actual and simulated power and frequency waveforms are of similar shape and reach the stability limit at the same integral gain.

In order to remove the 3.4 Hz oscillation found under P control a 3.4 Hz notch filter was included at the input to the dumpload controller. Fig 5.32(a) shows the response of the system at the dumpload controller P gain of 4kW/Hz, with the additional notch filter, when subjected to a stepload rejection of 2.7 to 0kW. As in the actual system, the sustained oscillation was removed and the reponse was well damped. The tenfold increase of the mechanical damping in the wind turbine drivetrain was also found to alleviate this problem, as illustrated by Fig 5.32(b). For comparison, Fig 5.32(c) illustrates the original response without the notch filter and at the original level of mechanical damping.

5.6 Autonomous Diesel Alternator Operation

5.6.1 Frequency Controlled Dumpload

Simulations were also carried out to determine the stability limit of the diesel supplied consumer load with frequency based dumpload control.

Figs 5.33(a) and (b) illustrate the actual and simulated frequency waveforms when the system was under frequency-based integral action dumpload control. Note, the frequencies do not appear to be at the same level, this is due to the choice of reference speed for the diesel engine (in the actual engine it varies over quite a large range depending on temperature). However, the stability limit is reached at the same integral gain (10kW/Hz/s) for both the actual and simulated tests. The period and amplitude of the oscillation (+/- 2.5Hz) appear to be in good agreement for the two tests.

5.6.2 Power Controlled Dumpload

Steploading testing of the actual diesel supplied system under power based dumpload control to find the stability limits initally revealed the controller to be stable up to 10kW/kW (limit of the P gain setting). However, the 3.4 Hz notch filter (used under frequency control) had been left in place.

A repeat of the steploading tests, after the removal of the notch filter, revealed a much reduced stability limit. Fig

5.34(a) is the actual waveform of the rms diesel power whilst Fig 5.34(b) is the simulated response using the discrete deadtime model of Section 3.9. Both reveal a sustained 19 Hz oscillation at a dumpload controller P gain of 5 kW/kW. Fig 5.35(a) demonstrates that at a similar P gain setting the system is perfectly stable with the inclusion of the 3.4Hz Notch filter, whilst, Fig 5.35(b) reveals that as in the actual system the inclusion of the filter increases the stability limit to 10kW/kW.

An examination of the Participation Matrix obtained from the linearised version of the simulation program (using a truncated Taylor series expansion to approximate the deadtime) revealed that this 19 Hz oscillation was due to the deadtime at the output of the dumpload controller (although the equivalent eigenvalues indicated small signal stability).

A study of the dumpload controller with power feedback via the double lag model of the power transducer (no diesel alternator model), as illustrated by Fig 5.36, using discrete control methods, revealed a stability limit of approximately 4kW/kW with a sustained 18.5 Hz oscillation. The combination of the deadtime at the output of the dumpload controller with the double lag of the power transducer in the feedback loop was therefore inherently unstable at P gains in excess of 5kW/kW.

As an interim measure, the 3.4 Hz notch filter was refitted to the input of the controller. A Bode plot of the "Twin-T" 3.4Hz notch filter (Fig 5.37), reveals that as the frequency

increases above 3.4 Hz the phase relationship moves from phase lag to phase advance thus countering the effect of the deadtime.

An alternative approach tested was the inclusion of a 1.3Hz low pass filter at the input of the controller to block the response of the dumpload controller to all but the 1Hz (approx) natural mode of the wind turbine. Fig 5.38 is the simulated step response of the system with this device in place and demonstrates the much improved stability at 5kW/kW whilst Fig 5.39(a) and (b) are its actual and simulated step responses at the stability limit of 10kW/kW.

5.7 Conclusions

The linear and non-linear techniques developed in Chapter 4 have been used to successfully characterise critical components in the system and to develop compensating methods that maintain system performance within acceptable bounds.

It has been demonstrated in Chapter 5 that:

1) A combination of the Wind Turbine blades' characteristics and its electromechanical equations can be used to accurately predict the Wind Turbine Generator's power peformance when grid connected.

2) Quadrature Droop Compensation is required to ensure that reasonable reactive power flows may be maintained over the full load range when the Unity Power Factor Exciter is replaced by the AVR 15R.

3) The Wind Turbine Generator may be safely Synchronised onto the Grid without autosynchronisation equipment due to the combination of the Wind Turbine Generator's large transient reactance and the overrunning clutch plus flexible coupling in its drivetrain.

4) The wind-excited 1Hz mode of oscillation was due to the insufficient mechanical damping in the Wind Turbine's drivetrain. The oscillation was made more severe at the higher power levels as a result of the inherent negative damping of the C_p/λ characteristic of the Wind Turbine.

5) Linearisation techniques have shown:

   i) the poor response of the UPF exciter.

   ii) the addition of Quadrature Droop Compensation did not adversely effect the stability of the Wind Turbine Generator.

   iii) the lightly damped nature of the Wind Turbine generator could be improved by a reduction in its untypically large transient reactance.

6) A simple Power System Stabiliser could be developed, using the Pole Placement Technique of Hsu and Chen, as an alternative method to dampen the wind-excited 1Hz mode of oscillation.

7) Under autonomous Wind Turbine operation, the frequency transducer of the dumpload controller was identified as the cause of the 3.4Hz non-linear instability. This instability was cured by the introduction of a 3.4Hz "Notch" filter at the input to the controller.

8) The stability limit of the power based dumpload controller, under autonomous wind turbine operation, could be greatly enhanced by either the 3.4Hz "Notch filter" or a 1.3Hz Low-Pass filter at its input.

9) The models were able to accurately predict the stability limits of the system under both power and frequency control.

Synch Angle (deg)	Max Power (pu)	Max Current (pu)	Max Diff (deg)
0.0	-0.28	0.29	80.0
90.0	0.57	0.74	144.0
180.0	0.54	1.43	311.0
270.0	-0.78	0.93	95.0

(a) Simulated

Synch Angle (deg)	Max Power (pu)	Max Current (pu)	Max Diff (deg)
0.0	-0.37	0.44	-----
270.0	-0.81	1.03	-----

(b) Actual

Table 5.1 Maximum transient power, current and shaft twist during synchronisation of the WTG onto the grid.

Level of Transient Reactance	σ_{lo}	σ_{hi}
Original	-0.07±j6.31	+1.87±j51.25
$(X_d', X_l, T_{do}')/10$	-0.07±j6.51	-0.09±57.51

Table 5.2 Effect of transient reactance upon the stability of the grid connected WTG.

Damping(pu)	σ_{lo}	ζ	σ_{hi}	ζ
0.00	-0.31±j5.9	0.052	+1.24±j44.9	-----
1.75	-0.53±j5.8	0.089	-5.87±j44.6	0.132
17.50	-3.29±j6.7	0.443	--------	-----

(a) 10% QDC

Damping(pu)	σ_{lo}	ζ	σ_{hi}	ζ
0.00	-0.26±j6.0	0.044	+1.33±j46.4	-----
1.75	-0.53±j6.0	0.088	-5.76±j46.1	0.125
17.50	-3.64±j6.9	0.466	--------	-----

(b) 25% QDC

Damping(pu)	σ_{lo}	ζ	σ_{hi}	ζ
0.00	-0.25±j6.0	0.042	+1.34±j46.7	-----
1.75	-0.52±j5.9	0.089	-5.74±j46.7	0.124
17.50	-3.64±j6.9	0.466	--------	-----

(c) 37.5% QDC

Damping (pu)	σ_{lo}	ζ	σ_{hi}	ζ
0.00	-0.25±j6.0	0.042	+1.35±j46.8	-----
1.75	-0.52±j6.0	0.087	-5.74±j46.4	0.124
17.50	-3.64±j7.0	0.465	--------	-----

(d) 50% QDC

Table 5.3 The effect of Quadrature Droop Compensation on the stability of the grid connected WTG.

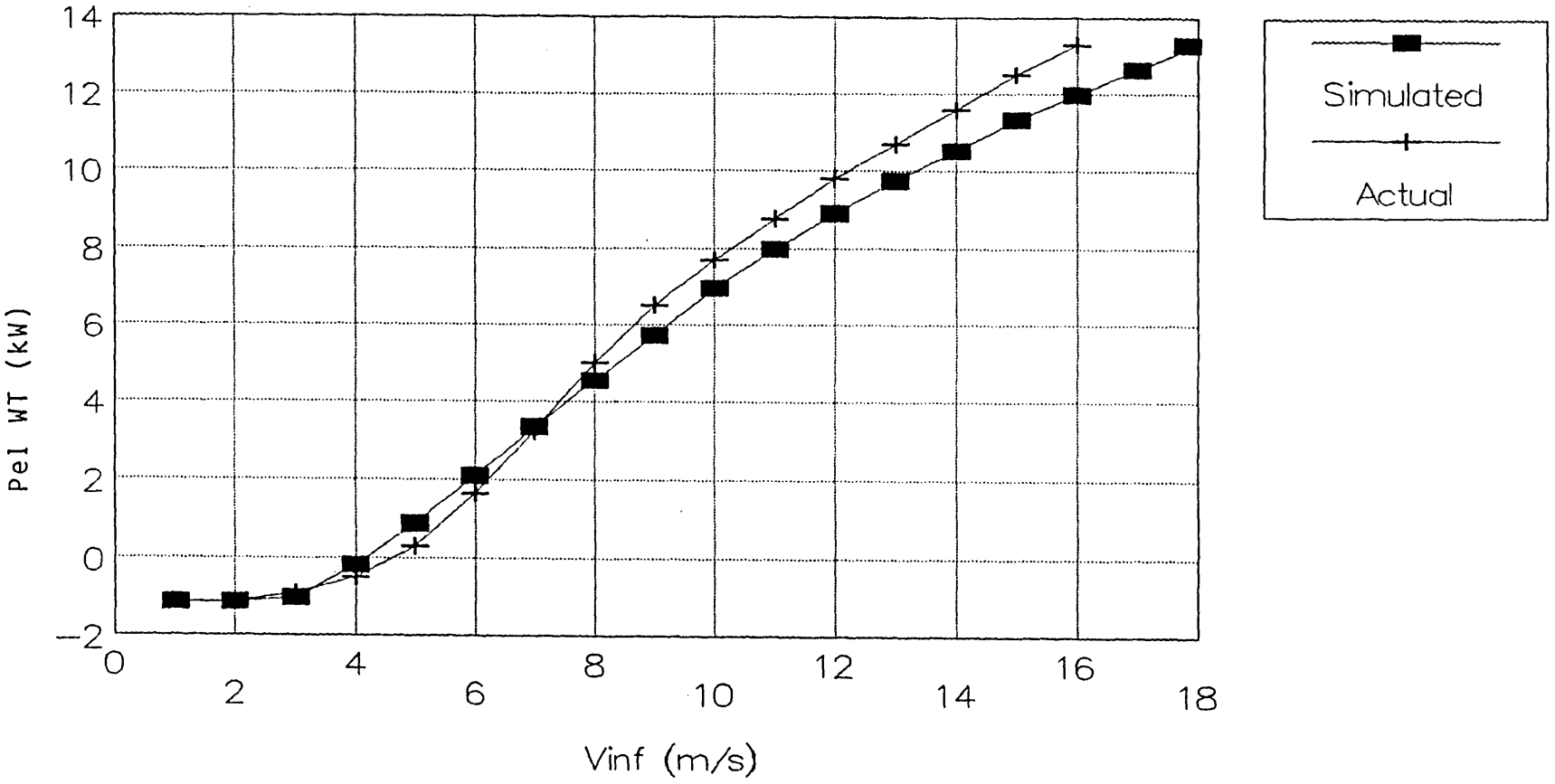

FIGURE 5.1 NWP Co WT (original) Performance curve
WT connected to the Grid

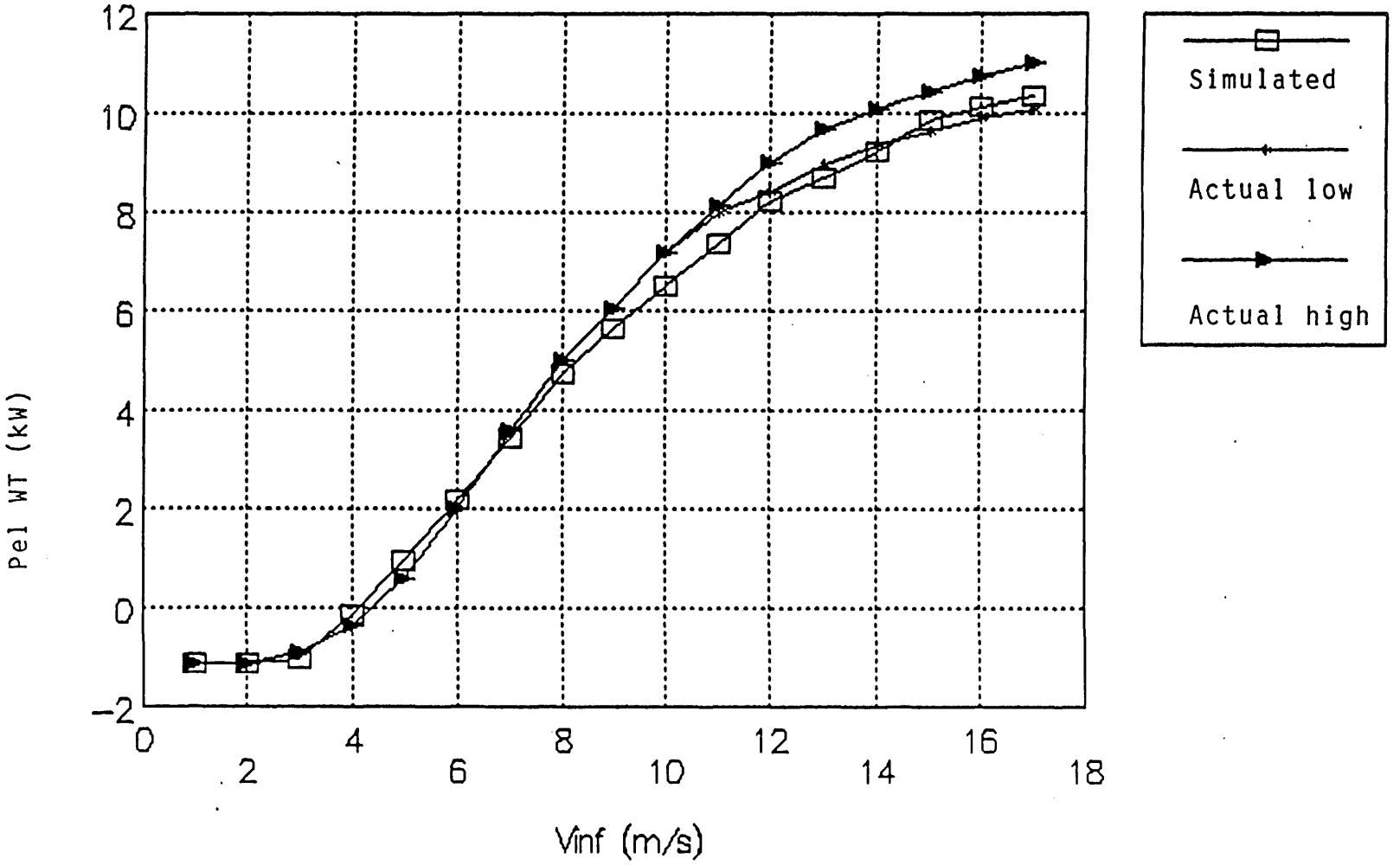

FIGURE 5.2 NWP Co WT (derated) Performance curve
WT connected to the Grid

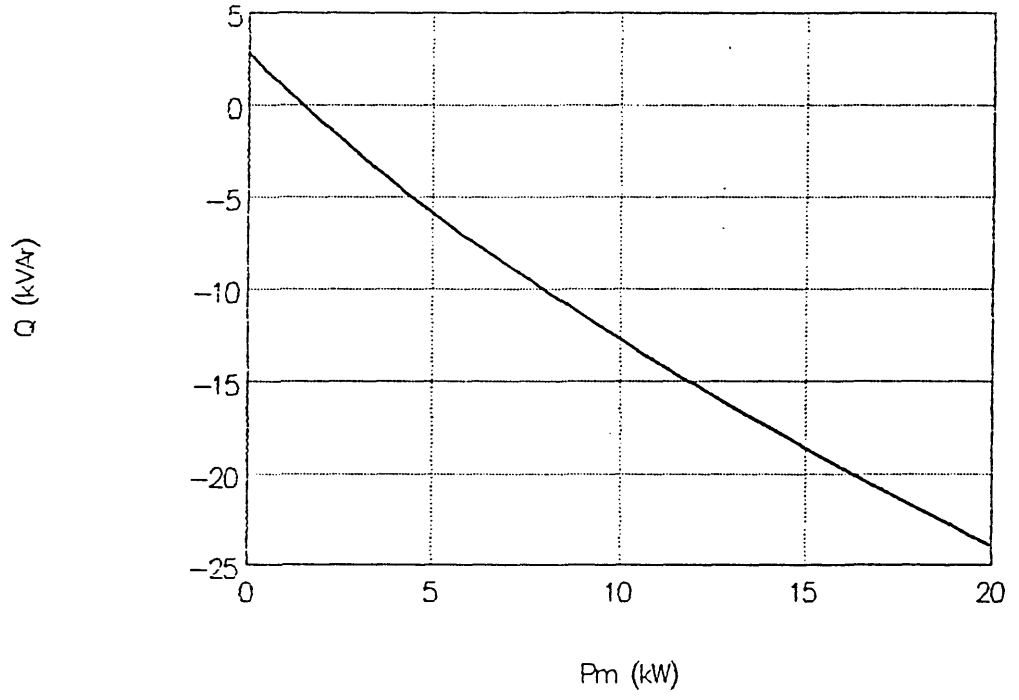

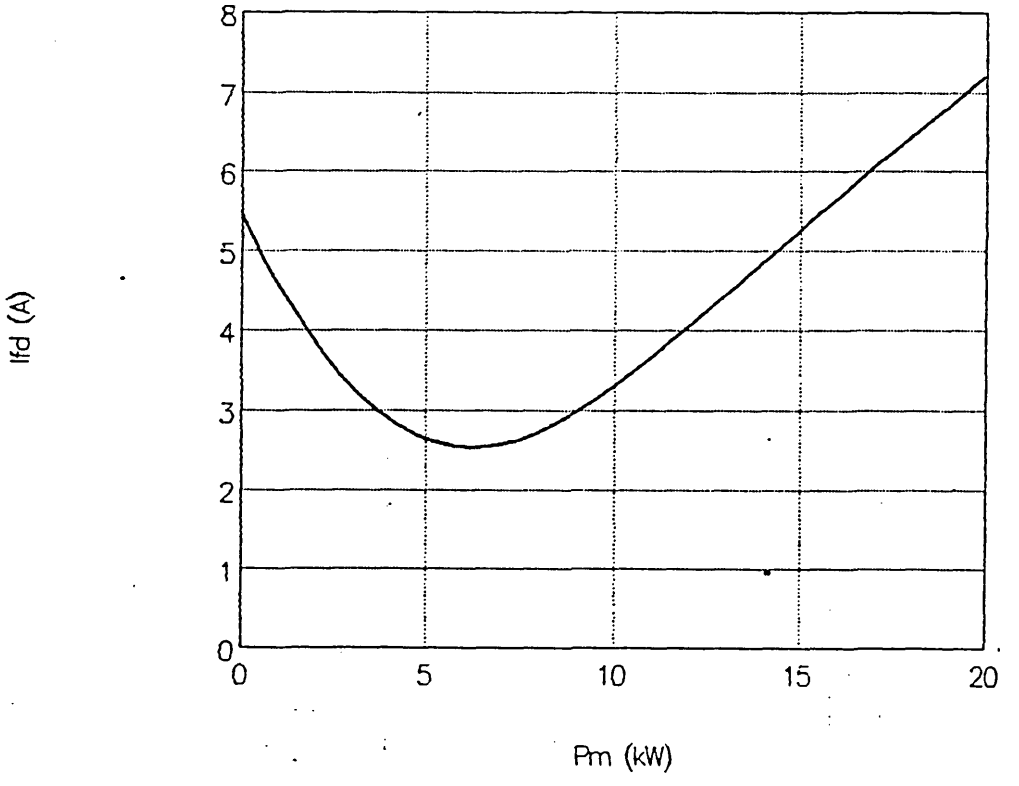

FIGURE 5.3 AVR with NO QDC
WTG Connected to the Grid

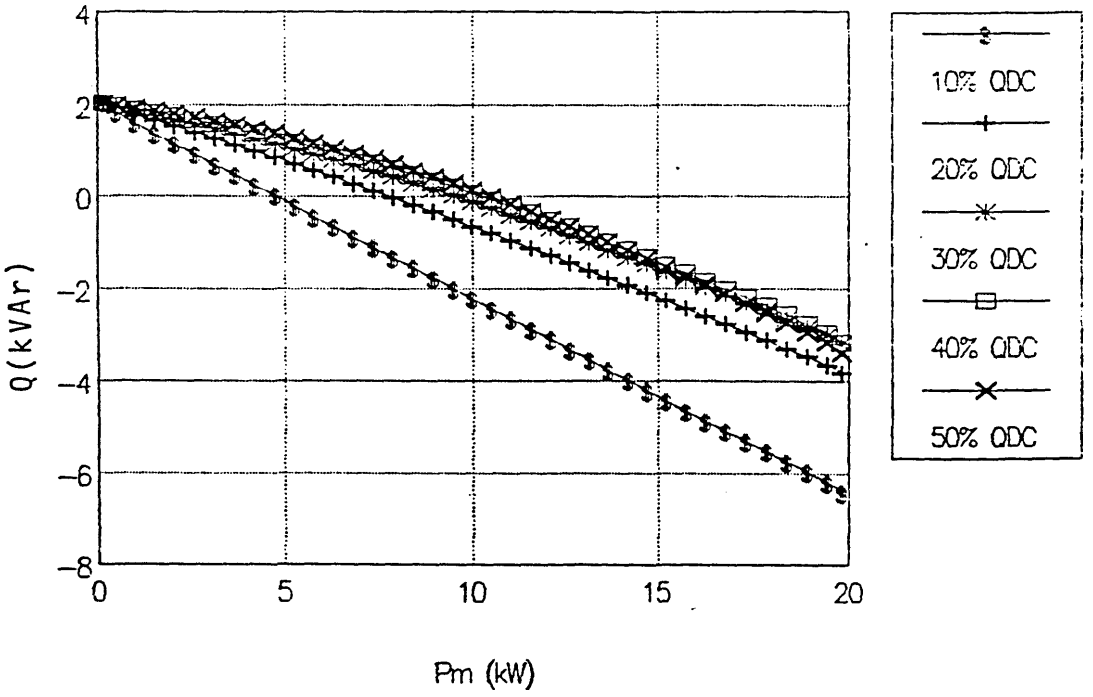

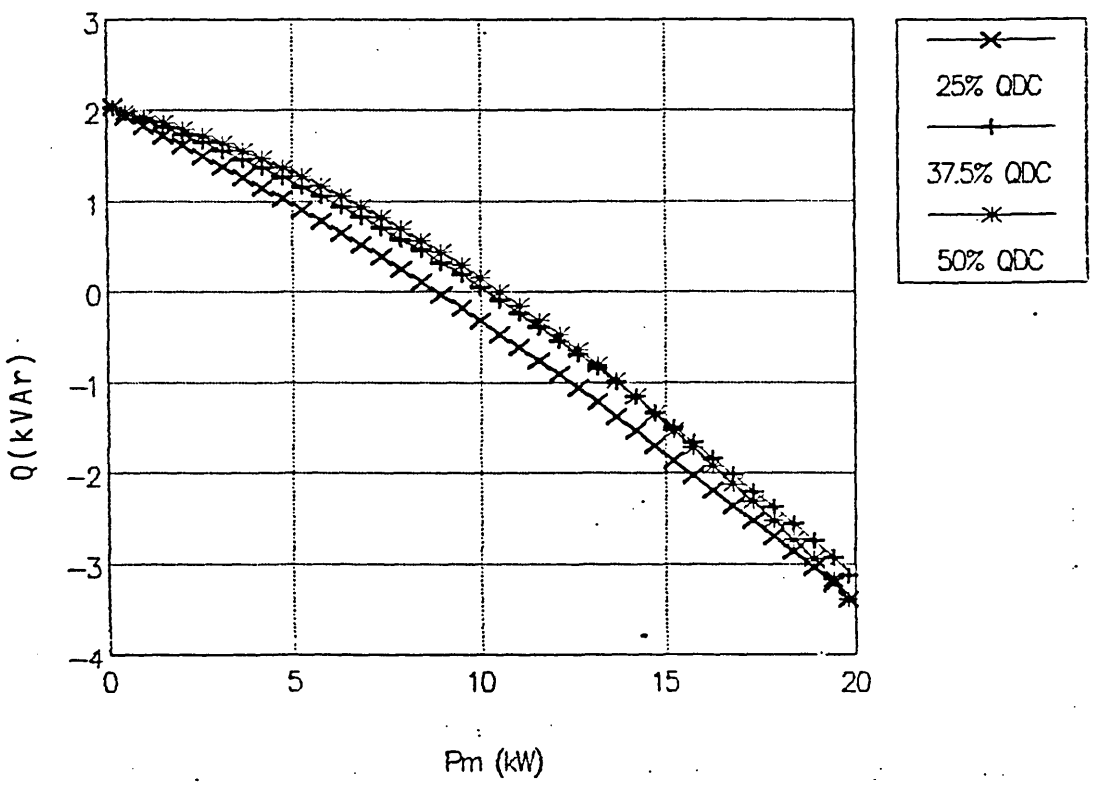

FIGURE 5.4 AVR with QDC
WTG connected to the Grid

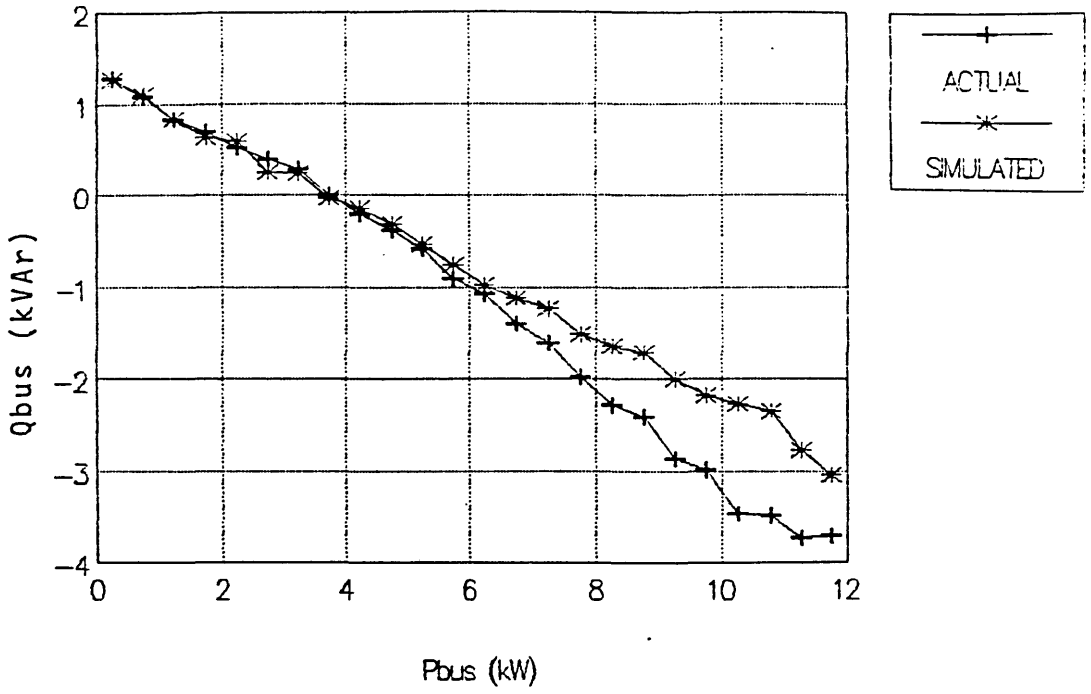

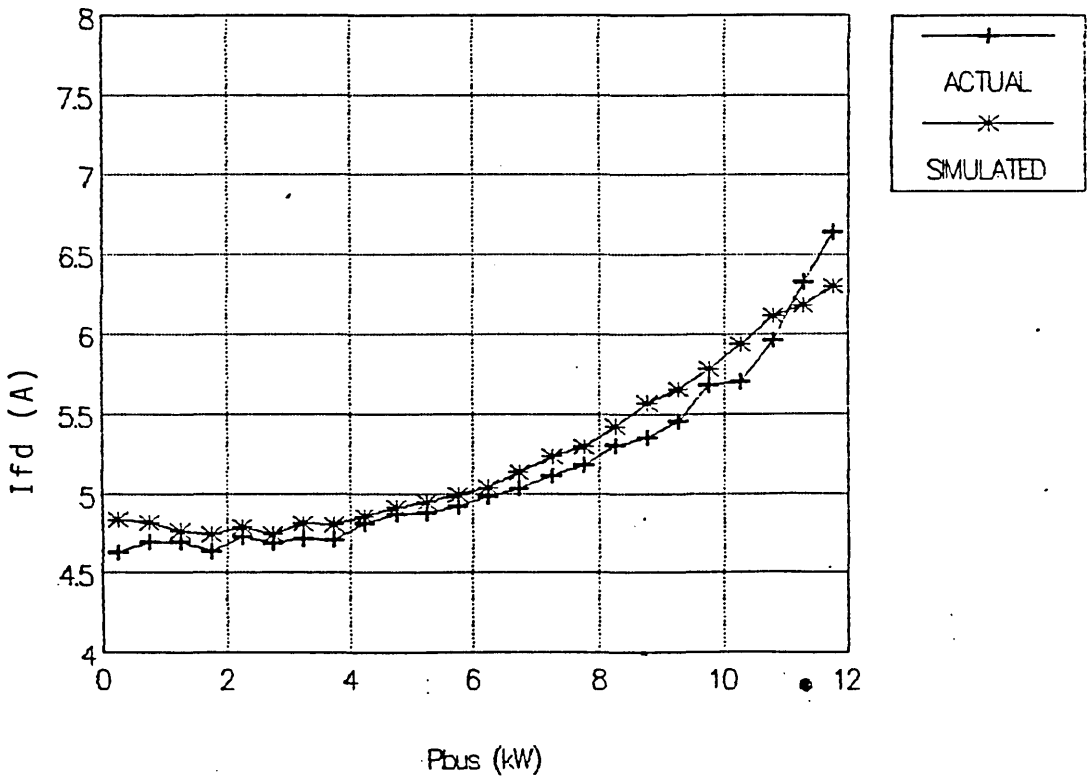

FIGURE 5.5 AVR with 25% QDC
WTG connected to the Grid

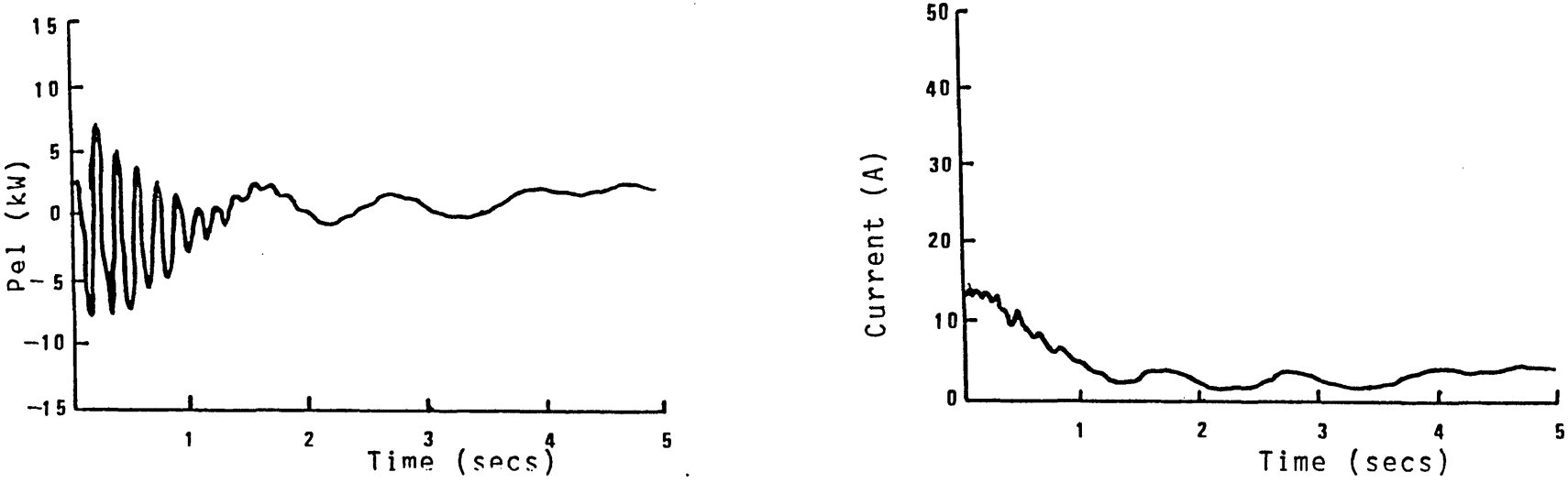

FIGURE 5.6 Synchronisation of the WTG on to the grid at 0.94pu speed (actual) - Relative load angle = 0°

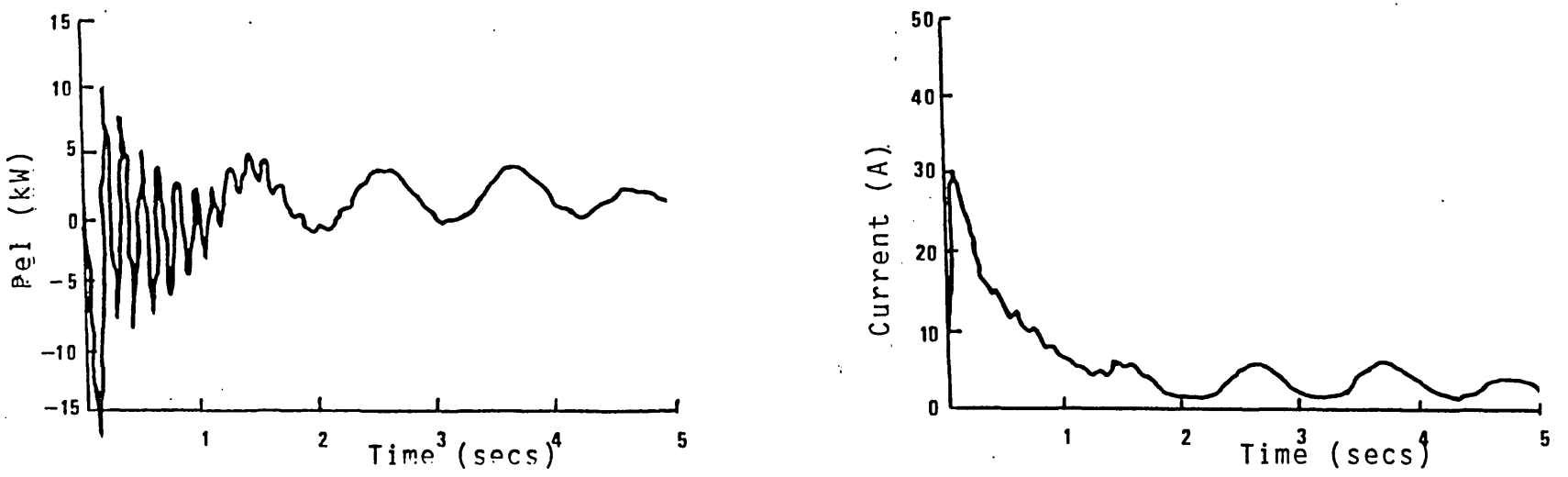

FIGURE 5.7 Synchronisation of the WTG on to the grid at 0.94pu speed (actual) - Relative load angle = 270°

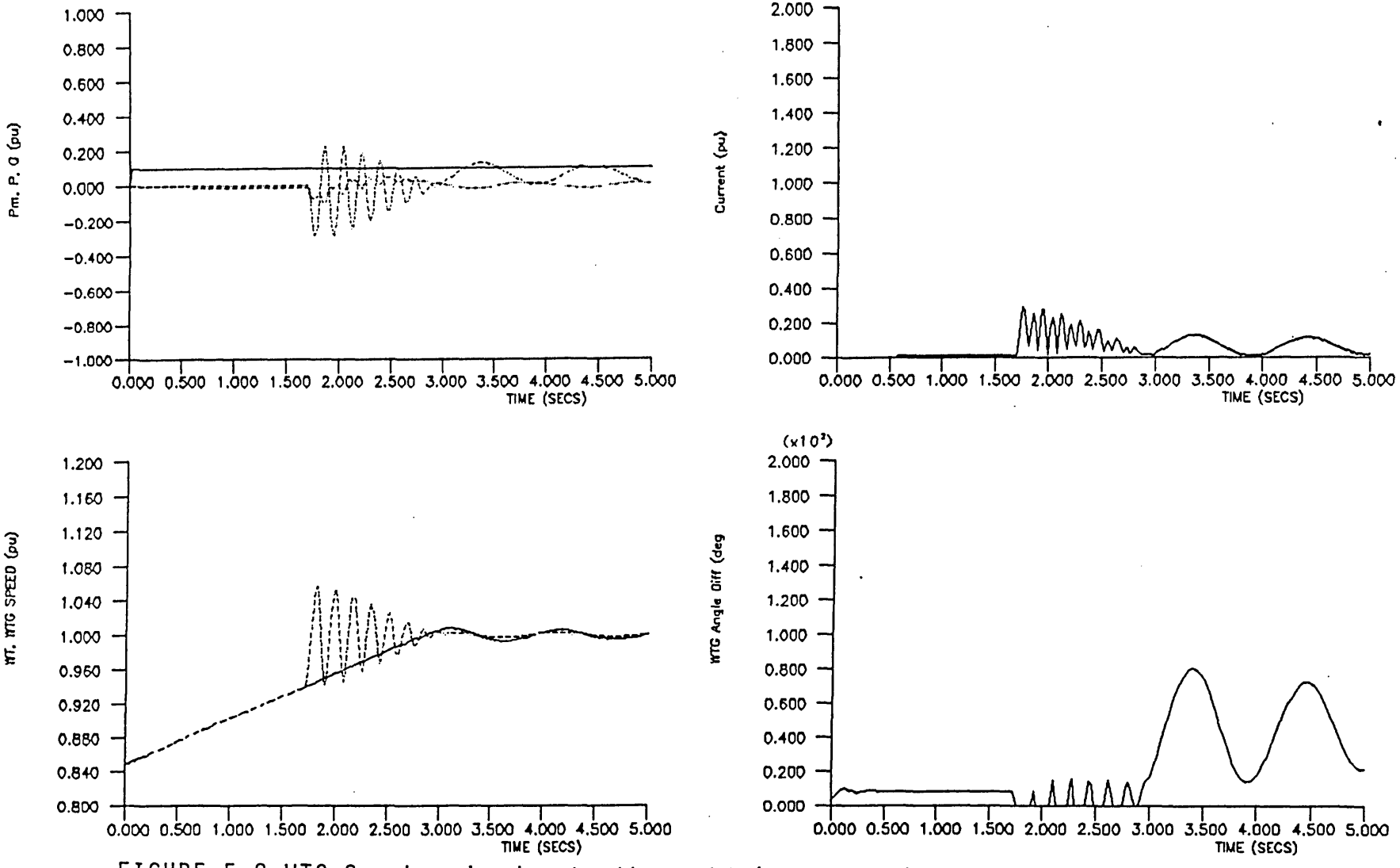

FIGURE 5.8 WTG Synchronised onto the grid (simulated) at 0.94pu speed
- Relative load angle = 0°

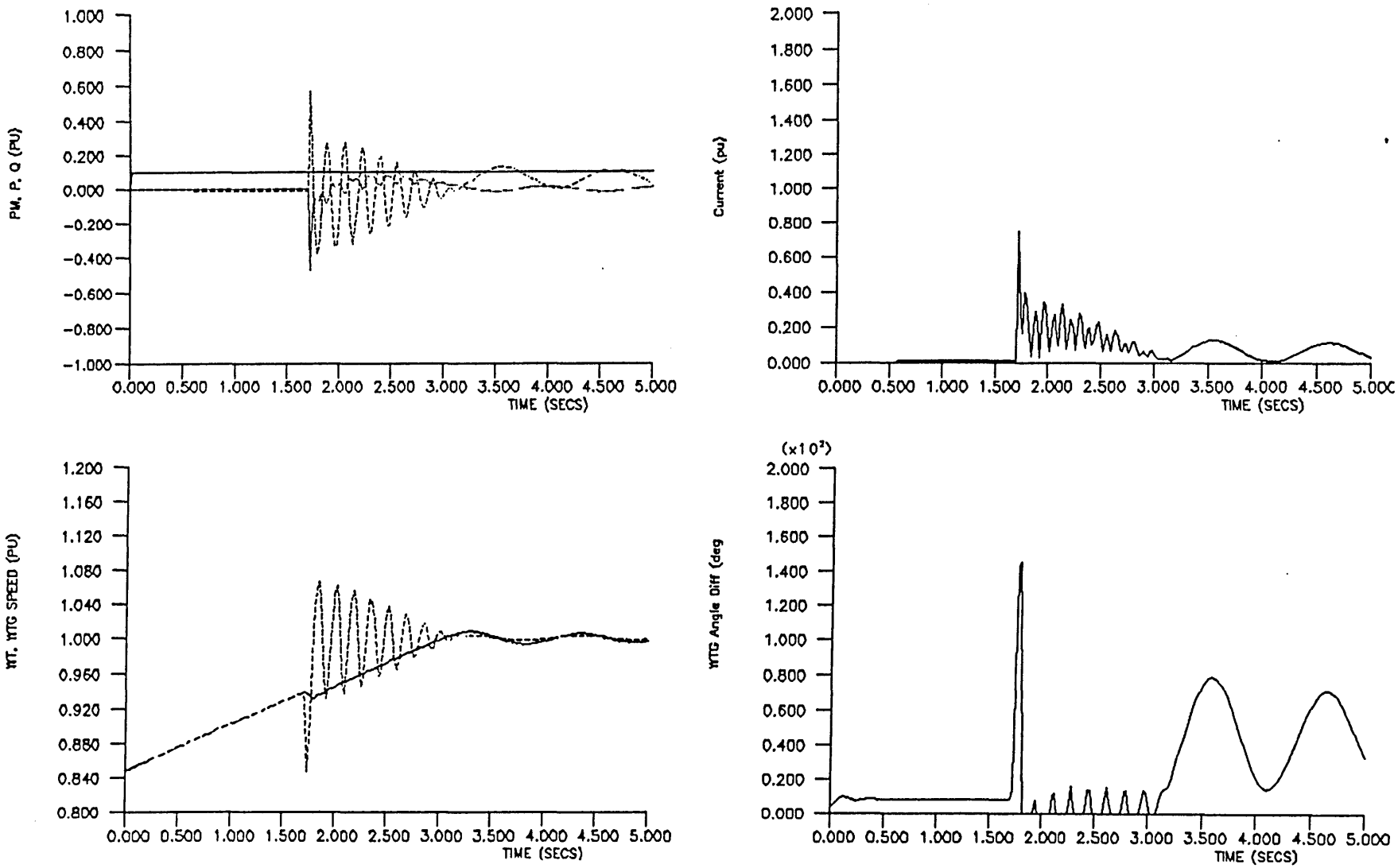

FIGURE 5.9 WTG Synchronised onto the grid (simulated) at 0.94pu speed - Relative load angle =90°

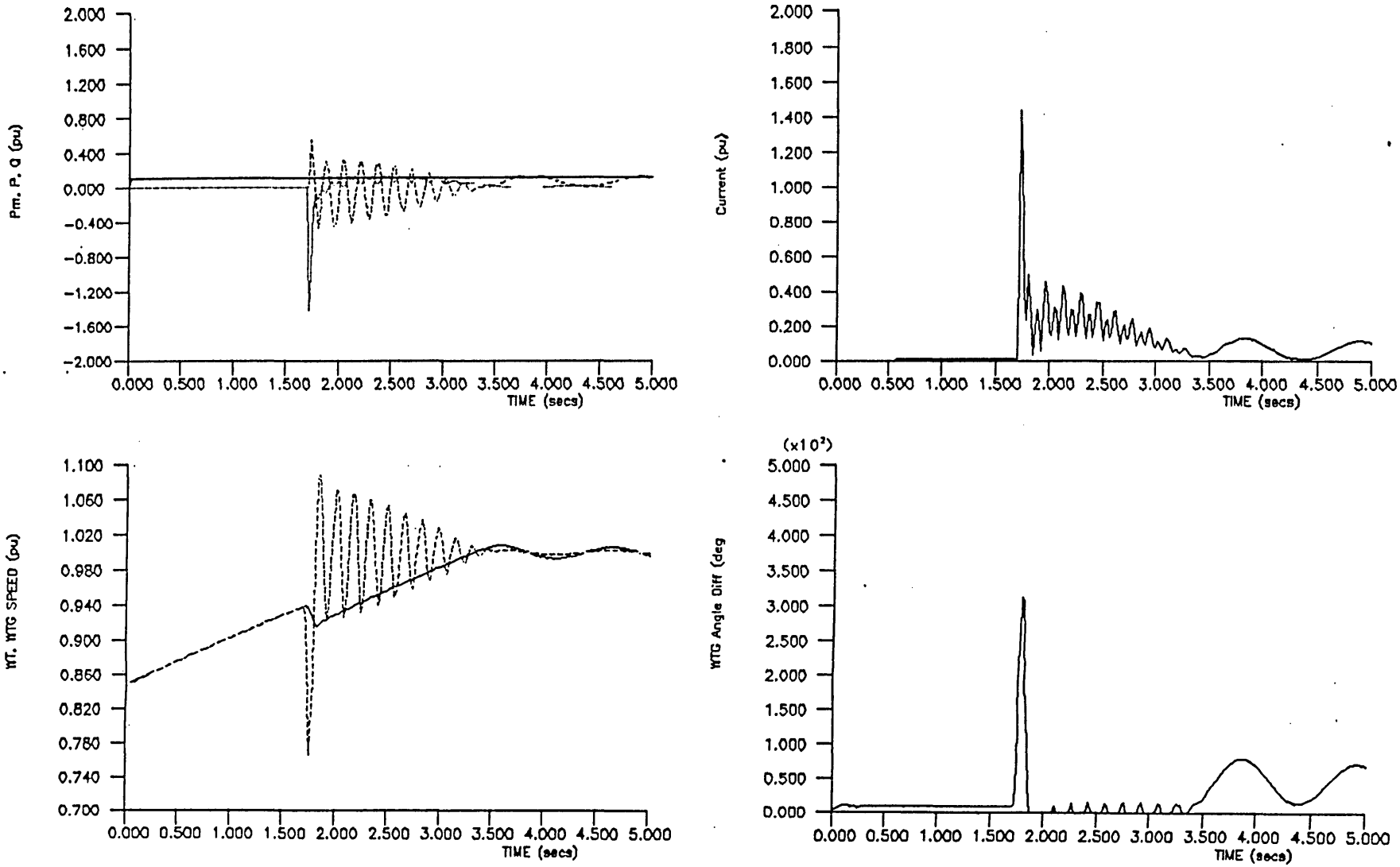

FIGURE 5.10 WTG Synchronised onto the grid (simulated) at 0.94pu speed
- Relative load angle =180°

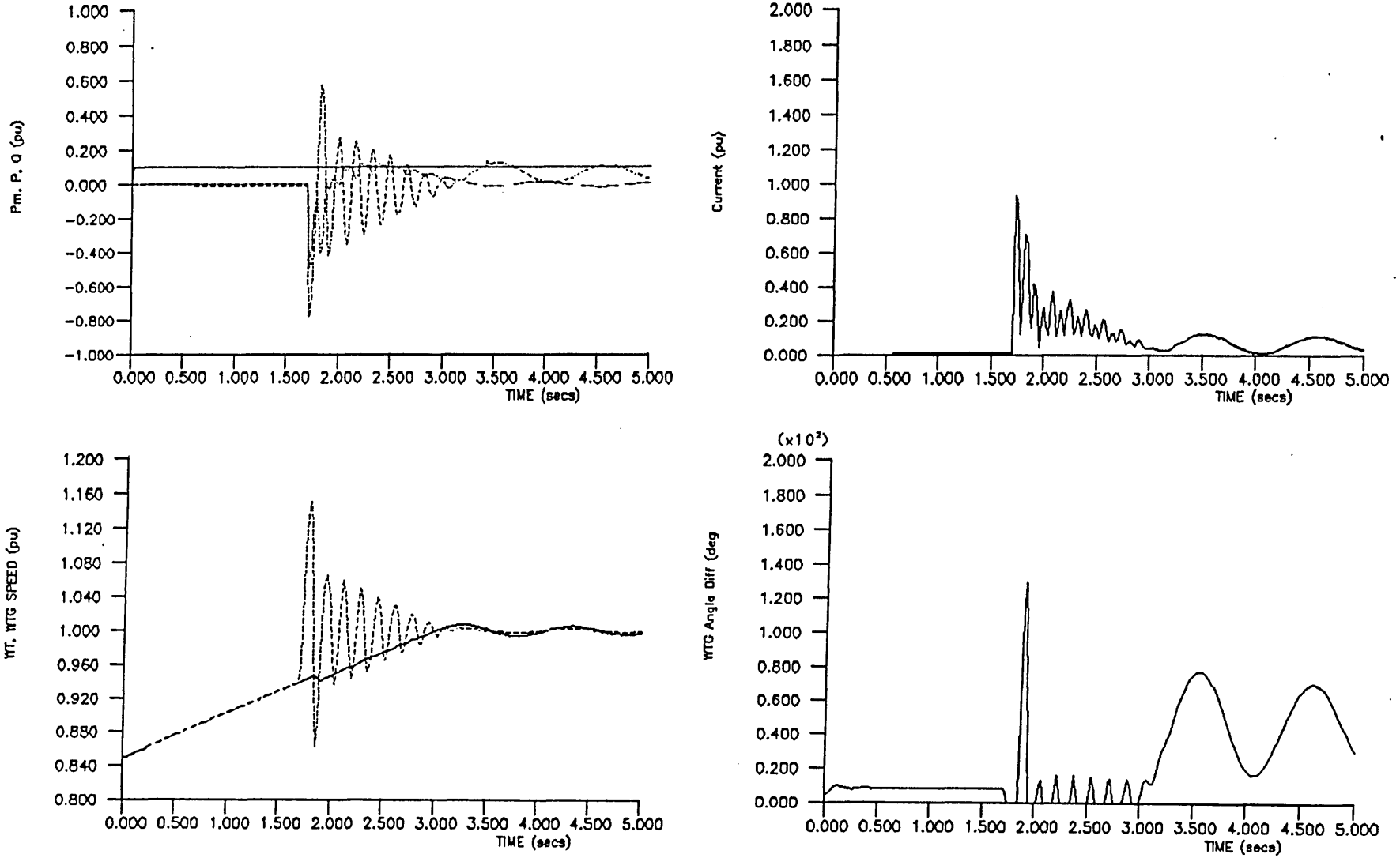

FIGURE 5.11 WTG Synchronised onto the grid (simulated) at 0.94pu speed
- Relative load angle = 270°

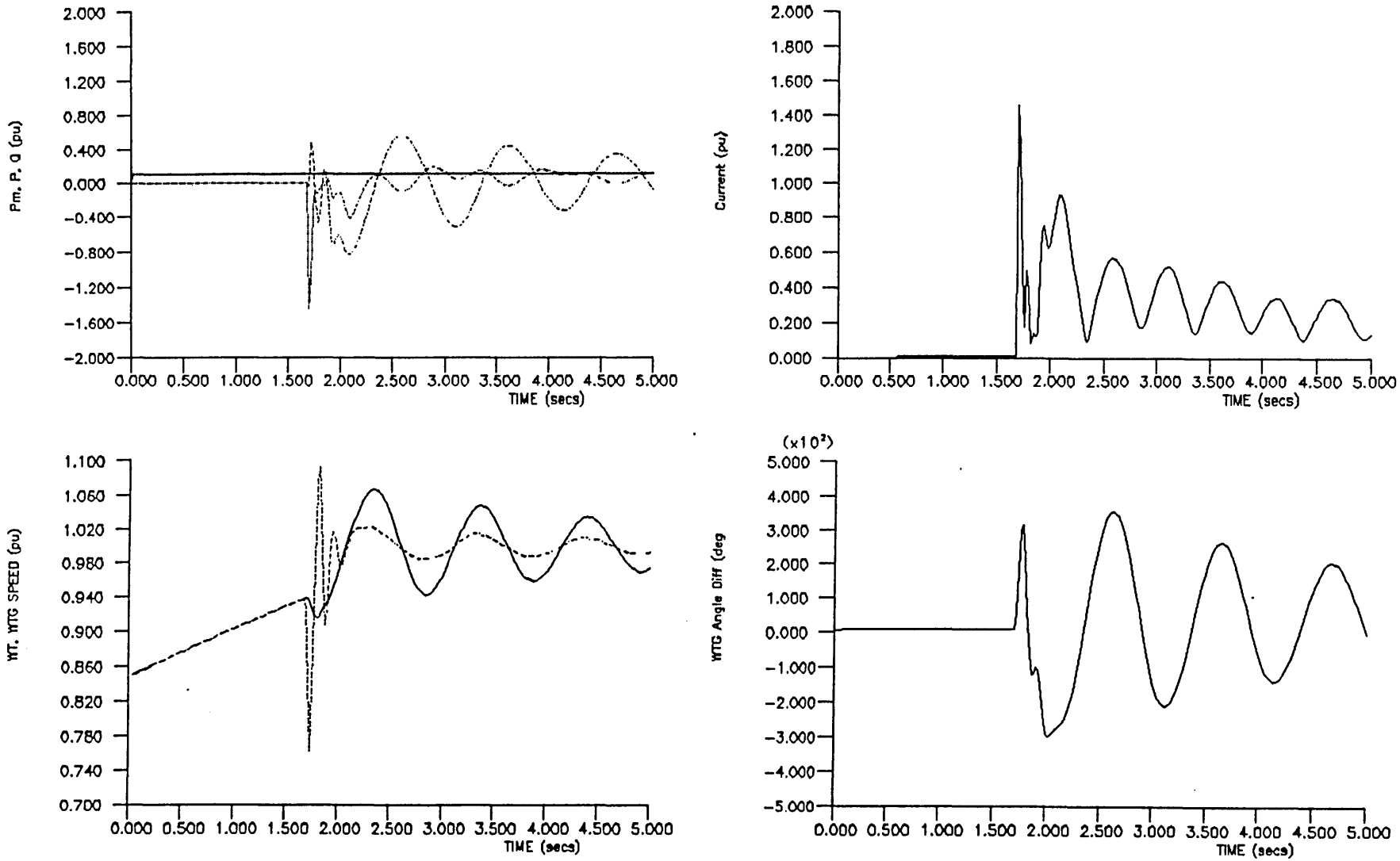

FIGURE 5.12 WTG Synchronised onto the grid (simulated) at 0.94pu speed with locked overrunning clutch - Relative load angle =180°

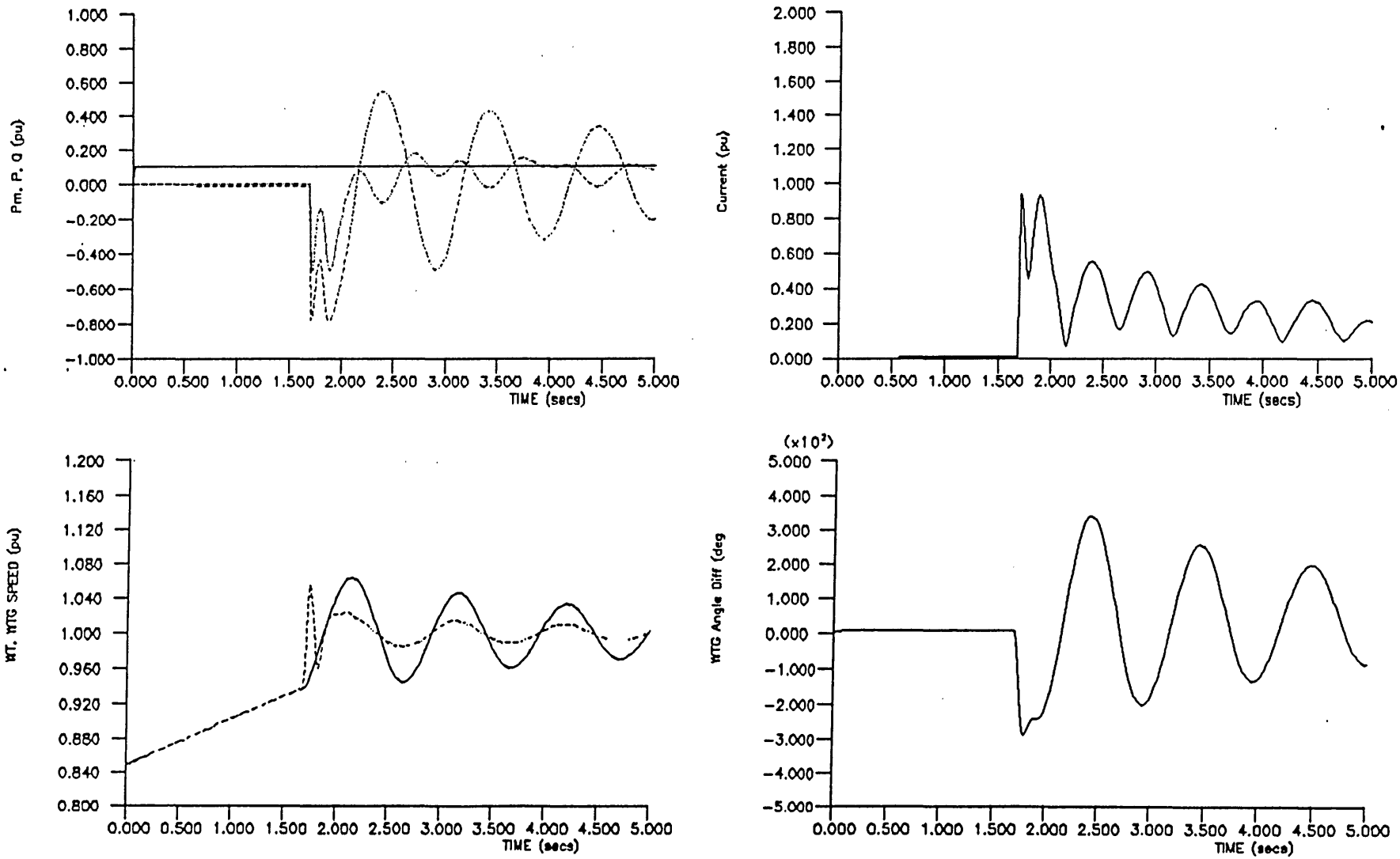

FIGURE 5.13 WTG Synchronised onto the grid (simulated) at 0.94pu speed with locked overrunning clutch - Relative load angle = 270°

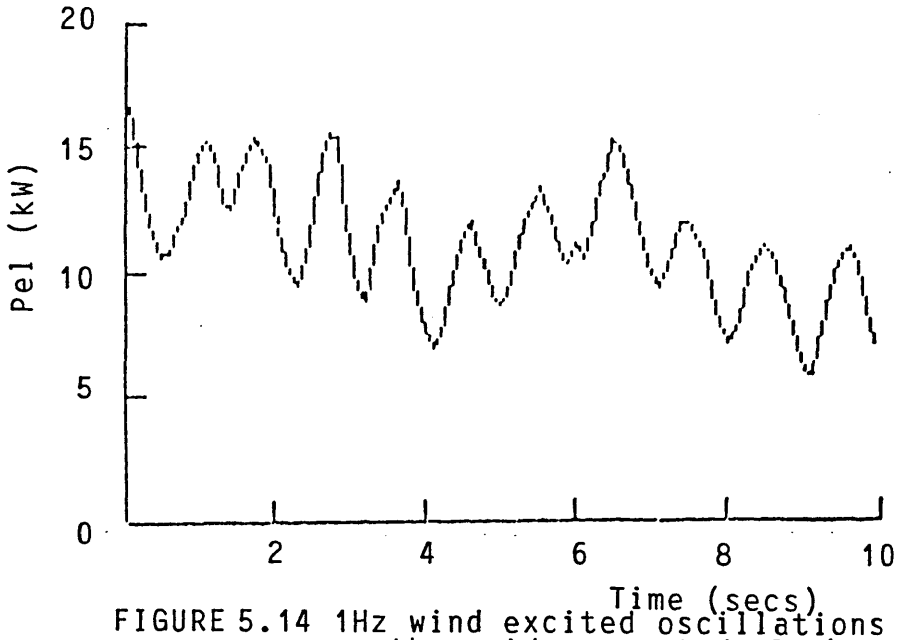

FIGURE 5.14 1Hz wind excited oscillations on the grid connected WTG (measured)

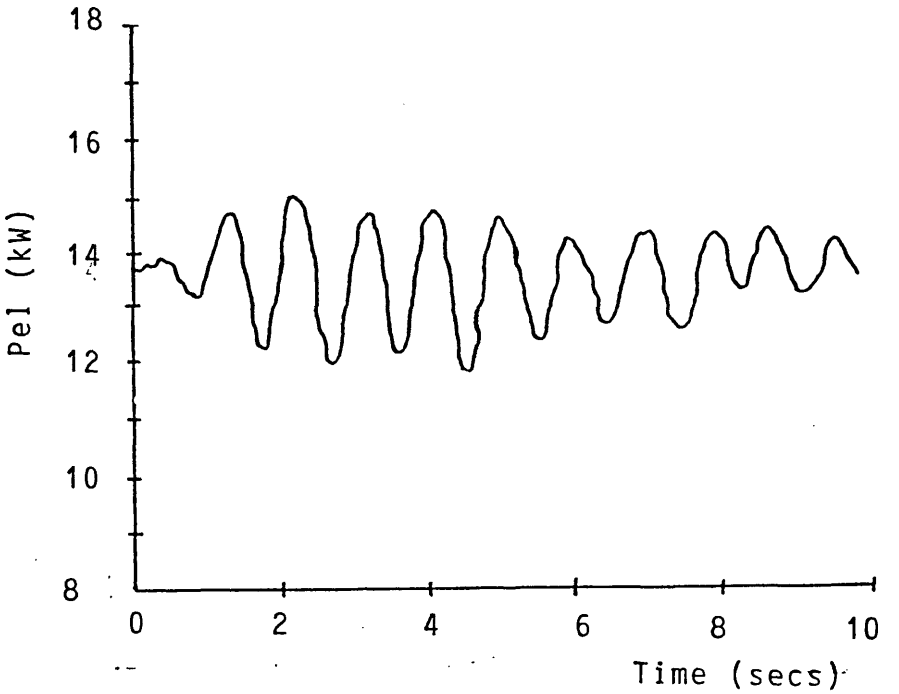

FIGURE 5.15 Simulation of 1Hz oscillation due to gaussian mechanical power inputted into the grid connected WTG

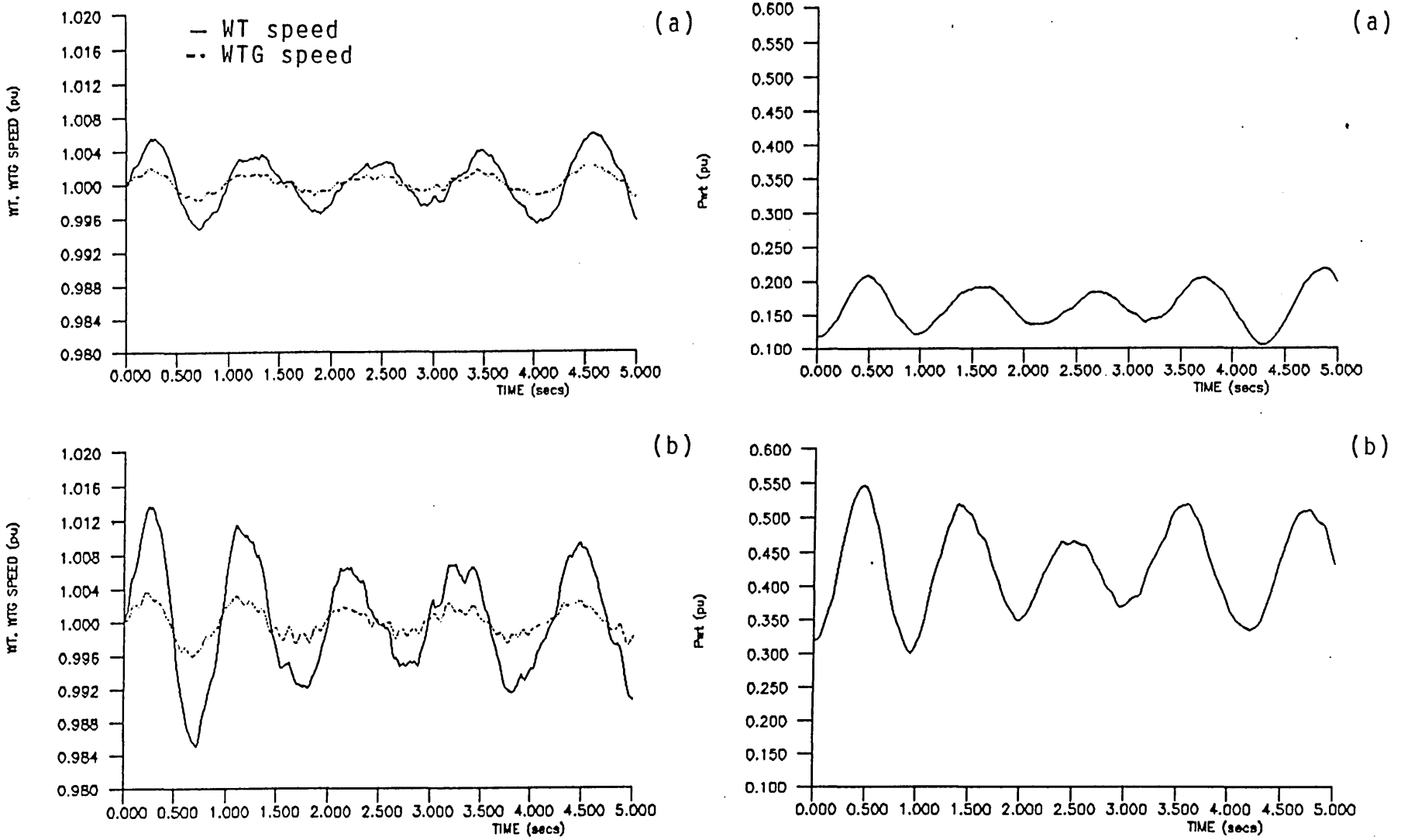

FIGURE 5.16 Simulation of the WTG connected to the grid (mechanical damping=220Nm/rad/s) when subjected to gaussian wind speeds at:(a) 4.5m/s (mean)
(b) 10 m/s (mean)

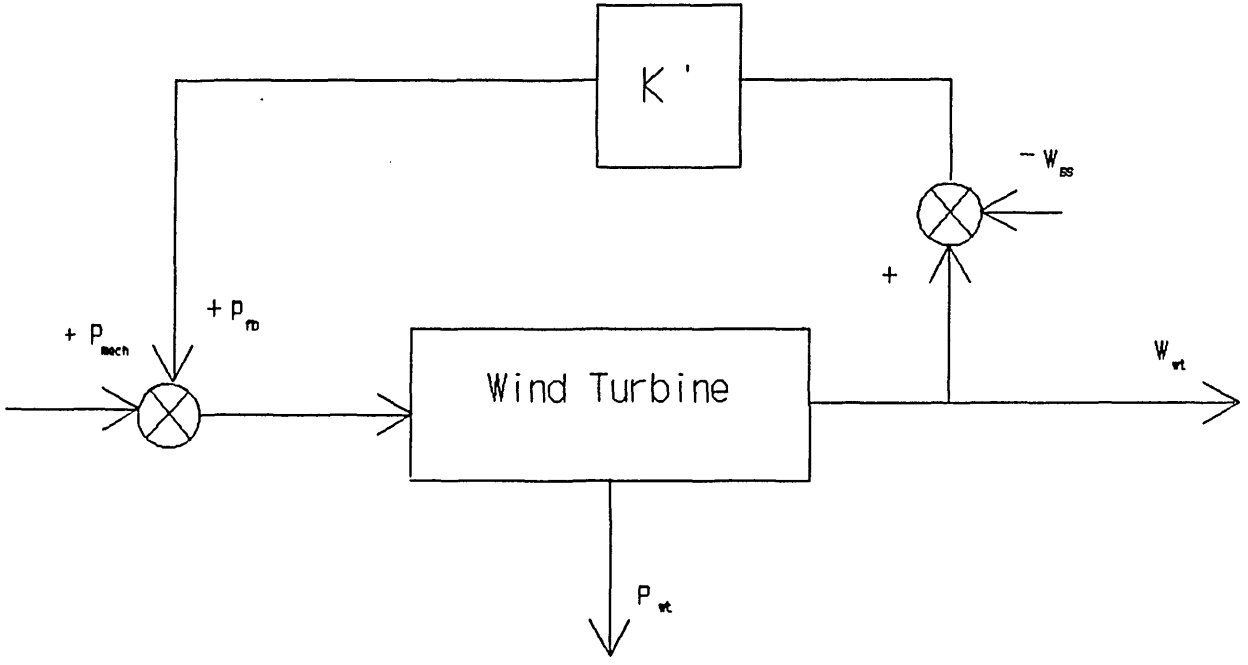

FIGURE 5.17 Block diagram representation of negative damping due to the Cp/lambda characteristic of the Wind Turbine at high wind speeds.

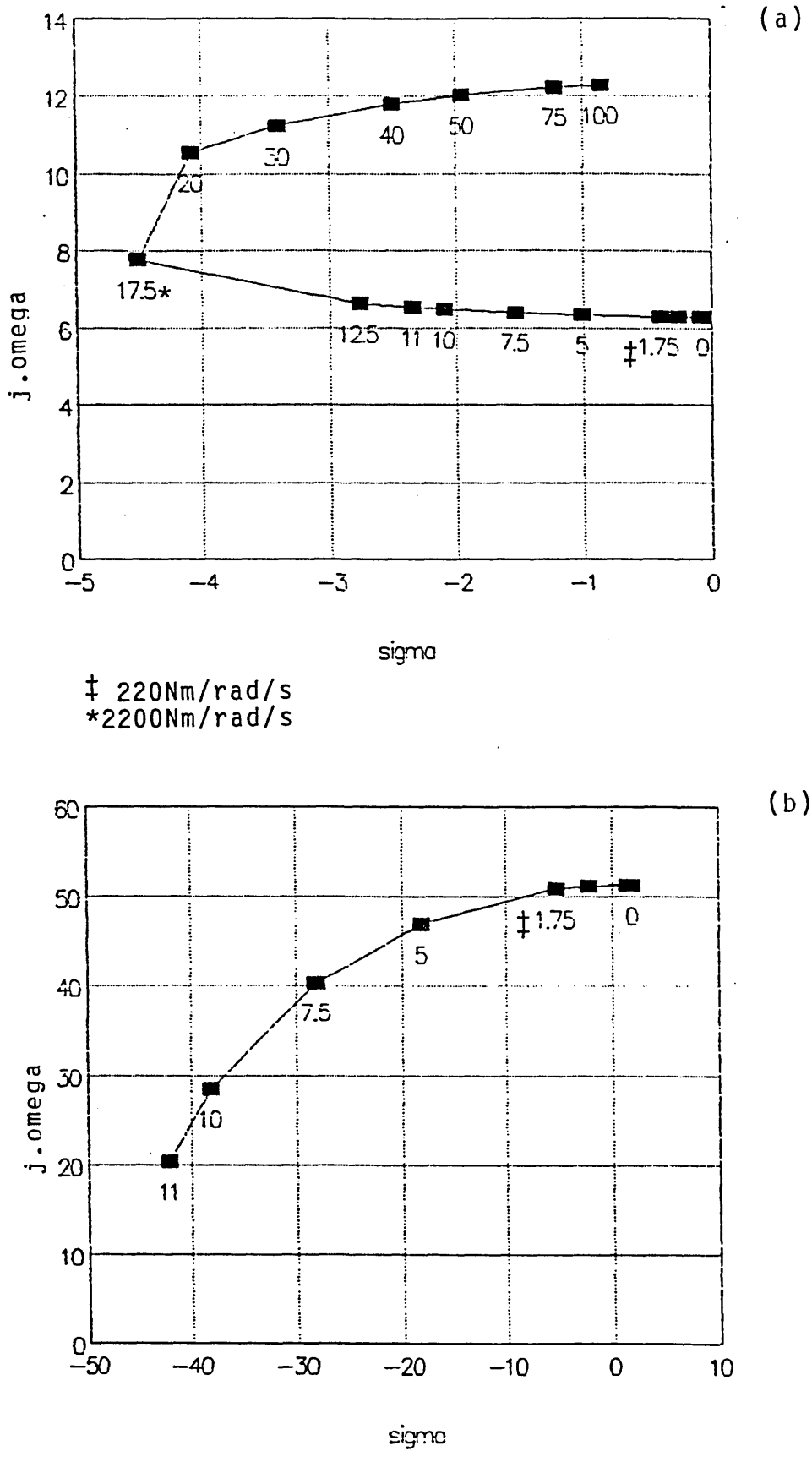

FIGURE 5.18 Root locus of the effect of increased mechanical damping on the WTG connected to the grid with UPF exciter
(a) low frequency (b) high frequency modes

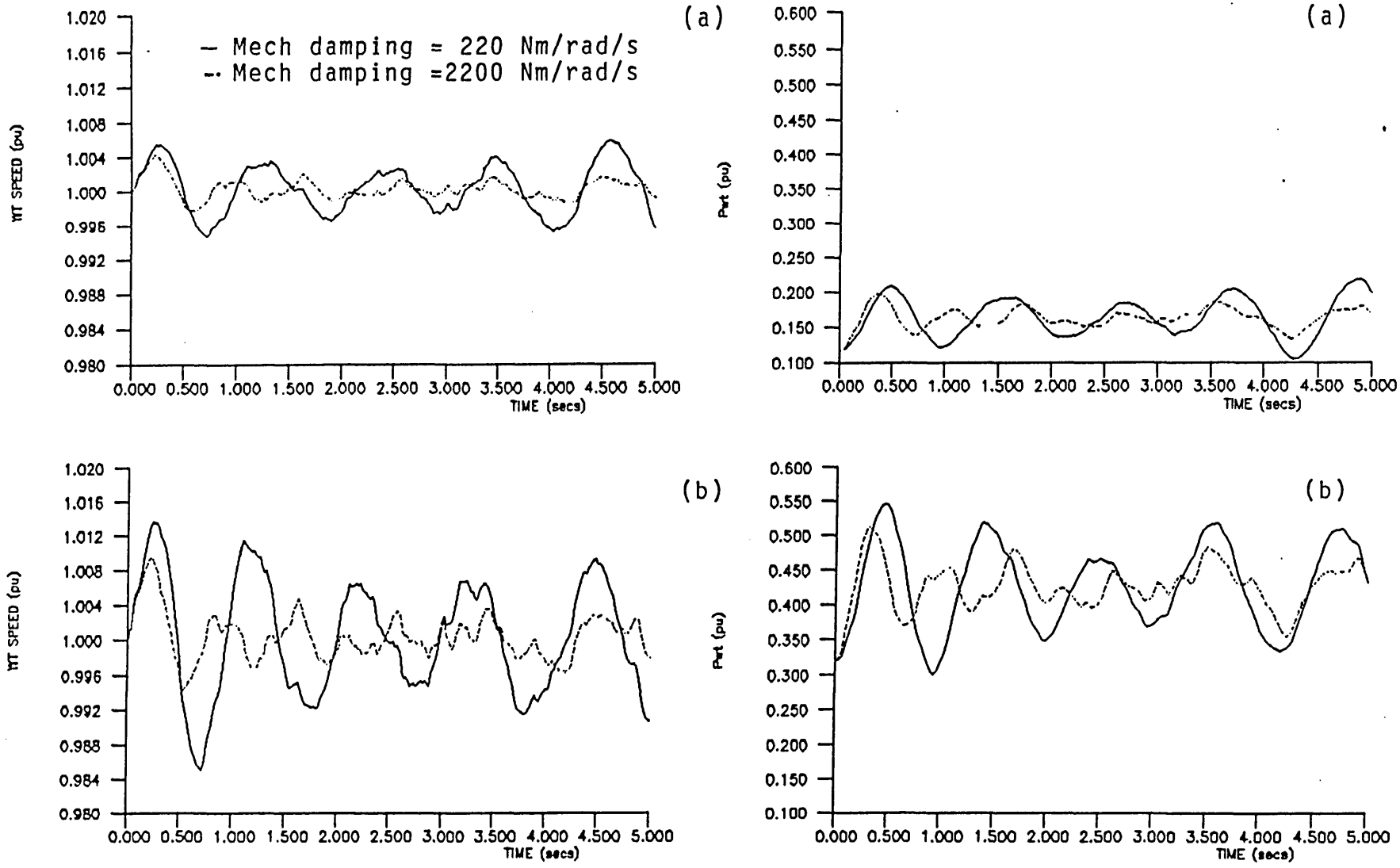

FIGURE 5.19 Effect of increased mechanical damping on the WTG connected to the grid (simulated) when subjected to gaussian wind speeds at: (a) 4.5 m/s (mean) (b) 10 m/s (mean)

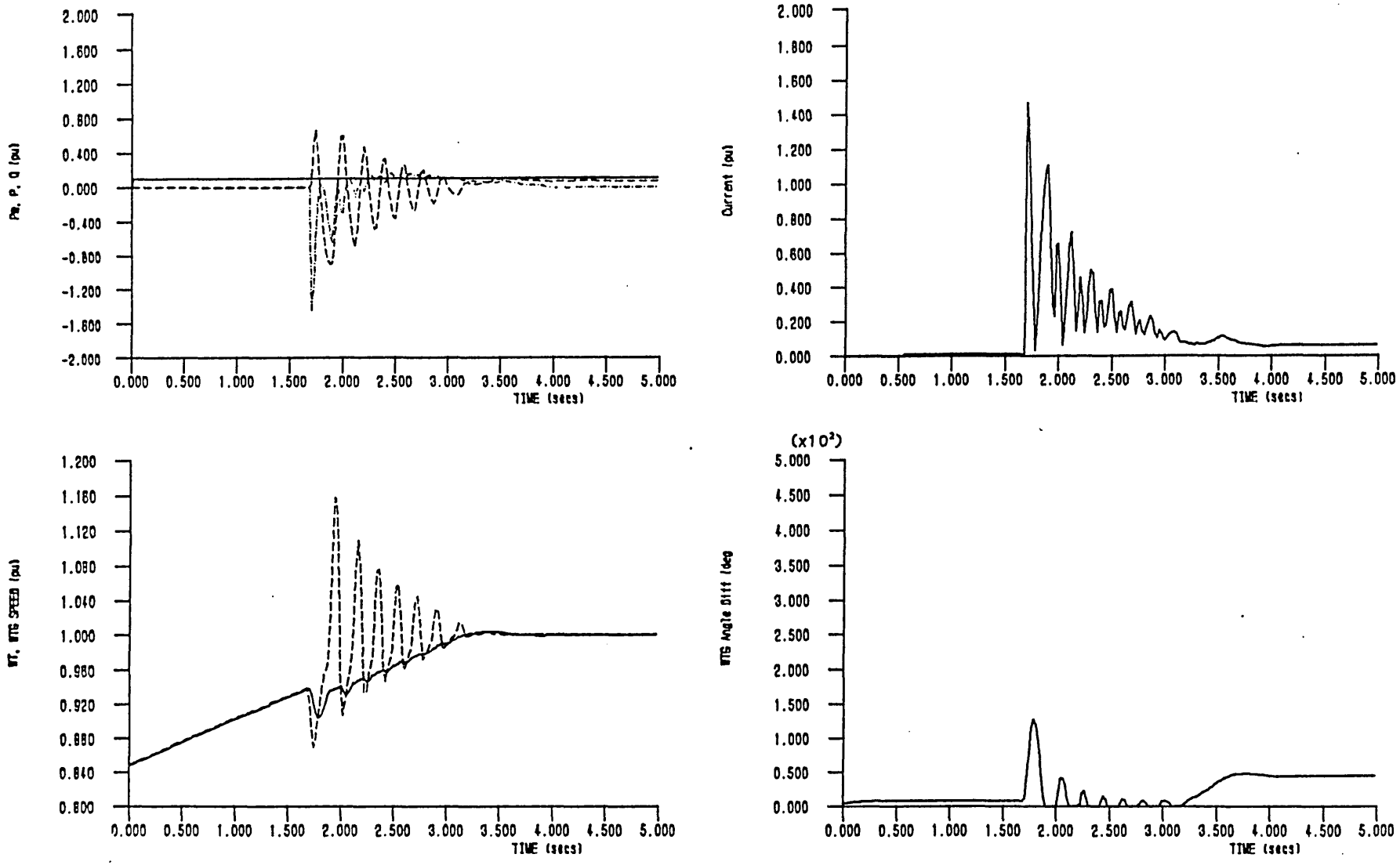

FIGURE 5.20 WTG Synchronised onto the grid (simulated) at 0.94 pu speed with mechanical damping = 2200 Nm/rad/s - Relative load angle =180°

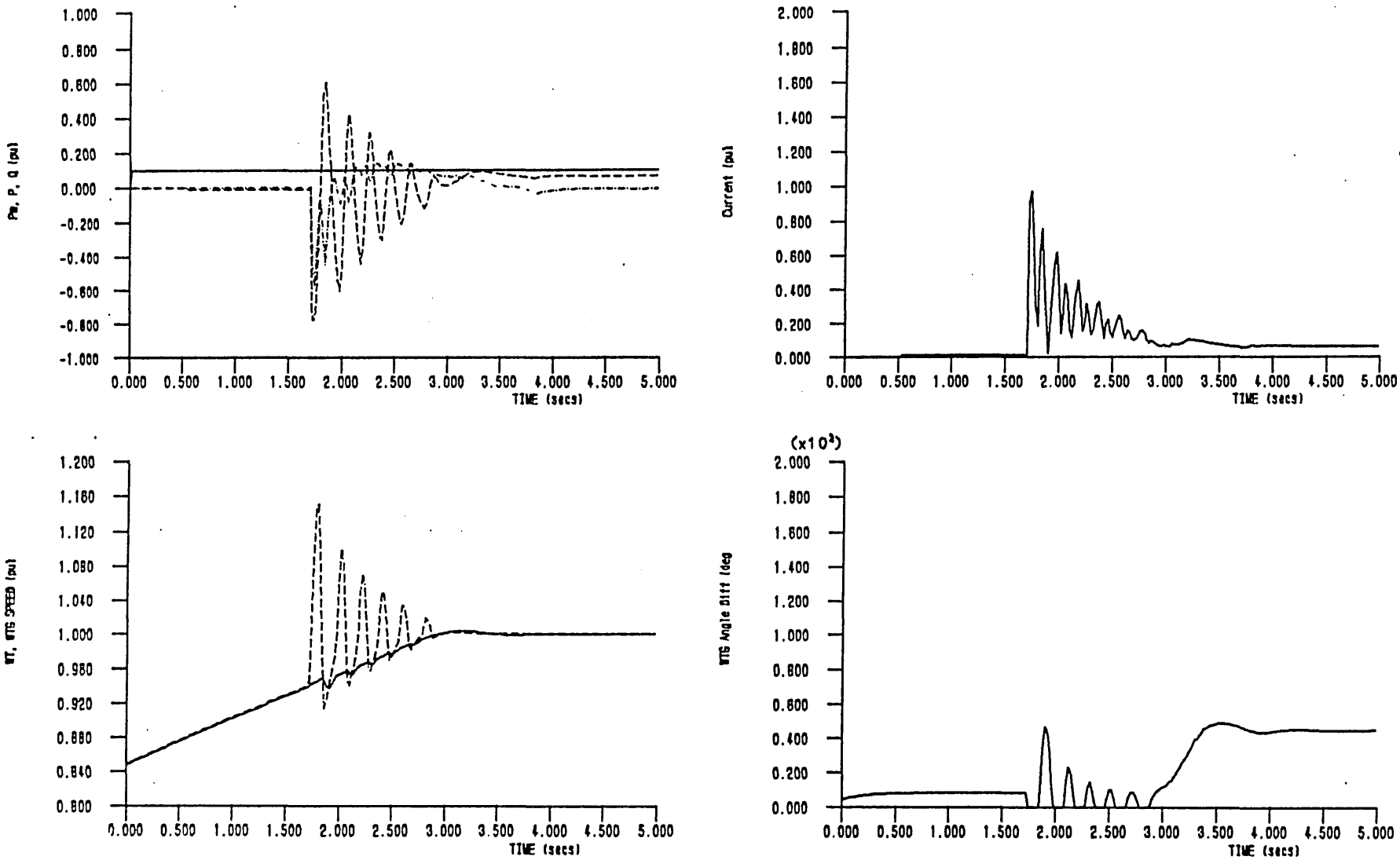

FIGURE 5.21 WTG Synchronised onto the grid (simulated) at 0.94pu speed with mechanical damping = 2200 Nm/rad/s - Relative load angle = 270°

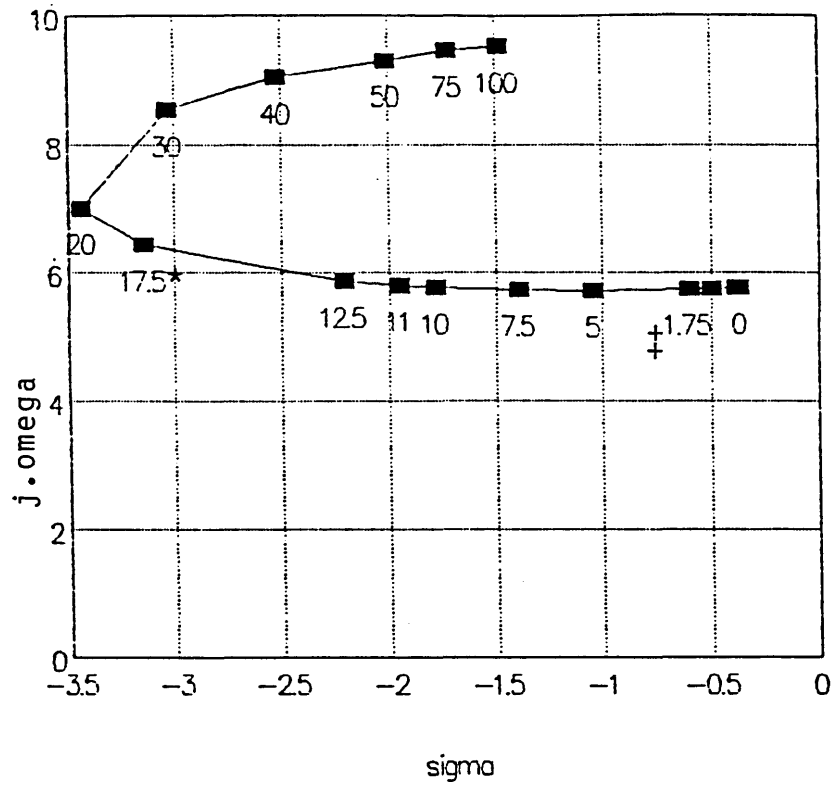

‡ 220 Nm/rad/s
* 2200 Nm/rad/s

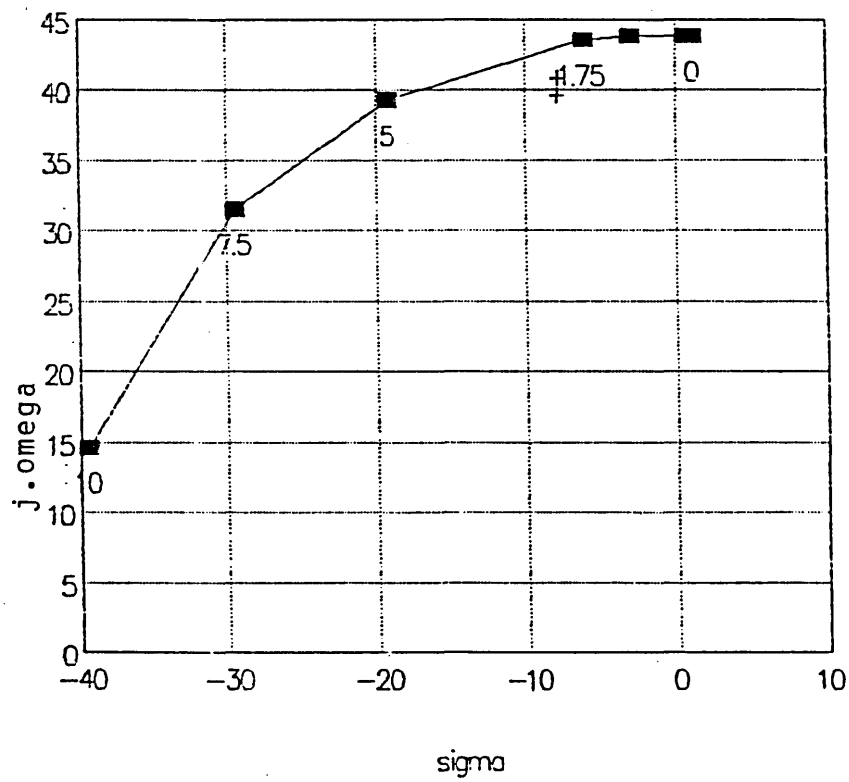

FIGURE 5.22 Root locus of the effect of increased mechanical damping on the WTG connected to the grid with constant excitation (a) low frequency (b) high frequency modes

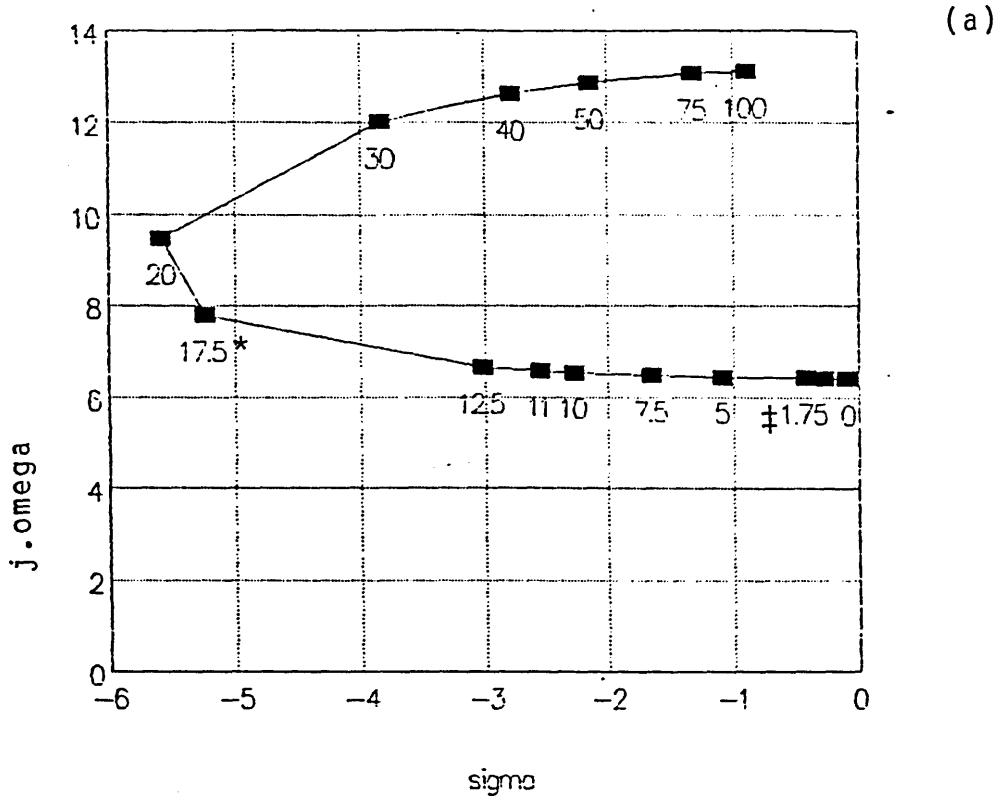

FIGURE 5.23 Root locus of the effect of increased mechanical damping on the WTG connected to the grid with the exciter time constant reduced one hundred fold (a) low frequency (b) high frequency modes

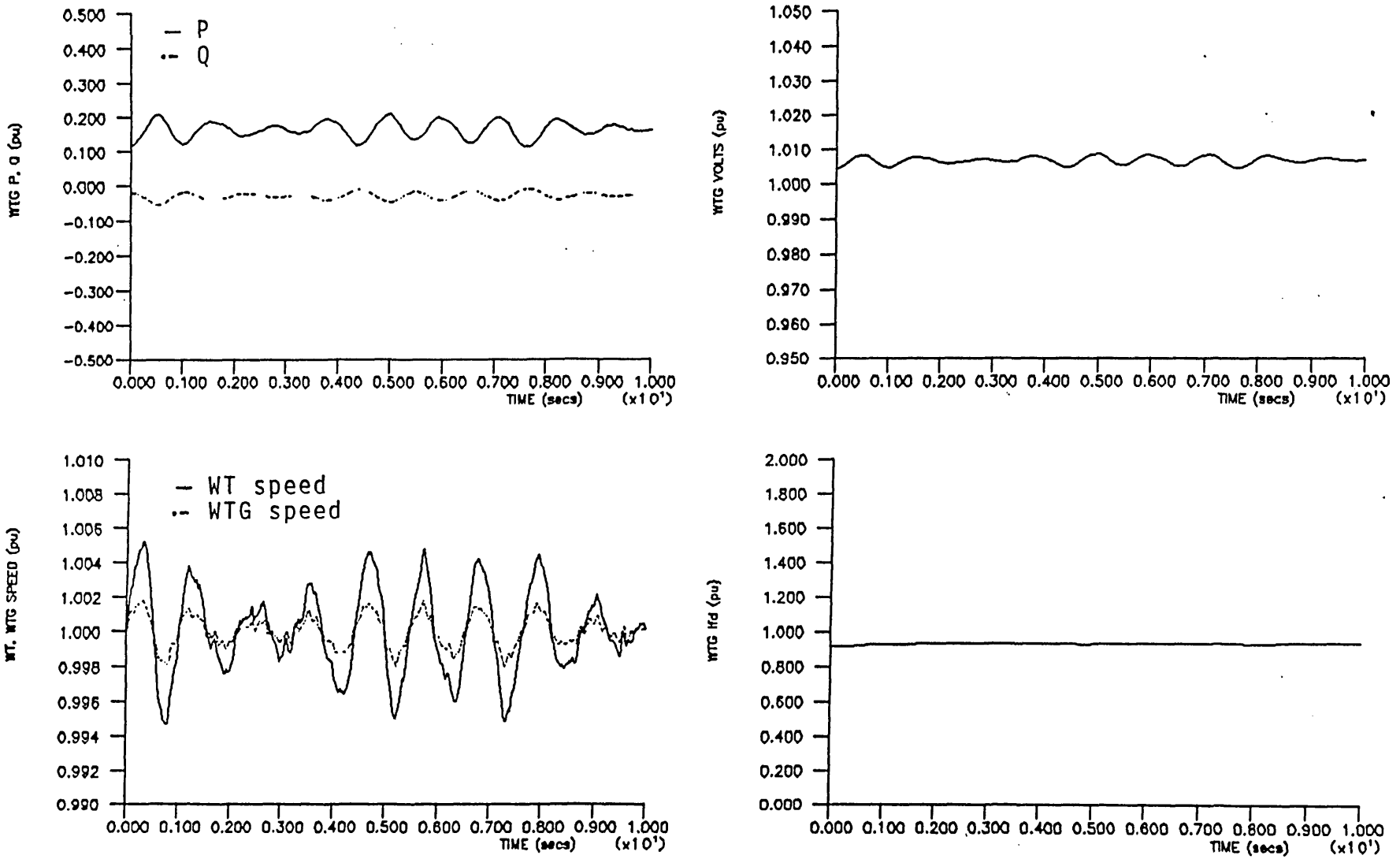

FIGURE 5.24 WTG plus AVR connected to the grid with gaussian WT mechanical power inputted - No PSS

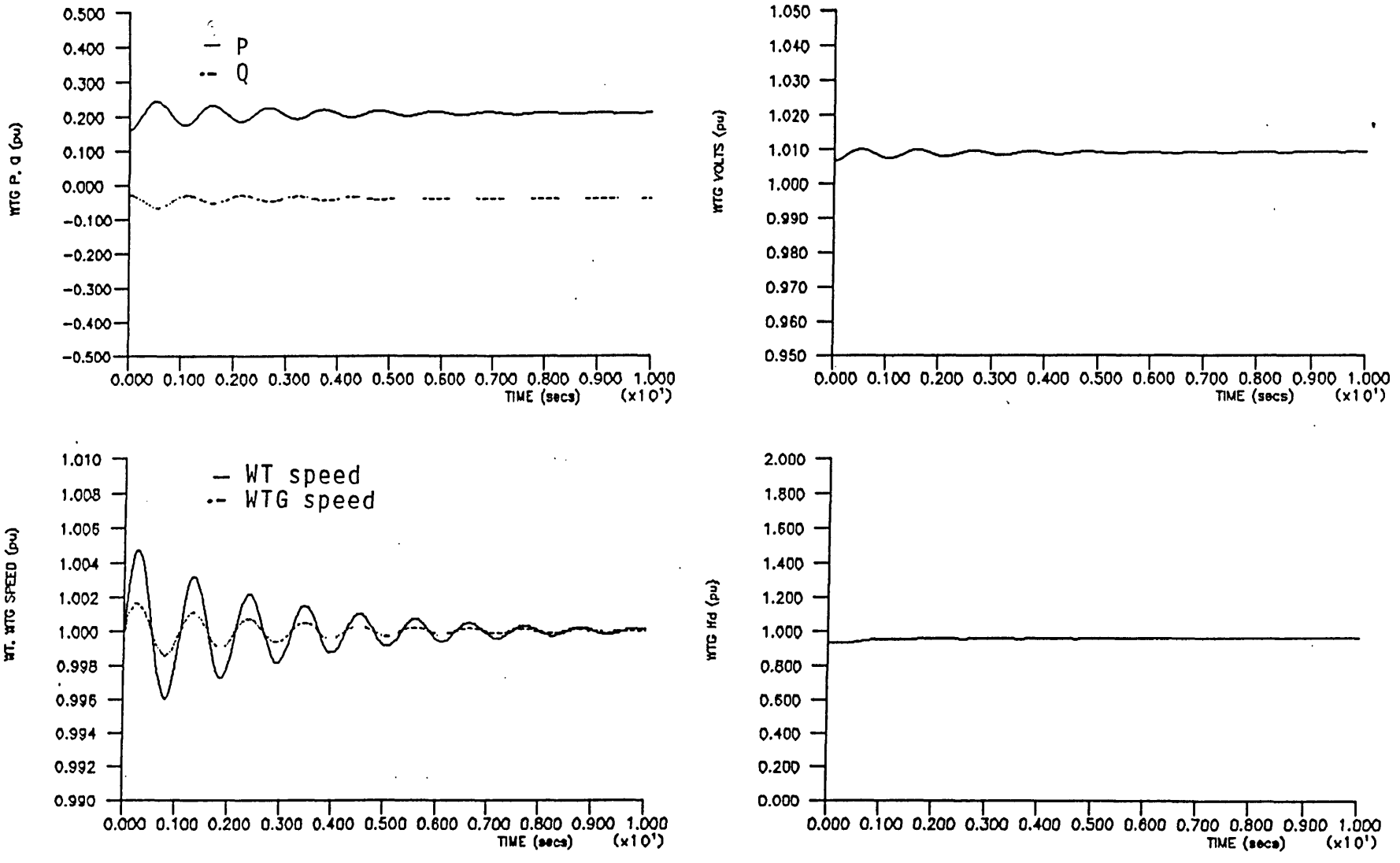

FIGURE 5.25 WTG plus AVR connected to the grid subjected to a step change in WT mechanical power - No PSS

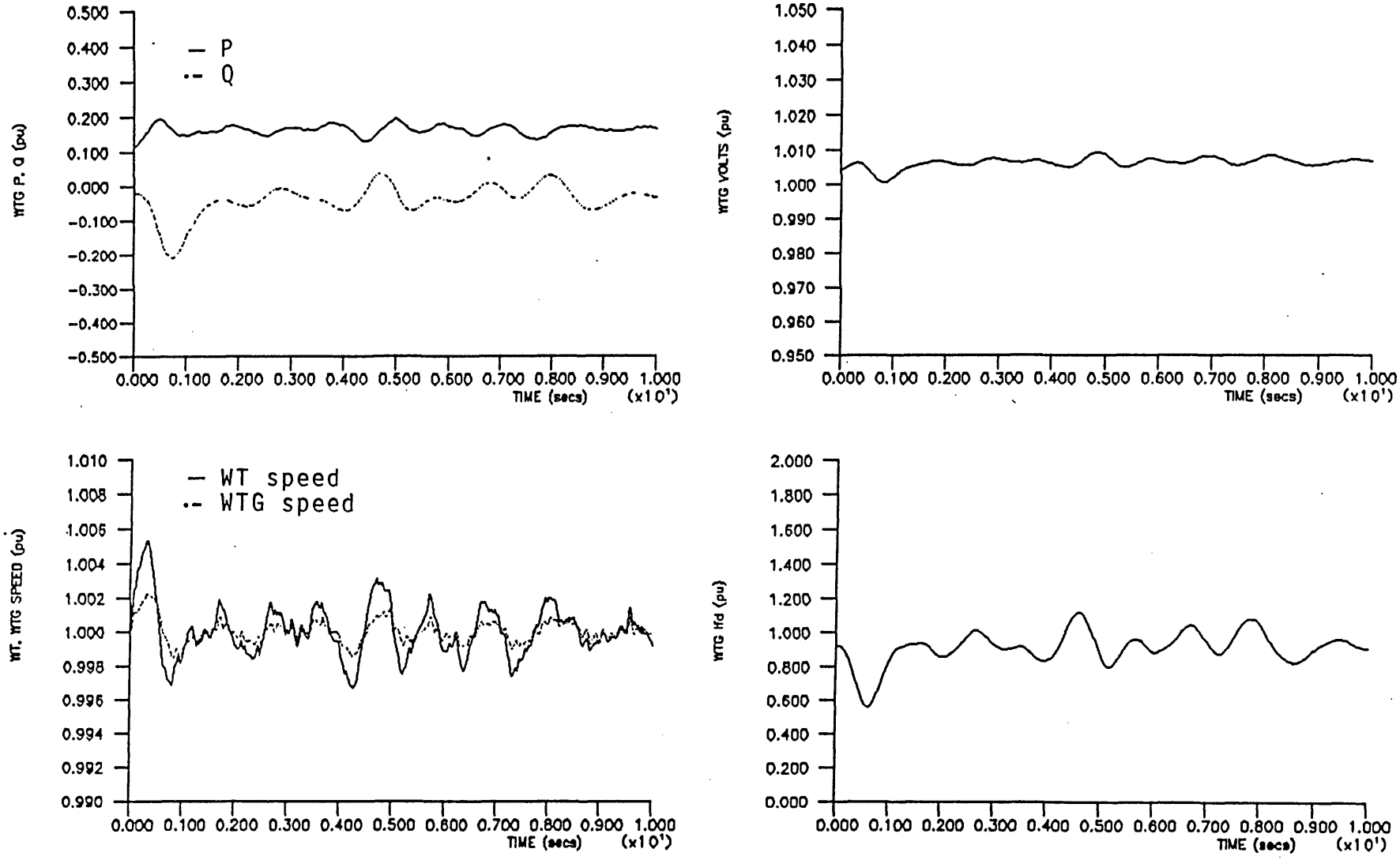

FIGURE 5.26 WTG plus AVR connected to the grid with gaussian WT mechanical power inputted - with PSS (T1 = -3.626, T2 = 0.2257)

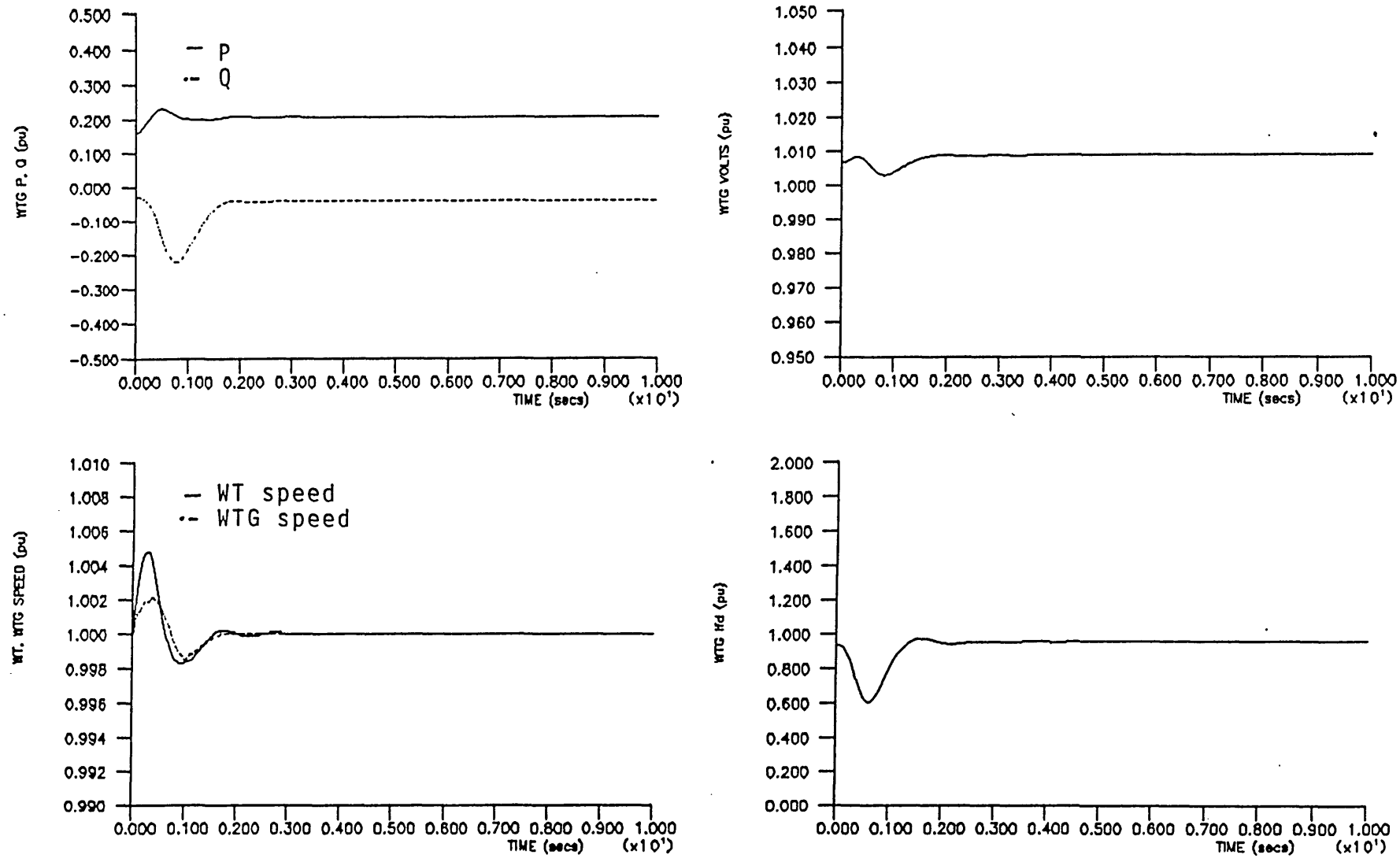

FIGURE 5.27 WTG plus AVR connected to the grid subjected to a step change in WT mechanical power - with PSS (T1 = -3.626,T2 = 0.2257)

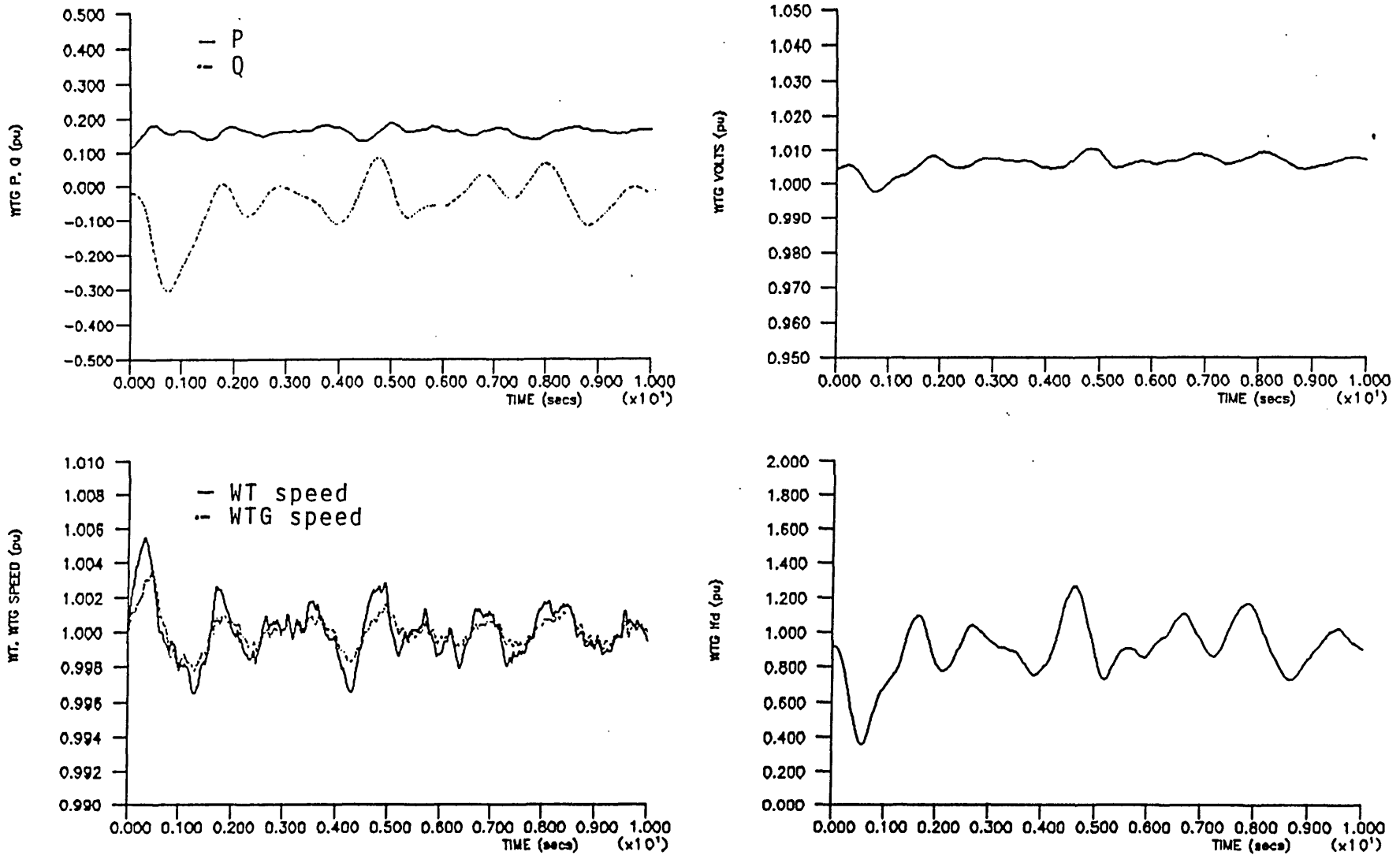

FIGURE 5.28 WTG plus AVR connected to the grid with gaussian WT mechanical power inputted - with PSS (T1 = -7.99, T2 = 0.178)

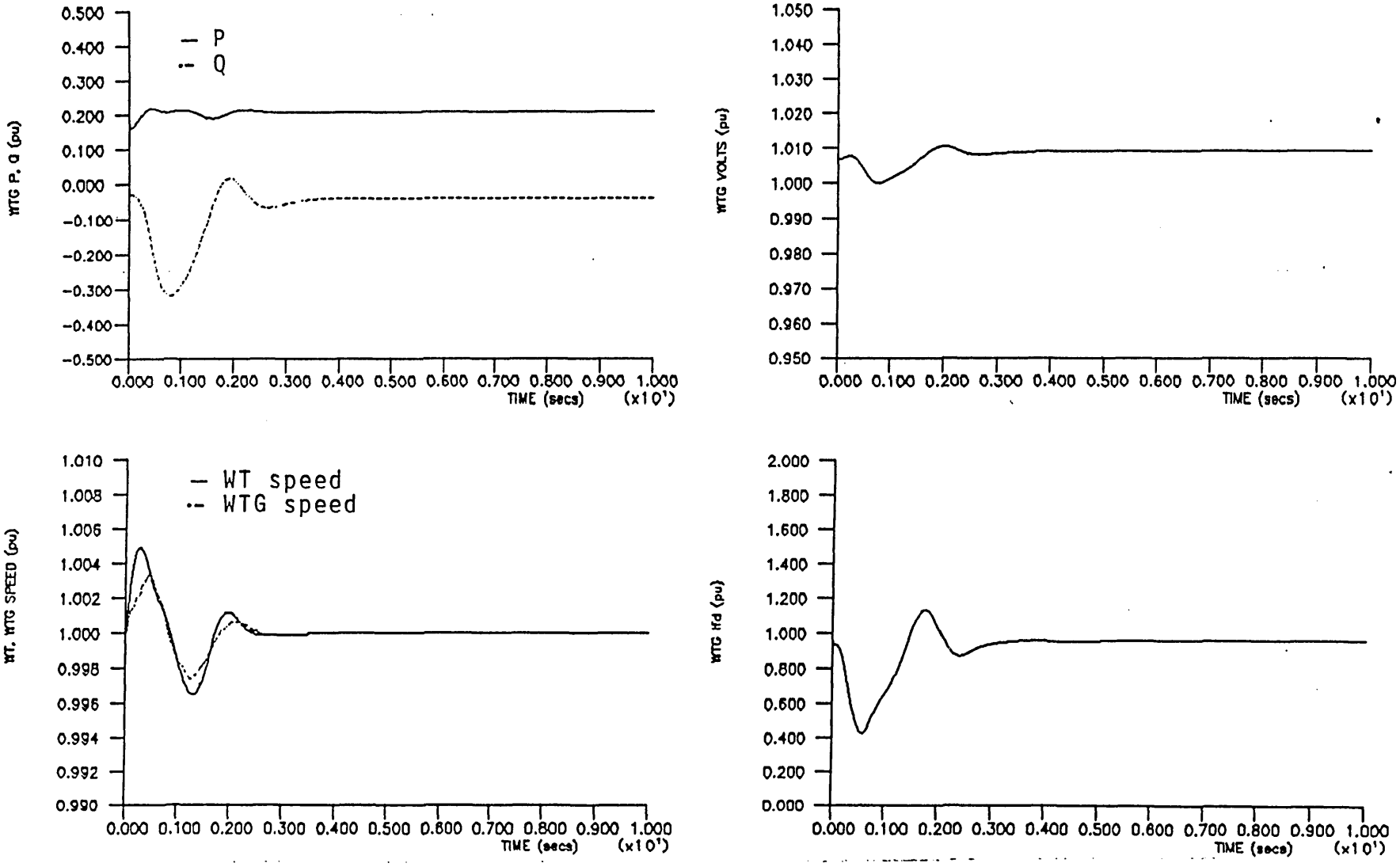

FIGURE 5.29 WTG plus AVR connected to the grid subjected to a step change in WT mechanical power - with PSS (T1 = -7.99, T2 = 0.170)

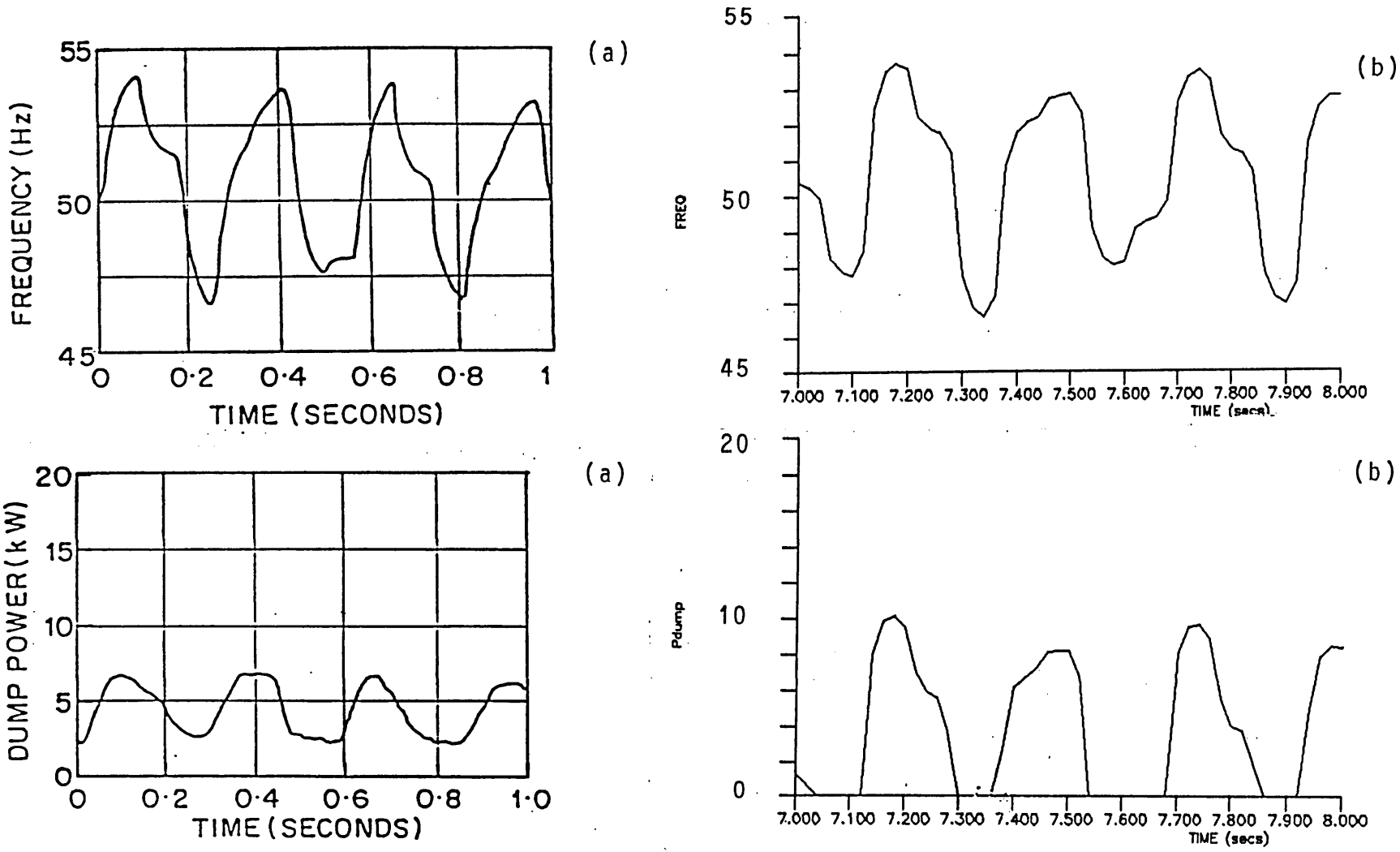

FIGURE 5.30 Effect of the frequency controlled dump load on the autonomous WTG
(a) measured (b) simulated

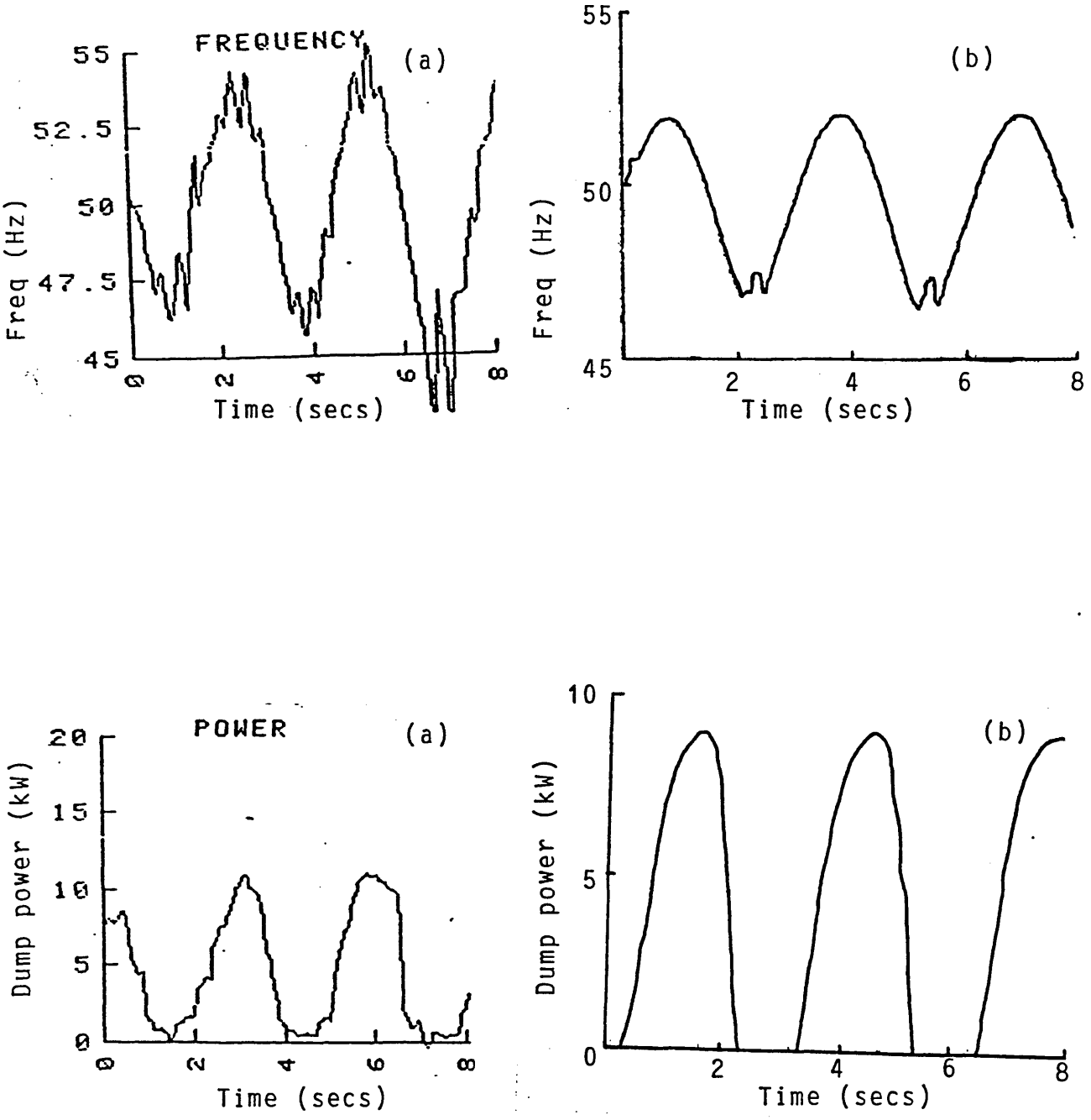

FIGURE 5.31 Effect of frequency control dumpload (integral control) on the autonomous WTG
(a) measured (b) simulated

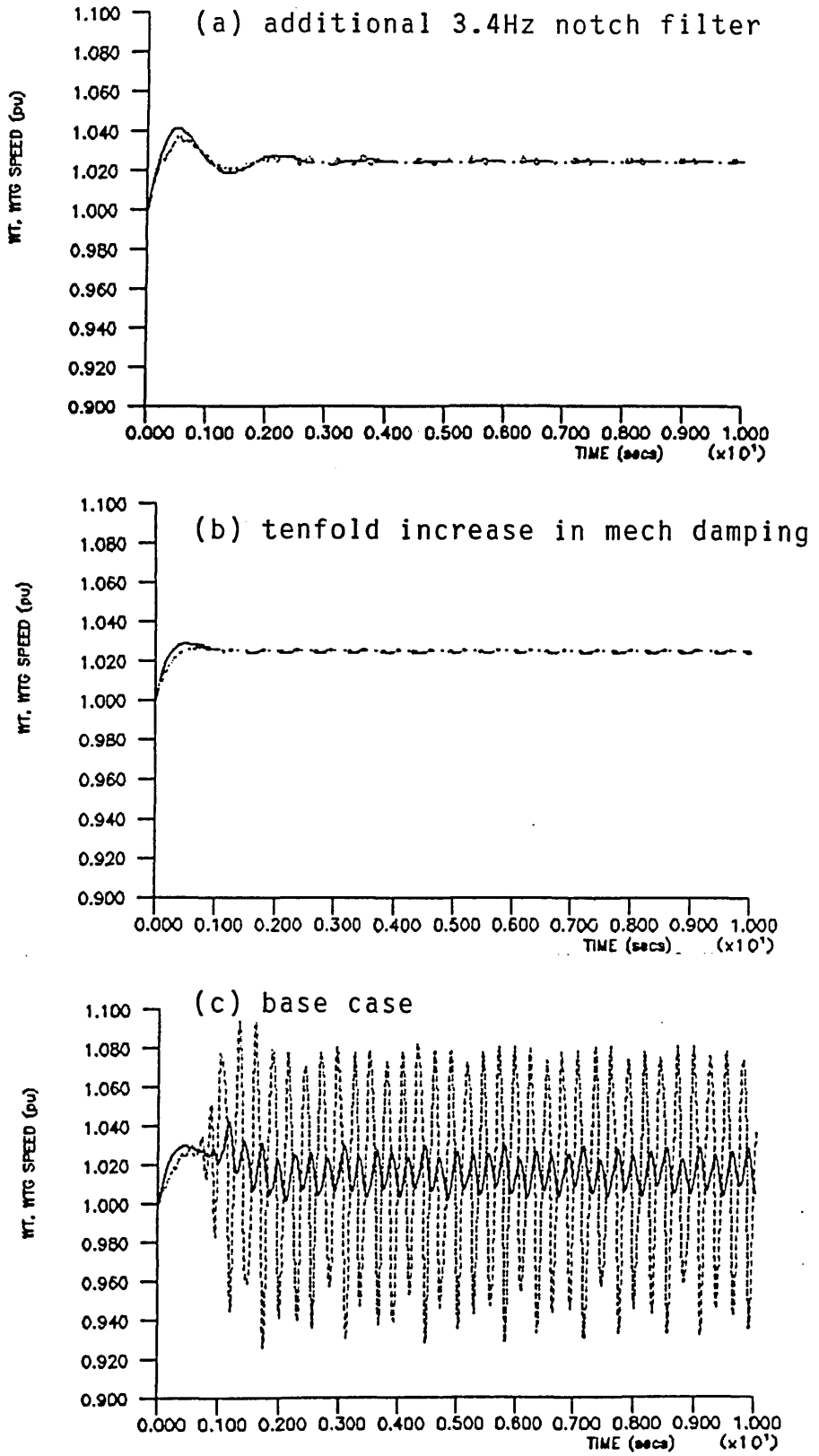

FIGURE 5.32 Methods to remove the 3.4Hz oscillation under proportional frequency control

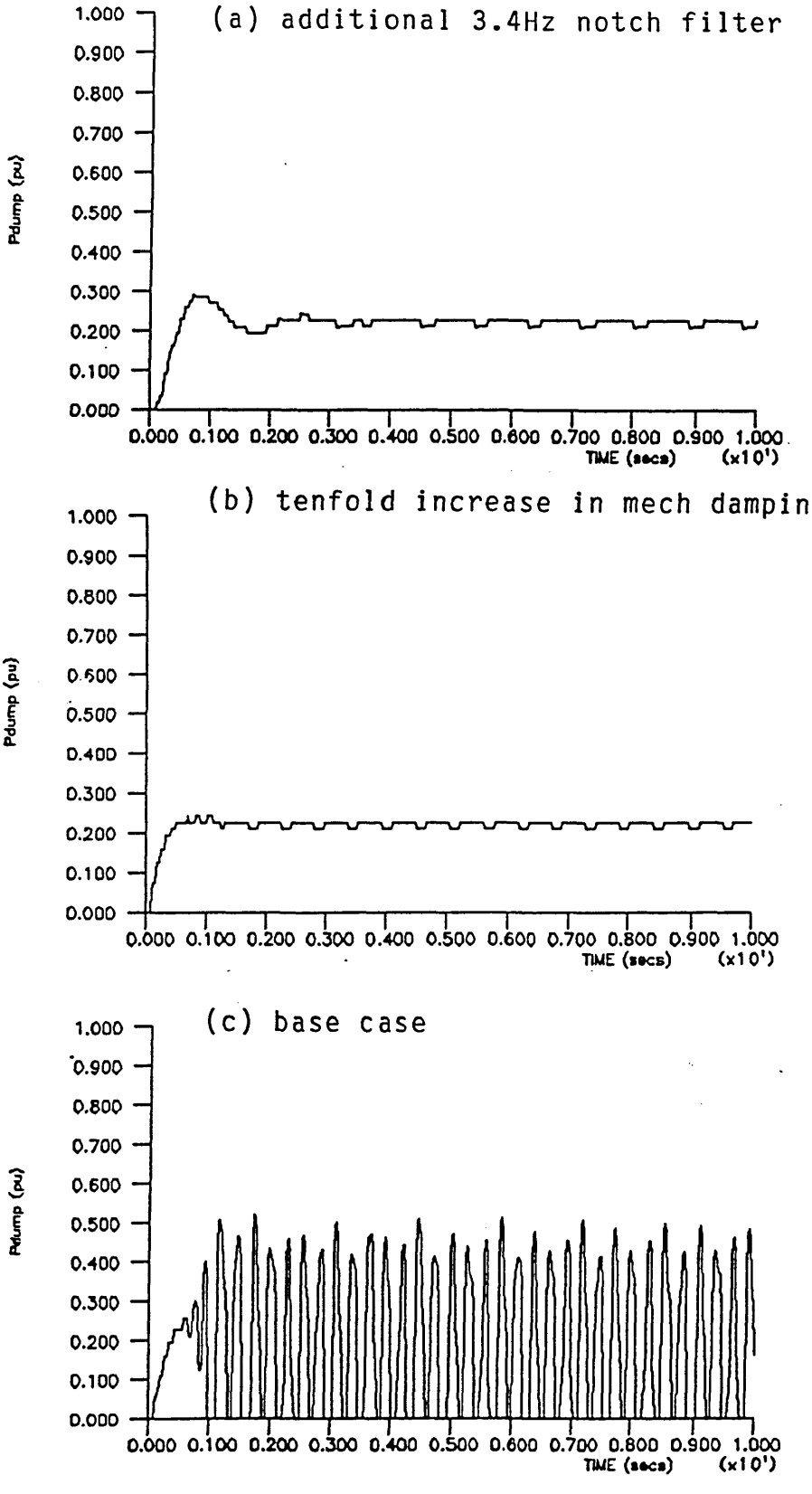

FIGURE 5.32 contd

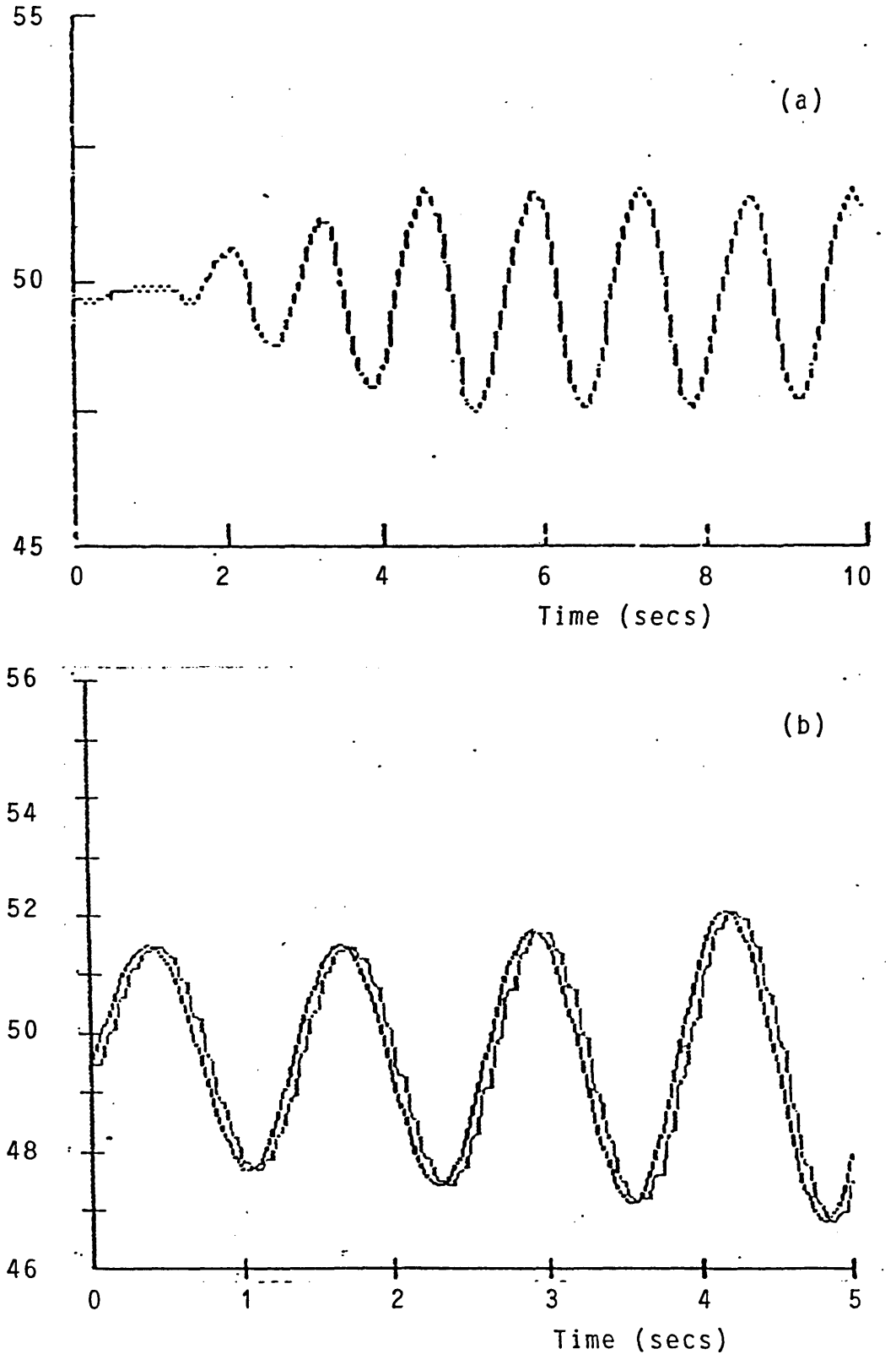

FIGURE 5.33 Stability limit with integral control of the frequency based dumpload controller under autonomous diesel generator operation (a) measured (b) simulated

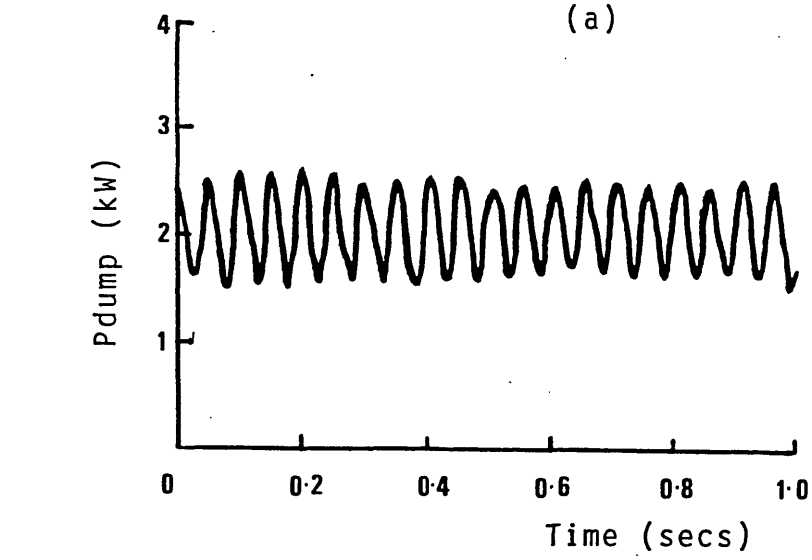

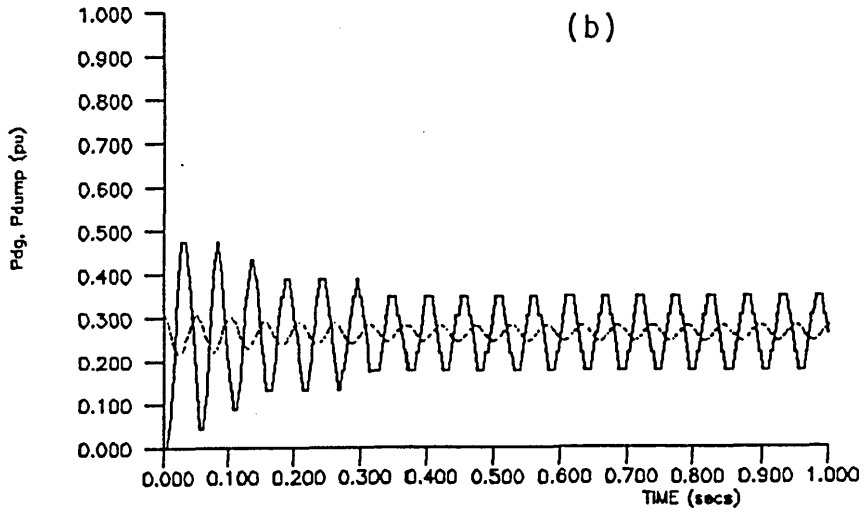

FIGURE 5.34 Stability limit with proportional control using power based dumpload controller under autonomous diesel generator operation (a) measured (b) simulated

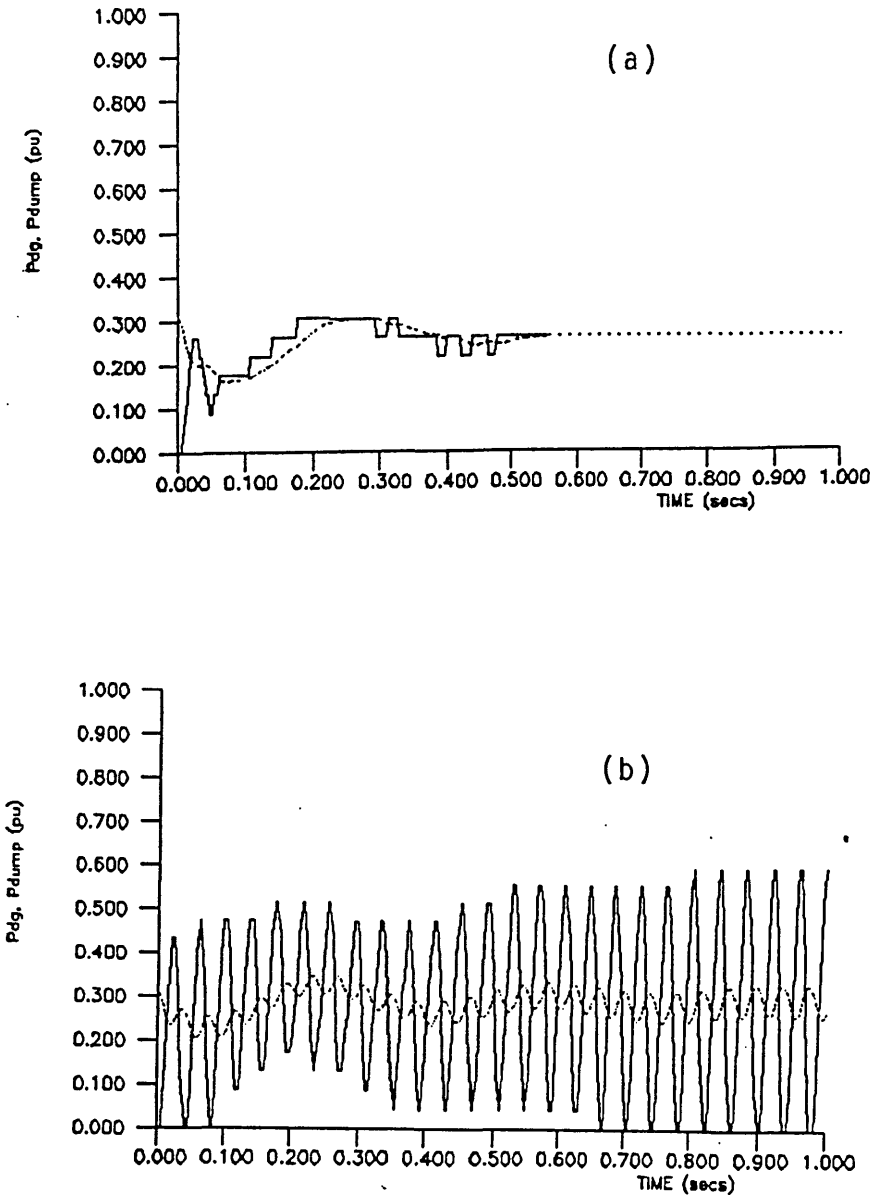

FIGURE 5.35 Inclusion of 3.4Hz notch filter in the power based dumpload controller under diesel generator operation
(a) Kpp = 5kW/kW
(b) Kpp =10kW/kW (stability limit)

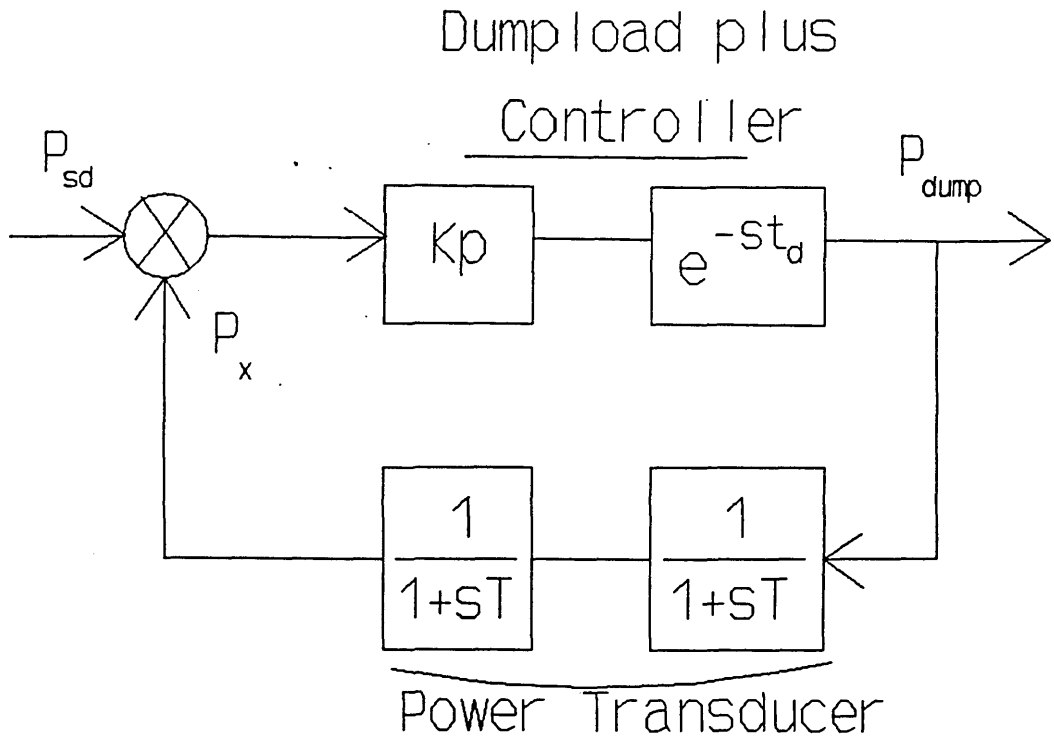

FIGURE 5.36 Discrete Control Representation of the Dumpload Controller with Power Feedback

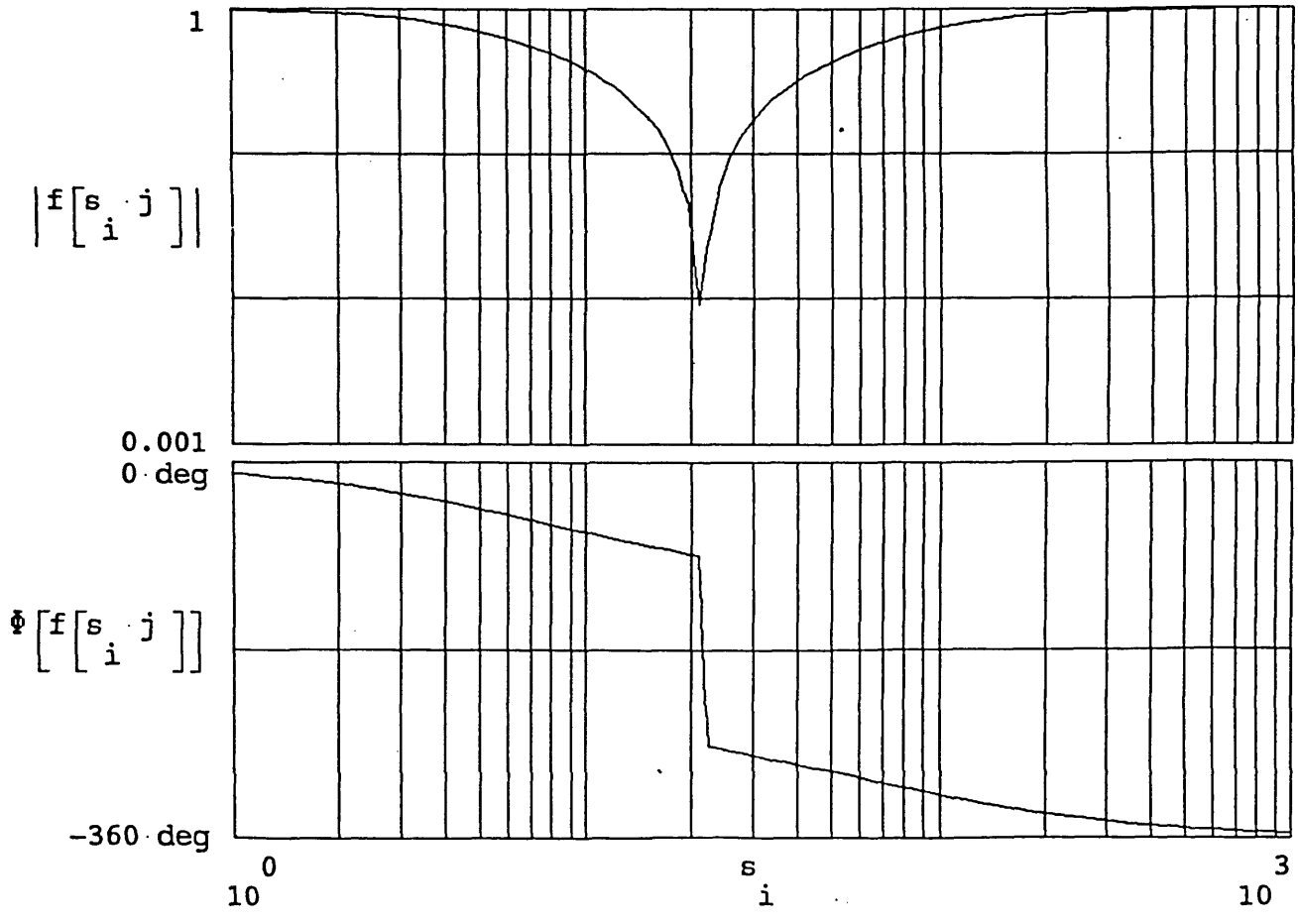

FIGURE 5.37 Bode Plot of the 3.4Hz "Notch" Filter

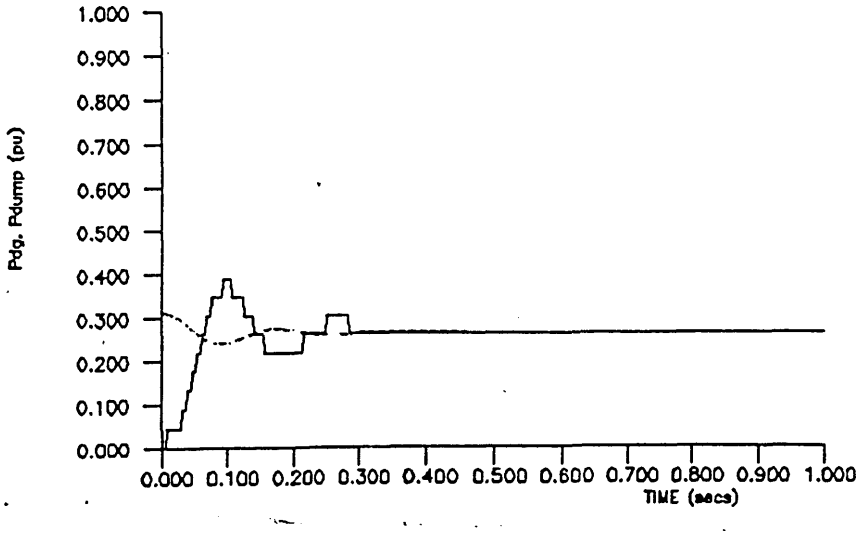

FIGURE 5.38 Inclusion of 1.3 Hz lowpass filter in the power based dump load controller under diesel generator operation (Kpp = 5kW/kW)

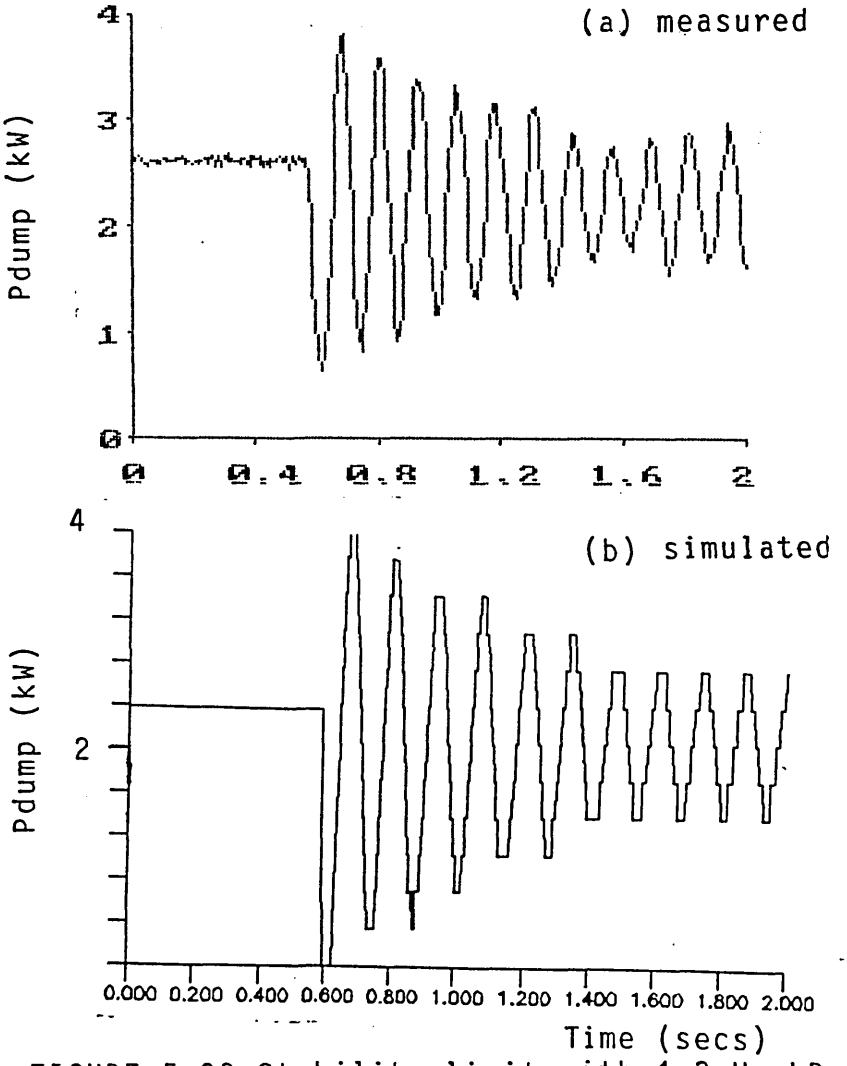

FIGURE 5.39 Stability limit with 1.3 Hz LP filter - Kpp = 10kW/kW

CHAPTER 6

THE AUTONOMOUS WIND/DIESEL/FLYWHEEL SYSTEM

6.0 Introduction

This chapter uses the lessons learnt from the validation and single prime-mover studies of the previous chapters in order to examine certain options that enable the autonomous wind/diesel/flywheel system to perform as a stable electrical platform.

Initially, an examination was carried out into the effect of the wind turbine excitation system on the steady-state behaviour of the wind/diesel/flywheel system.

As in the previous chapter, small signal analyses were used to examine certain critical effects:

1) Wind Turbine mechanical damping.
2) Wind Turbine exciter.
3) Flywheel size.
4) The Wind Turbine's C_p/λ curve at low and high wind speeds.

Such studies therefore provide guides to the small signal stability of the wind/diesel/flywheel system and will also point to the viability of the full non-linear model options.

The full non-linear models were used to examine the effects of the following on system stability:

1) The dump-load under frequency and power plus frequency control.
2) Diesel engine disengagement from the system.
3) Diesel engine crash-started onto the system.

In order to make comparison with experimental results from the RAL equipment, three sizes of flywheel are considered:

1) Jfly=0.0kg m^2 (wind/diesel system).
2) Jfly=11.8kg m^2 (ω_{fly}=1125 rpm).
3) Jfly=58.0kg m^2 (ω_{fly}=2500 rpm).

The flywheel sizes allow the study of this form of storage at the hundreds of seconds, tens of seconds and no storage levels.

6.1 Steady-State Behaviour of the Wind/Diesel/Flywheel System

One of the main areas of concern identified in the previous chapter was the ability of the wind turbine excitation system to satisfactorily control the reactive power flow over the full load range whilst grid-connected. A similar study was therefore carried out to examine the effect of the wind turbine as a main prime-mover in the autonomous wind/diesel system with:

1) The Unity Power Factor exciter.
2) The CONTROLOGY AVR15R.
3) The CONTROLOGY AVR15R plus Quadrature Droop Compensation.

Two versions of program PARDYN were adapted to allow the study of the effects of both wind turbine excitation systems on the steady-state behaviour of the wind/diesel system at increasing levels of wind turbine mechanical power and consumer load.

6.1.1 Wind Turbine Generator with UPF Exciter

Fig 6.1 illustrates the effect of increasing wind turbine mechanical power input at consumer loadings of 0%, 25%, 50%, 75% and 100% of full load. Throughout the study, the reference voltage of the diesel generator AVR15E is held at 1.0 pu.

Fig 6.1(a) is the graph of wind turbine generator reactive power output versus wind turbine mechanical power input. It shows that as the mechanical power is increased the wind turbine generator changes from a sink of reactive power into a source. The effect of increasing consumer load approximates to that of an overall reduction in the excitation level. At low levels of wind turbine mechanical power, there is an increase of reactive power into the wind turbine. Whilst at high levels of wind turbine mechanical power, the reactive power flow out of the wind turbine generator is reduced. This

is borne out by Fig 6.1(b) which is the graph of wind turbine field current versus wind turbine mechanical power. As the consumer loading increases, the field current is reduced across the range of wind turbine mechanical power.

The graph of wind turbine terminal voltage versus wind turbine mechanical power, Fig 6.1(c), also demonstrates the effect of increased excitation for increased wind turbine mechanical power and decreased excitation at higher consumer loadings. However, as the mechanical power increases, a maximum voltage of approximately 415V (1.0 pu) is reached. A further increase in mechanical power results in a gradual fall in the wind turbine terminal voltage as the excitation system increasingly fails to deliver sufficient field current.

Over the ranges tested in this simulation the wind turbine reactive power flows are from -0.6kVAr to +3.2kVAr whilst the wind turbine terminal voltage regulation is from 398V to 415V.

The graphs therefore demonstrate the poor reactive power flow performance due to the UPF exciter, whilst, the voltage regulation at the terminals of the wind turbine is satisfactory (4%).

Two possible alternatives to improve reactive power flow are available:

1) The excitation current of the UPF exciter is reduced across its range via the preset excitation current potentiometer. Although this would result in a more balanced reactive power flow across the range it would also lead to a worsening of the wind turbine generator terminal voltage regulation.

2) The replacement of the UPF exciter by the CONTROLOGY AVR15R.

6.1.2 Wind Turbine Generator with the CONTROLOGY AVR15R

Similar studies were carried out on the wind/diesel system as per the previous section, but with the UPF exciter replaced by the CONTROLOGY AVR15R.

From Fig 6.2 it is apparent that although the inherent integrating action of this device leads to a constant terminal voltage, the large reactive power flows (to 3.7kVAr) are totally unsuitable for this small system. At this high level of reactive power flow, the diesel generator not only has to totally supply the consumer load at full load (plus system losses) but must also absorb the kVArs produced by the wind turbine generator. The apparent power rating of the diesel generator (8.5kVA) is therefore exceeded. Furthermore, its field is weakened, resulting in a worsening of the diesel generator's stability. The inclusion of Quadrature Droop

Compensation (QDC) into the wind turbine excitation system was therefore studied.

6.1.3 Wind Turbine Generator with the CONTROLOGY AVR15R plus QDC

As in the single prime-mover studies, the results with 25% and 35% QDC are presented. Again, simulation studies of the form carried out in the previous two sections were undertaken.

Fig 6.3 shows that with 25% QDC, reactive power flows are limited to +0.5kVAr to -0.7kVAr, whilst voltage regulation is between 407V to 412V (1.2%) over the full wind turbine mechanical power and consumer load ranges. With 35% QDC, reactive power flows are limited to +0.7kVAr to -0.3kVAr and voltage regulation of 407V to 412V, as illustrated by Fig 6.4.

The results demonstrate that both levels of QDC enable satisfactory ranges of reactive power flows to be attained whilst voltage regulation is good. It is apparent that fine tuning could be achieved by adjustment of the QDC to approximately 30% to provide a slightly more balanced reactive power flow range.

6.2 Small Signal Eigenvalue Analyses

The small signal perturbation techniques described in Chapter 4 were used to investigate the effect of certain critical components upon the dynamic stability of the wind/diesel/flywheel system.

6.2.1 Wind Turbine Mechanical Dampers (UPF Exciter)

As discussed in the previous chapter, tuning of the wind turbine mechanical dampers had helped to lessen the susceptibility of the wind-excited 1Hz mode of oscillation when it was grid-connected. A similar study was therefore undertaken to examine the benefits of retuning the mechanical dampers when the wind turbine formed part of the wind/diesel/flywheel system.

Fig 6.5 illustrates the effect of varying the wind turbine mechanical damping upon the two critical modes of oscillation of the wind/diesel system (J_{fly}= 0.0 kg m^2). Fig 6.5(a) is the Root Locus of the low frequency mode from which several points can be made:

1) Without the wind turbine mechanical dampers, the wind/diesel system is inherently unstable.

2) At the original level of wind turbine mechanical damping (220 Nm/rad/s) the wind/diesel system is very poorly damped (zeta=0.013) as compared to

zeta = 0.1 for the same mechanical damping whilst the wind turbine was grid connected. The frequency of this mode of oscillation has also increased from 0.94Hz to 1.27Hz.

3) The wind turbine mechanical dampers are optimally set at 2200Nm/rad/s. However, their benefit to the damping of this low frequency mode has been greatly reduced (zeta = 0.23 from zeta= 0.44 for the grid connected wind turbine).

From Participation Matrix analysis, the low frequency mode is due to the wind turbine swinging in anti-phase with the diesel. As with the grid connected wind turbine, it is susceptible to excitation from the wind.

The high frequency mode is shown in Fig 6.5(b). Again several points should be noted:

1) The inherently unstable nature of the system without the wind turbine mechanical damping is again demonstrated in this mode of oscillation.

2) At 220Nm/rad/s the mode has a slightly improved damping factor of 0.2 as opposed to 0.18 for the grid connected wind turbine.

3) At 2200Nm/rad/s this mode no longer exists for both system configurations.

The higher frequency mode is caused by the wind turbine generator and the busbar swinging against the wind turbine or the diesel engine. This mode can therefore be easily excited by incorrect action of the wind turbine generator excitation system or busbar activity (eg dumpload action).

Bleijs [6.1] using a simple mass/spring analogy (neglecting damping) of the wind/diesel system provides a succinct insight into the form of the two modes of oscillations as illustrated by Fig 6.6(a). However, the method did not include the effects of damping and does not suggest that without the wind turbine mechanical damping, the system is inherently unstable.

An immediate conclusion that can be drawn from this basic study is that further means, such as the use of an AVR (with Power System Stabilisation), must be investigated to improve the damping of the wind-excited low frequency mode.

6.2.2 Wind Turbine Mechanical Dampers (UPF Exciter)-Effect of Flywheel Size

Table 6.1 consists of the critical eigenvalues at wind turbine mechanical damper values of 220 and 2200Nm/rad/s for flywheel inertias of 0.0, 11.8 and 57.8 Kg m^2.

Several conclusions can be drawn from these results:

1) Low frequency mode

a) From a Participation Matrix analysis, at the original level of wind turbine mechanical damping, the low frequency mode shape has noticeably changed from that of the system without the flywheel. The wind turbine now swings against the diesel/flywheel and therefore any beneficial damping from this node would be largely ineffective. The analysis also suggests that this mode may still be excited by the wind. This is concisely explained by the Mode shape diagram of Fig 6.6(b) [6.1].

b) The increase in flywheel size results in a slight worsening of the stability of this mode at the original damper setting (zeta=0.038, 0.034, 0.032). The Participation Matrix analysis had indicated that worsening stability could be due to a reduction in the ability of the diesel governor to aid in the damping of this mode as the flywheel size increases. However, these results demonstrate that the damping factor is only slighly worsened by the inclusion of the flywheel. Therefore, it appears that the diesel governor contributes little to the damping of the wind/diesel system. In all three cases the wind/diesel/flywheel system is very close to the stability limit. The system could therefore not satisfactorily operate with this level of mechanical damping.

c) At the larger mechanical damper setting the trend is reversed as the damping factor improves with increased flywheel size (zeta=0.233, 0.247, 0.248).

2) High Frequency Mode

a) The natural frequency (6.3Hz) and damping factor (zeta=0.17) of this mode is little effected by flywheel size, but can be stimulated by action at the busbar as can be seen from the high frequency mode shapes of Figs 6.6(a) and (b).

Also included in Table 6.1 are the eigenvalues for each flywheel size when the wind turbine rotor is decoupled (via the overrunning clutch) from its generator. Only one important oscillatory mode exists due to wind turbine generator swinging against the busbar. For all three cases this mode is very close to the system's stability limit (zeta=0.004). Again the natural frequency of this mode is little affected by flywheel size.

6.2.3 Wind/Diesel/Flywheel System (UPF Exciter)- Diesel Engine Disengaged

The wind/diesel/flywheel system was tested with the diesel engine mechanically disengaged, via the electromagetic

clutch, from the diesel generator/flywheel system. Table 6.2 lists the eigenvalues for the two natural frequency modes.

Without the flywheel, the dominant eigenvalue is at 8.2Hz and has a very poor damping factor of zeta=0.074. From the Participation matrix it appears that this mode is most sensitive to changes in the wind turbine generator speed or angle and to the internal emf of the diesel generator (Eqd'). A similar oscillatory mode has been identified at RAL whilst the diesel generator (without its engine) was coupled to the grid. Although no hard copies exist of the actual event, oscillations at approximately 8Hz were noted to develop leading to the tripping of the protection equipment. This leads to the conclusion that the diesel generator is itself inherently unstable and therefore relies upon its engine to provide the necessary damping.

Referring back to Fig 6.6, the mode shape of the low frequency mode changes from the wind turbine rotor swinging in anti-phase to the diesel engine (wind/diesel system) to that of the wind turbine rotor being unaffected by the action of the diesel generator and its engine (wind/diesel/flywheel system). Therefore, with the inclusion of the flywheel, the low frequency mode again becomes critical even though the diesel engine is disengaged. Likewise, the high frequency modes are similar to the full wind/diesel/flywheel system results.

6.2.4 Effect of Wind Turbine C_p/λ curve (UPF Exciter)

Table 6.3 lists the critical eigenvalues when the positive damping effect of the C_p/λ curve at high wind speeds is included in the model.

Table 6.3 demonstrates a large deterioration in stability at the original level of mechanical damping for both oscillatory modes. The low frequency mode is in fact unstable with the introduction of either flywheel size. At the higher level of mechanical damping the deterioration in stability is less pronounced.

6.2.5 CONTROLOGY AVR15R WITH 30% QDC

Table 6.4 lists the critical eigenvalues for the wind/diesel/flywheel system when the wind turbine UPF exciter is replaced by the CONTROLOGY AVR15R with 30% QDC.

When compared with Table 6.1, it shows practically no change in system stability for both oscillation modes. However, the replacement of the UPF exciter by the AVR allows supplementary signals to be fedback into the device to aid in the damping of these natural modes of oscillations. A Power System Stabiliser of the form simulated in Chapter 5 along with the associated method of tuning will therefore be studied.

6.2.6 The effect of Power System Stabilisers

As described in Section 5.4, an additional method to improve the damping of the low frequency mode is via the use of a Power System Stabiliser. The wind turbine generator electrical power is fedback into the AVR in order to provide an increased damping torque for the low frequency mode.

The simple controller of the form of Equation 5.1 along with the method of "Pole Placement" described in Appendix 5.A was used to improve the low frequency mode of the Wind/diesel/flywheel with a flywheel inertia of 11.8 kg m^2. In order to demonstrate more easily the advantages and disadvantages of such a method the original level of wind turbine mechanical damping (220 Nm/rad/s) is used throughout the study.

Without stabilisation, the system suffers from extreme 1Hz oscillations as illustrated by Fig 6.7. The graphs show the time response of the wind/diesel/flywheel system without Power System Stabilisation when subjected to a stepchange in the wind turbine mechanical power from 2.5 to 6kW (this steptest was used as a benchmark throughout this study).

1) With PSS (sigma = -2.0 +/- j 5.65)

Using the Pole Placement technique, controller gains of:
Kp = -8.48, Tw = 0.191 secs

were needed to move the critical low frequency eigenvalues from sigma = -0.21 +/- j5.65 to sigma = -2.0 +/- j5.65.

However, Fig 6.8 demonstrates that even though the 1 Hz mode is damped out within 2 cycles when subjected to the steptest, the level of reactive power flow is much too great, especially during the first swing.

As in Chapter 5, a compromise must be reached between satisfactory damping of the 1Hz mode and sustainable levels of reactive power.

2) With PSS (sigma = -0.6 +/- j5.65)

Fig 6.9 illustrates the time response of the wind/diesel/flywheel system with the effect of the PSS reduced so that the eigenvalues were only moved to sigma = -0.6 +/- j5.65 (Kp = -2.91, Tw = 0.331 secs). The response shows that the 1Hz oscillation has not been totally damped out within 5 seconds and that the reactive power flow although much improved is still very large.

3) With PSS ("Bang-Bang" Method)

An alternative method to a reduction in the Power System Stabiliser's gains, is to limit the output of the controller as illustrated by Fig 6.10. The limiters therefore "cap" the action of the PSS when the system is subjected to large

disturbances, as during the initial transient stages of the steptest, therefore preventing the large reactive power flows of case 1). However, it is able to provide a higher level of damping than case 2) when responding to smaller disturbances.

Fig 6.11 illustrates the time response of the wind/diesel/flywheel system using such a method and demonstrates that the 1Hz mode is damped out within 4 cycles. There is also a reduction in the magnitude of the transient reactive power flow.

Therefore it may be concluded that "bang-bang" control represents the most viable method of Power System Stabilisation from the three options under test.

6.2.7 Problem with the Pole-Placement Method

Whilst attempting to undertake a similar study on the wind/diesel system, without flywheel energy storage, the Pole Placement Method failed to provide sensible values for the PSS controller gains, Kp and Tw. Upon examination of the system eigenvalues it was noticed that the pole-pair to be moved (sigma = -0.25 +/-j7.91) shared an almost identical frequency component to the much more well damped eigenvalues (sigma = -4.64 +/-j8.0) due to the interaction of the DG's internal emf with that of its AVR.

As no similar problems were encountered with the Pole Placement method whilst using the wind/diesel/flywheel system

it may be concluded that the method breaks down if two pole-pairs share similar frequency components.

6.3 Time-Step Simulation of the Wind/Diesel/Flywheel System

The time-stepping methods described in Chapter 4 will now be used to investigate the normal and abnormal running conditions to which the wind/diesel/flywheel system is subjected. The section will be broken down into the following areas:

1) Continuous wind/diesel/flwheel operation
2) Wind turbine decoupled from its generator
3) Diesel engine disengagement
4) Diesel engine "crashstarted"

Throughout the study, particular attention will be paid to the effect of the dumpload plus its controller, damping and the effect of flywheel size.

6.3.1 Continuous Wind/Diesel/Flywheel System

6.3.1.1 Without Dumpload Control

In order to compare with the results of the small signal eigenvalue analysis studies carried out in Section 6.2, the time-stepping model was used to investigate the effect of the wind turbine mechanical dampers upon system stability. At

each flywheel size (0.0, 11.8 and 57.8 kg m^2) the system was subjected to Gaussian wind turbine mechanical power with a mean of 5kW and a consumer load of 7kW.

Fig 6.12 illustrates the time responses at a wind turbine mechanical damping of 220Nm/rad/sec for the wind turbine/diesel generator real power outputs and wind turbine speed at the three flywheel sizes. In all three cases, the power responses show a pronounced low frequency oscillation of 1.3Hz (wind/diesel system), 0.95 Hz (Jfly=11.8 kg m^2) and 0.925 Hz (Jfly=57.8 kg m^2) which is in reasonable agreement with that obtained from the eigenvalue analysis. Also, increased flywheel size is again demonstrated to worsen system stability.

At 2200Nm/rad/s the time responses of Fig 6.13 indicate much reduced levels of low frequency oscillations with stability again worsening with increased flywheel size.

The positive damping effect of the wind turbine's C_p/λ curve at the higher wind turbine mechanical power of circa 8kW is shown by Fig 6.14 to worsen stability at this higher level of mechanical damping but to be still satisfactory.

6.3.1.2 Frequency Controlled Dumpload

Due to the non-linear/discrete nature of the dumpload and its controller, the eigenvalue analysis methods previously discussed, are unable to provide any indication of the

performance of the wind/diesel/flywheel system with the inclusion of such a device. In order to gain an insight into its performance, time-stepping methods were again used.

In order to benchmark the wind/diesel model and its frequency controlled dumpload, a comparative study was made between the results of a step-load test carried out on the actual system with that of the simulated system under similar conditions. Fig 6.15 (a) and (b) illustrate the actual and simulated responses of the wind/diesel system (Jfly=0.0 kg m^2) whilst under frequency control with a proportional gain of Kfp=2.5kW/Hz and subjected to a steploadchange of 0 to 3.4kW after 1.5 secs.

Both actual and simulated results appear to be in good agreement in both magnitude and frequency of oscillation (1.4Hz). The overall damping of this low frequency mode is poor in both the actual and simulated responses and is not aided by the action of the dumpload. The initial spike in both the real and reactive powers is due to the deadtime in the frequency transducer and the delay in the setting of the relays in the dump load whilst it responds to the sudden stepchange in consumer load.

Using the model, an investigation was carried out into the effect of the frequency controlled dumpload whilst subjected to gaussian wind turbine mechanical power as described in Section 6.3.1, however, with the consumer load set to zero.

For the wind/diesel system, Fig 6.16, initially a 1.4Hz oscillation can be seen, however, this is superseded after 3 seconds by the steady growth of a 6Hz oscillation, which at the gain of Kfp=7kW/Hz appears to be slightly past the stability limit for the system. A similar (but more stable) high frequency mode was apparent in the eigenvalue analysis study (Section 6.2.1) which could be excited by wind turbine generator or busbar action (ie dumpload operation).

Fig 6.17(b) also shows that the wind turbine generator is stimulated into this 6Hz mode via the action of the dumpload which is connected to the busbar. This 1 second segment of the time response demonstrates that the dumpload power is in anti-phase to the power output of the wind turbine generator. The effect is due to the sample-and-hold action of the frequency transducer causing the dumpload to respond out-of-phase with the wind turbine power variations, thus providing negative damping to this mode. For comparison, the actual wind/diesel system's response under similar conditions is shown as Fig 6.17(a)

An effect that is not seen in the eigenvalue analysis is that the 6Hz mode is slightly better damped with increasing flywheel size (Figs 6.18 and 6.19). However, as with the eigenvalue analysis, the 1Hz oscillation worsens with increased flywheel size.

Figs 6.20 (a), (b) and (c) illustrates the system with the wind turbine mechanical damping at 2200Nm/rad/s and demonstrates that the 6Hz mode appears to be satisfactorily

removed for all three flywheel sizes. Although no traces exist, the actual system has been reported to go unstable and eventually collapse due to a 6Hz oscillation which did not immediately appear. The system model was therefore tested over a 30 second period (limited by excessive computer runtime and the inaccuracy of such models over long time periods). However, no evidence was found of this mode of oscillation nor did the system go unstable. Attempts were made to introduce imperfections into the wind turbine mechanical damper model in the forms of backlash and poor high frequency performance. Both types of modifications to the model failed to produce this 6Hz instability at the higher level of mechanical damping.

In order to ensure that the developed controller was able to deal with this oscillatory problem it was decided that the wind turbine mechanical damping would in future simulations be reduced until such oscillatory effects became apparent.

6.3.1.3 Wind Turbine Motored

The Eigenvalue Analysis of Section 6.2.2 suggested that if the wind turbine was decoupled from its generator, the wind/diesel/flywheel system would again suffer from sustained severe oscillations. Study of the Participation Matrix suggested that the oscillations at approximately 4.9Hz were due to the wind turbine generator swinging against the diesel generator/flywheel.

Fig 6.21(a) shows the synchronisation of the wind turbine generator onto the actual wind/diesel/flywheel system during very low wind speeds. After synchronisation, the wind turbine is motored due to the poor wind conditions. In this condition the wind turbine is decoupled from its generator and as predicted by Eigenvalue Analysis, a sustained 4.9Hz oscillation results. Fig 6.21(b) illustrates the time response of the simulation when subjected to similar conditions. Although, the magnitude of the oscillation (0.3pu =2.4kW) is not as large as the actual response, both the actual and simulated responses demonstrate that the system is at its stability limit.

If the frequency controlled dumpload is also in operation, the system becomes totally unstable as illustrated by Fig 6.22(a) (actual) and Fig 6.22(b) (simulated). Again, there is an anti-phase relationship between the simulated wind turbine generator power with that of the dumpload power. This causes a negative damping effect which pushes the system past its stability limit eventually leading to system collapse.

As in the previous chapter, control of the dumpload using real power as its feedback signal was also investigated.

6.3.1.4 Power Controlled Dumpload

As discussed in Chapter 5 and 6, due to the problems of using frequency feedback in the dumpload controller, the wind/diesel/flywheel system was tested with a power

controlled dumpload. In this configuration, the real power output of the diesel generator was fedback into the dumpload controller as described in Section 3.11 and Fig 3.28(b).

Initial testing of the actual wind/diesel/flywheel system under this form of control had left the 3.4Hz notch filter, used to improve the performance of the frequency controlled device, in place.

Fig 6.23(a) illustrates the response of the actual wind/diesel system when subjected to windspeeds at approximately 8m/s, whilst Fig 6.23(b) similarly illustrates the response of the wind/diesel model when subjected to a gaussian wind turbine mechanical power @ 5kW (mean) under no-load conditions. For both the actual and simulated runs, controller gains were set at Kp=5.6kW/kW, Ki=5.6kW/kW/s and Pset=2.56kW.

Both sets of graphs illustrate that the system is satisfactorily stable under these conditions. Unlike the frequency controlled dumpload, the power controlled dumpload is acting in-phase with the power output of the wind turbine generator thereby ensuring a very stable electrical platform.

With the removal of the 3.4Hz notch filter, synchronisation of the wind turbine onto the wind/diesel system led to the immediate development of a 6Hz oscillation causing the system to become unstable. Fig 6.24(a) (actual) and Fig 6.24(b) (simulated) illustrate the system's response to this severe

disturbance using the previously described controller gain settings. With the inclusion of the 3.4Hz notch filter, the system's response is again well damped when subjected to a similar severe disturbance, Fig 6.25. Referring to Fig 5.37, two possible mechanisms in the notch filter's characteristics are responsible for the damping out of the 6Hz oscillation:

1) The 6Hz oscillation is sufficiently close to the 3.4Hz notch to be greatly attenuated.

2) As in Section 5.6.2, the phase advancing feature of the notch filter above 3.4Hz helps to counteract the effects of the deadtime at the output of the dumpload controller.

As the continuous wind/diesel system was satisfactorily stable, it was decided to leave the 3.4Hz notch filter in place throughout the rest of the project.

The wind/diesel/flywheel model was also tested with additional derivative control to provide full P+I+D control. However, Fig 6.26 illustrates that even with small amounts of derivative control (Kd=0.2kWs/kW) the system is immediately subjected to a large 14Hz oscillation. Derivative control is therefore totally inappropriate due to the high level of noise in such a system and to the stepload action of the dumpload being converted to an impulse by its own controller.

A further test run carried out on the model was to examine the effect of high wind speeds on the wind/diesel/flywheel system under power controlled dumpload action. Two levels of mechanical damping were studied, namely 220NM/rad/s (original) and 2200Nm/rad/s (uprated). Fig 6.27(a) shows the actual response of the wind/diesel/flywheel system (J_{fly}=57.8kg m^2) at the uprated level of mechanical damping when subjected to high windspeeds. The graphs show a pronounced (approximately) 1Hz oscillation with a maximum power swing of 3kW.

Fig 6.27(b) and 6.27(c) show the simulated responses of the system with the original and uprated levels of mechanical damping under similar conditions. A comparison of the simulations at the two levels of mechanical damping suggests that although the oscillation frequency of the higher damping level is approximately correct, the lower damping level shows similar magnitudes of power swings to the actual response. As in the wind/diesel study, both demonstrate that the wind turbine generator power swings are largely consumed by the dumpload ensuring a reasonably stable electrical platform.

However, quite large swings occur in the reactive power output of the wind turbine generator. This suggests that the excitation systems, even with 30% QDC on the wind turbine generator AVR, would be unable to maintain satisfactory levels of reactive power flow at very high windspeeds.

6.4 Disengagement of the Diesel Engine

At times of sufficient wind speeds and stored flywheel energy, the diesel engine may be decoupled via its electromagnetic clutch from the diesel generator/flywheel and shutdown in order to save fuel.

6.4.1 Diesel Engine Disengaged Without Dumpload Control

Eigenvalue Analysis had suggested that upon disengagement of the diesel engine a very lightly damped 8.2Hz oscillation would develop in the wind/diesel system (J_{fly}=0.0kg m^2). Fig 6.28 illustrates the simulated time repsonse of such an occurrence without dumpload control. Almost immediately after disengagement at 0.2 secs, the 8.2 Hz oscillation develops and is only damped out after approximately 40 cycles (5 secs). With the inclusion of a flywheel into the system, all traces of the 8.2Hz mode had disappeared as predicted by the Eigenvalue Analysis.

6.4.2 Diesel Engine Disengaged Whilst Under Dumpload Control

During the disconnection of the diesel engine from the system, not only may a large disturbance occur due to this disengagement, but also new control objectives must be brought in for the dumpload to maintain a stable electrical platform. Consider the control objectives of the two configurations:

1) Continuous Wind/Diesel/Flywheel System

The dumpload is used to maintain a minimum diesel loading. This it achieves by comparing the power output of the diesel generator with that of a power setpoint.

2) Diesel Engine Disengagement from the Wind/Diesel/Flwheel System

Without the diesel engine, a minimum diesel loading is no longer required. However, three new constraints must be met:

a) Whilst the diesel is being motored, the power flow into the device must be limited to below that of its rating. This is achieved by readjustment of the dumpload setpoint to ensure that the dumpload diverts any excessive power flow away from the diesel/flywheel.

b) The dumpload must ensure that the system frequency does not exceed an upper limit. A frequency loop must therefore be included in the dumpload controller to ensure that above a frequency setpoint, power is again diverted into the dumpload.

c) A decision must be reached when to restart and re-engage the diesel engine onto the wind/diesel/flywheel system. However, this is a logistical decision and will not be discussed in this thesis.

In order to investigate methods to fulfill these operating constraints in both the transitional state and the reconfigured system, simulation studies were carried out at

ICSTM and tests were carried out at RAL on the actual system.

6.4.3 Power Controlled Dumpload Operation

Initially a dumpload controller of the form illustrated by Fig 6.29 was tested on the wind/flywheel system. Previously discussed problems with frequency based dumpload control led to the decision to minimise its use. The dumpload controller was therefore designed to operate as follows:

1) continuous wind/diesel

The power setpoint was used to maintain the minimum diesel loading.

2) Diesel disengaged

a) Below frequency upper limit

The power setpoint was used to limit power flow into the diesel generator/flywheel to below the generator rating.

b) At or above the frequency limit

The power setpoint was set to zero to prevent further power flow into the diesel generator/flywheel. The frequency transducer was therefore only used as a flag to the controller when the system frequency had reached the upper limit.

However, upon initial testing of the model it immediately became apparent that although the disengagement of the diesel

engine and the resetting of the power setpoint could be achieved successfully, the system became unstable when it reached the upper frequency limit. Fig 6.30 is the output from an early simulation which illustrates the response of the system under such conditions.

When the frequency setpoint is reached, power is diverted away from the flywheel into the dumpload. If the frequency drops, the setpoint immediately changes to allow power to flow into the flywheel and hence increase the system's speed/frequency. The upper frequency limit is again exceeded and the setpoint is reset. The system therefore cycles between these two states.

This method to maintain an upper frequency limit was abandoned and attention turned to the use of a dumpload controller that used both power and frequency.

6.4.4 Frequency Controlled Dumpload Operation

In order to investigate further methods of maintaining an upper frequency limit, the dumpload was tested solely under frequency control during diesel disengagement (the 3.4Hz notch filter was included at the input to the dumpload controller).

Fig 6.31(a) illustrates the actual response of the wind/diesel/flywheel ($J_{flywheel}$=11.8kg m^2) system to the disengagement of the diesel engine whilst under low gain P+I

(Kfp=5kW/Hz, Kfi=2kW/Hz/s) frequency controlled dumpload operation. Fig 6.31(b), is the simulated repsonse at the uprated level of mechanical damping (2200Nm/rad/s). At this low windspeed, system stability is maintained for both the actual and simulated runs. Furthermore, the wind turbine generator power smoothly transfers to the new "steady-state" conditions as the diesel moves from its generating to motoring mode. Wind excitation of the 1Hz mode apppears to be mimimal in the power signal but is more pronounced in the reactive power flow (2 to 5 seconds).

For comparison, Fig 6.31(c) is the equivalent simulated response at the original level of wind turbine mechanical damping (220Nm/rad/s). Upon disconnection of the diesel engine, a 6Hz oscillation quickly develops and leads to system instability.

Both actual and simulated results bear out that if sufficiently low P+I gains are used, a frequency loop may be used to maintain an upper frequency limit.

6.4.5 Power Plus Frequency Controlled Dumpload

Modifications were made to the design of the dumpload controller of Fig 6.29 to allow the inclusion of a frequency loop that became operational upon diesel disengagement and at a frequency above the upper limit, Fig 6.32. In order to provide a "soft" changeover at the upper frequency limit the frequency loop was used to gradually adjust the power

setpoint. However, two problems were immediately detected when this configuration was simulated:

1) P+I Frequency loop

With the frequency loop under P+I control (ensuring a zero "steady-state" error) another hard reset problem became apparent. When the frequency passes the upper limit, the frequency control loop becomes active and reduces the power setpoint accordingly. If the power into the diesel generator/flywheel exceeds this setpoint, it is diverted into the dumpload. When the system frequency falls to the upper frequency limit, the output of the integrator will not necessarily be at zero, thereby still adjusting the power setpoint. However,when the frequency falls below the upper limit, the frequency loop is switched out leading to a stepchange in the power setpoint. The frequency then rises again above the upper limit and the already charged integrator causes another stepchange in the power setpoint. Cyclic operation between the two states then occurs as illustrated by the simulation results of Fig 6.33 (NB the frequency setpoint is set artificially low at 51.3Hz).

Two alternative methods were therefore investigated:

1) The frequency loop is left active once the upper limit is initially passed. This removes the "hard" changeover conditions, but, as illustrated by Fig 6.34, the system goes into a much longer timeframe oscillation around the

upper frequency limit. This oscillation is dependent upon the integrator time constant in the frequency loop.

2) The frequency loop is operated solely under proportional control. In order to minimise the steady-state frequency error, a large gain must be used.

Fig 6.35(a) and (b) are the actual and simulated time responses of the wind/flywheel system under power plus frequency dumpload control (Kpp=3kW/kW, Kfp=7kW/Hz) when the upper frequency limit (54Hz actual, 51Hz simulated) has been reached. Even with the inclusion of the notch filter, 6Hz oscillations have devloped and swamp the response due to the sample/hold effect of the frequency transducer being magnified by the combined gains of the proportional terms in both the power and frequency loops (Kfp*Kpp). In order to use this form of control the gain of the frequency loop must be drastically reduced. However, this leads to a large steady-state error above the upper frequency limit.

In order to be able to use a large proportional gain in the frequency loop, the frequency transducer may be replaced by speed signals fedback from tachogenerators mounted on the wind turbine generator or on the shaft of the diesel flywheel. The use of such devices remove the sample/hold problem.

Fig 6.36 illustrates the time response of the wind/flywheel system with the "frequency" loop now fed by; (a) wind turbine generator speed and (b) diesel flywheel speed. Both

methods of control show no sign of the 6Hz oscillation, whilst the wind turbine speed control demonstrates a slightly better damping characteristic than the diesel flywheel method. To date, neither method has been tried on the actual wind/diesel/flywheel system.

In order to test more fully the "power plus wind turbine generator speed" dumpload controller, the speed loop was increased to a gain of 10kW/Hz at a frequency set point of 55Hz. The system was subjected to high windspeeds (including the positive damping effects of the C_p/λ curve), at no-load and with the wind turbine mechanical dampers set deliberately low to allow for the apparent imperfections in the actual devices. Fig 6.37 shows the time response of this study.

Upon diesel engine disengagement (t=0.02secs), the power output of the wind turbine drives the diesel alternator at a level that exceeds its rated power causing dumpload activity. After 4.5 seconds, the upper frequency limit is reached and the speed loop becomes active. Over the next 3 seconds the dumpload increasingly diverts power away from the diesel alternator until it reaches its steady-state condition at 55.8Hz. Even though the system is still being subjected to high gaussian wind speeds the controller ensures a stable electrical platform at a steady-state frequency error of 0.8Hz.

6.5 Diesel "Crashstarted onto the Wind/Flywheel System

The remaining and most onerous test to be applied to the wind/diesel/flywheel system and to the computer simulation is the "crashstarting" of the diesel engine onto the wind/flywheel system.

If insufficient stored energy remains in the system a logistical decision has to be made to restart the diesel engine and mechanically re-engage it via the electromagnetic clutch. The system must therefore bring the diesel up to speed before the system frequency falls below the lower frequency limit (eg 45Hz).

Tests were carried out on the actual wind/diesel/flywheel system at RAL and a comparative study was carried out using the computer simulation programs at ICSTM. The smaller of the two flywheel sizes (J_{fly}=11.8kg m^2) was chosen as this would present the more arduous challenge thereby ensuring that the system maintained voltage and frequency constraints.

In addition to the characteristics of the diesel/flywheel rig described in section 3.9, an important lesson was learnt during early crashstart tests. It was noticed that after re-engagement of the diesel engine, some seconds elapsed before the diesel engine's characteristics matched that of the normally fixed power versus frequency relationship. A computer simulation (Fig 6.38) reveals this to be due to the fuel rack of the diesel engine being held fully open, causing overfueling, for a number of seconds after the diesel had run

up to speed. An overhaul of the diesel engine revealed that the fuel rack was sticking fully across for much longer than the desired overfueling time. However, this period of overfueling remained and so this characteristic has been built into the diesel crashstart procedure of the model.

Fig 6.39(a) (actual) and Fig 6.39(b) (simulated) demonstrate that the diesel engine can be brought back online within 0.6 seconds and is capable of maintaining the system frequency within the lower frequency limit. The actual test used a decision frequency of 50Hz (1500rpm, 1.0 pu) resulting in a frequency dip to 46.6Hz (1400rpm, 0.93 pu) whilst the simulation used a more onerous decision frequency of 49Hz (1470rpm, 0.98 pu) resulting in a frequency dip to 45.3Hz (1359rpm, 0.90 pu).

Fig 6.40 shows more extensive results of the simulated study with the diesel being crashstarted after 1.0 secs. After the initial peak of power from the wind turbine (used to run-up the diesel engine), the wind speed is sufficiently low to motor it. This causes the wind turbine to decouple from its generator. Immediately a 4.9Hz oscillation develops, which is only damped down when the dumpload commences operation at 49Hz (the dumpload is disabled at frequencies below 49Hz). Several large spikes occur around this point due to the sudden enabling/disabling of the dumpload as the frequency rises and falls about this point. Although the wind turbine is still being motored the frequency/speed of the system continues to rise due to the diesel engine being at full output due to overfueling. After 9 secs the diesel engine

ceases overfueling and returns to the normal dynamic characteristics described in Section 3.3. At approximately 10 secs the windspeed increases so that the wind turbine is recoupled to its generator. The dumpload responds to the inherent 1Hz oscillation that devlops eventually damping it down in the remaining period.

For comparison, Fig 6.41 shows results from the actual wind/diesel/flywheel system test on which this simulation study was based. Due to the data acquisition system limiting the samples to 250 readings over the 20 second period, a similar process has been applied to the simulated results displayed alongside.

Fig 6.42 illustrates a similar study with the flywheel size increased to 57.8kg m^2. The disturbance to the system is much reduced with the frequency dip being limited from 49Hz to 48Hz. Due to this much reduced dip, the decision to crashstart the diesel engine could be left to a much lower level of system speed/frequency. This would allow more energy to be extracted from the device, would decrease the number of diesel on/off cycles and save more fuel.

Both the actual and simulated results demonstrate that the system is able to maintain satisfactory frequency and voltage levels and that control is maintained throughout these most onerous conditions for both flywheel sizes.

6.6 Conclusions

Building upon the performance criteria developed in the previous chapters, Chapter 6 investigated the characteristics and control of the full wind/diesel plus flywheel system. The following points should be noted:

6.6.1 Steady-State Behaviour

The Wind Turbine Generator's UPF exciter demonstrated poor reactive power flow performance even though voltage regulation was satisfactory.

Replacement of the UPF exciter with the AVR15R again required additional QDC. 30% QDC was found to provide satisfactory reactive power flow performance and voltage regulation over the full load range.

6.6.2 Small Signal Analysis

As in the studies of the wind turbine generator connected to the grid, Eigenvalue Analysis revealed two critical oscillation modes.

The wind/diesel system proved more susceptible to the approximately 1Hz wind-excited oscillation and led to the wind turbine swinging in anti-phase to the diesel generator.

Increased wind turbine mechanical damping improves system stability, however, its benefit is not so great as in the grid connected arrangement.

The addition of a flywheel worsens the stability of this mode and results in a change of mode shape that has the wind turbine swinging against the diesel-flywheel. Any beneficial damping that may have been due to this node has therefore been lost.

The addition of power system stabilisation using the wind turbine generator real power output as the controlling signal was demonstrated as an alternative means of damping the low frequency mode. However, a tradeoff exists between improved damping and worsening reactive power flows. This resulted in the limiting of the output of the device using "bang-bang" control.

The higher frequency (6Hz mode), due to wind turbine generator or busbar activity (ie dumpload action) is slightly better damped than in the grid connected system. Increasing flywheel size little effects this mode whilst a tenfold increase in wind turbine meachanical damping successfully removes it.

Mechanically decoupling the wind turbine via its overrunning clutch results in a very poorly damped 4.7Hz mode which is unaffected by the inclusion of a flywheel.

The decoupling of the diesel engine from the wind/diesel system results in a very poorly damped 8.2Hz oscillation and leads to the two generators swinging in anti-phase. This mode does not occur in the wind/diesel/flywheel system.

At high windspeeds, the wind turbine's C_p/λ characteristic causes a negative damping effect which leads to a deterioration in stability of both modes. With either flywheel size the system is unstable at the original level of wind turbine mechanical damping.

30% QDC was found not to significantly effect the stability of the wind/diesel/flywheel system.

6.6.3 Dynamic Behaviour

The use of time-stepping methods provided further confirmation of the results predicted using Eigenvalue Analysis and also allowed the comparison with actual time responses. Additionally, the simulations investigated the development of the dumpload controller and examined large system disturbances, including transitional conditions, which could not be undertaken using the small signal analysis techniques.

Under frequency controlled dumpload operation the wind/diesel system demonstrated a 6Hz oscillation which at a controller gain of 7kW/Hz was at its stability limit. This mode is stimulated by the incorrect action of the dumpload due to the

sample/hold element of the frequency transducer causing the dumpload to respond in anti-phase to the required action. The dumpload also leads to system instability at much lower controller gains if the wind turbine is decoupled.

Under power controlled dumpload operation a 3.4Hz notch filter at the input to the controller was required to ensure stability. However, under P+I control the dumpload was able to maintain a minimum diesel loading and provided additional damping. Derivative control was demonstrated to be unsatisfactory due to the high level of system "noise" and the stepload action of the dumpload being converted into impulses by its own controller.

During diesel disengagement the power setpoint was adjusted to limit the power into the alternator-flywheel. Additionally, in order to maintain an upper frequency limit an additional "speed" (wind turbine generator or flywheel) loop was used to adjust this power setpoint in the dumpload controller. This method demonstrated that large gains could be used to minimise the steady-state frequency error and aided in system stability.

Under the most onerous condition of a diesel "crashstart" the computer models demonstrated their ability to accurately predict actual system behaviour. The simulated and actual results also demonstrated that the wind/diesel/flywheel system was able to maintain satisfactory voltage and frequency levels for both sizes of flywheel under examination.

J_{fly} (kg m^2)	D_{sh} (Nm/rad/s)	σ	$\pm j\omega$	σ	$\pm j\omega$
0.0	220	-0.30	7.92	-3.60	39.49
	2200	-2.37	9.88	-----	-----
	WT OFF	-----	-----	-0.115	31.38
11.8	220	-0.20	5.85	-6.74	39.18
	2200	-1.82	7.13	-----	-----
	WT OFF	-----	-----	-0.13	30.37
57.8	220	-0.18	5.64	-6.75	39.04
	2200	-1.74	6.79	-----	-----
	WT OFF	-----	-----	-0.132	30.3

Table 6.1 Effect of Flywheel Inertia on the Wind/Diesel System's Critical Eigenvalues

J_{fly} (kg m^2)	D_{sh} (Nm/rad/s)	σ	$\pm j\omega$	σ	$\pm j\omega$
0.0	220	-----	-----	-3.83	51.48
	2200	-----	-----	-3.80	39.98
11.8	220	-0.25	5.84	-6.80	39.17
	2200	-2.00	7.06	-----	-----
57.8	220	-0.28	5.59	-6.8	39.12
	2200	-1.88	6.64	-----	-----

Table 6.2 Effect of Diesel Disengagement on the Wind/Diesel/flywheel System's Critical Eigenvalues

J_{fly} (kg m^2)	D_{sh} (Nm/rad/s)	σ	$\pm j\omega$	σ	$\pm j\omega$
0.0**	220	-0.41	8.23	-5.4	42.1
0.0	220 2200	-0.18 -2.58	8.24 11.52	-5.41 -----	42.1 -----
11.8	220 2200	0.025 -1.99	6.15 7.89	-5.53 -----	41.59 -----
57.8	220 2200	0.056 -1.85	5.94 7.50	-5.54 -----	41.55 -----

**Eigenvalues of the wind/diesel system at the higher wind speeds without the effect of the Cp/Lambda curve

Table 6.3 Effect of the Wind Turbine's C_p/λ Characteristics on the Wind/Diesel/Flywheel System's Critical Eigenvalues

J_{fly} (kg m^2)	D_{sh} (Nm/rad/s)	σ	$\pm j\omega$	σ	$\pm j\omega$
0.0	0 220 2200 WT OFF	0.05 -0.29 -1.92 -----	7.75 7.78 9.89 -----	0.42 -6.59 ----- -0.11	38.99 38.26 ----- 30.3
11.8	0 220 2200 WT OFF	0.025 -0.21 -1.69 -----	5.65 5.65 6.74 -----	0.43 -6.73 ----- -0.11	38.5 37.9 ----- 29.3
57.8	0 220 2200 WT OFF	0.019 -0.19 -1.61 -----	5.43 5.44 6.39 -----	0.43 -6.77 ----- -0.11	38.5 37.86 ----- 29.2

Table 6.4 Effect of the Wind Turbine Generator AVR with 30% QDC on the Wind/Diesel/Flywheel System's Critical Eigenvalues

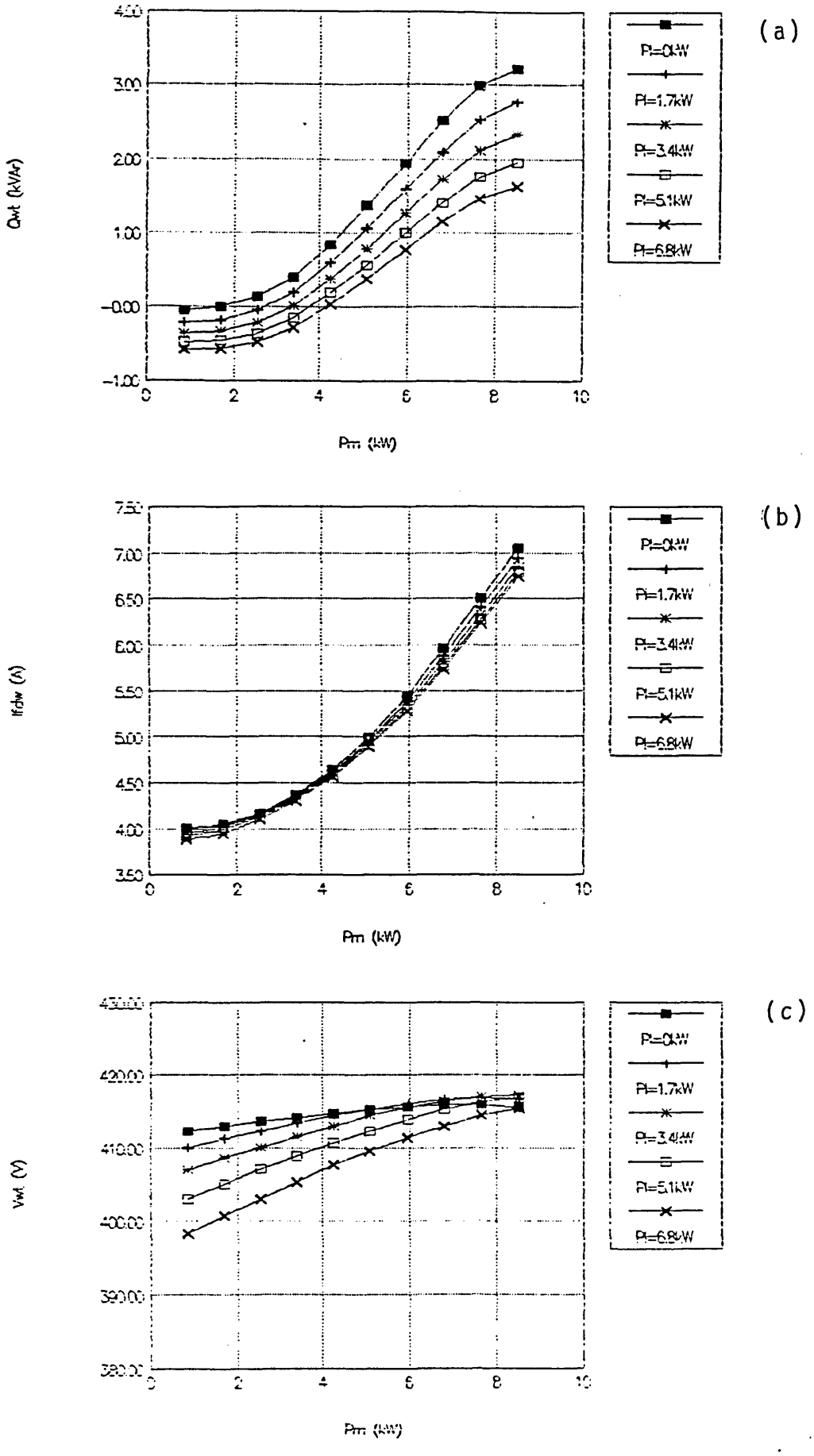

FIGURE 6.1 Steady-state performance of the wind/diesel system - wind turbine generator with UPF exciter

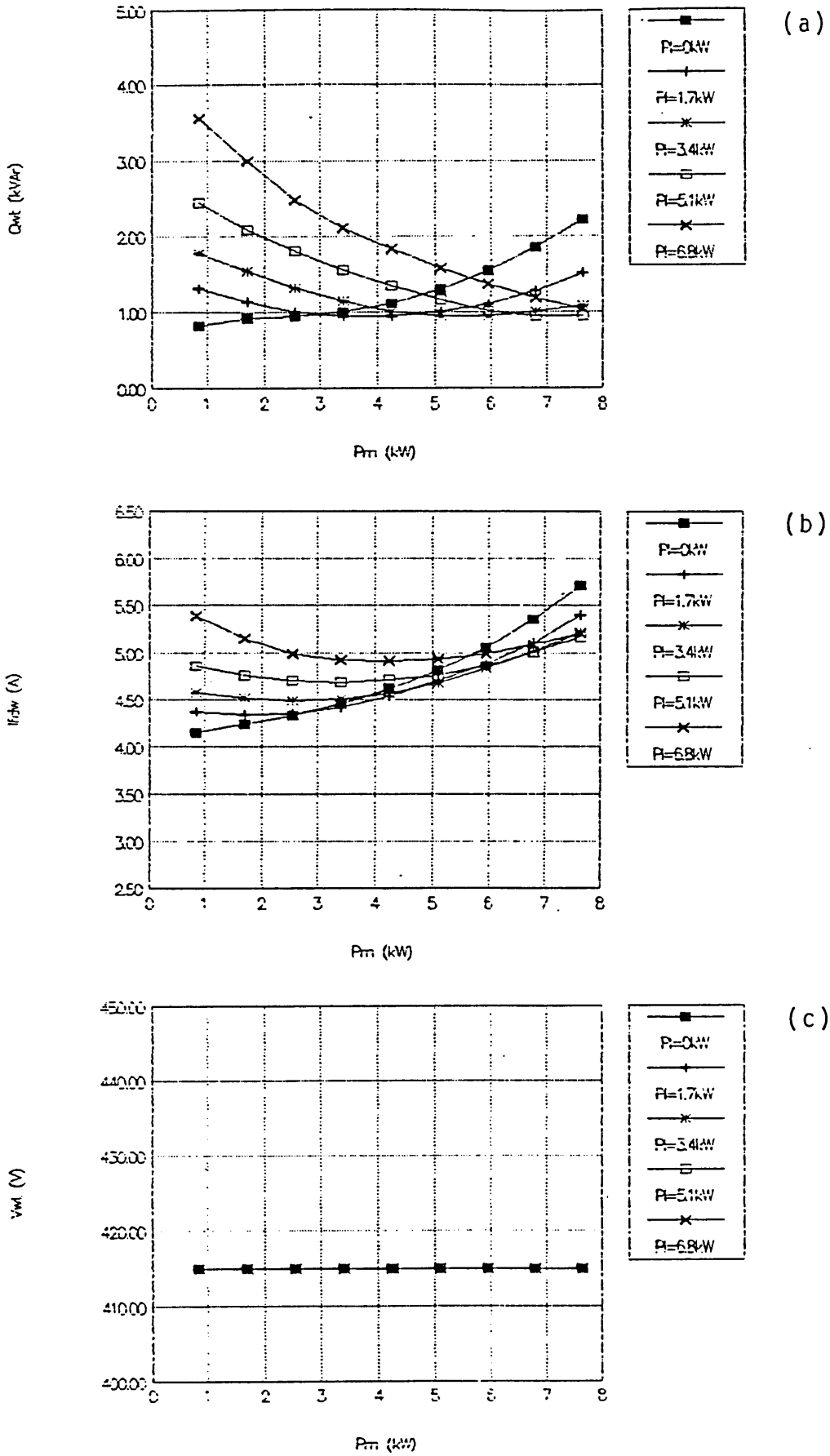

FIGURE 6.2 Steady-state performance of the wind/diesel system - wind turbine generator with AVR

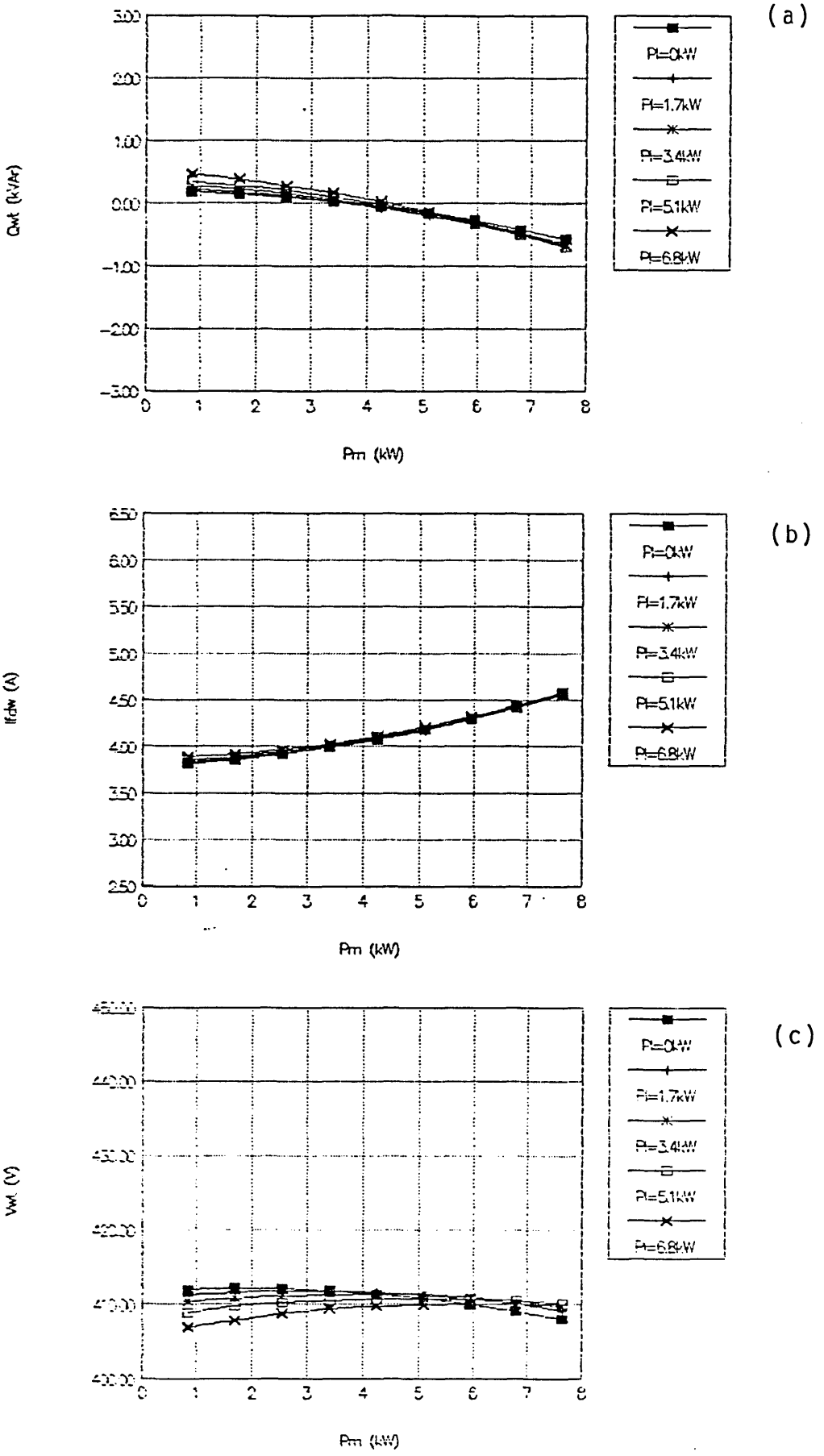

FIGURE 6.3 Steady-state performance of the wind/diesel system - wind turbine generator with AVR + 25% QDC

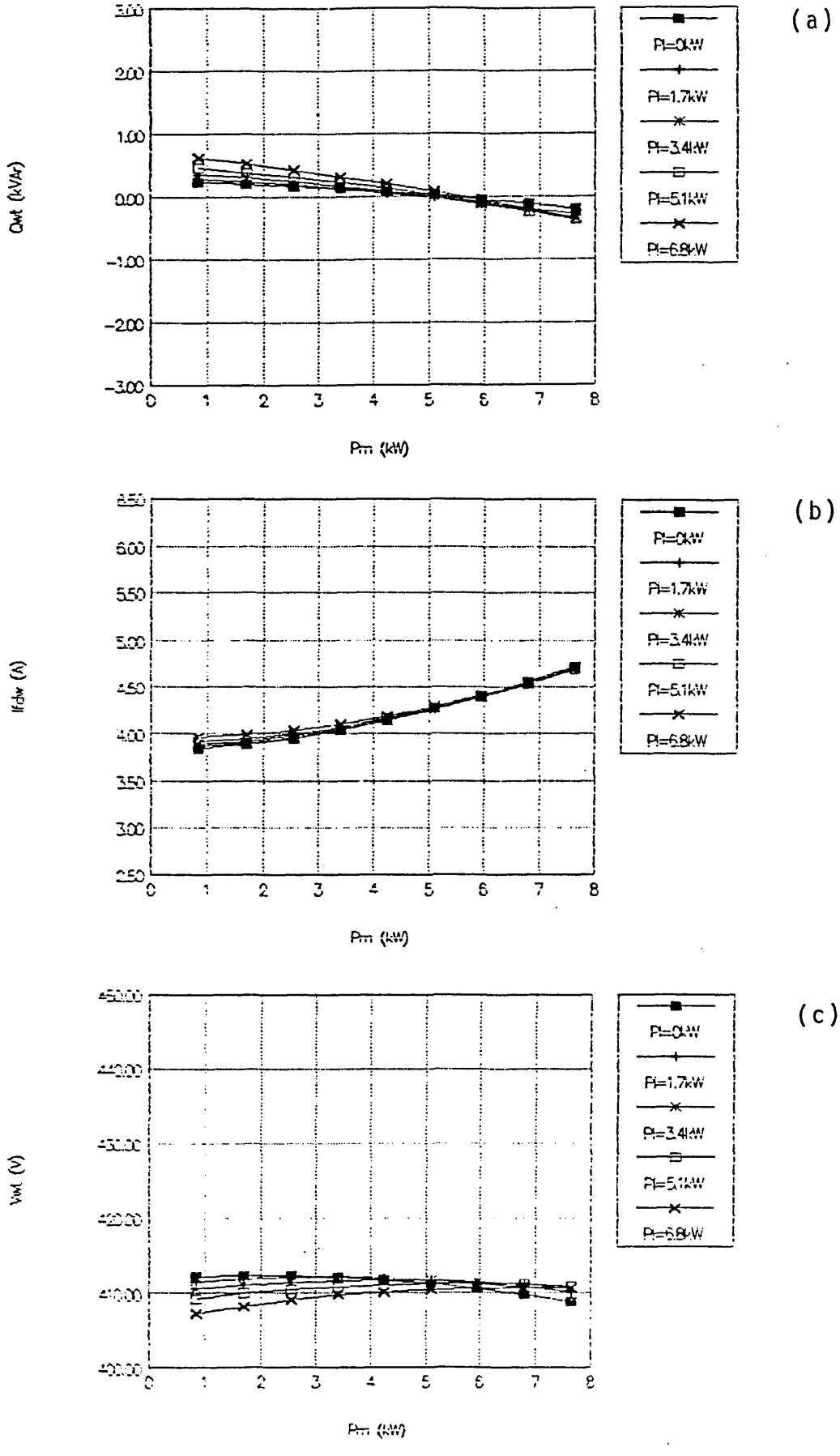

FIGURE 6.4 Steady-state performance of the wind/diesel system - wind turbine generator with AVR + 35% QDC

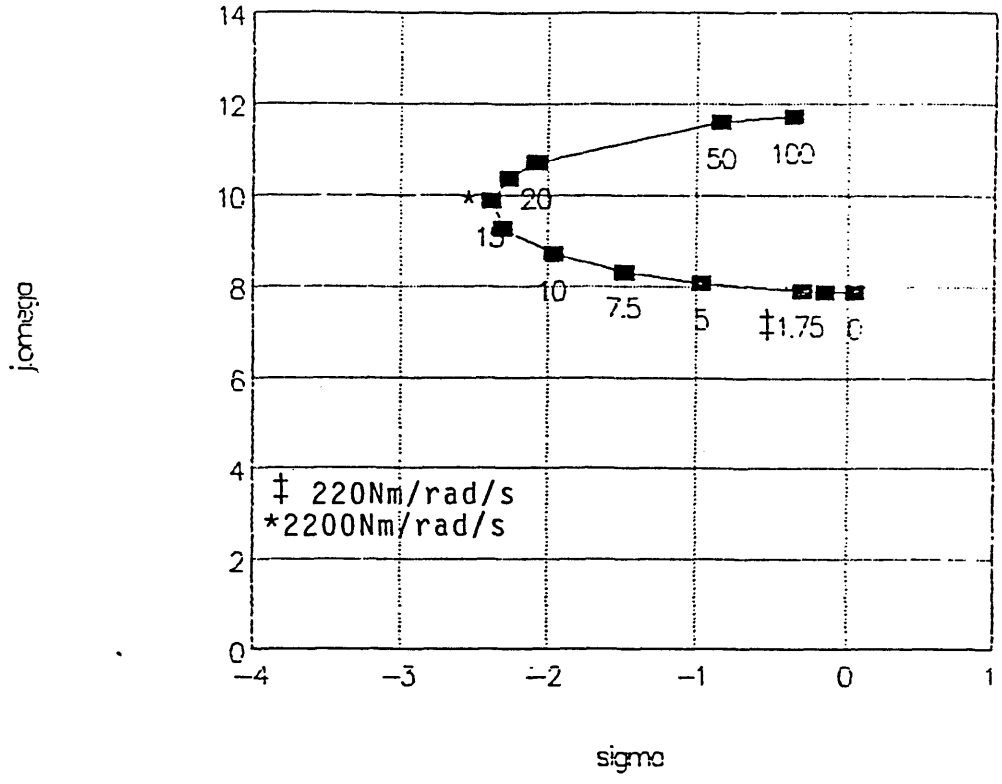

(a) low frequency

FIGURE 6.5 Root locus of the effect of increased mechanical damping on the WTG (with UPF exciter) connected to the wind/ diesel system.

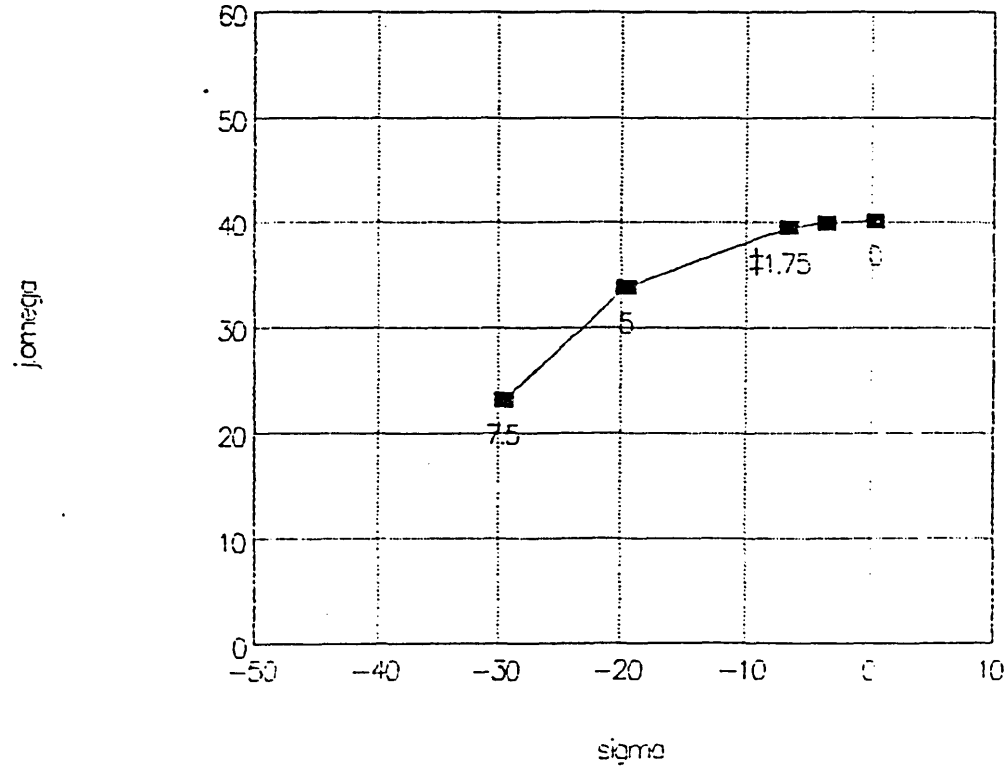

(b) high frequency

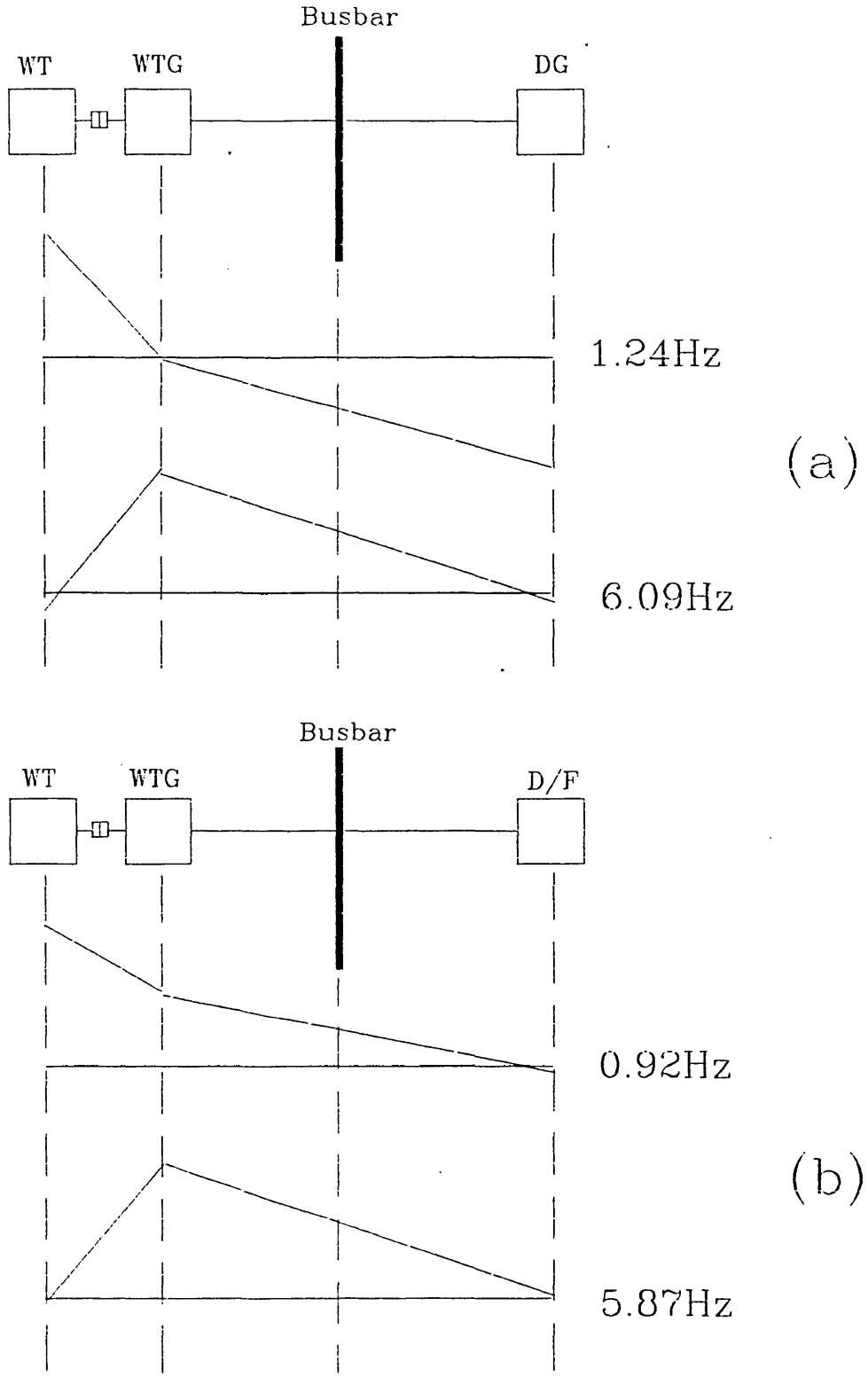

FIGURE 6.6 Modes of oscillation in (a) Wind Diesel (b) Wind Diesel Flywheel System using the mass/spring analogy (neglecting damping)

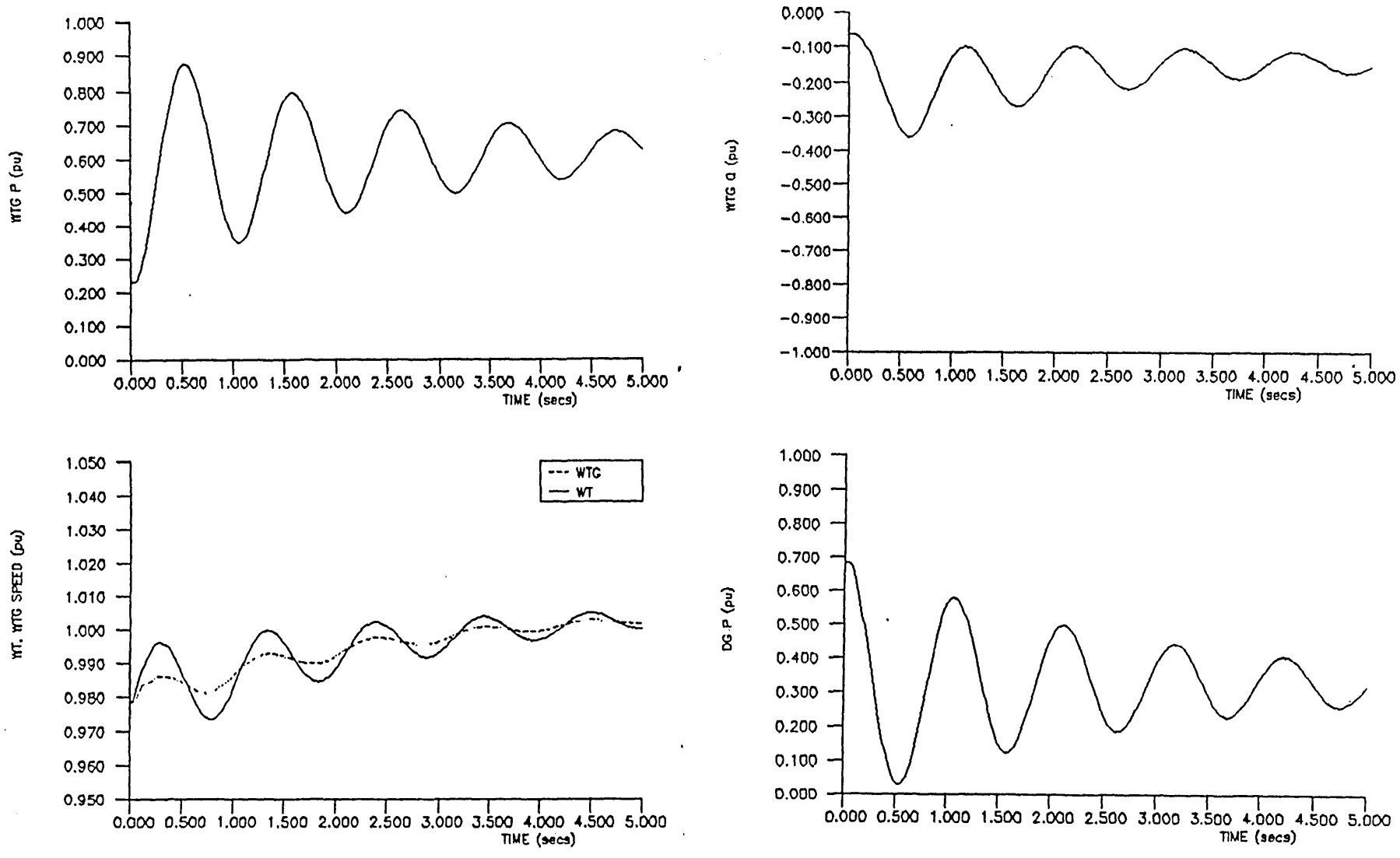

FIGURE6.7 Response of the wind/diesel/flywheel system without Power System Stabilisation - wind turbine mechanical power step change from 2.5 to 6kW

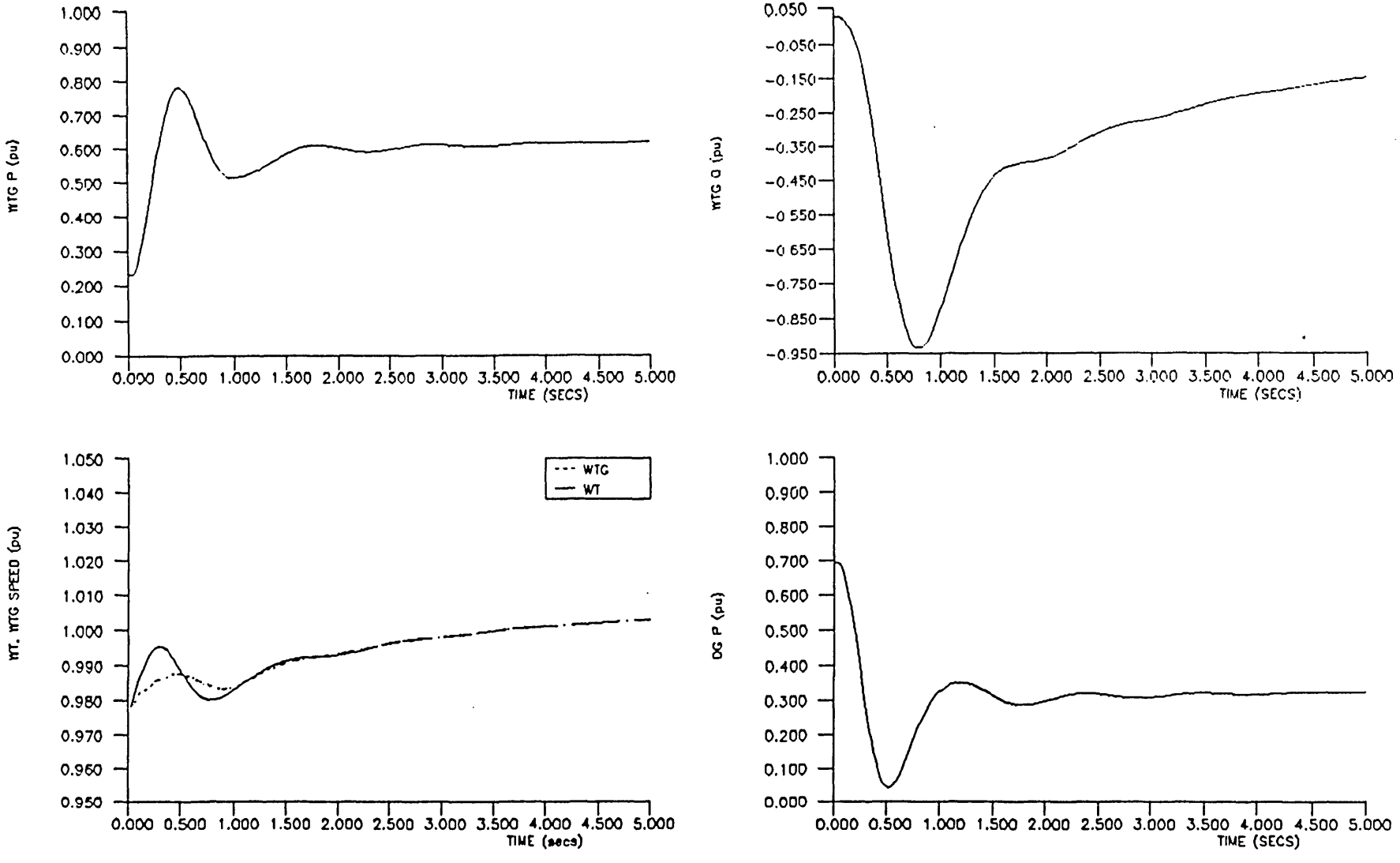

FIGURE 6.8 Response of the wind/diesel/flywheel system with Power System Stabilisation (sigma = -2.0 +/-j5.65) -wind turbine mechanical power step change from 2.5 to 6kW.

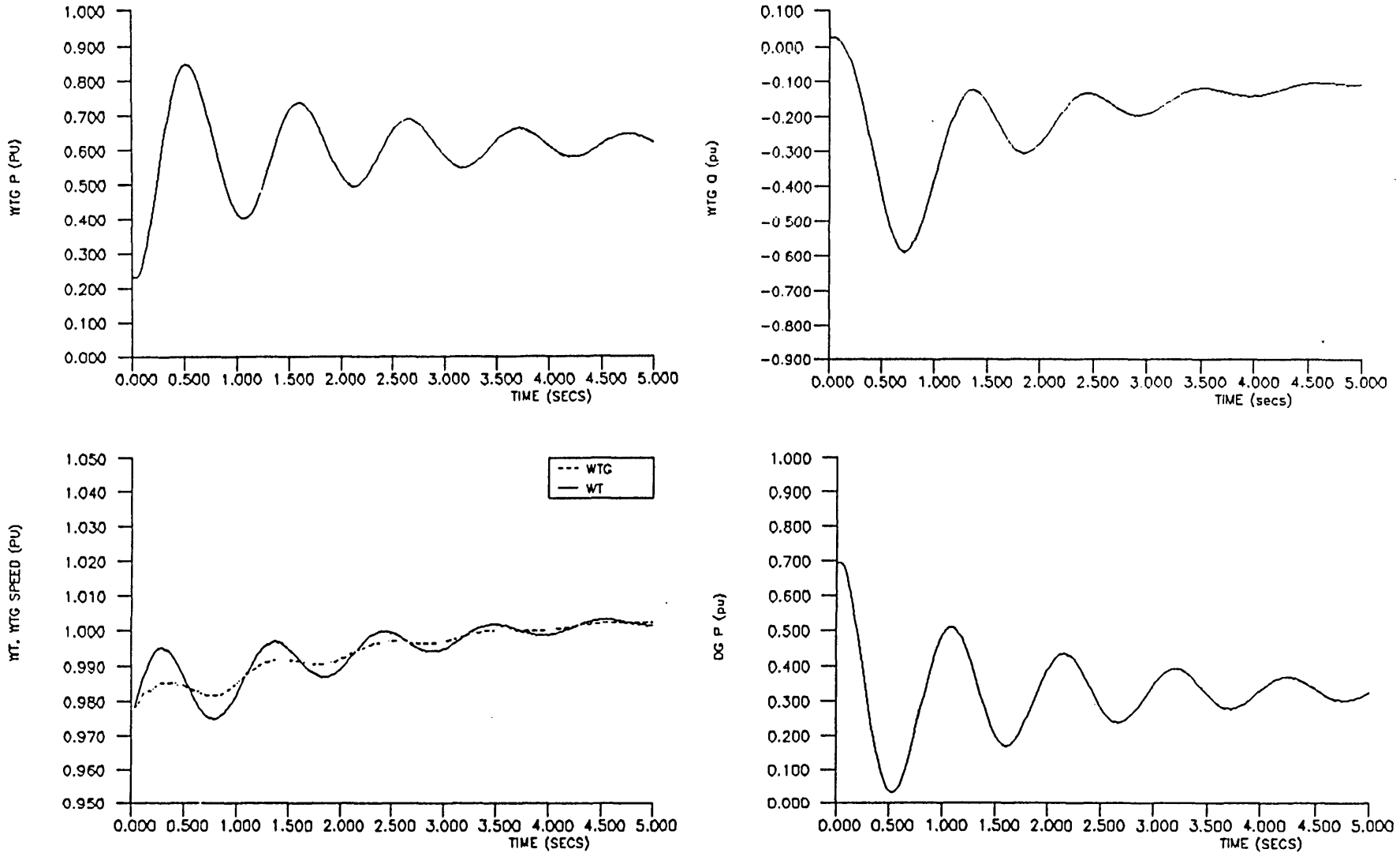

FIGURE 6.9 Response of the wind/diesl/flywheel system with Power System Stabilisation (sigma = -0.6 +/-j5.65) - wind turbine mechanical power step change from 2.5 to 6kW.

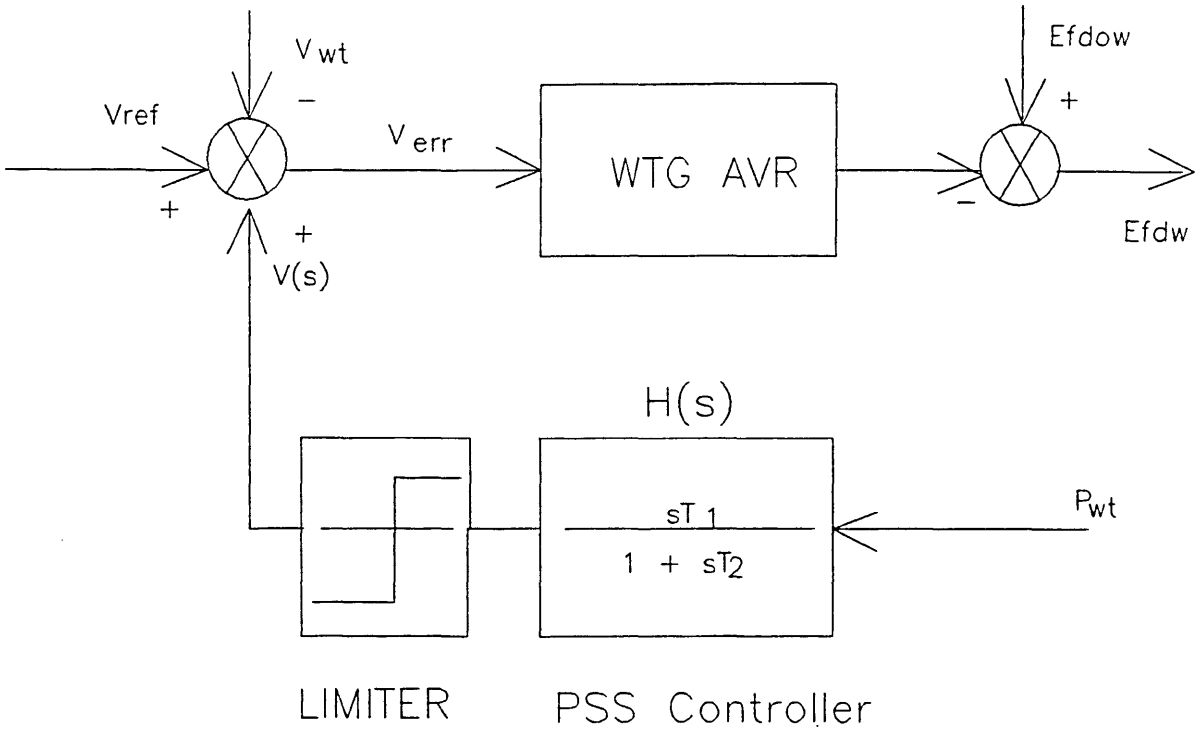

FIGURE 6.10 Power System Stabiliser with "Bang-Bang" controller

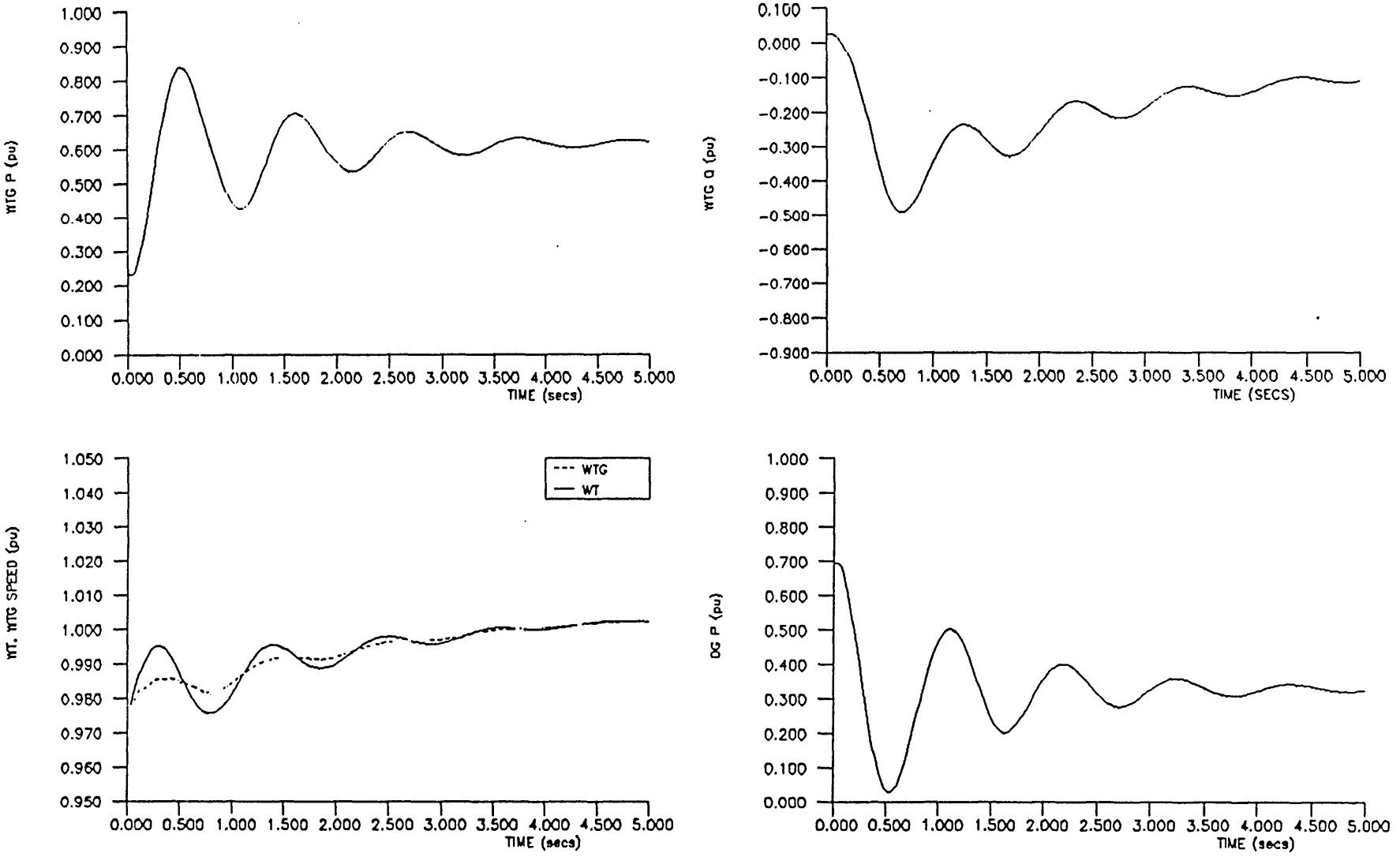

FIGURE 6.11 Response of the wind/diesel/flywheel system with Power System Stabilisation ("Bang-Bang" method) - wind turbine mechanical power step change from 2.5 to 6kW.

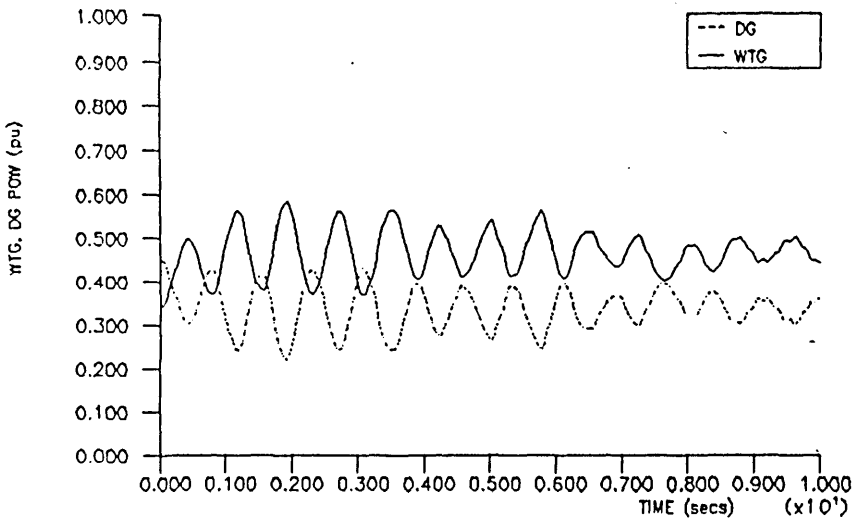

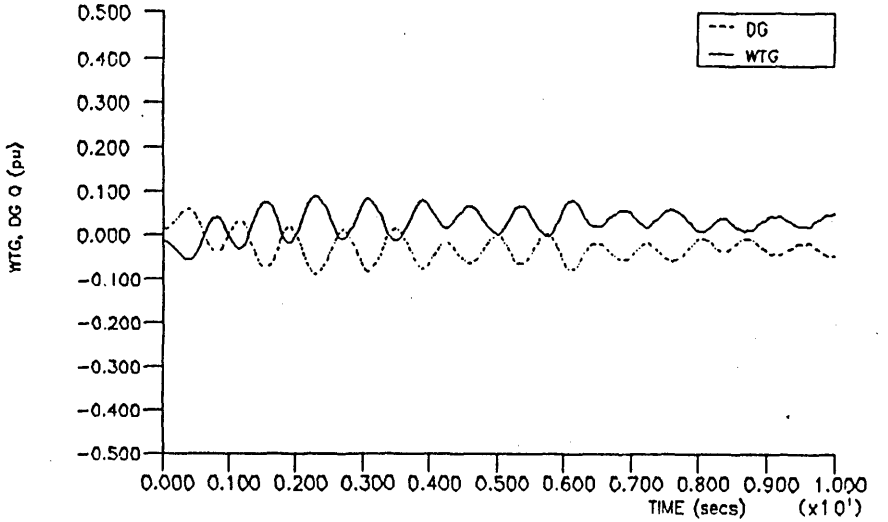

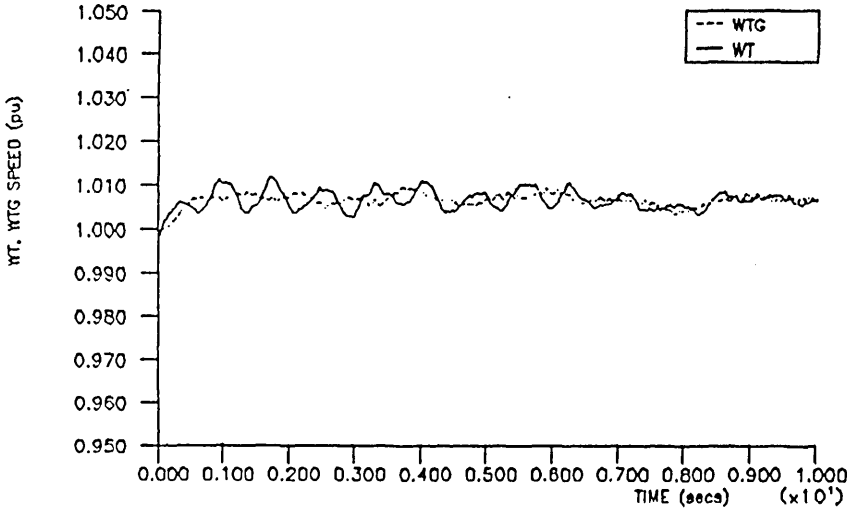

FIGURE 6.12 (a)
The effect of wind turbine mechanical damping upon system stability (Dsh=220Nm/rad/s)
-wind/diesel
-gaussian wind turbine mechanical power @ 5kW, consumer load = 7kW

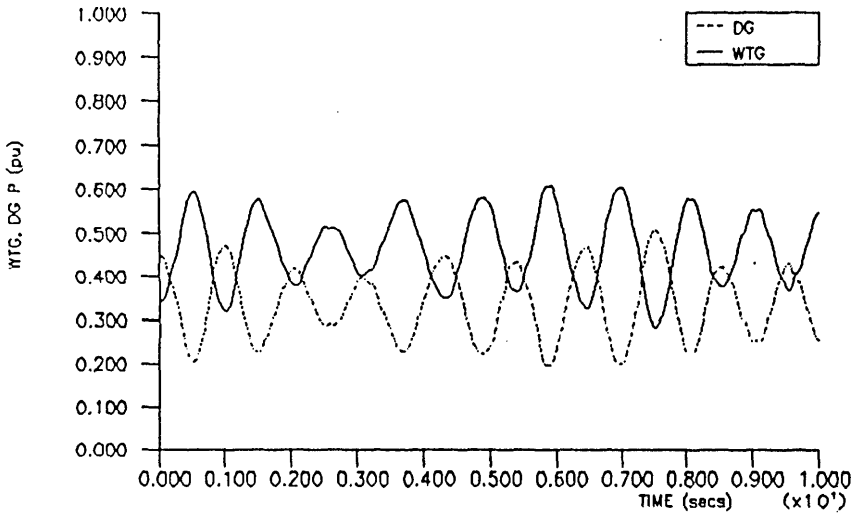

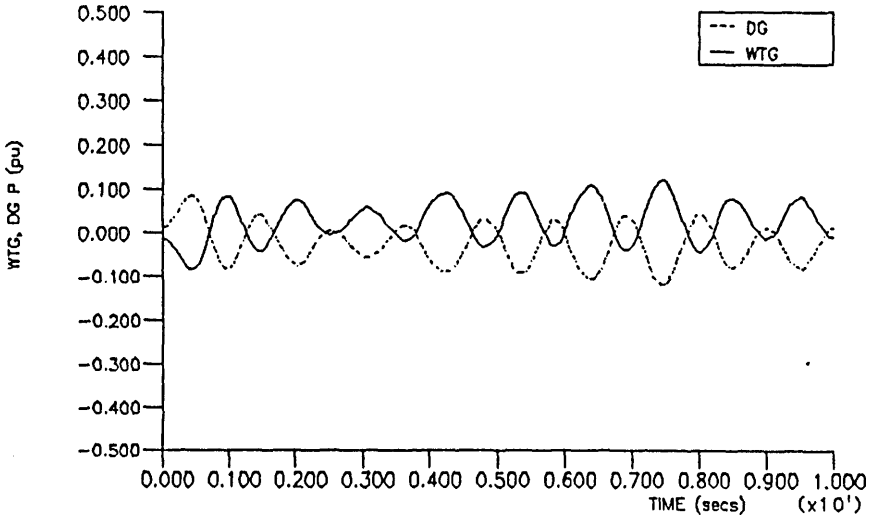

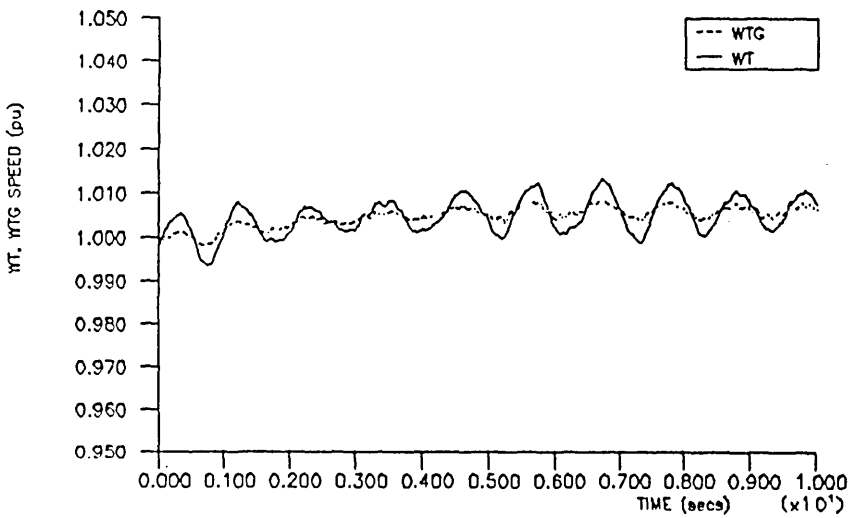

FIGURE 6 12 (b)
The effect of wind turbine mechanical damping upon system stability (Dsh=220Nm/rad/s)
-wind/diesel/flywheel(Jfly=11.8kgm²)
-gaussian wind turbine mechanical power @ 5kW, consumer load = 7kW

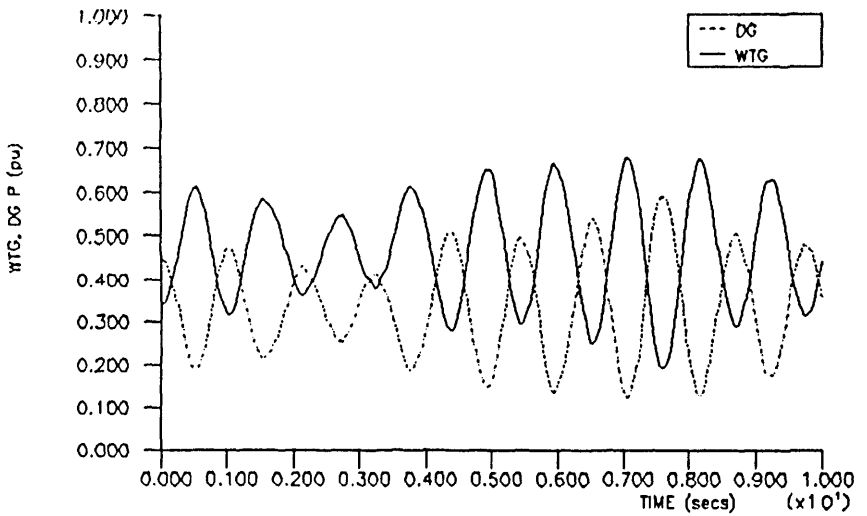

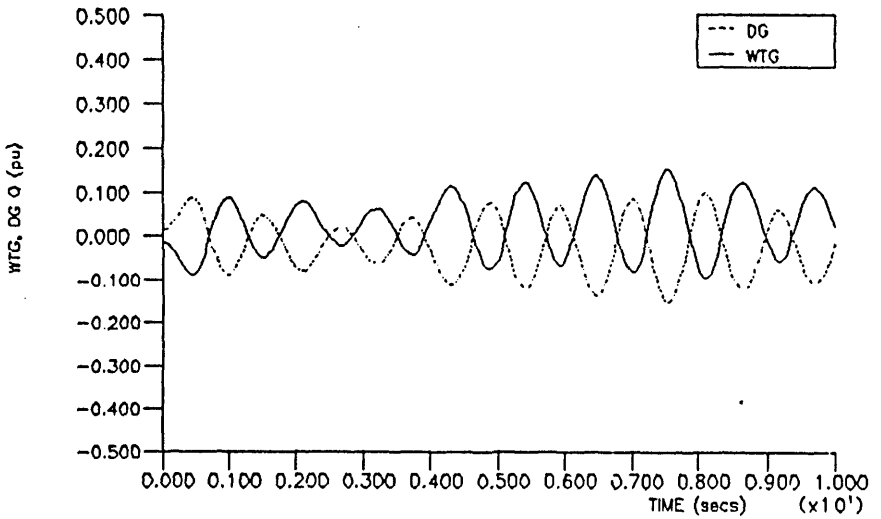

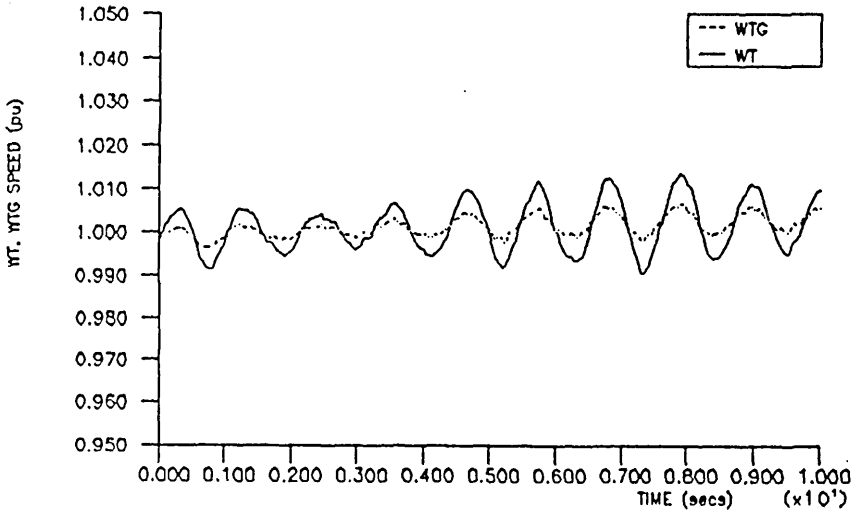

FIGURE 6.12 (c)
The effect of wind turbine mechanical damping upon system stability (Dsh=220Nm/rad/s)
-wind/diesel/flywheel(Jfly=58kgm²)
-gaussian wind turbine mechanical power @ 5kW, consumer load = 7kW

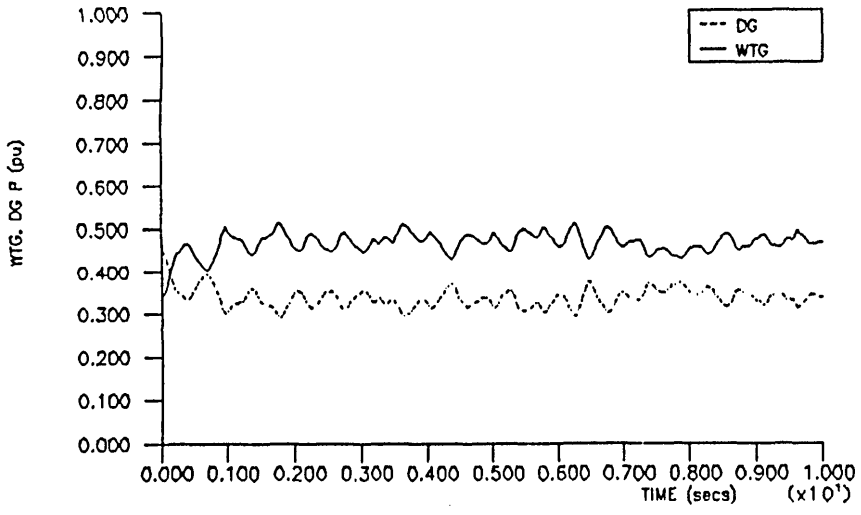

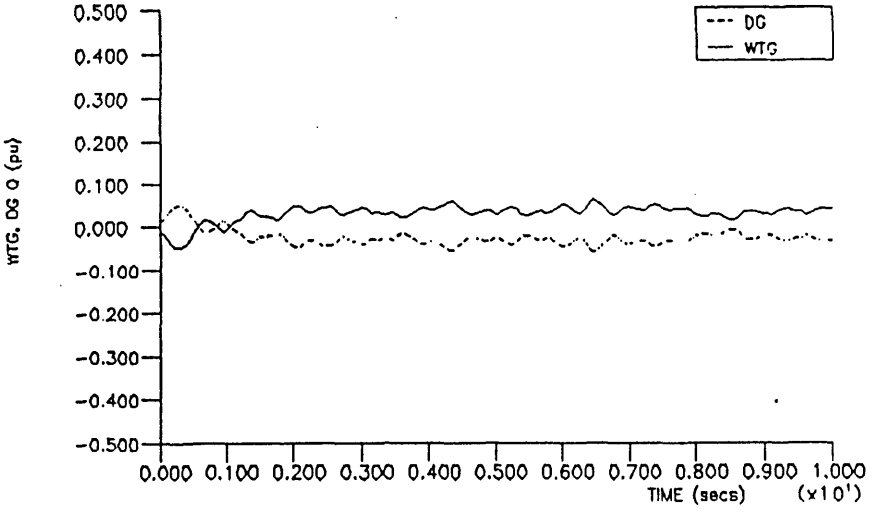

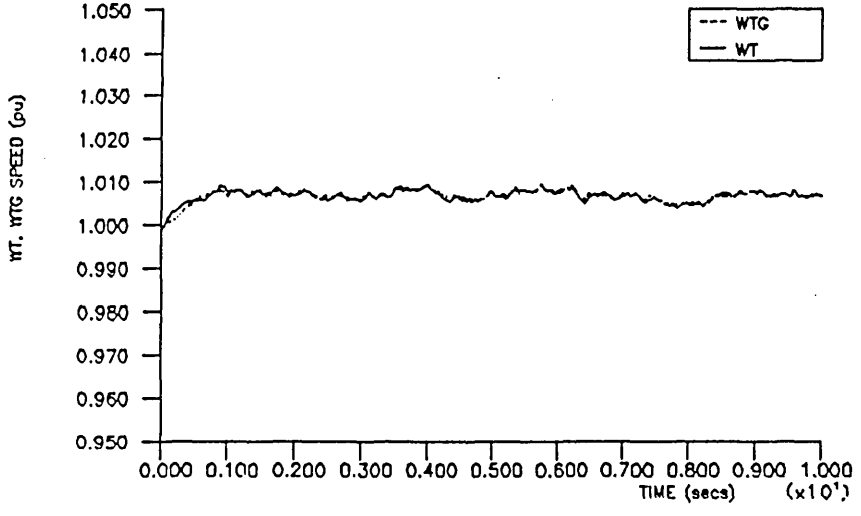

FIGURE 6.13 (a)
The effect of wind turbine mechanical damping upon system stability (Dsh=2200Nm/rad/sec)
-wind diesel
-gaussian wind turbine mechanical power @ 5kW, consumer load = 7kW

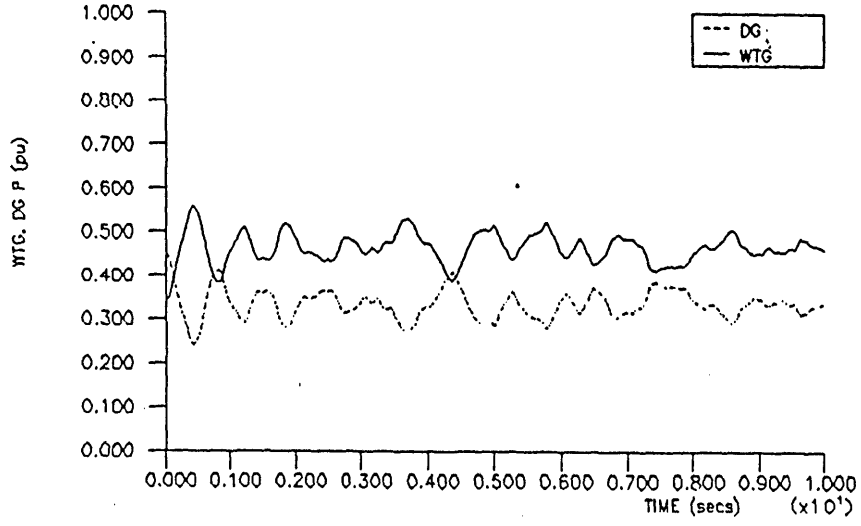

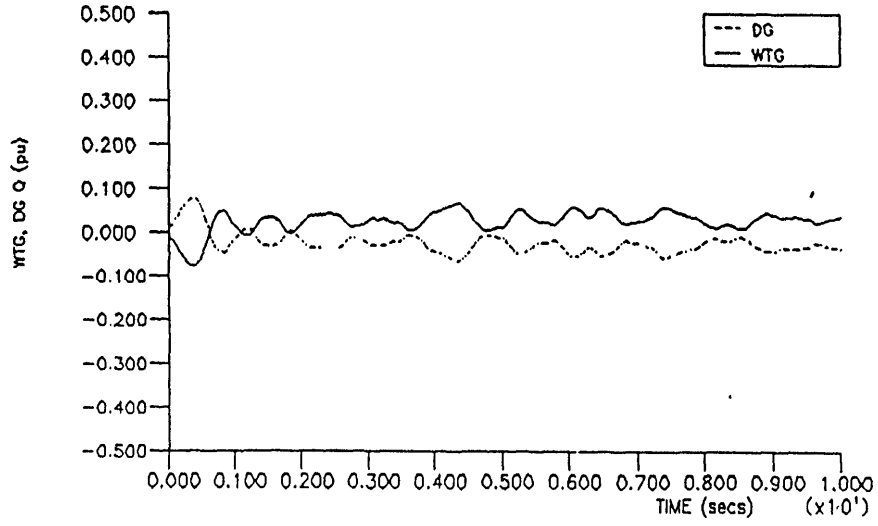

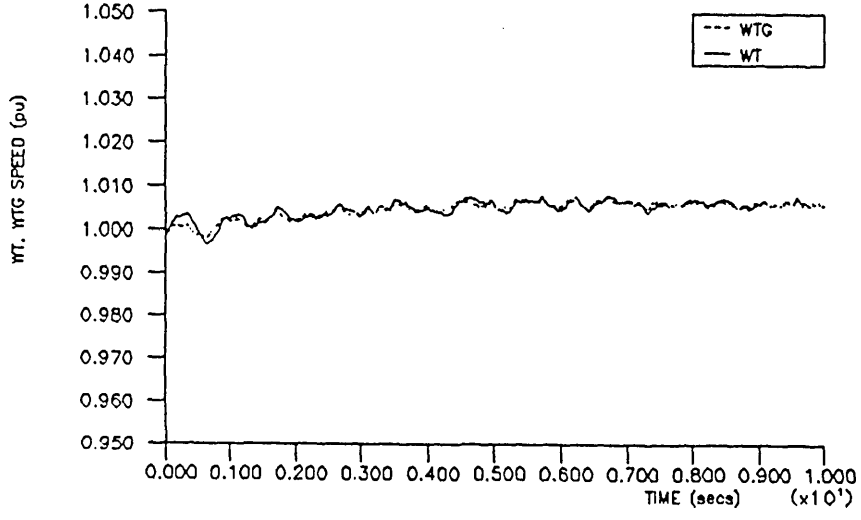

FIGURE 6.13 (b)
The effect of wind turbine mechanical damping upon system stability (Dsh=2200Nm/rad/s)
-wind/diesel/flywheel(Jfly=11.8kgm²)
-gaussian wind turbine mechanical power @ 5kW, consumer load = 7kW

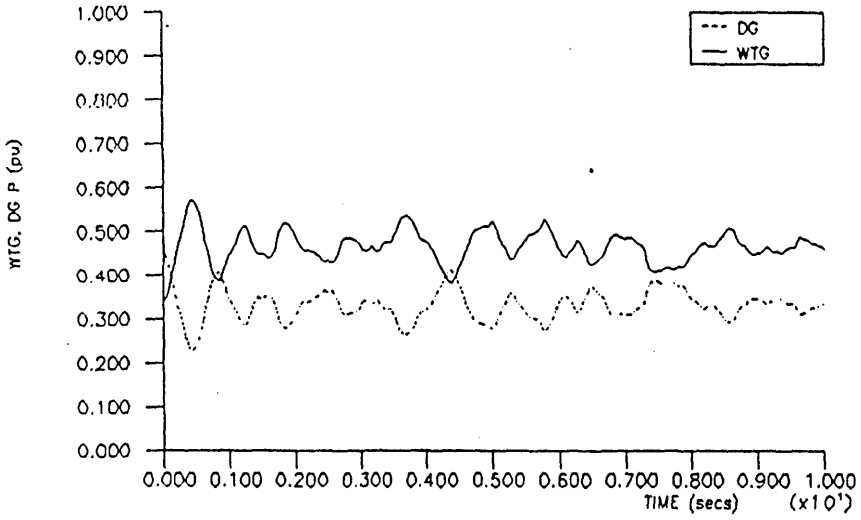

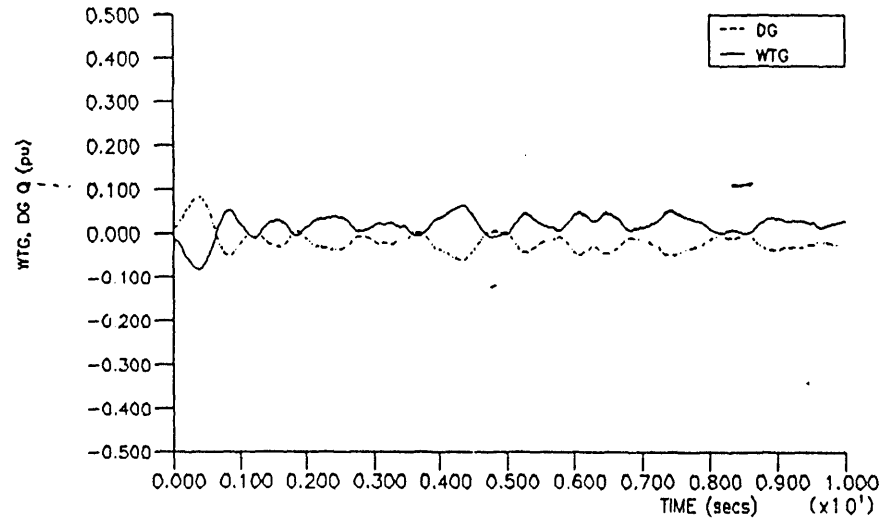

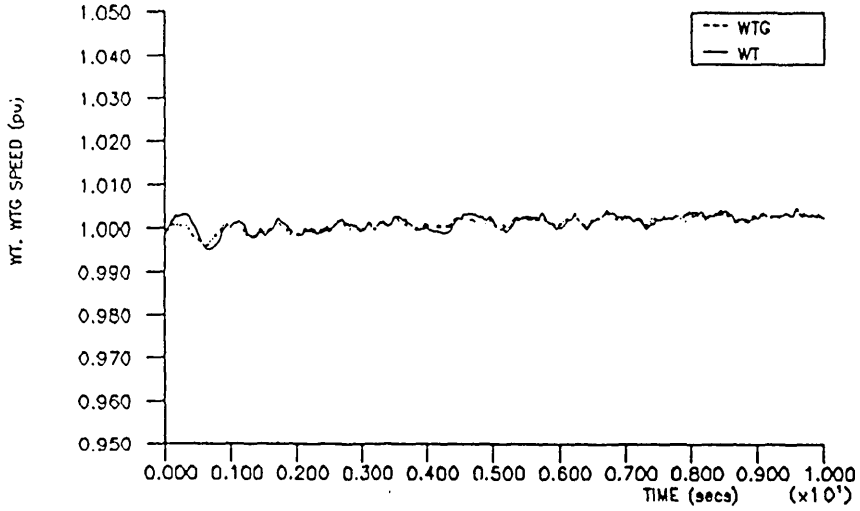

FIGURE 6.13 (c)
The effect of wind turbine mechanical damping upon system stability (Dsh=2200Nm/rad/s)
-wind/diesel/flywheel(Jfly=58kgm²)
-gaussian wind turbine mechanical power @ 5kW, consumer load = 7kW

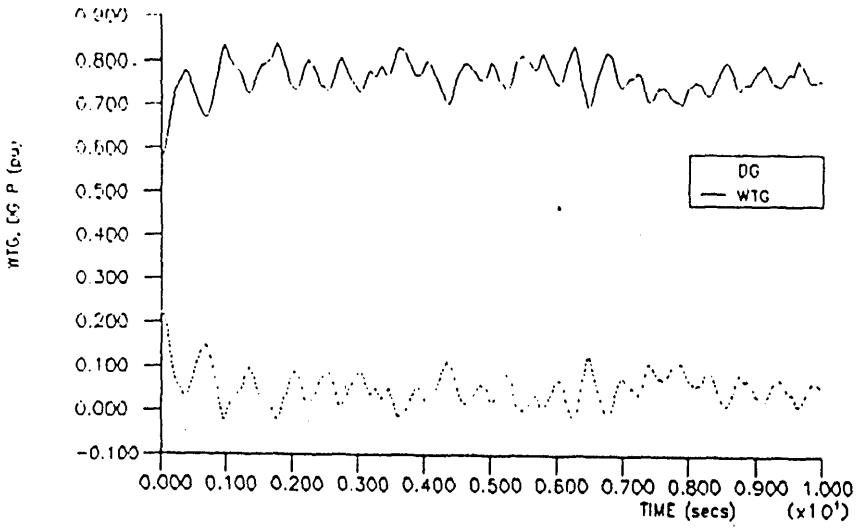

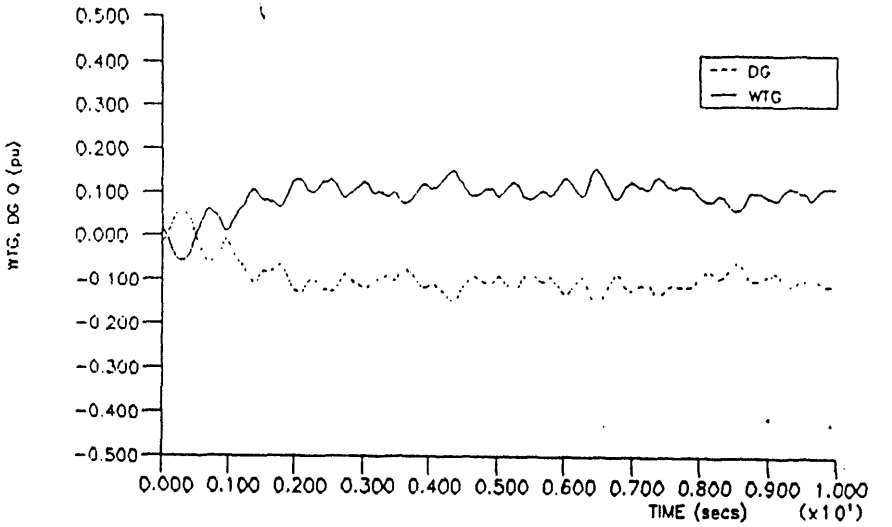

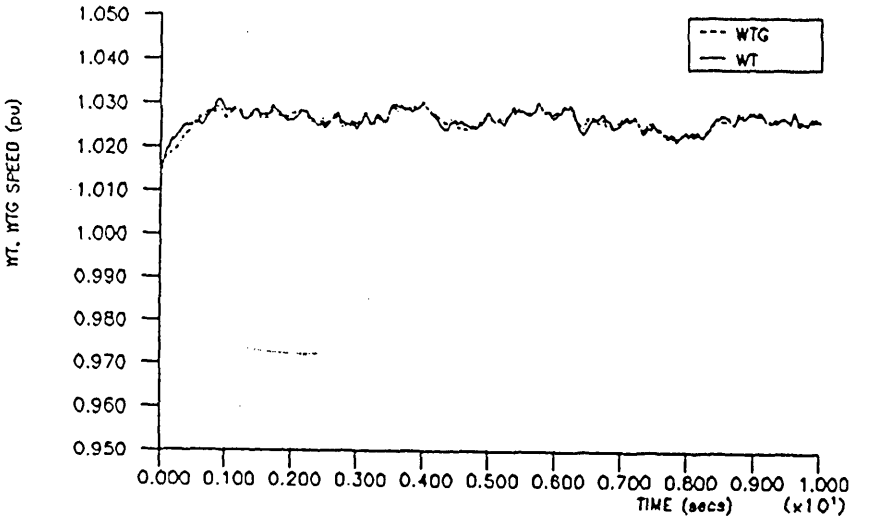

FIGURE 6.14 (a)
The effect of wind turbine mechanical damping upon system stability (Dsh=2200 Nm/rad/s)
-wind diesel
-gaussian wind turbine mechanical power @ 5kW, consumer load = 7kW
- positive damping effect of Cp/lambda (Vinf=11m/s)

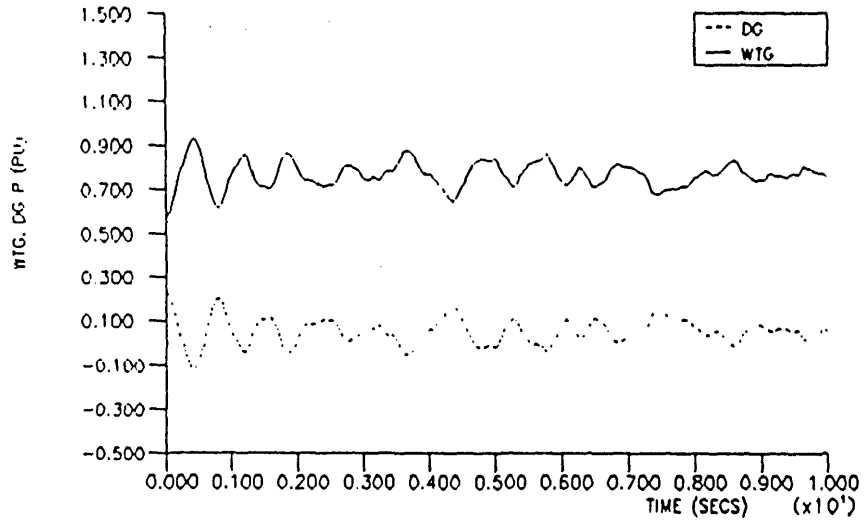

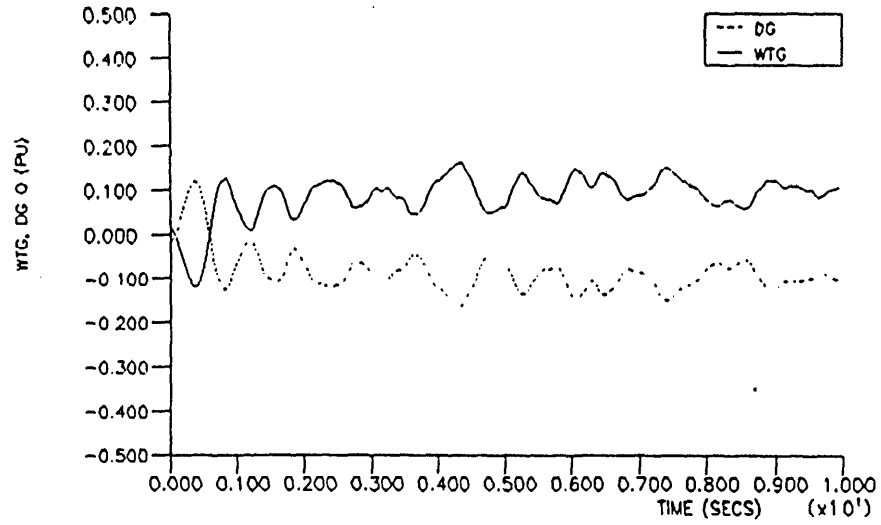

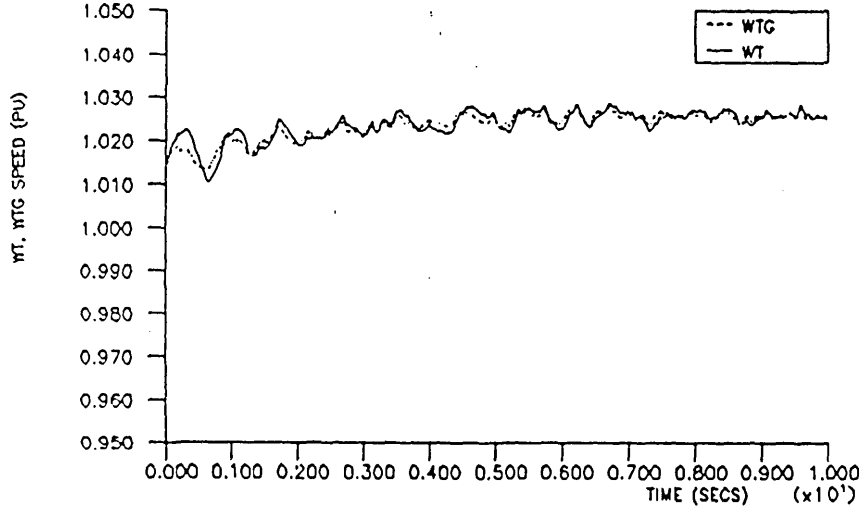

FIGURE 6.14 (b)
The effect of wind turbine mechanical damping upon system stability (Dsh=2200 Nm/rad/s)
-wind diesel/flywheel(Jfly=11.8kgm²)
-guassian wind turbine mechanical power @ 5kW, consumer load = 7kW

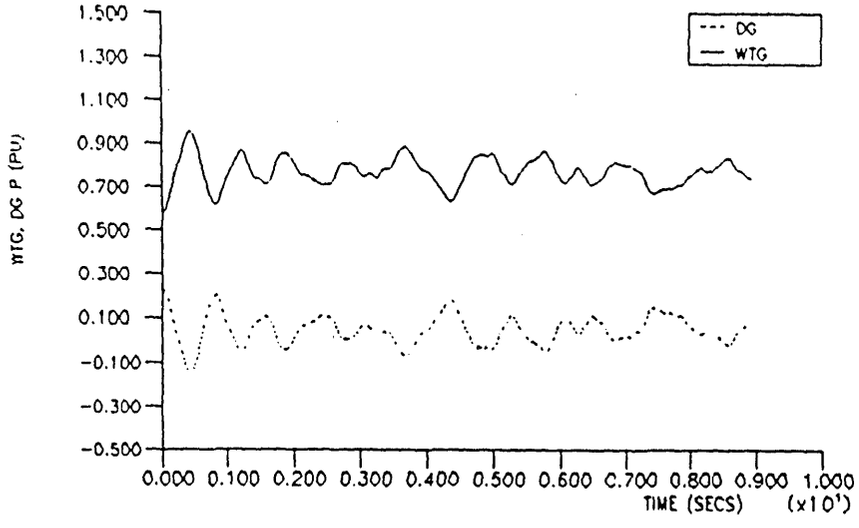

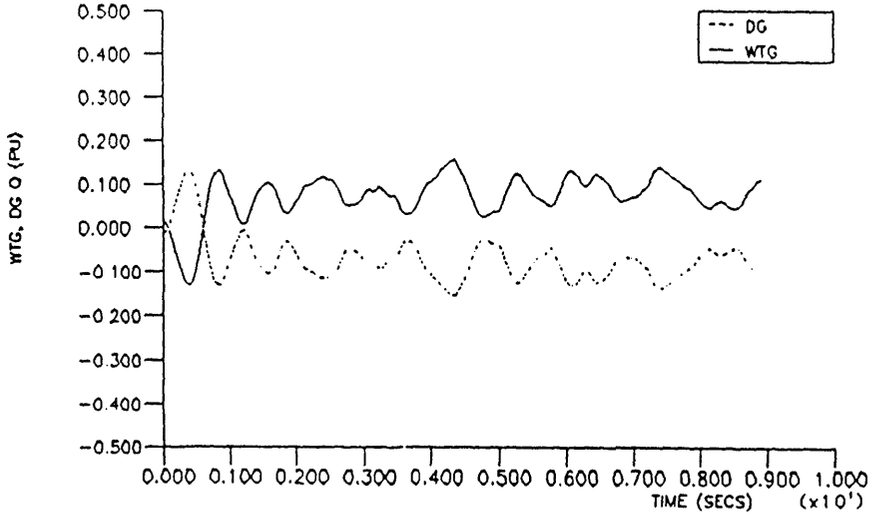

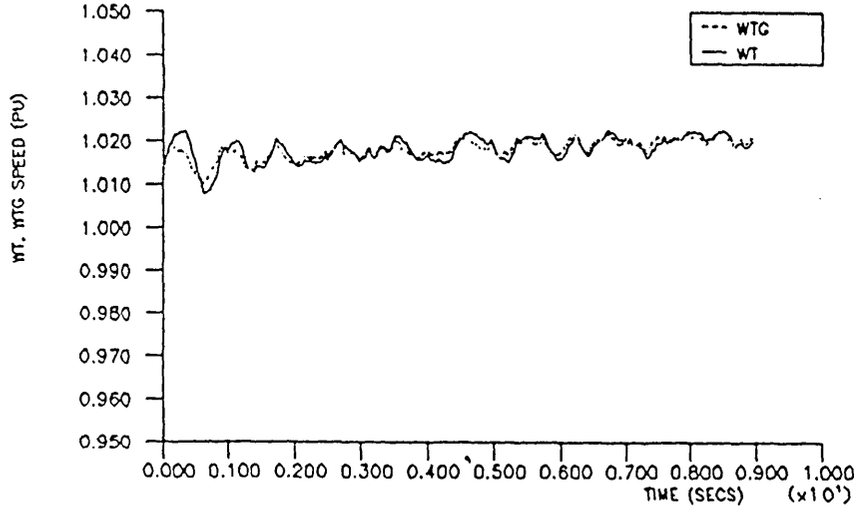

FIGURE 6.14 (c)
The effect of wind turbine mechanical damping upon system stability (Dsh=2200 Nm/rad/s)
-wind diesel/flywheel(Jfly=58kgm^2)
-gaussian wind turbine mechanical power @ 5kW, consumer load = 7kW

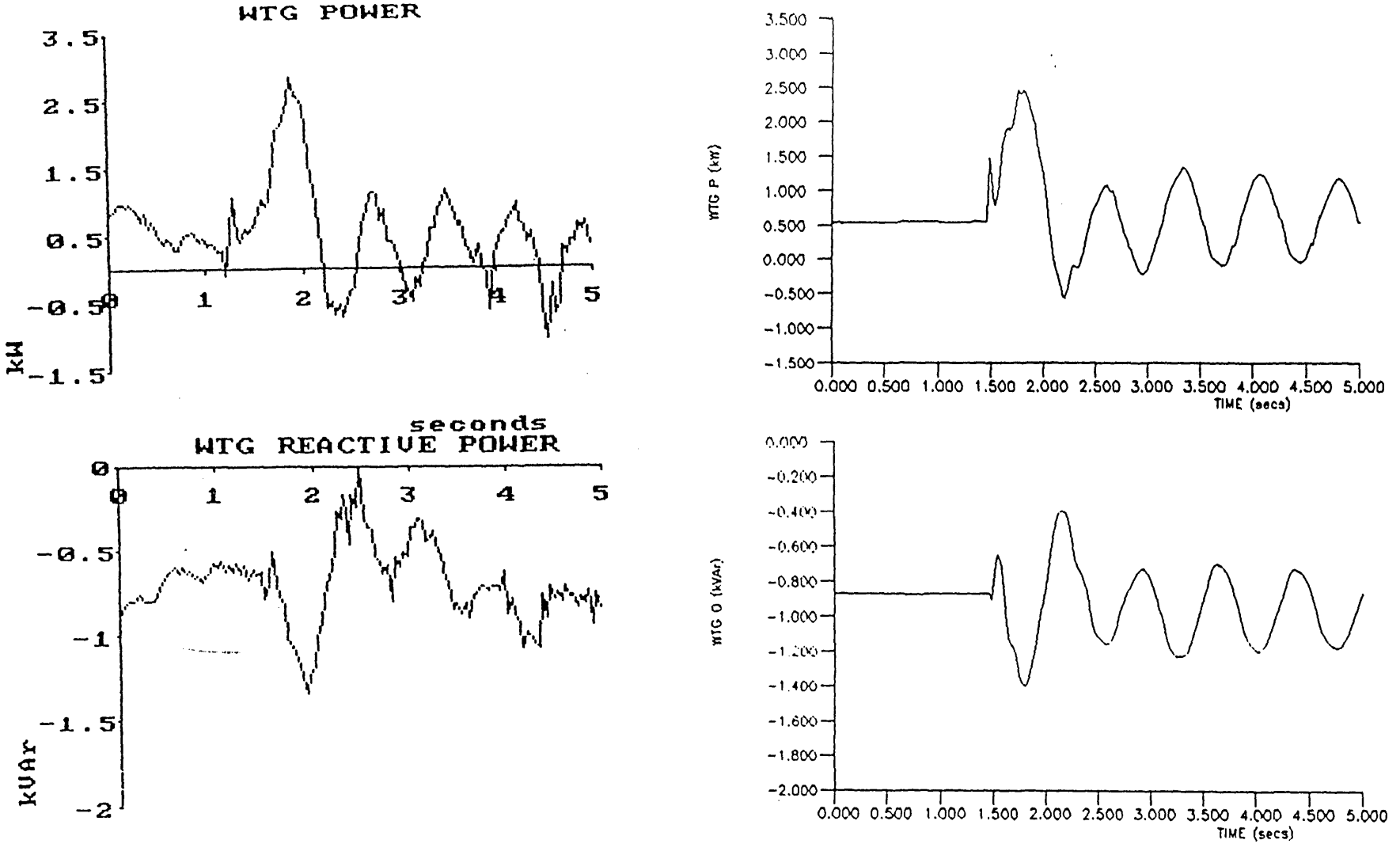

FIGURE 6.15 Step load test on the wind/diesel system with frequency controlled dumpload (consumer load = 0 to 3.4kW after 1.5 secs, Kfp=2.5kW/Hz)
(a) actual (b) simulated

FIGURE 6.15 Contd (a) actual

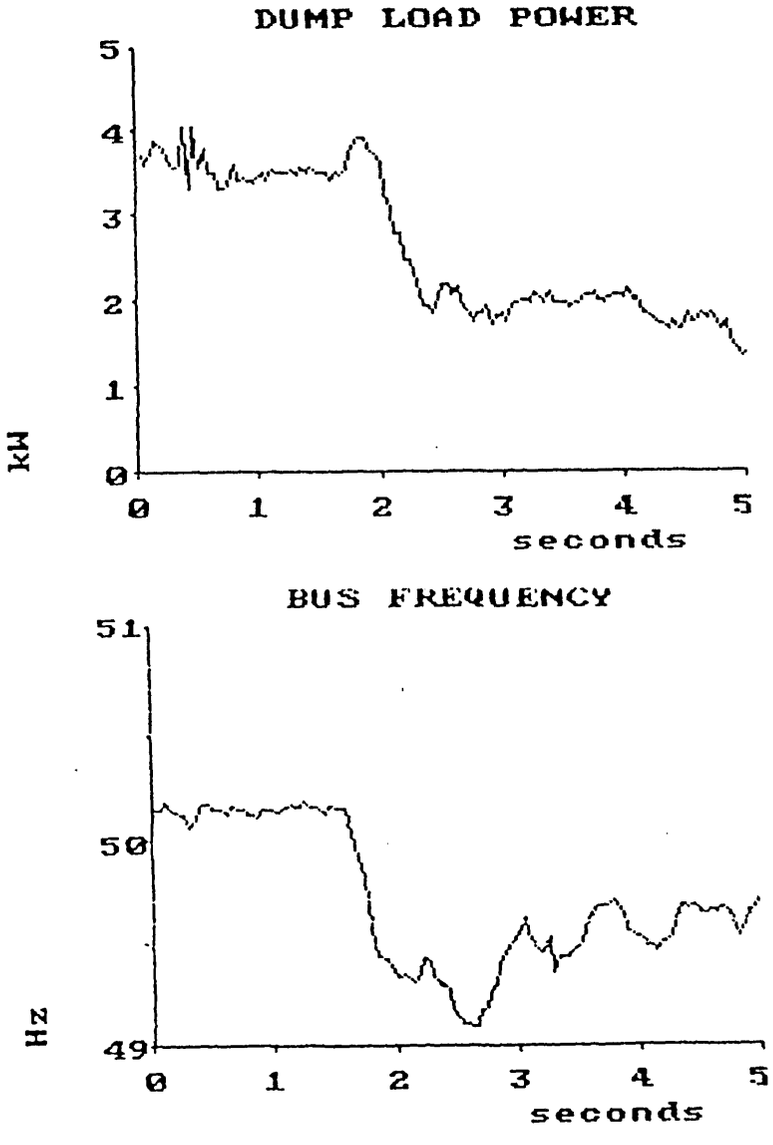

(b) simulated

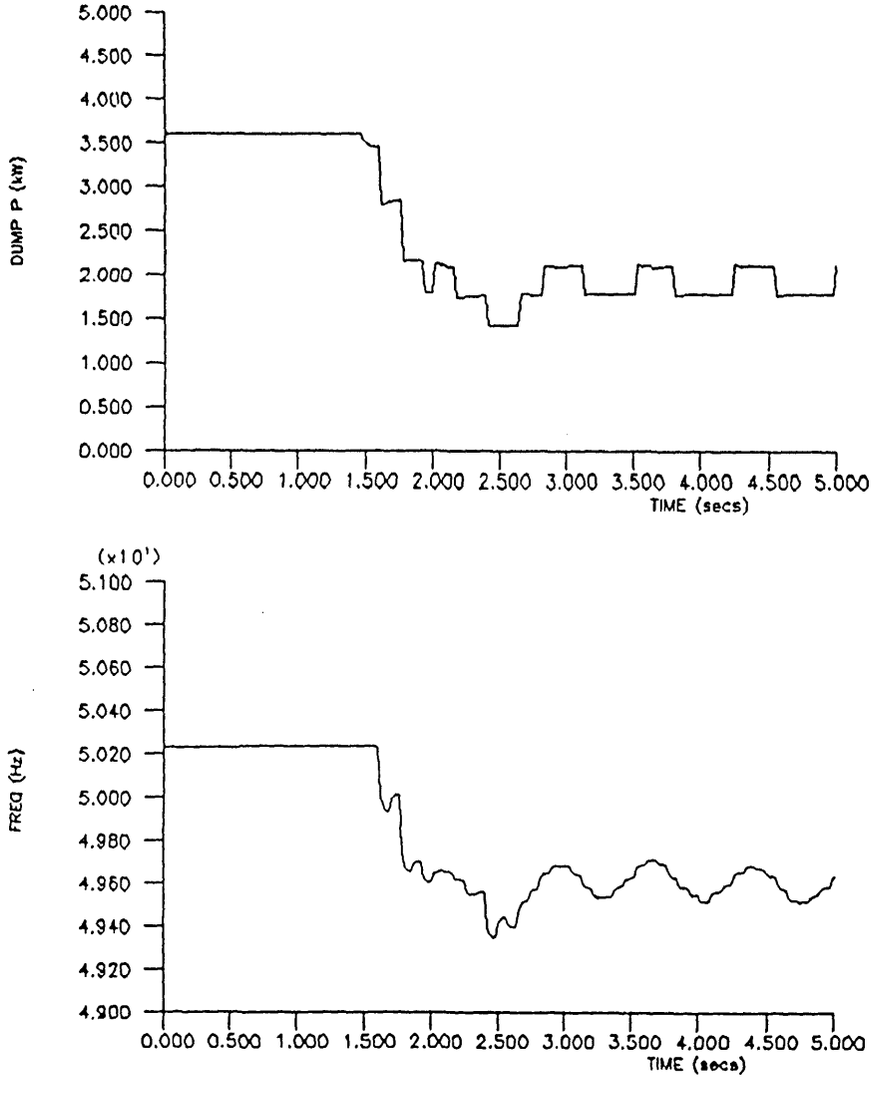

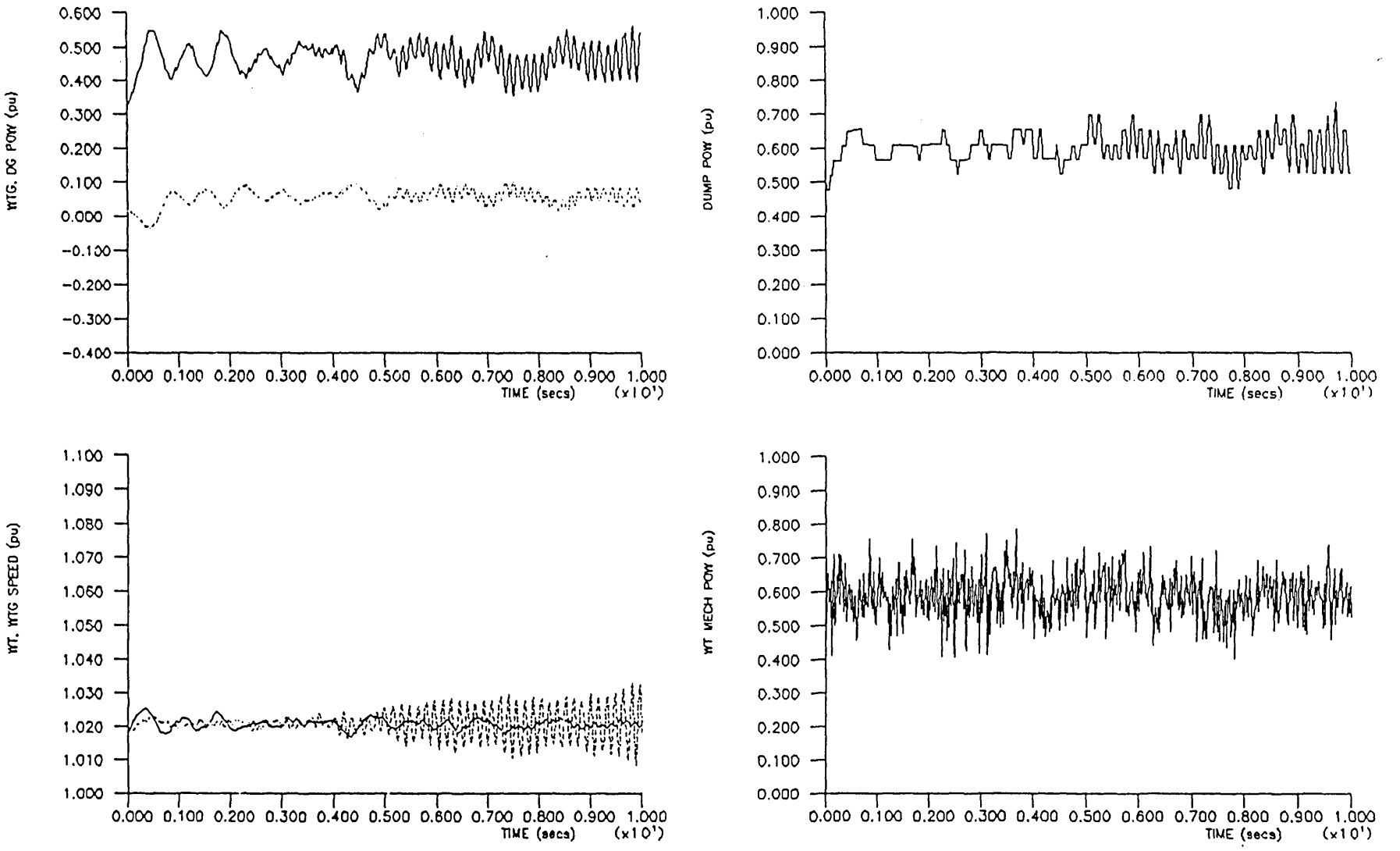

FIGURE 6.16 Effect of gaussian wind turbine mechanical power on the wind/diesel system under the frequency control dump load, Pmwt @ 5kW, consumer load = 0kW

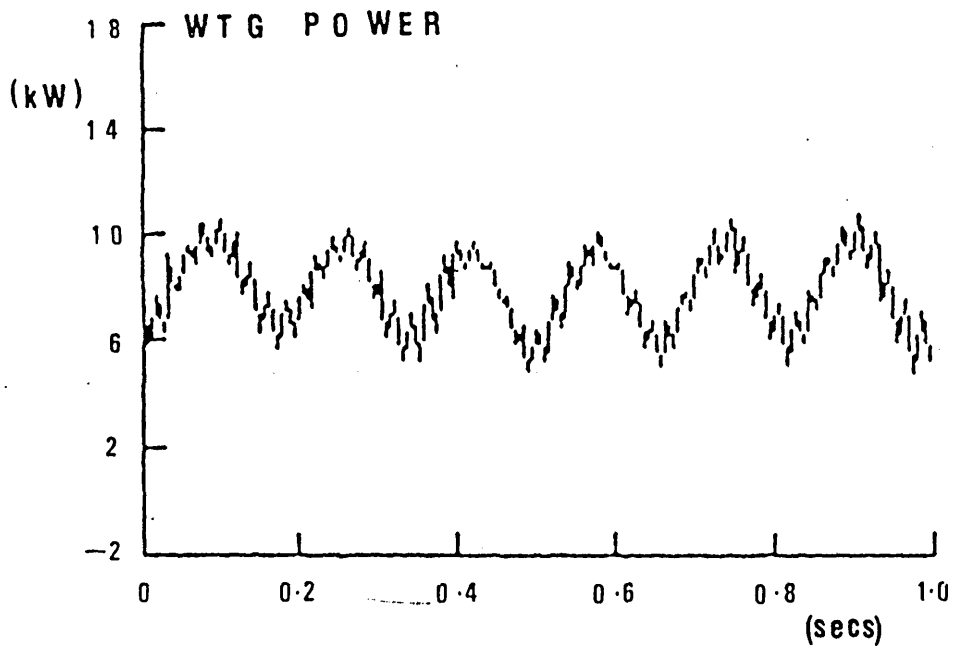

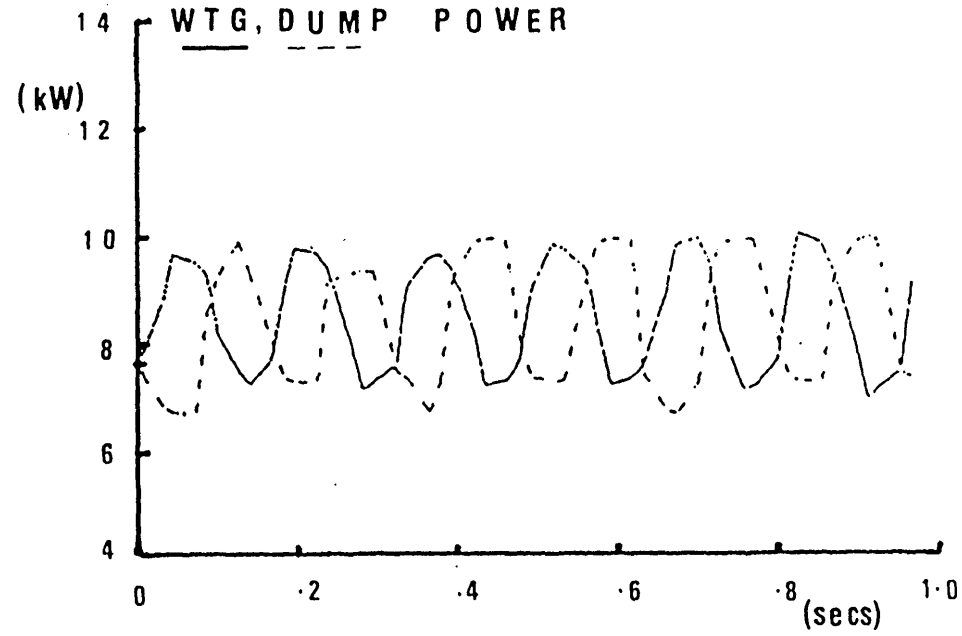

FIGURE 6.17 1 sec segment demonstrating anti-phase relationship of the frequency control dump load to the wind turbine generator
(a) actual (b) simulated

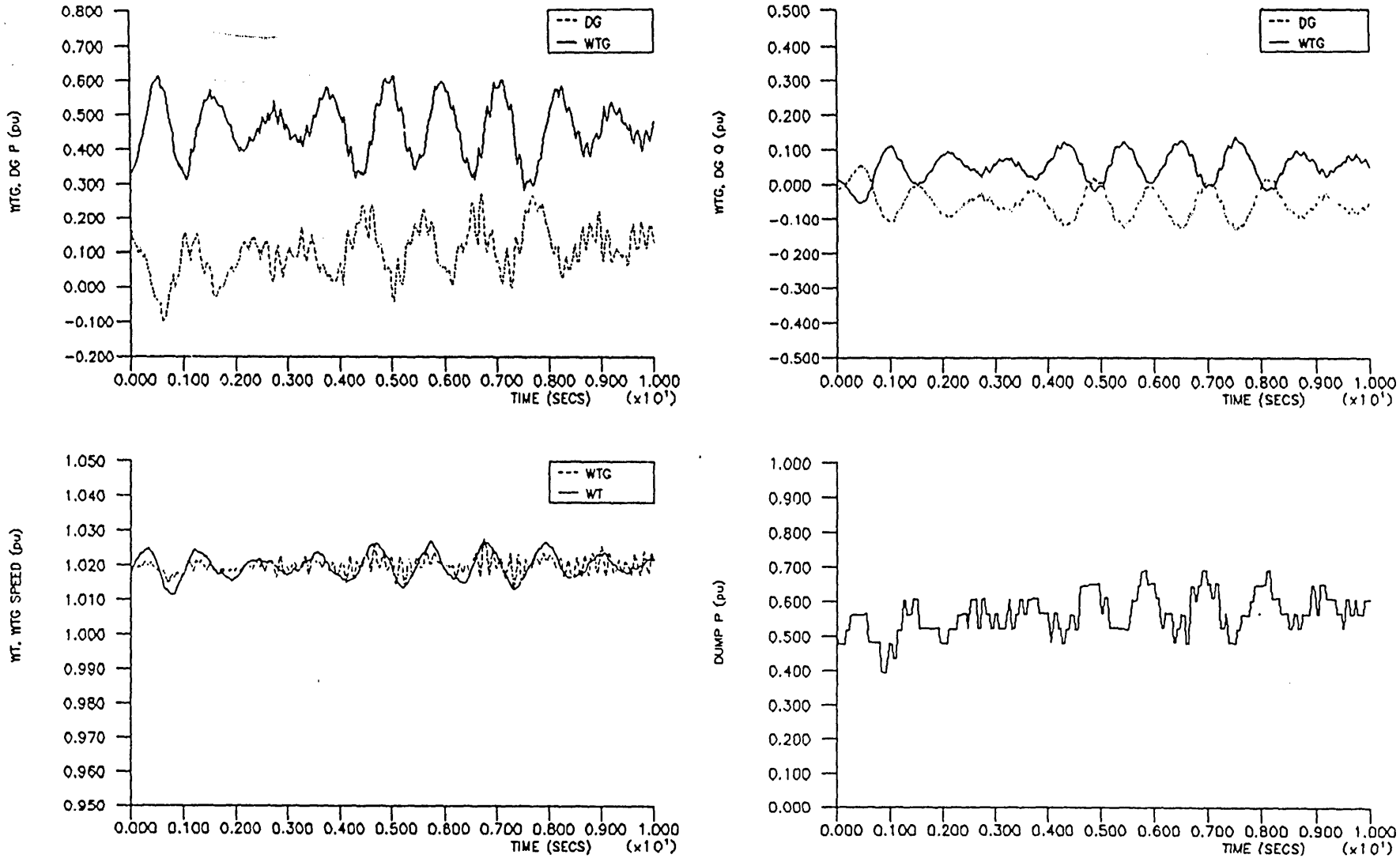

FIGURE 6.18 Effect of guassian wind turbine mechanical power on the wind/diesel/ flywheel (Jfly=11.8kgm^2) under the frequency control dump load, Pmwt @ 5kW, consumer load = 0kW

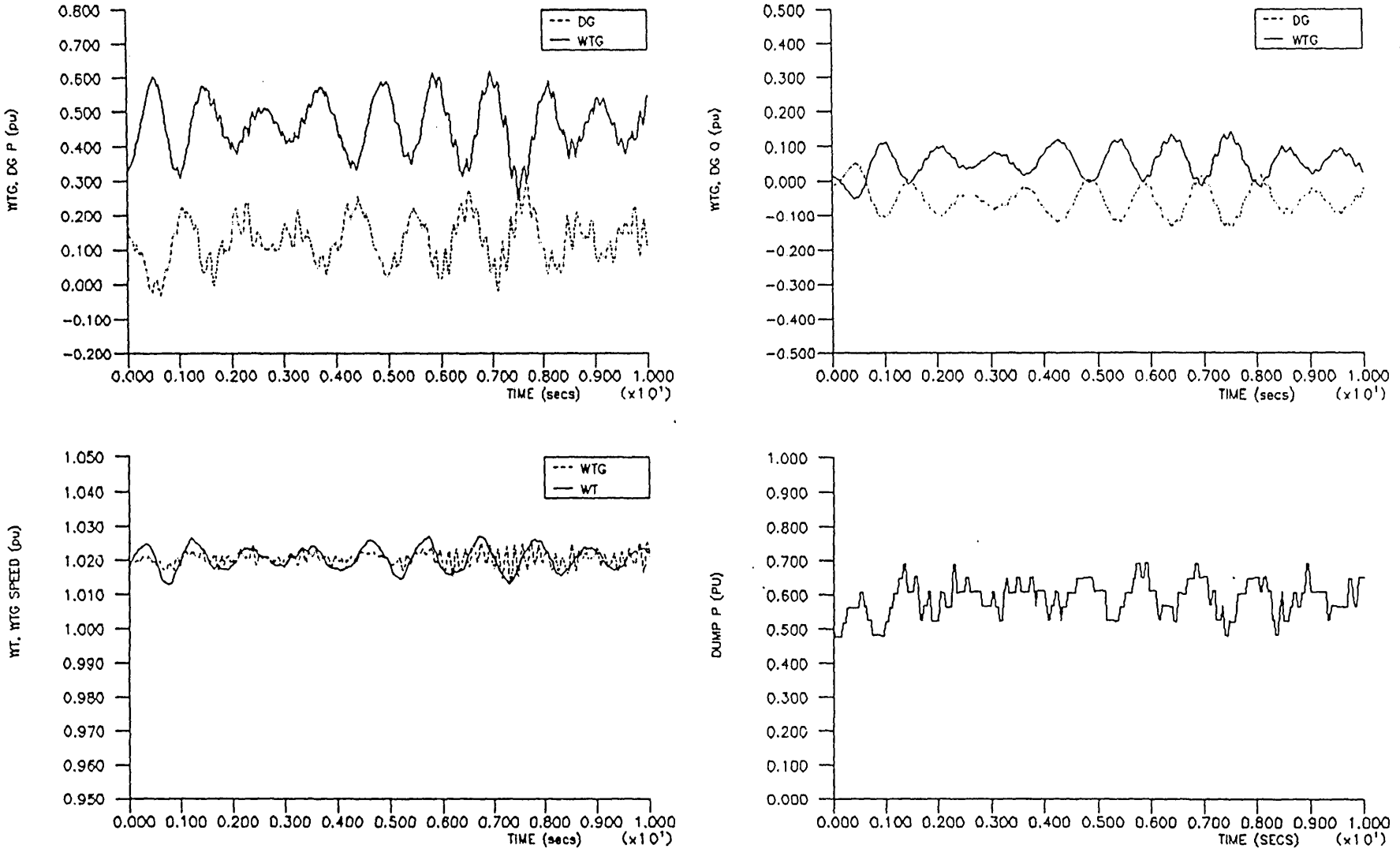

FIGURE 6.19 Effect of guassian wind turbine mechanical power on the wind/diesel/ flywheel (Jfly=58kgm²) under the frequency control dump load, Pmwt @ 5kW, consumer load = 0kW

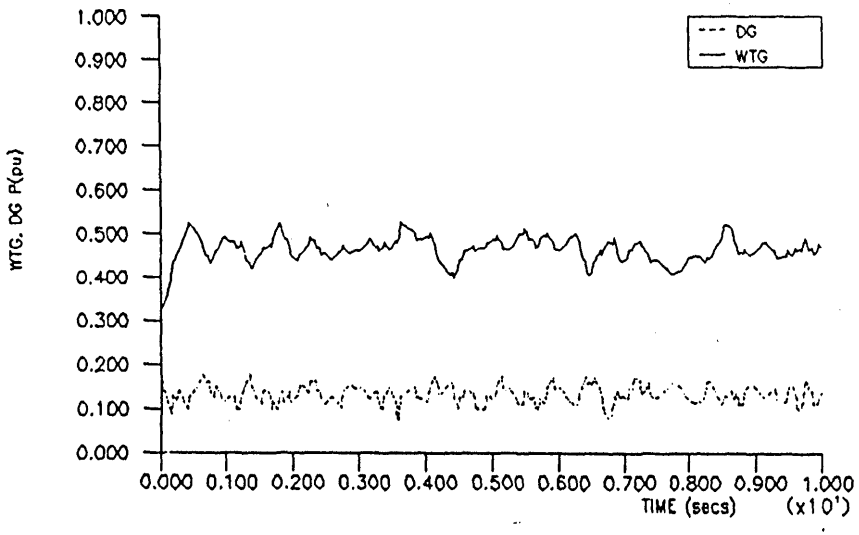

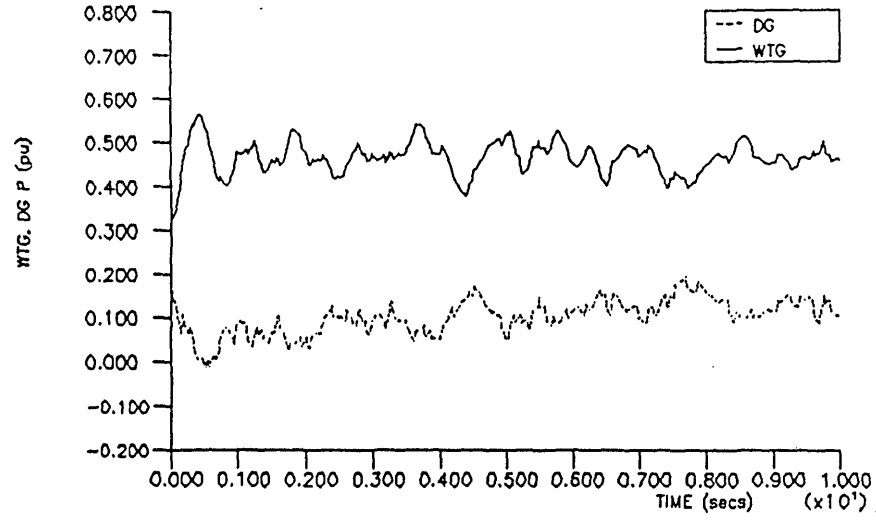

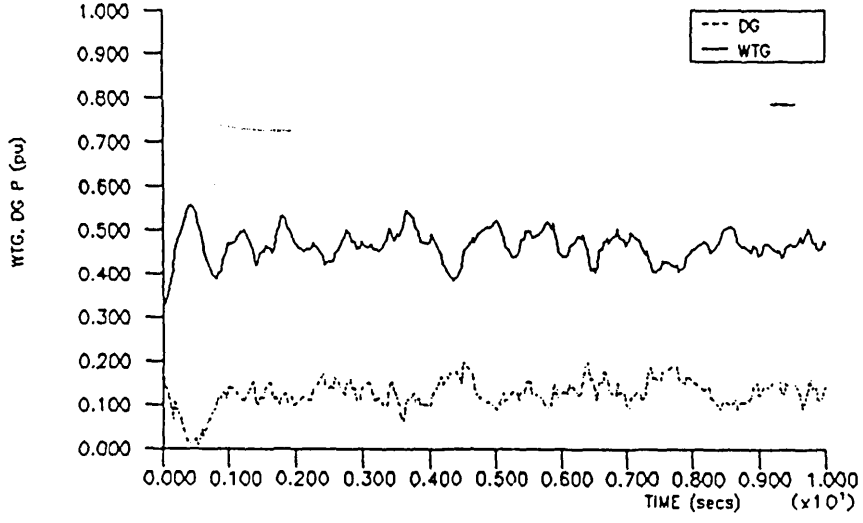

FIGURE 6.20 Effect of guassian wind turbine mechanical power on the wind/diesel/flywheel system under the frequency control dumpload, Pmwt @ 5kW consumer load = 0kW, Dsh = 2200Nm/rad/s.
(a) Jfly=0kgm²
(b) Jfly=11.8kgm²
(c) Jfly=58kgm²

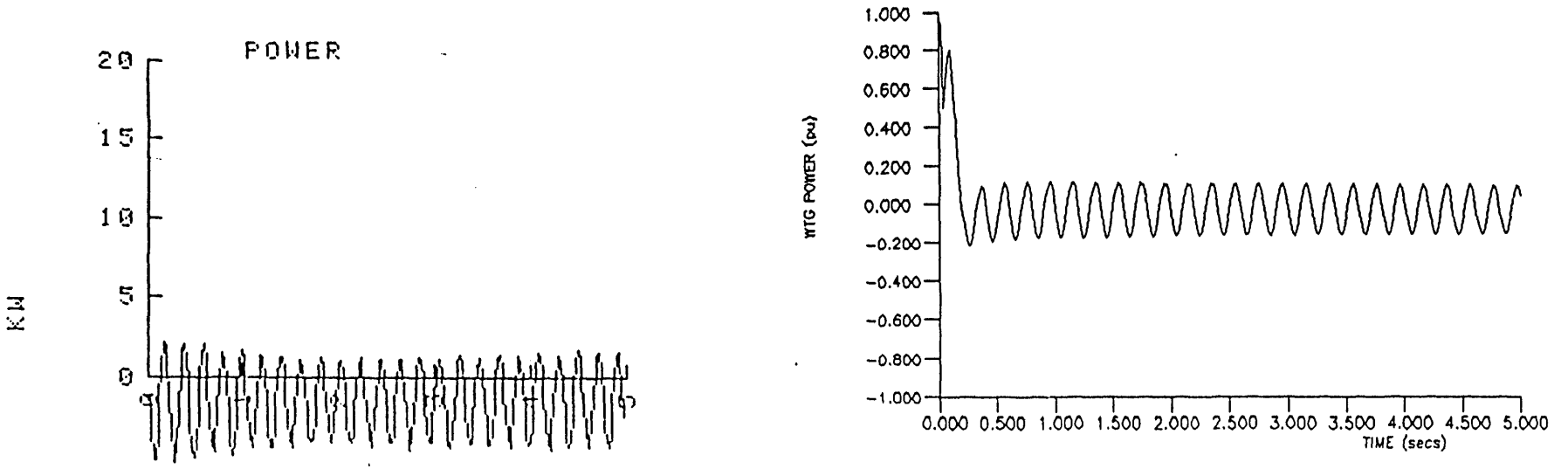

FIGURE 6.21 Motoring of the wind turbine following severe disturbance on the wind/diesel/flywheel system at low wind speed - no dumpload
(a) actual (b) simulated

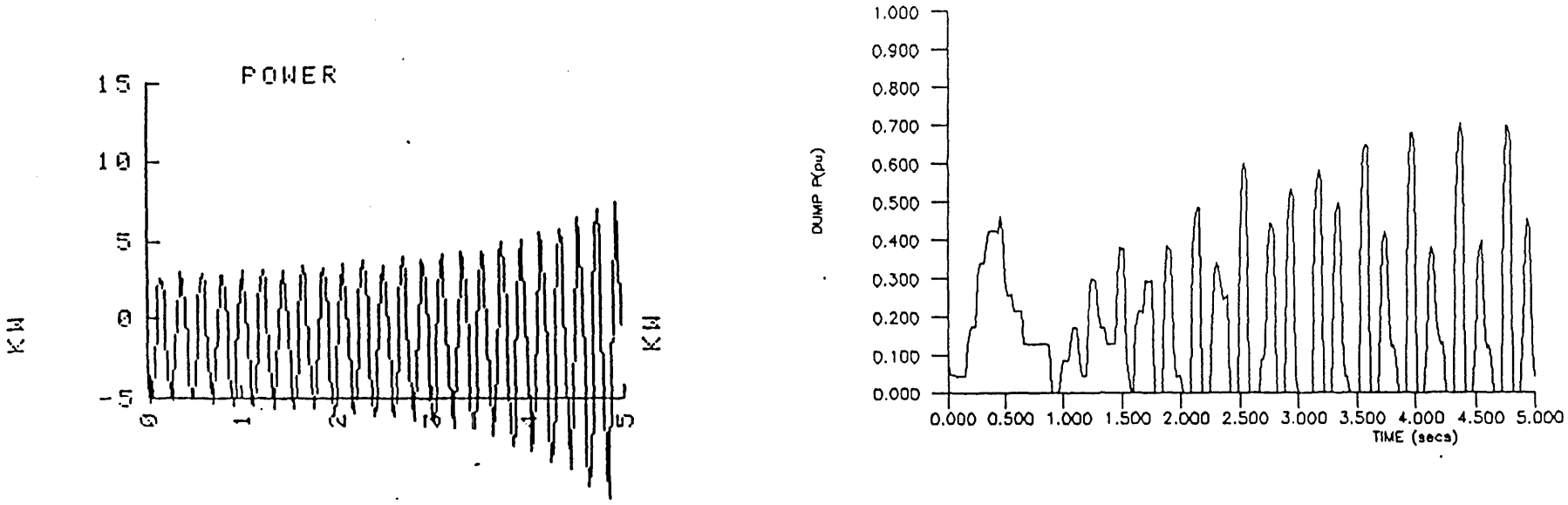

FIGURE 6.22 Motoring of the wind turbine following severe disturbance on the wind/diesel/flywheel system at low wind speed - frequency controlled dumpload

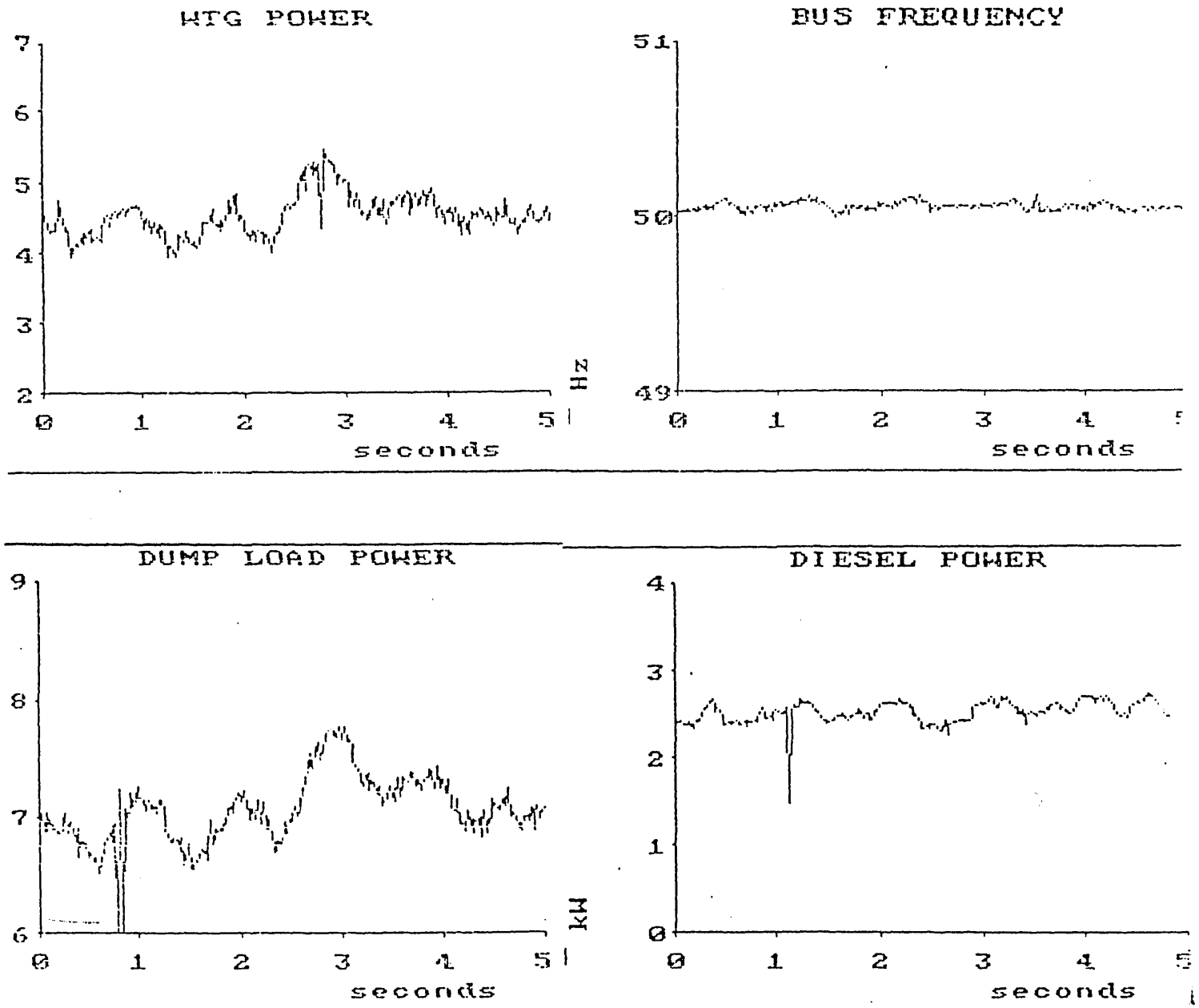

FIGURE 6.23 Wind/diesel system under power controlled dumpload operation (+ notch filter) (a) actual

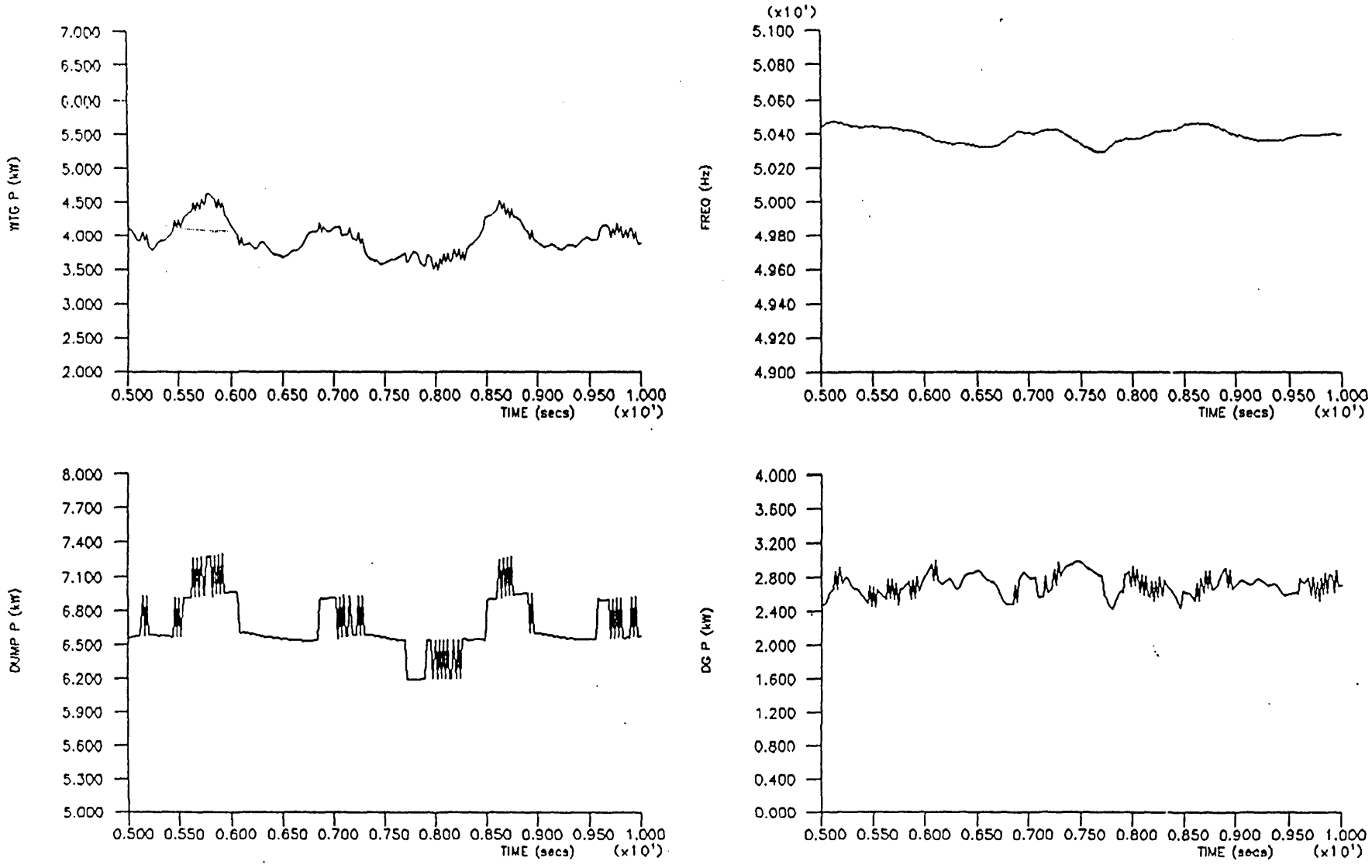

FIGURE 6.23 contd (b) simulated

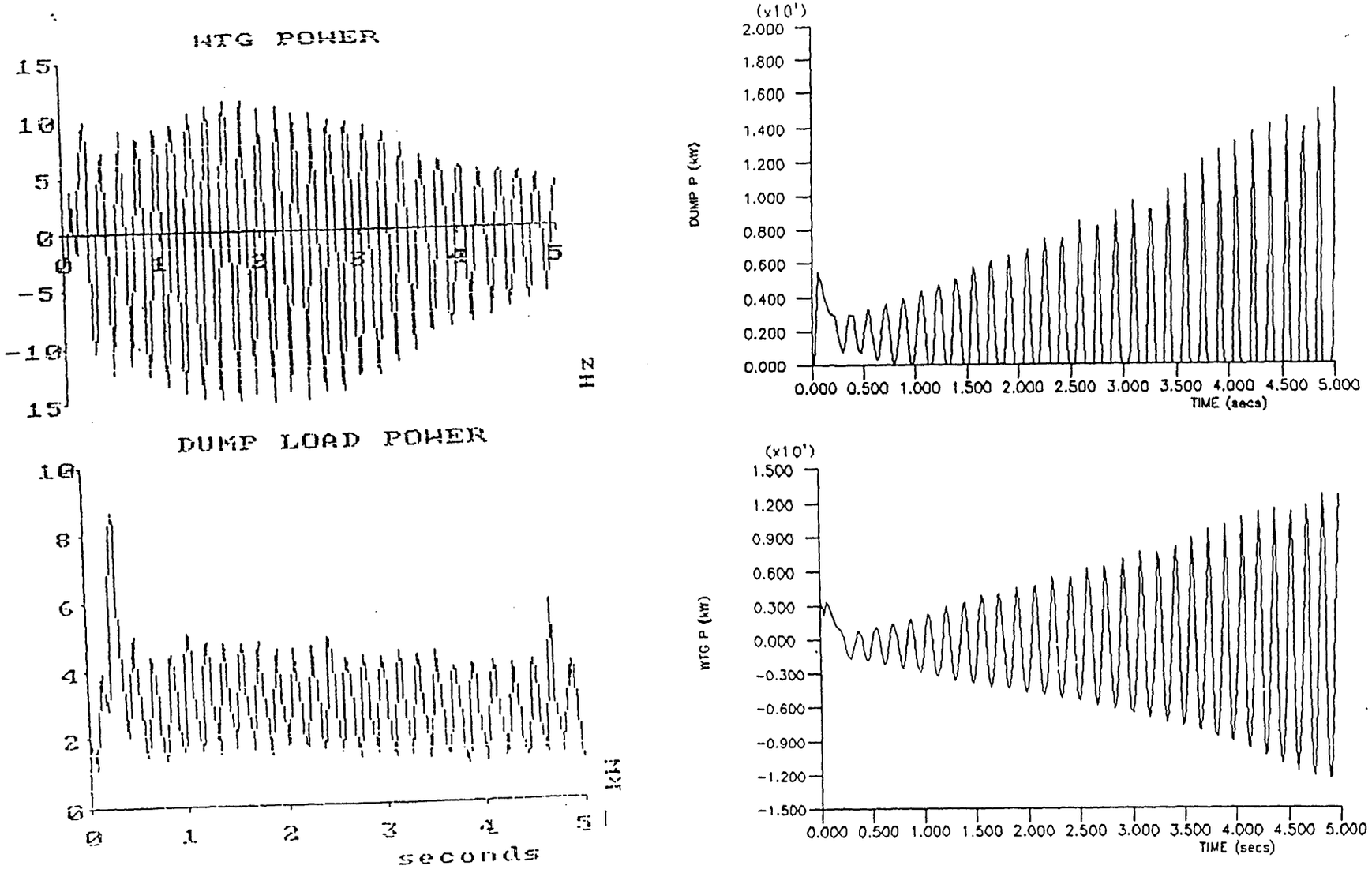

FIGURE 6.24 Severe disturbance on the wind/diesel system under power controlled dumpload - notch filter
(a) actual (b) simulated

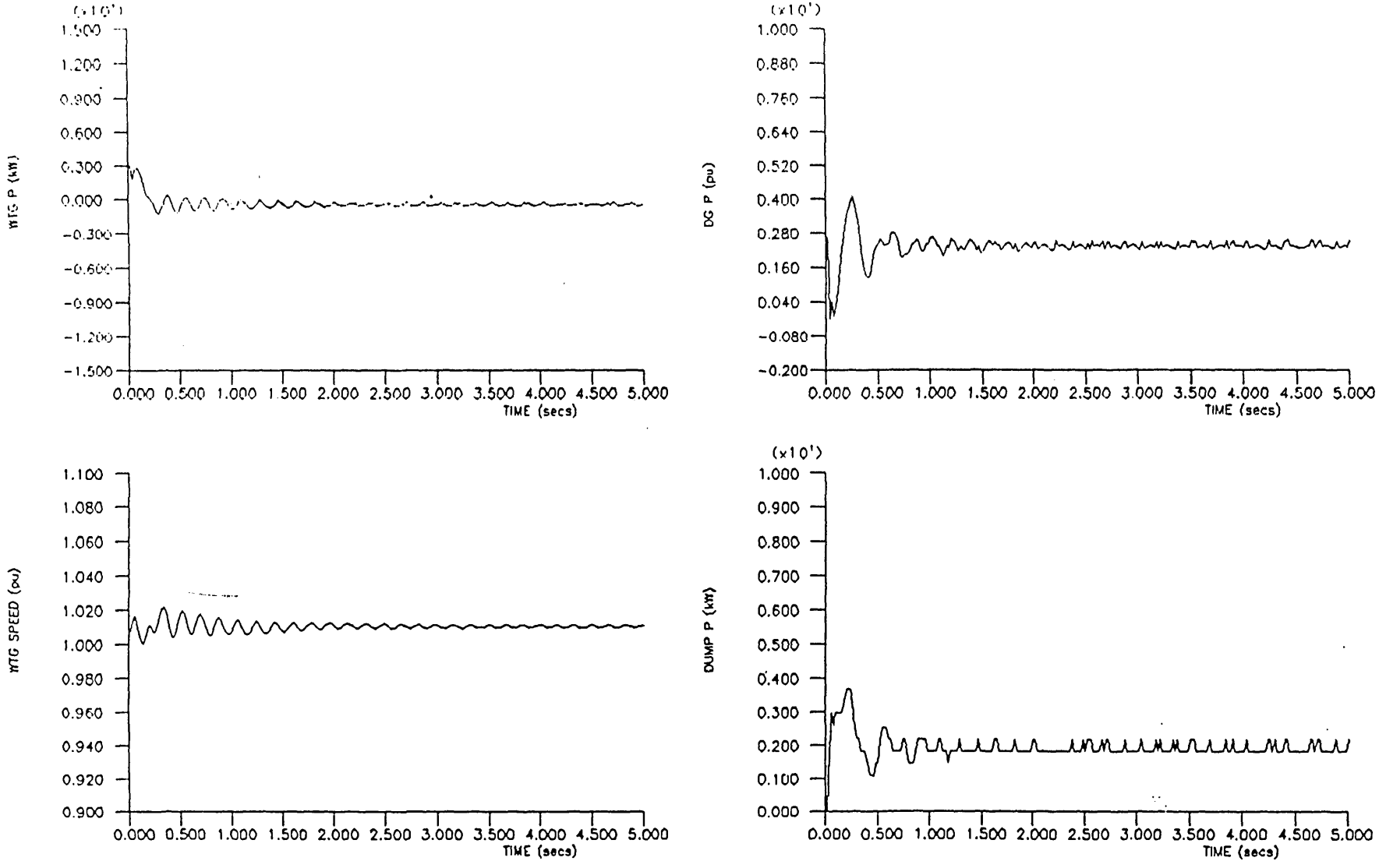

FIGURE 6.25 Severe disturbance on the wind/diesel system under power controlled dumpload + notch filter- simulated

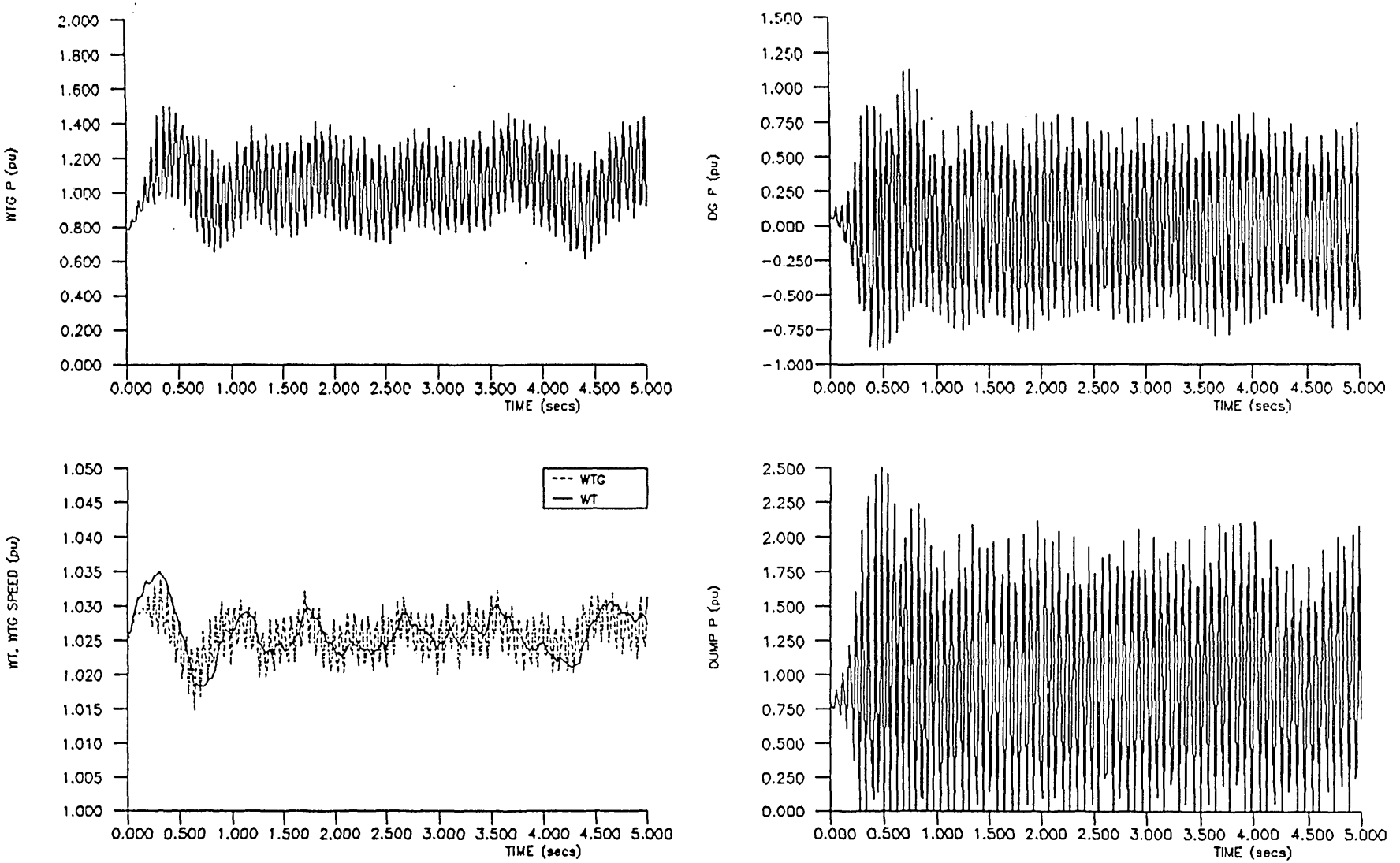

FIGURE 6.26 Effect of derivative action on the wind/diesel/flywheel system with power controlled dumpload operation

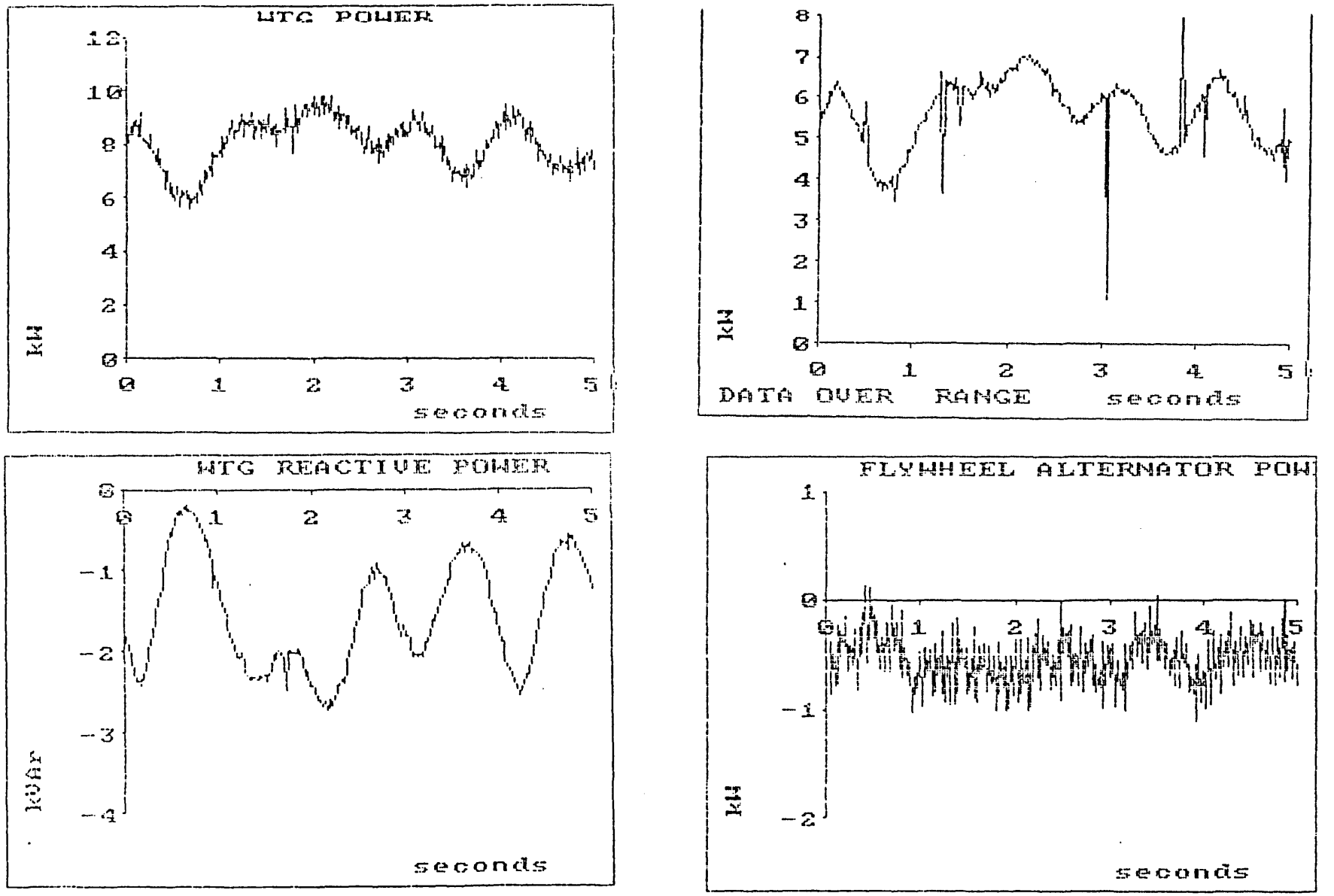

FIGURE 6.27(a) Parallel wind/diesel/flywheel operation under power controlled dumpload operation (actual)

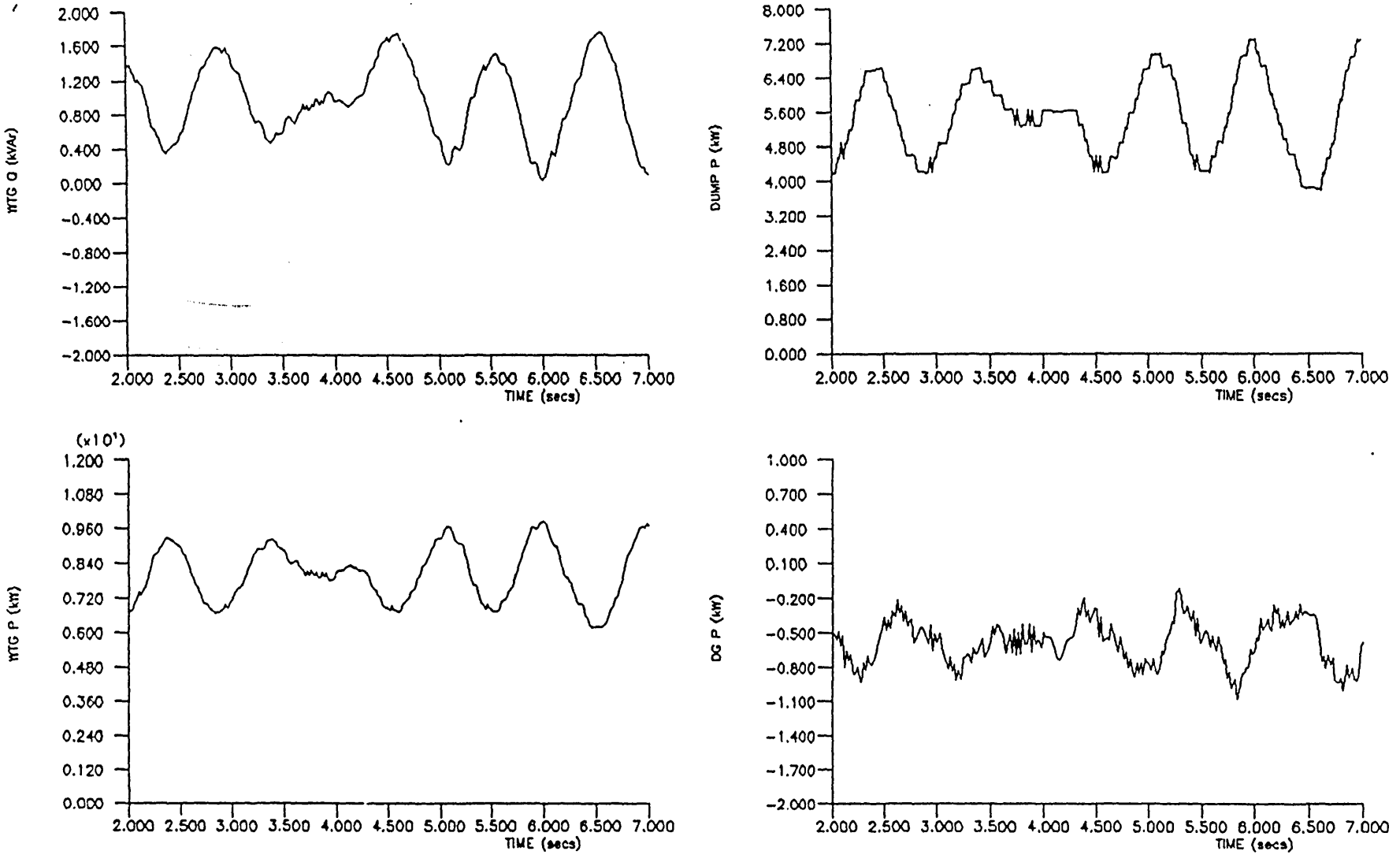

FIGURE 6.27(b) Parallel wind/diesel/flywheel operation under power controlled dumpload operation (Dsh=220Nm/rad/s)

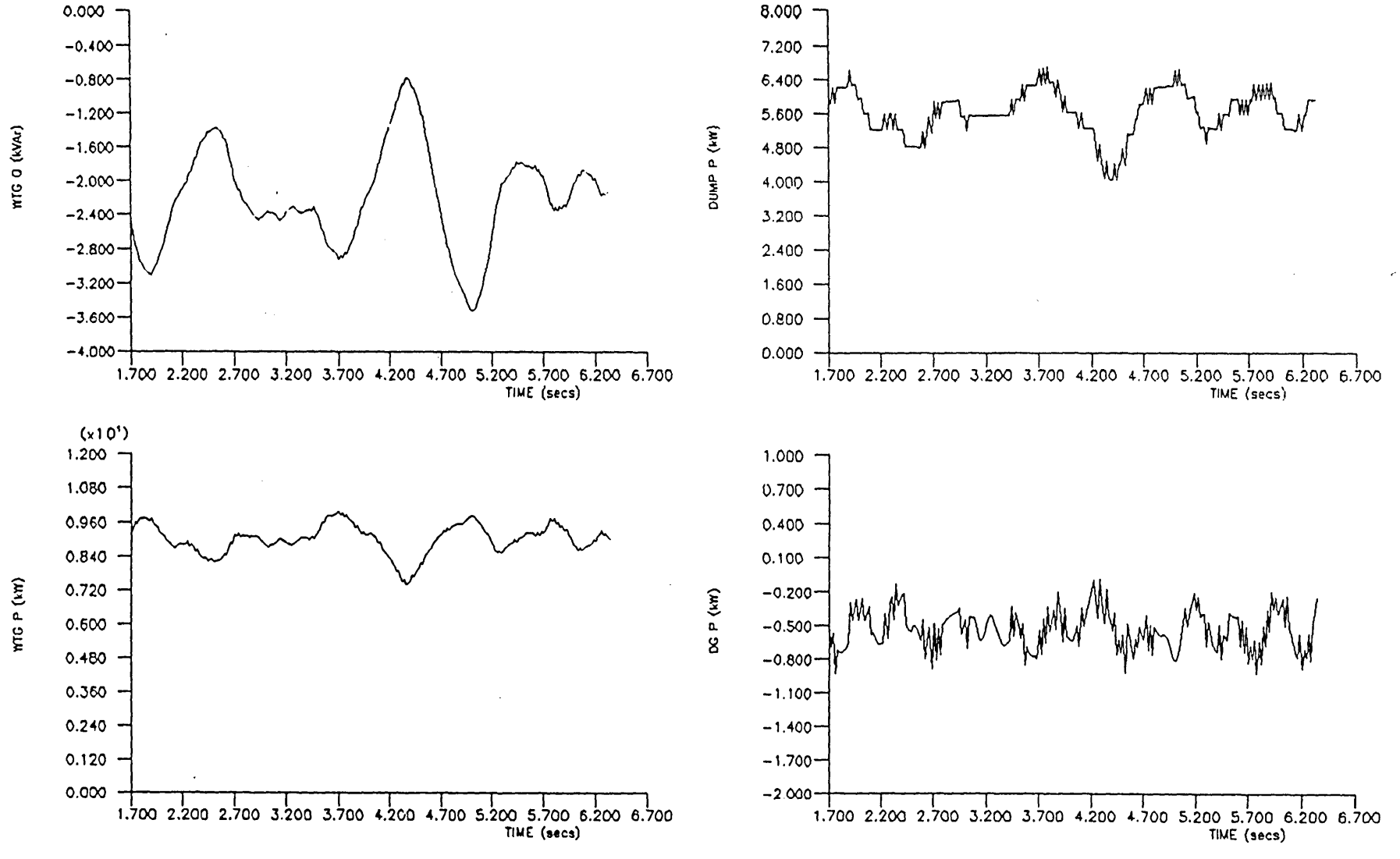

FIGURE 6.27(c) Parallel wind/diesel/flywheel operation under power controlled dumpload operation (Dsh=2200Nm/rad/s)

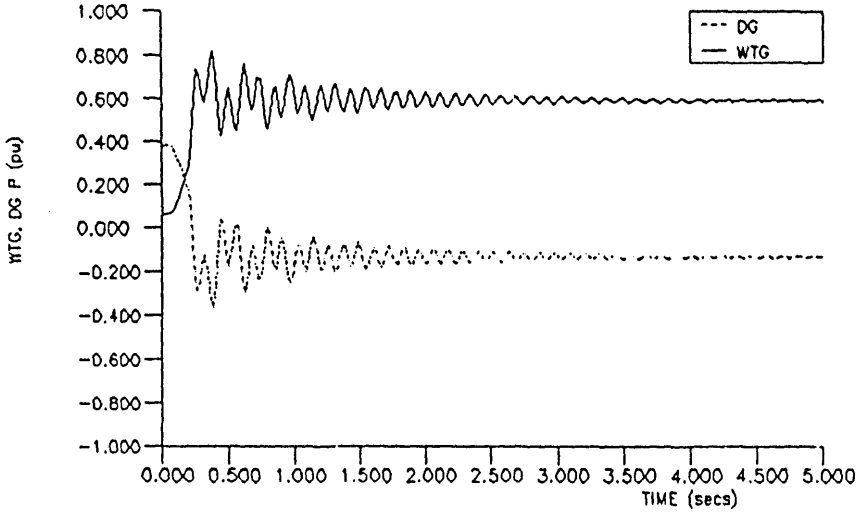

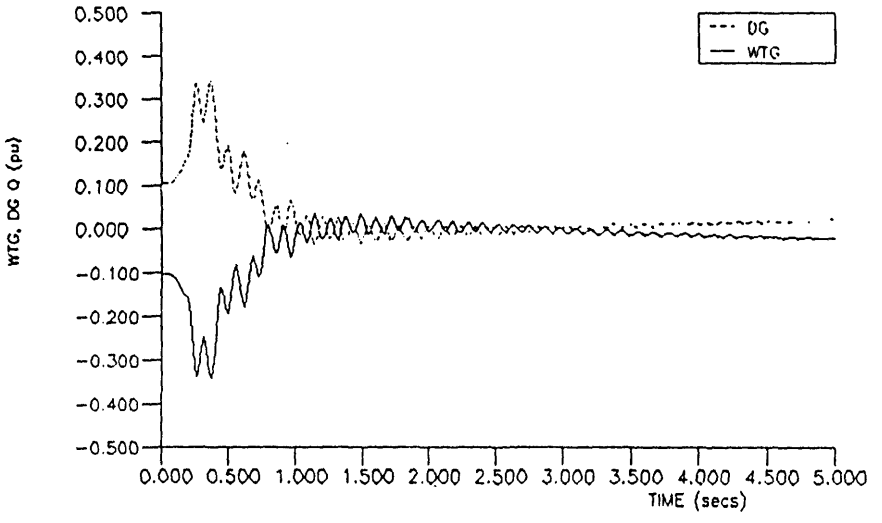

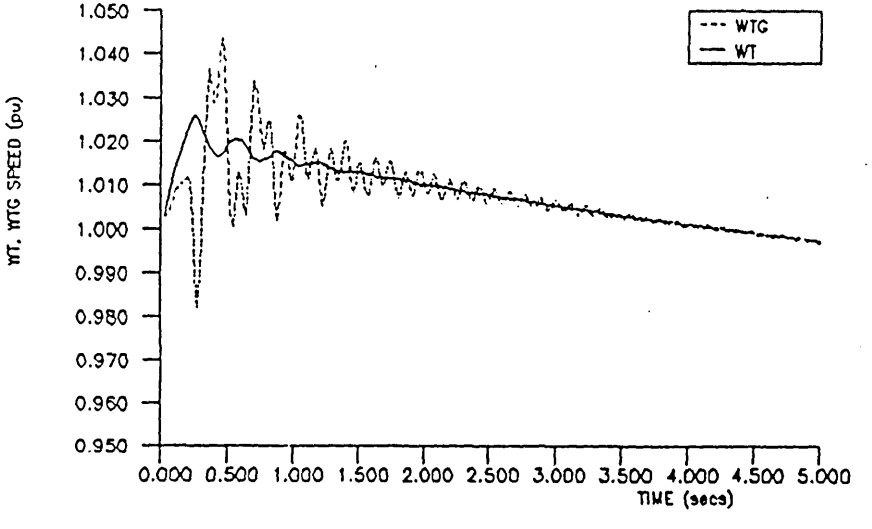

FIGURE 6.28 Disengagement of the diesel engine from the wind/diesel system

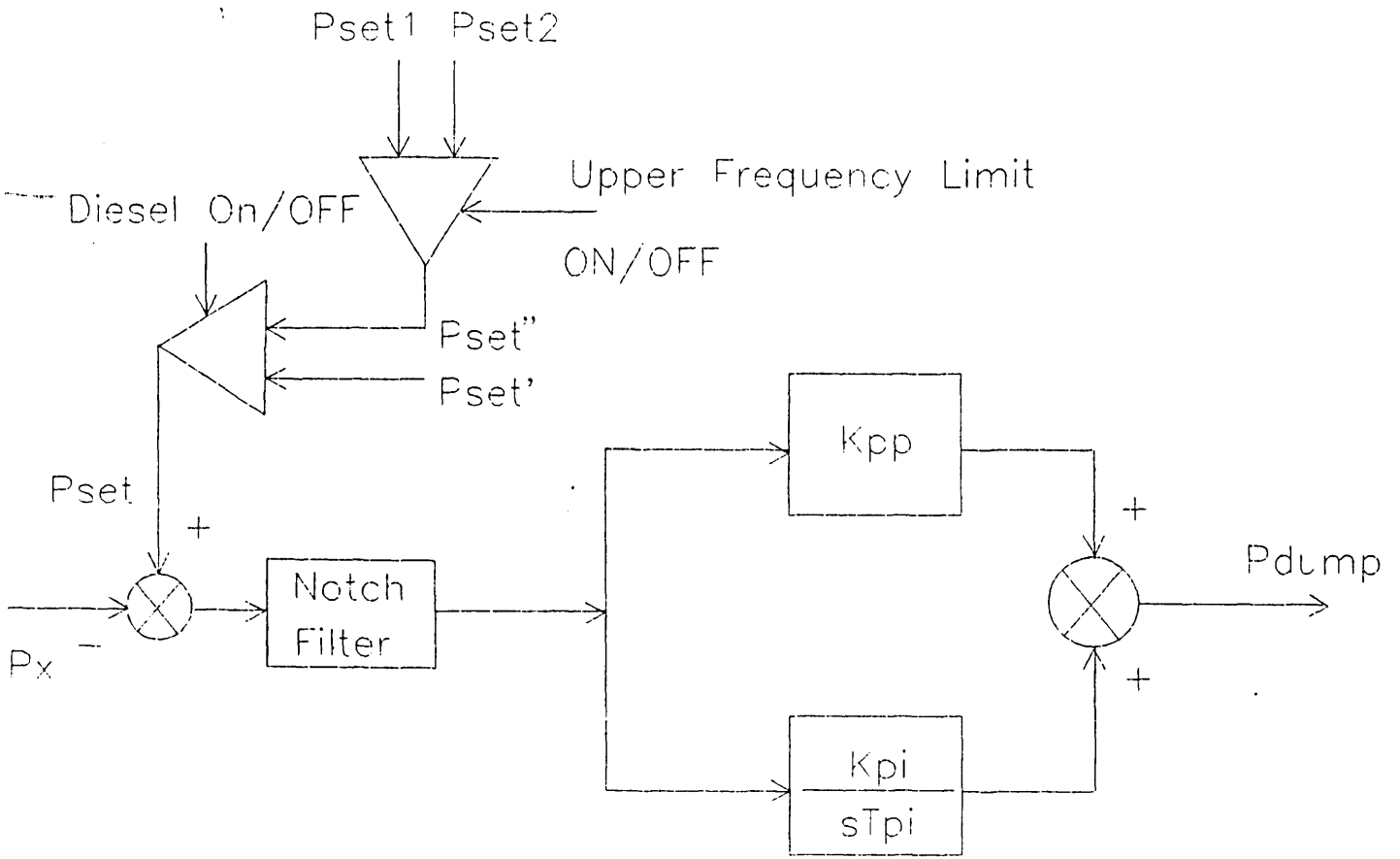

FIGURE 6.29 Power Based Dumpload Controller with; (i) set point adjusted when diesel disengaged by max power into generator flywheel (ii) Upper Frequency Limit switches power setpoint to zero

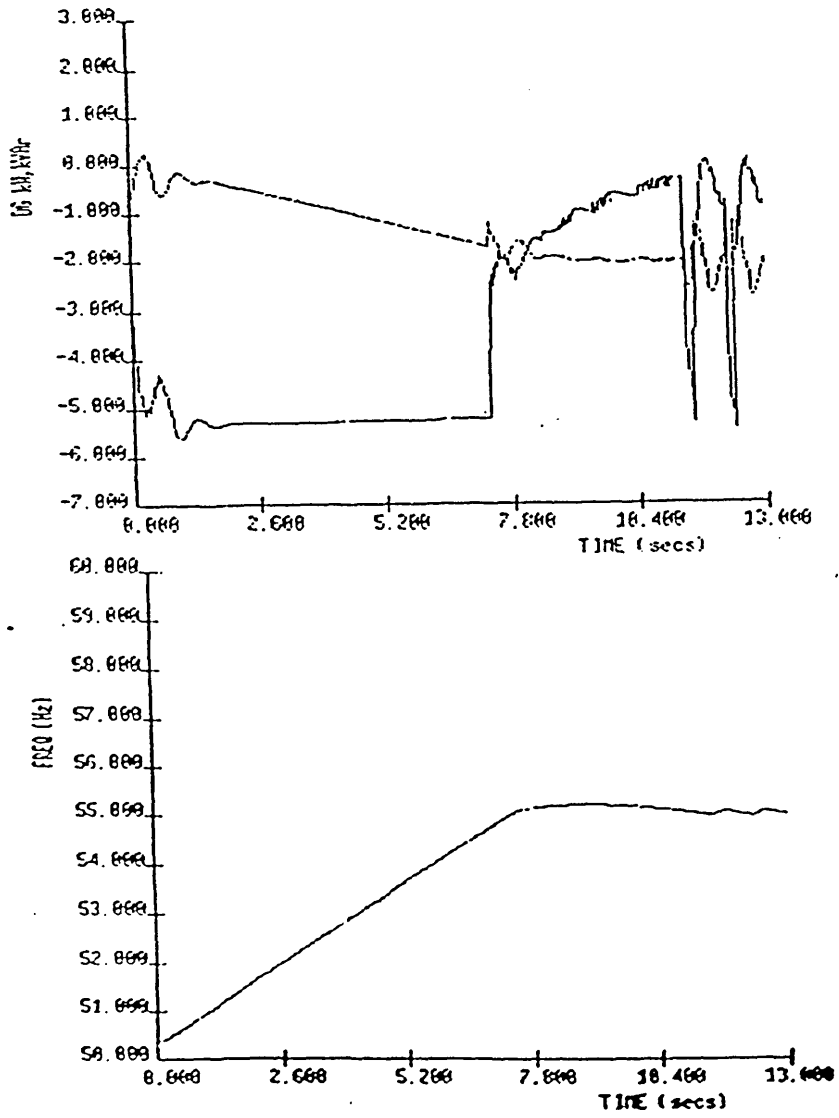

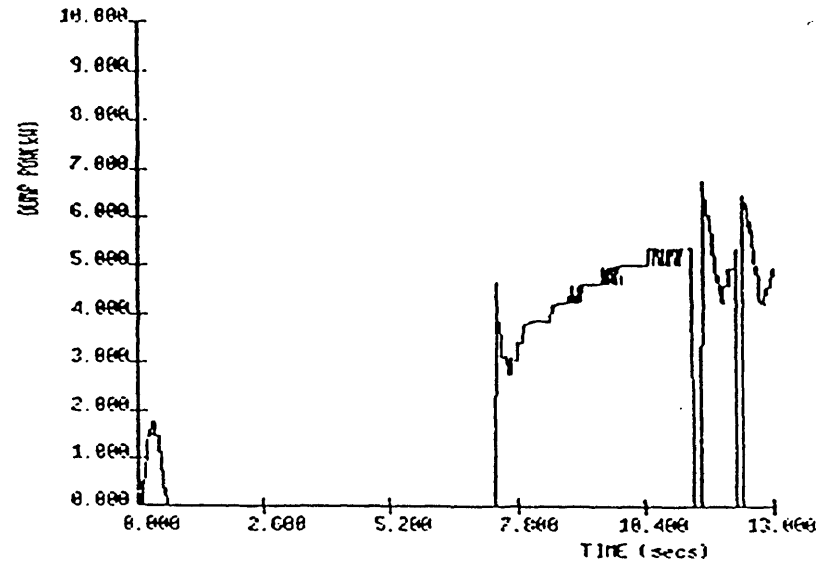

FIGURE 6.30 Diesel engine disengaged under power controlled dumpload operation - frequency signal used to flag upper frequency limit

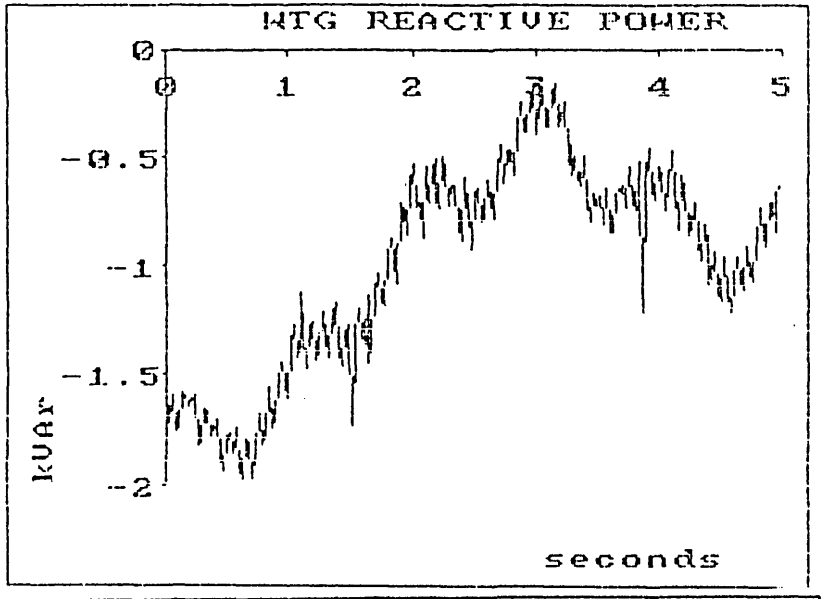

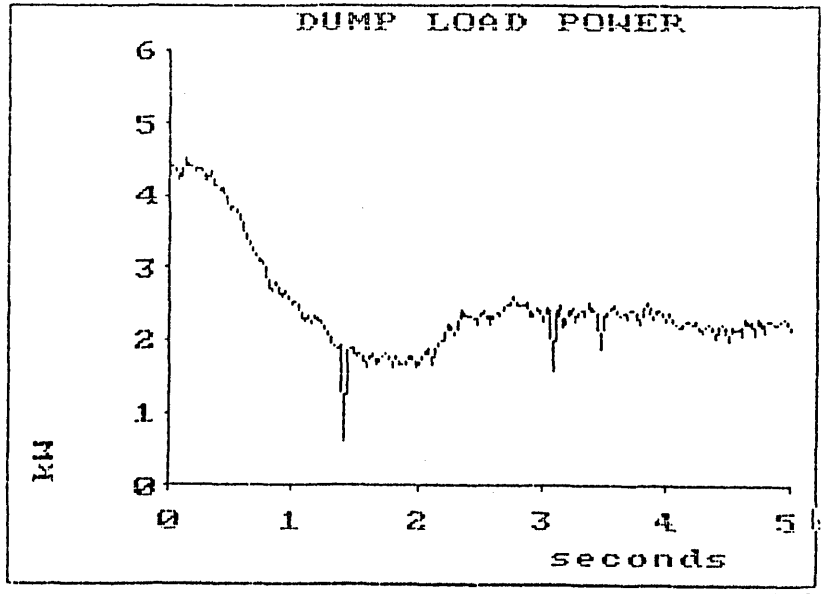

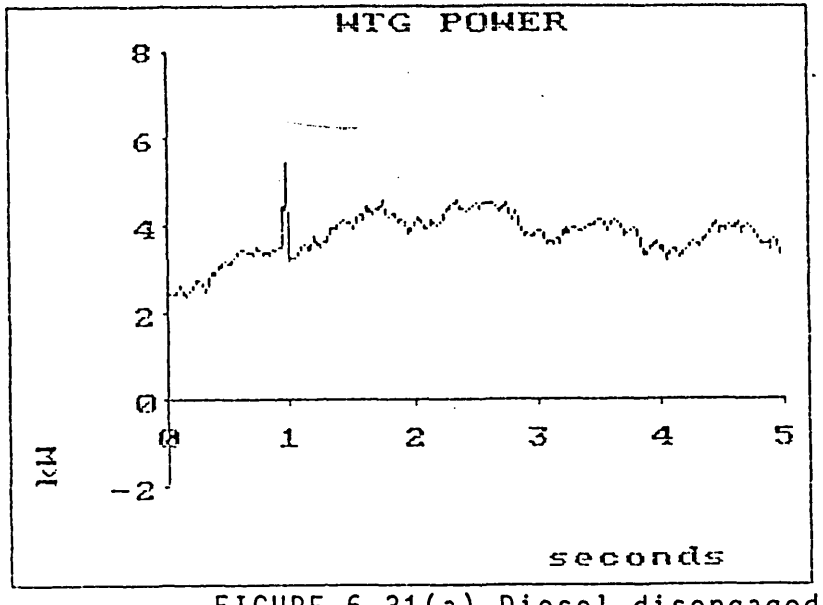

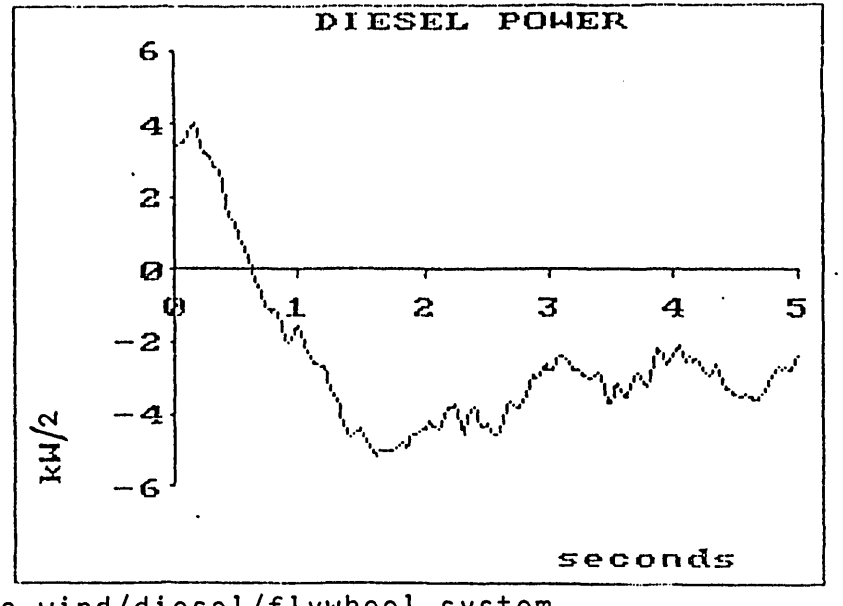

FIGURE 6.31(a) Diesel disengaged from the wind/diesel/flywheel system under frequency (P+I) controlled dumpload operation - actual

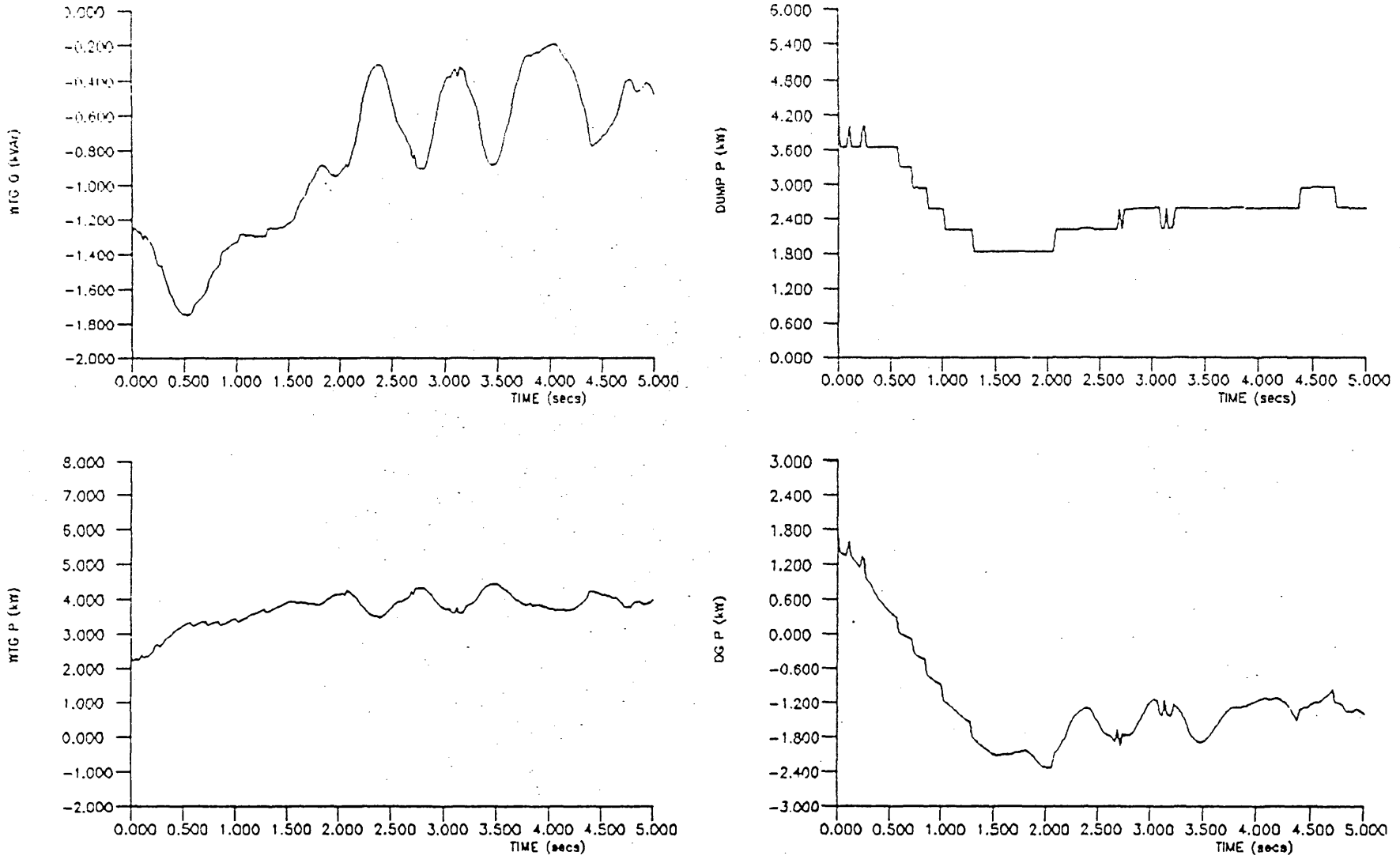

FIGURE 6.31(b) Diesel disengaged from the wind/diesel/flywheel system under frequency (P+I) controlled dumpload operation - simulated (Dsh=2200Nm/rad/s)

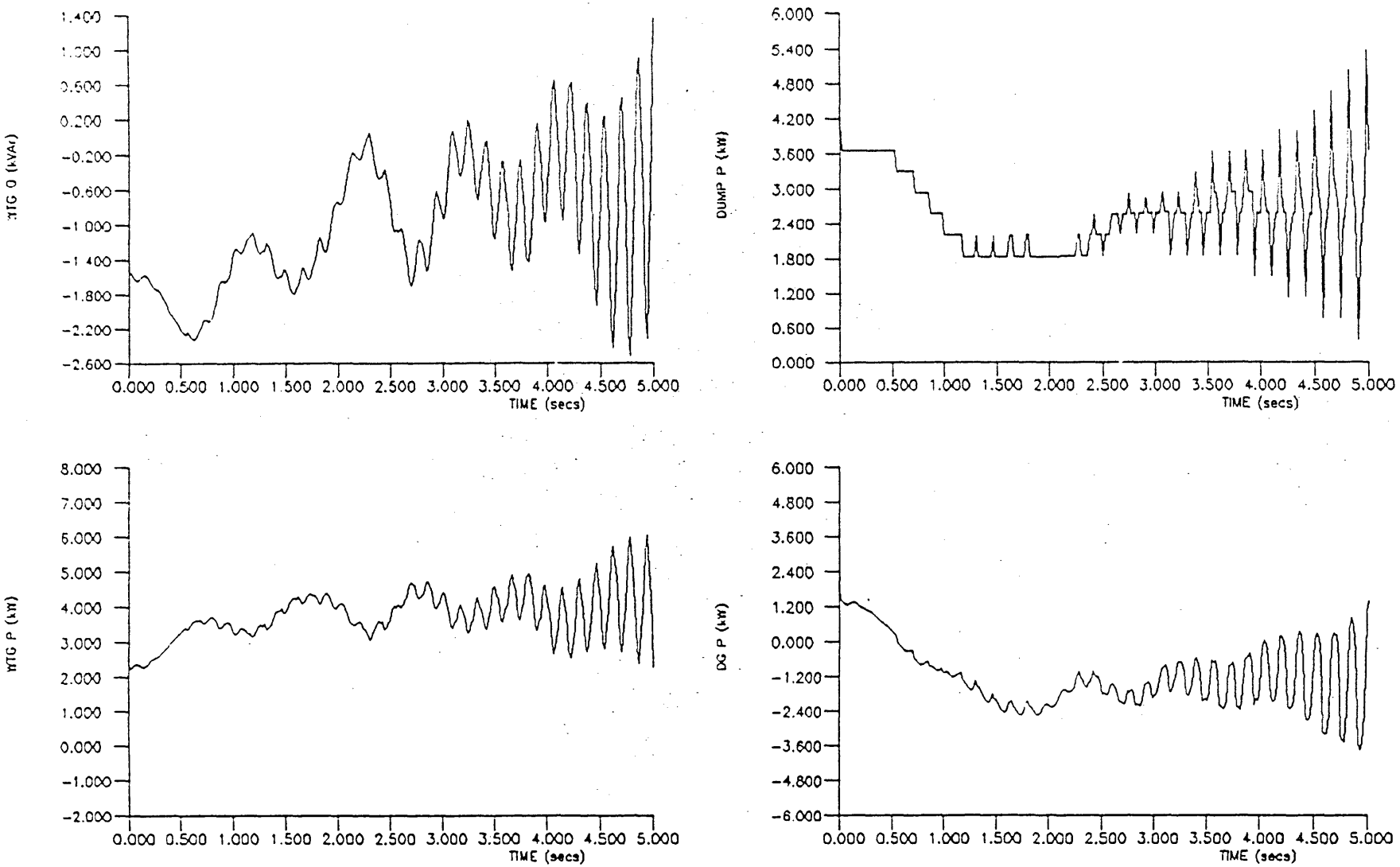

FIGURE 6.31(c) Diesel disengaged from the wind/diesel flywheel system under frequency (P+I) controlled dumpload operation - simulated (Dsh=220Nm/rad/s)

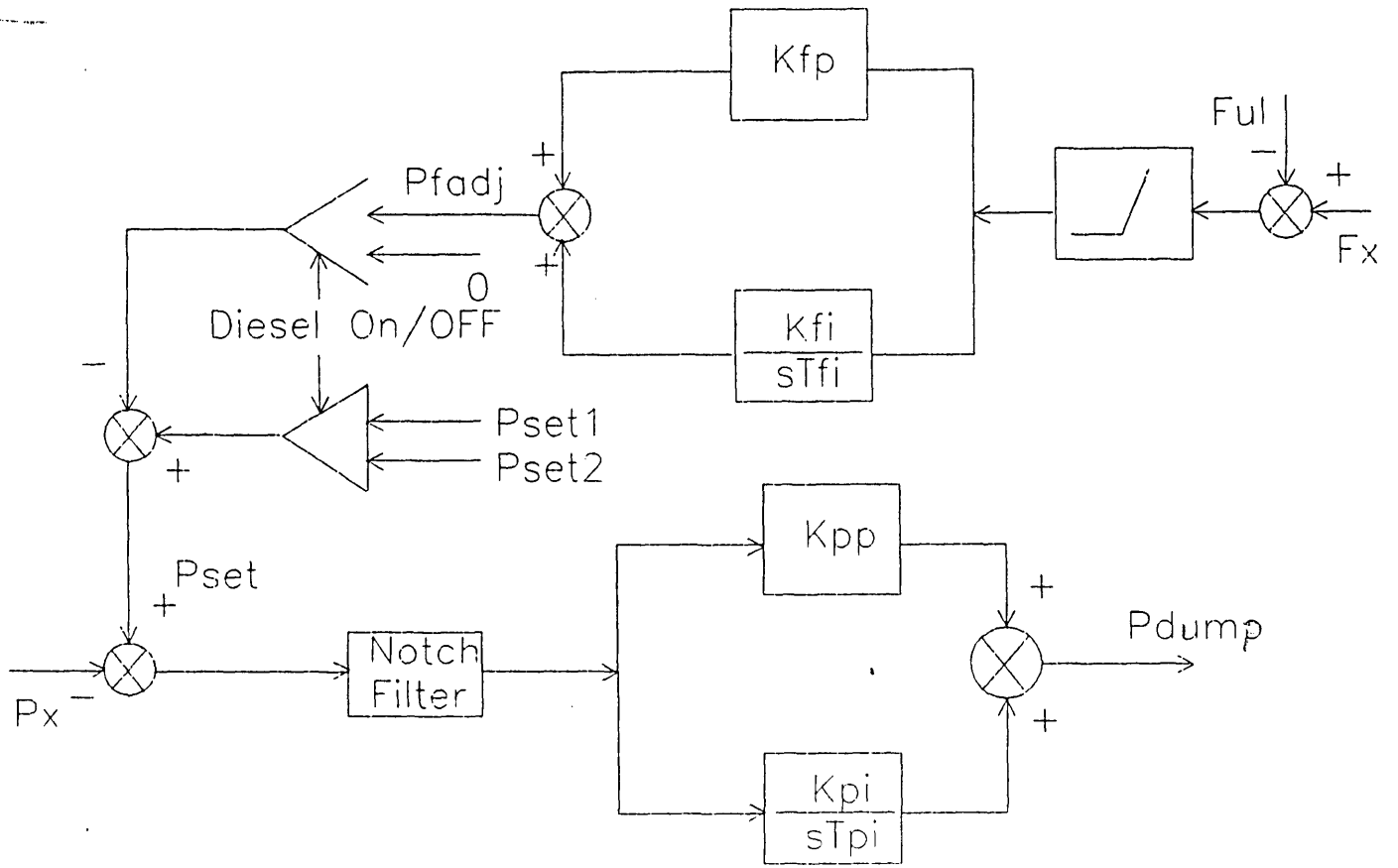

FIGURE 6.32 Power Based Dumpload Controller with set point adjusted when diesel disengaged by; (i) max power into generator flywheel (ii) Upper Frequency Limit

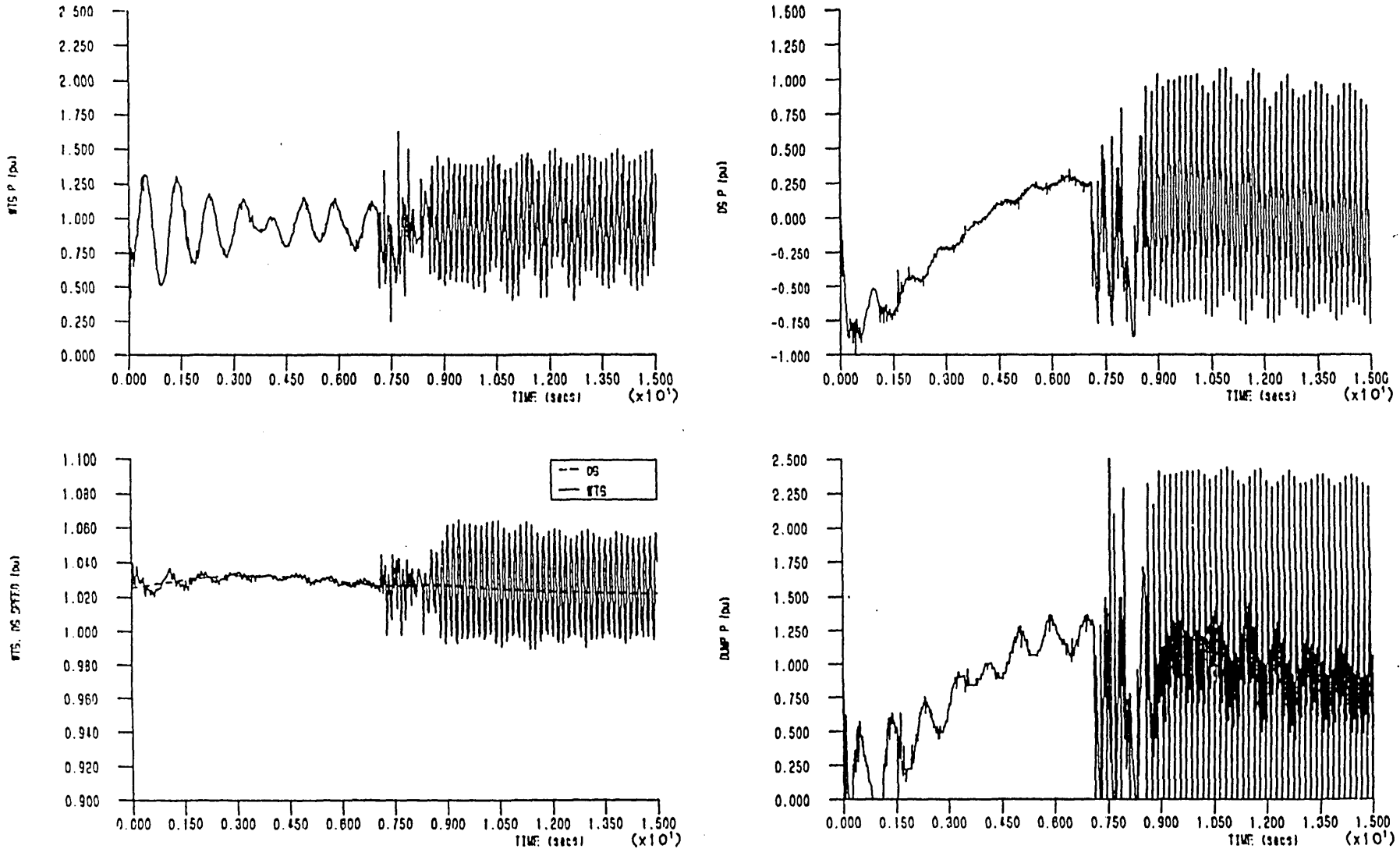

FIGURE 6.33 Diesel disengaged from the wind/diesel/flywheel system under Power (P) plus frequency (P+I) controlled dumpload operation - problem with integrator reset

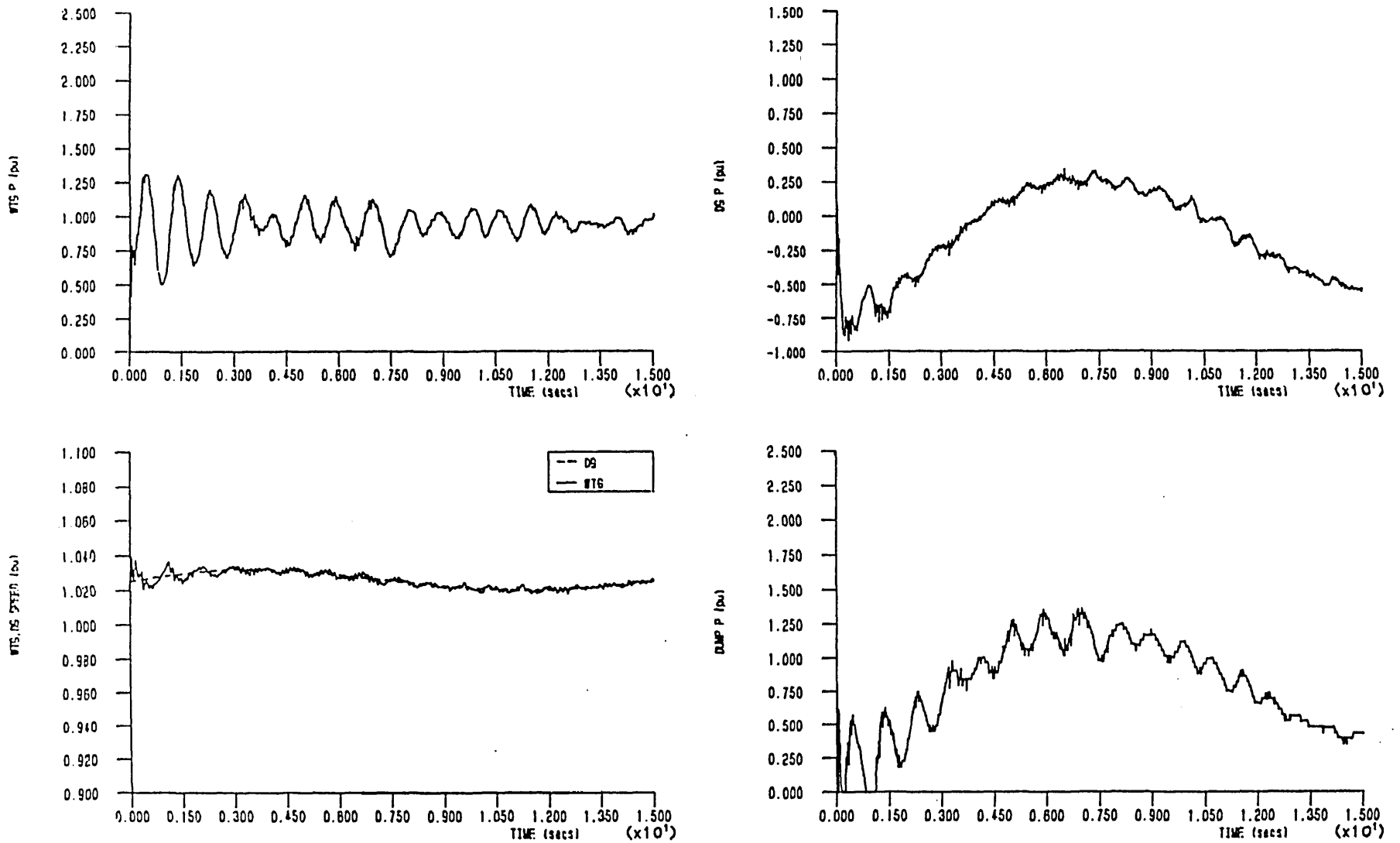

FIGURE 6.34(a) Diesel disengaged from wind/diesel/flywheel system under power (P) plus frequency (P+I) controlled dumpload operation - frequency loop remains in operation after first crossing of upper frequency limit (Kfp=3kW/kW,Kfp=5kW/Hz, Kfi=5kW/Hz/s)

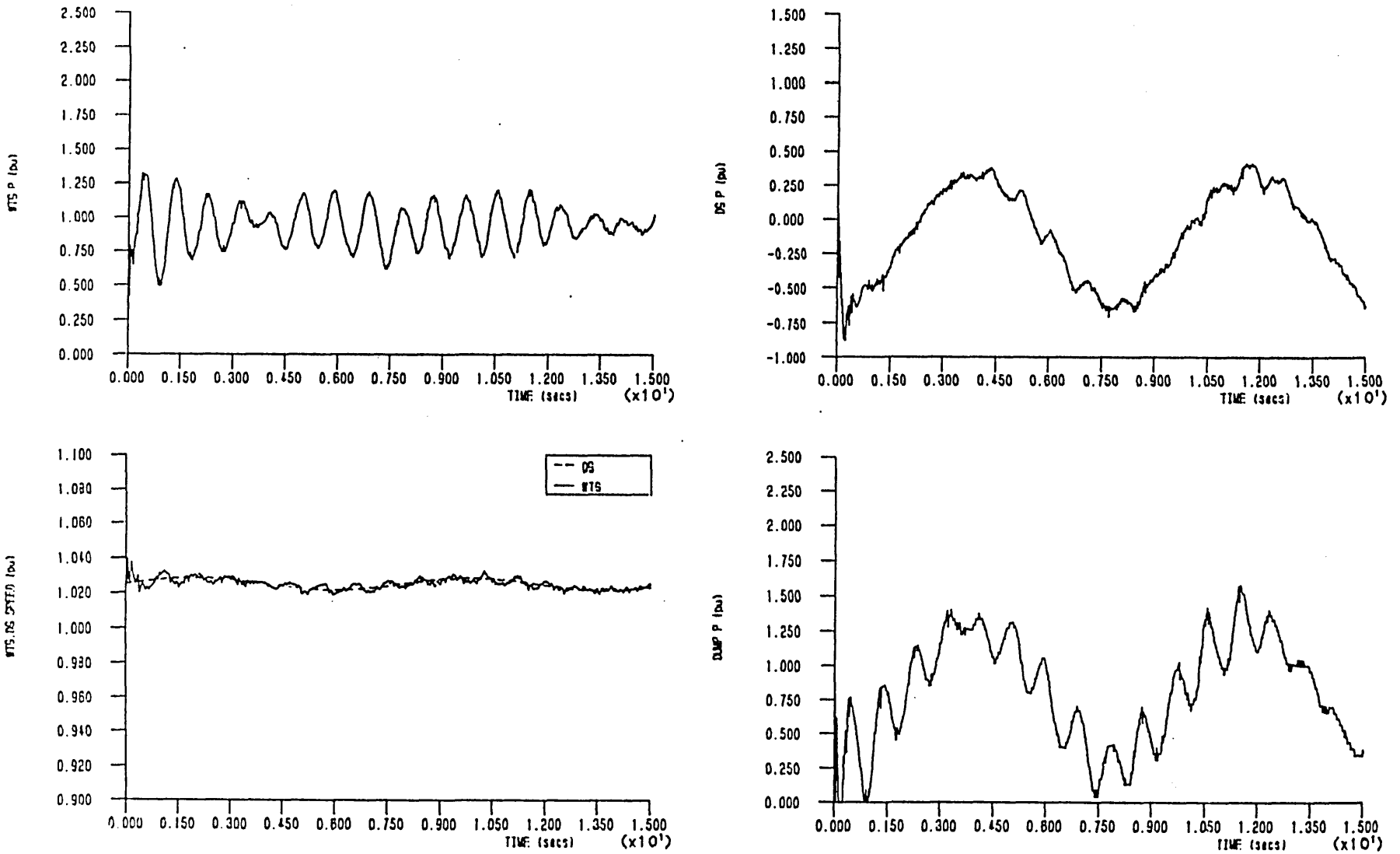

FIGURE 6.34(b) Diesel disengaged from wind/diesel/flywheel system under power (P) plus frequency (P+I) controlled dumpload operation - frequency loop remains in operation after first crossing of upper frequency limit (Kpp=3kW,Kfp=5kW/Hz,Kfi=20kW/Hz/s)

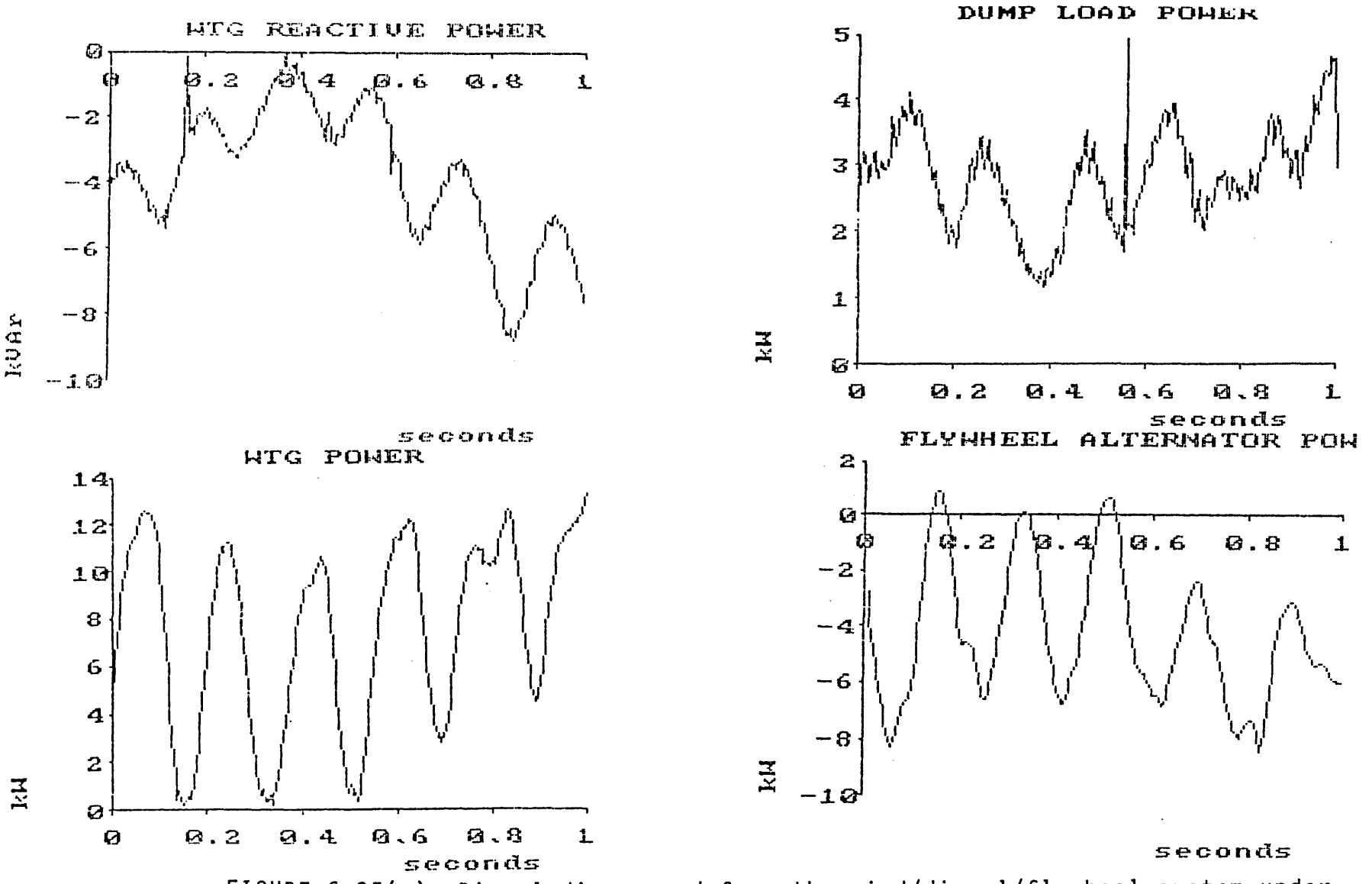

FIGURE 6.35(a) Diesel disengaged from the wind/diesel/flywheel system under Power (P) plus frequency (P) controlled dumpload operation- Problem with high proportional gain frequency loop (Kpp=3kW/kW, Kfp=7kW/Hz) - actual

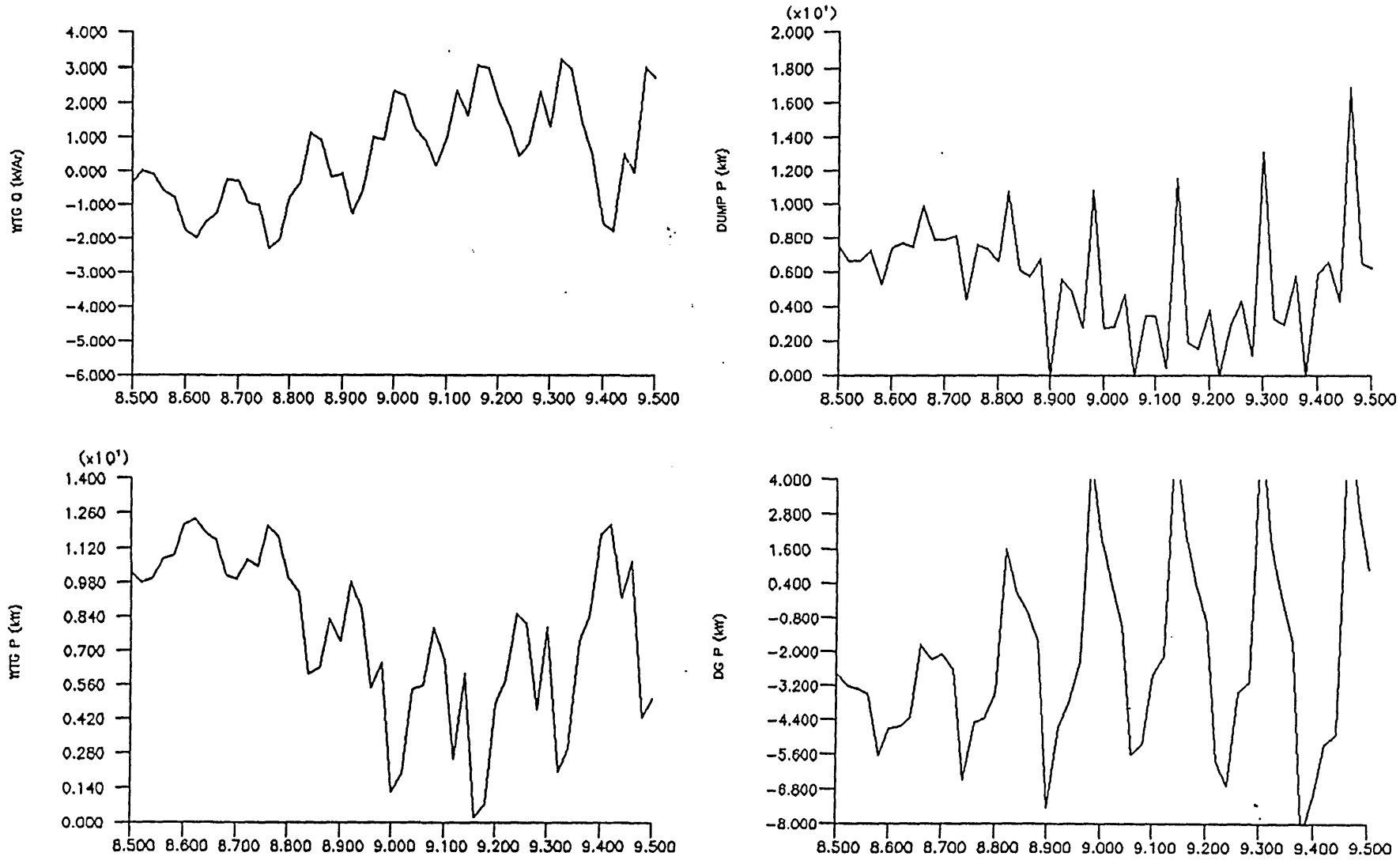

FIGURE 6.35(b) Diesel disengaged from the wind/diesel/flywheel system under Power (P) plus frequency (P) controlled dumpload operation - Problem with high proportional gain frequency loop (Kpp=3kW/kW, Kfp=7kW/Hz - simulated

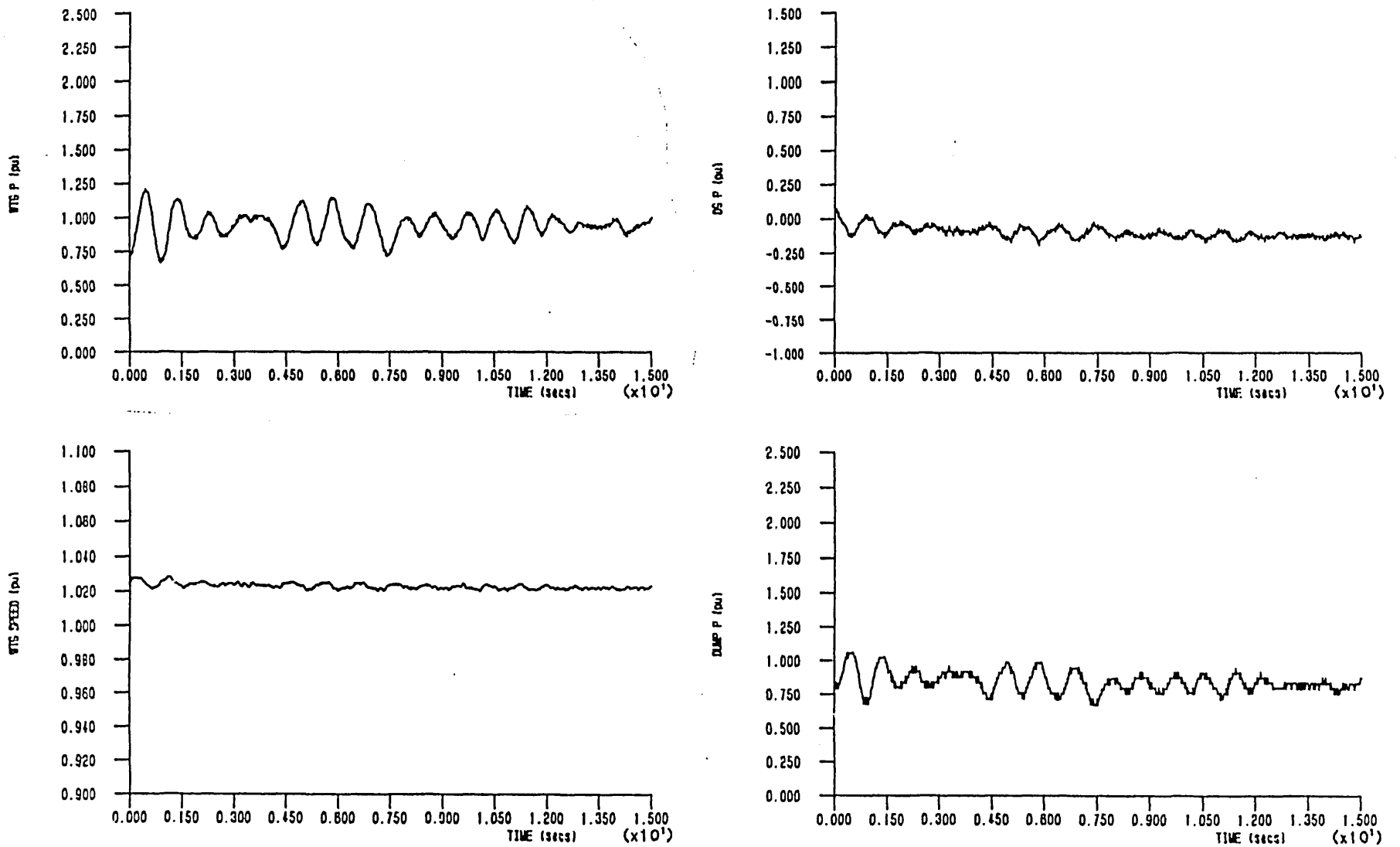

FIGURE 6.36(a) Control of system using "wind turbine generator speed" to maintain the upper frequency limit following diesel disengagement
(Kpp=3kW/kW,Kfp=7kW/Hz,fset=51.3Hz(1.026pu)

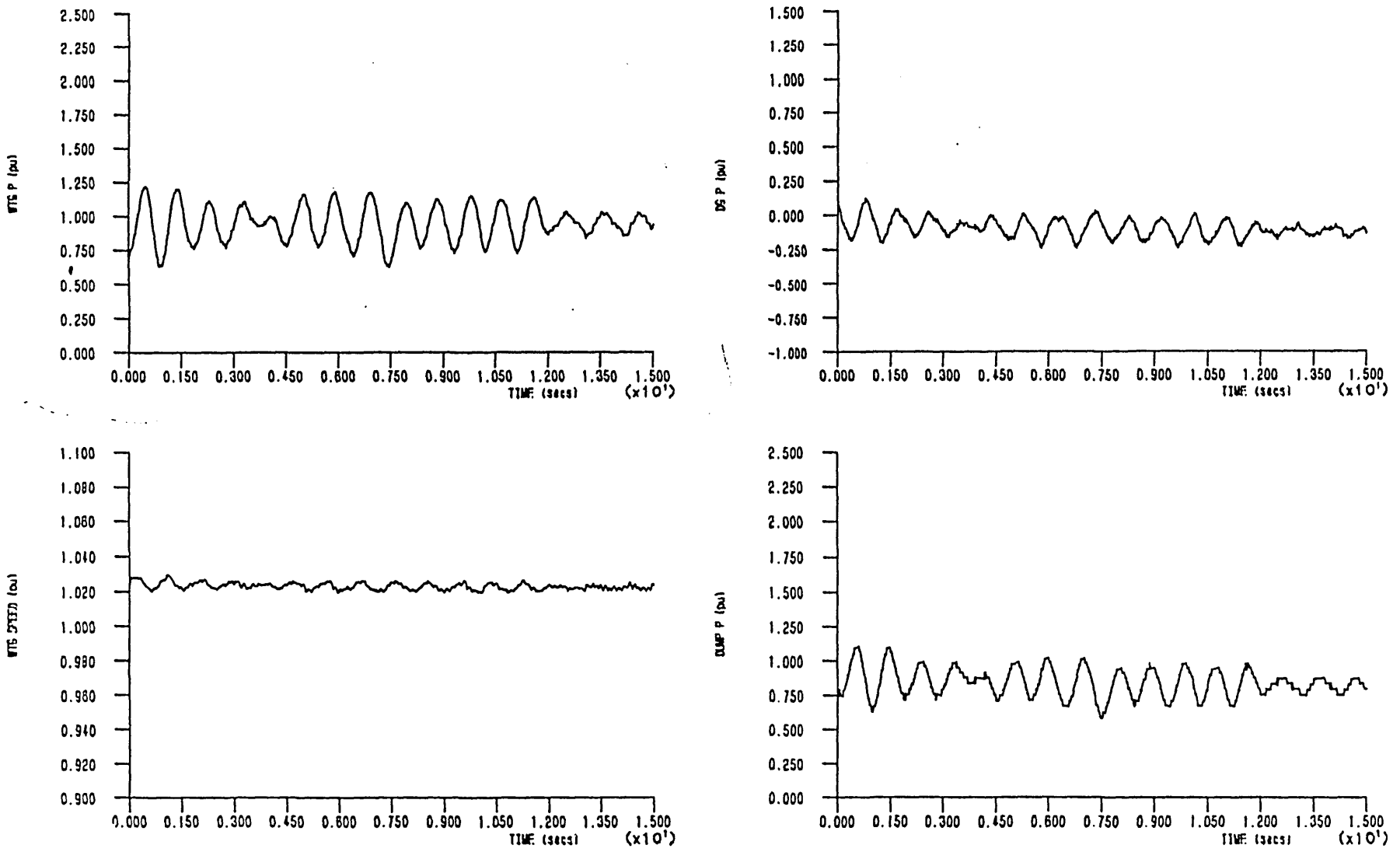

FIGURE 6.36(b) Control of system using "flywheel speed" to maintain the upper frequency limit following diesel disengagement.
(Kpp=3kW/kW Kfp=7kW/Hz, fset=51.3Hz(1.026pu)

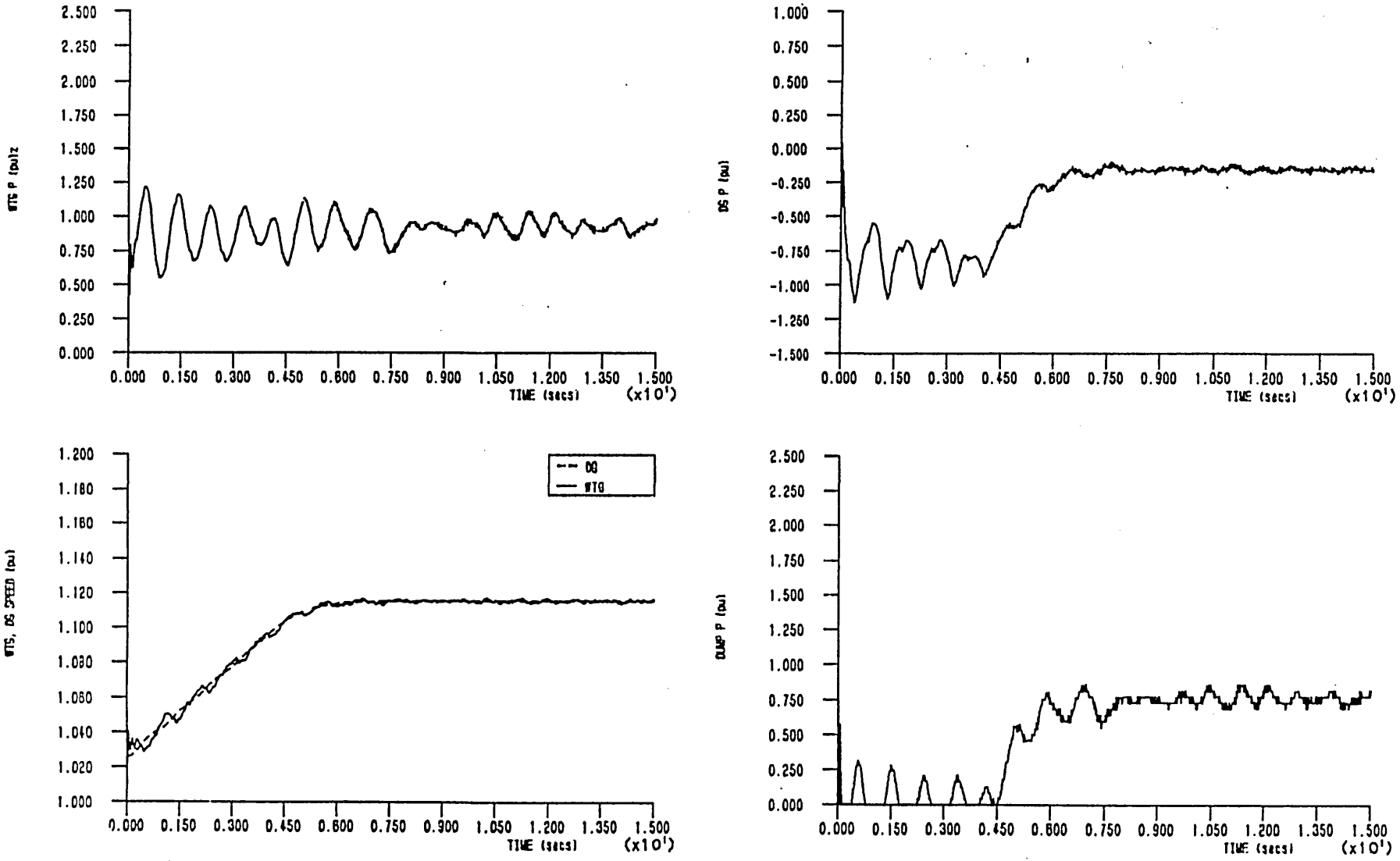

FIGURE 6.37 Control of system using "wind turbine generator speed to maintain the upper frequency limit following diesel disengagement.
(Kpp=3kW/kW, Kfp=10kW/Hz, fset=55Hz(1.1pu))

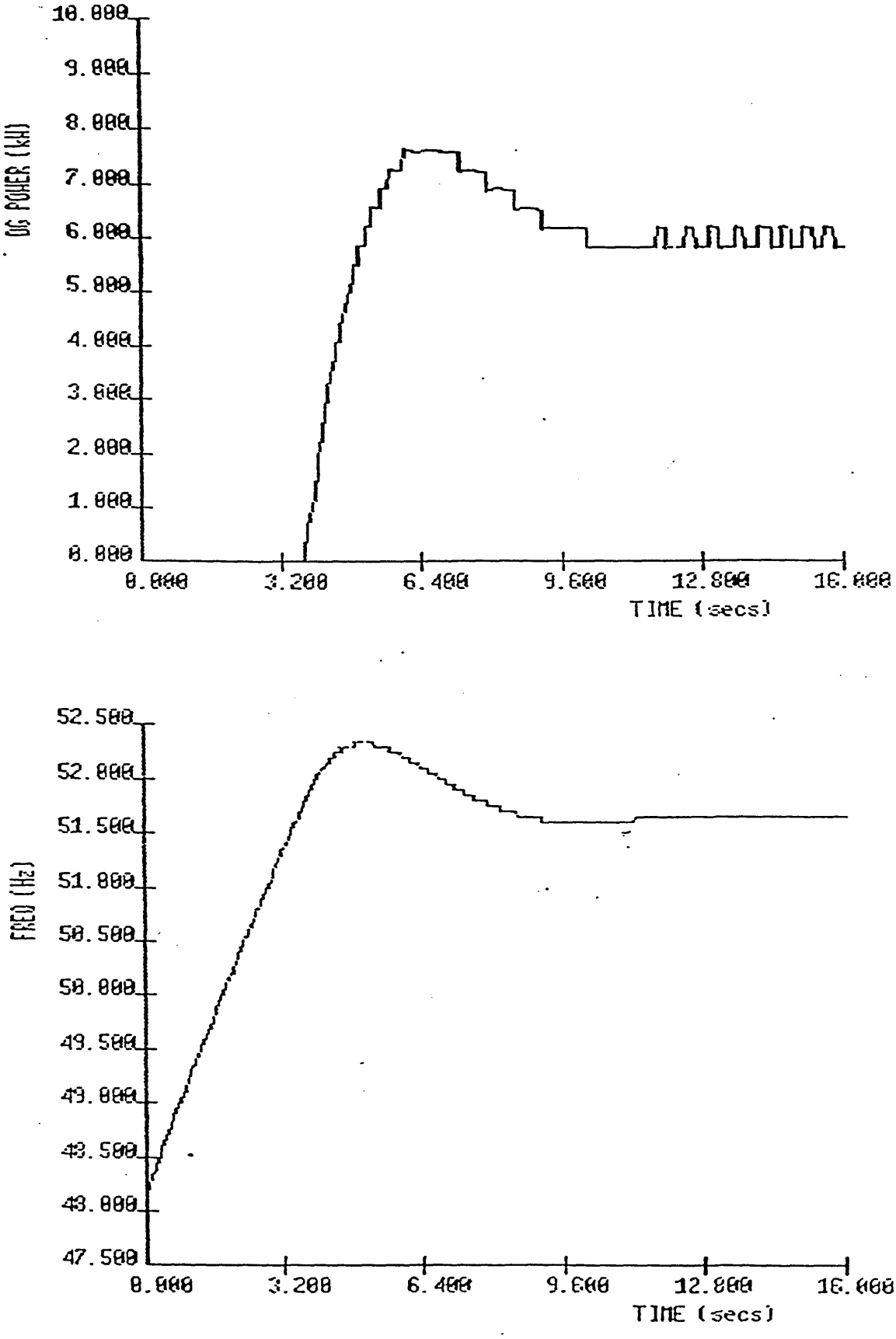

FIGURE 6.38 Wind/Diesel/Flywheel system, diesel crashstarted with initially fuel off, fuel rack then held fully across "overfuelling effect"

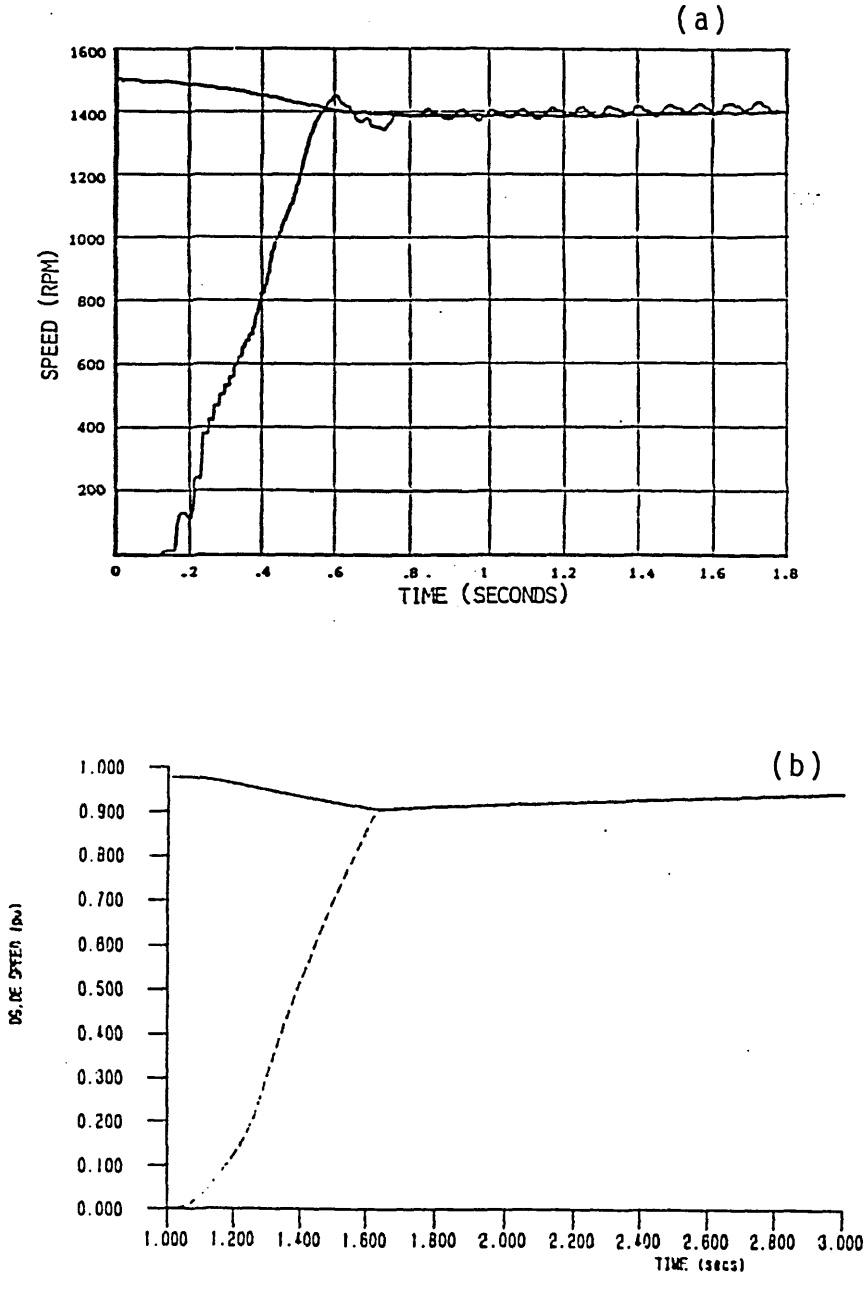

FIGURE 6.39 Diesel run up characteristics during its crashstart onto the wind/flywheel ($J_{fly}=11.8 kgm^2$) system -(a) actual (b) simulated

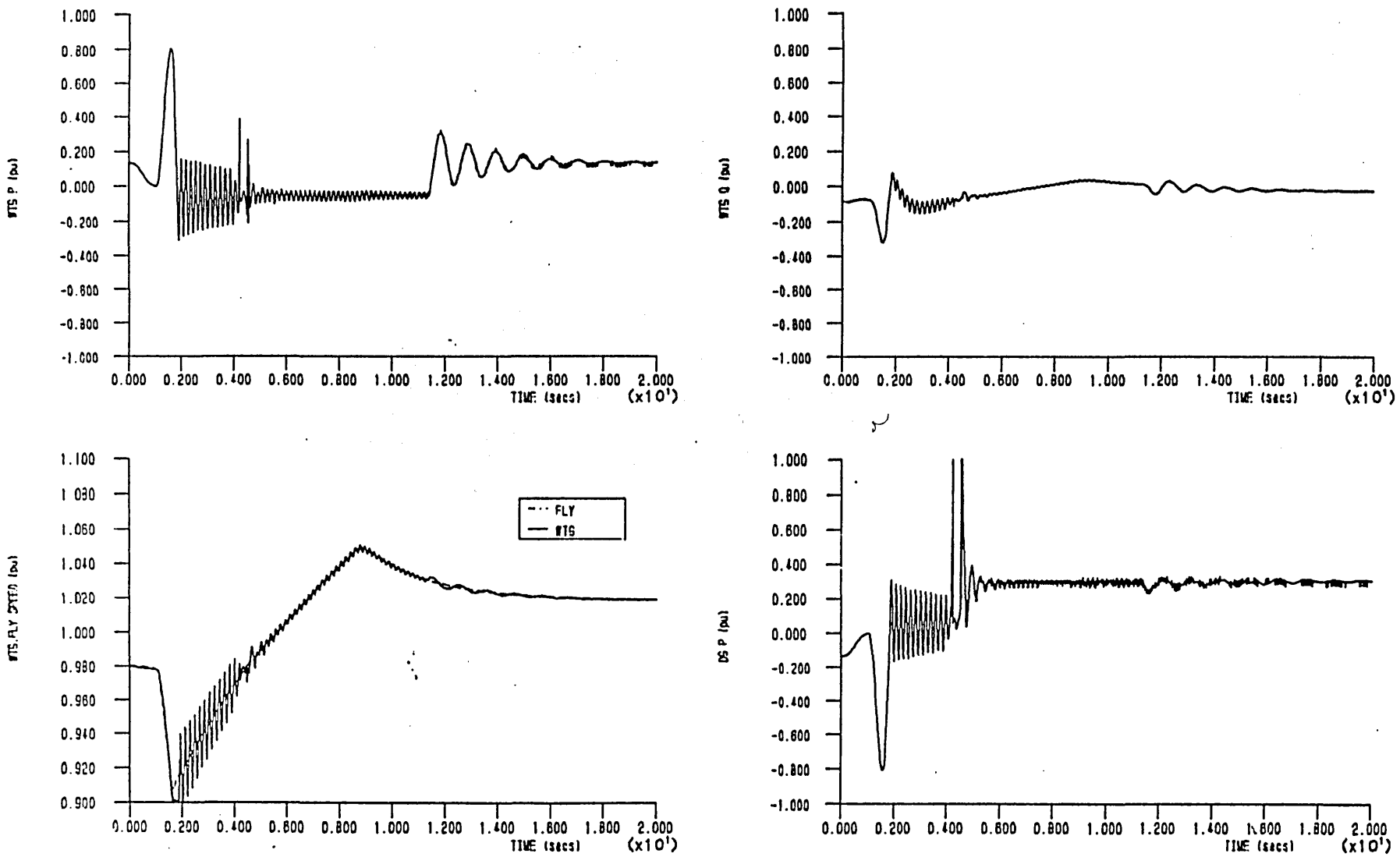

FIGURE 6.40 Response of the wind/diesel/flywheel (Jfly=11.8kgm^2) system following diesel "crashstart" - simulated

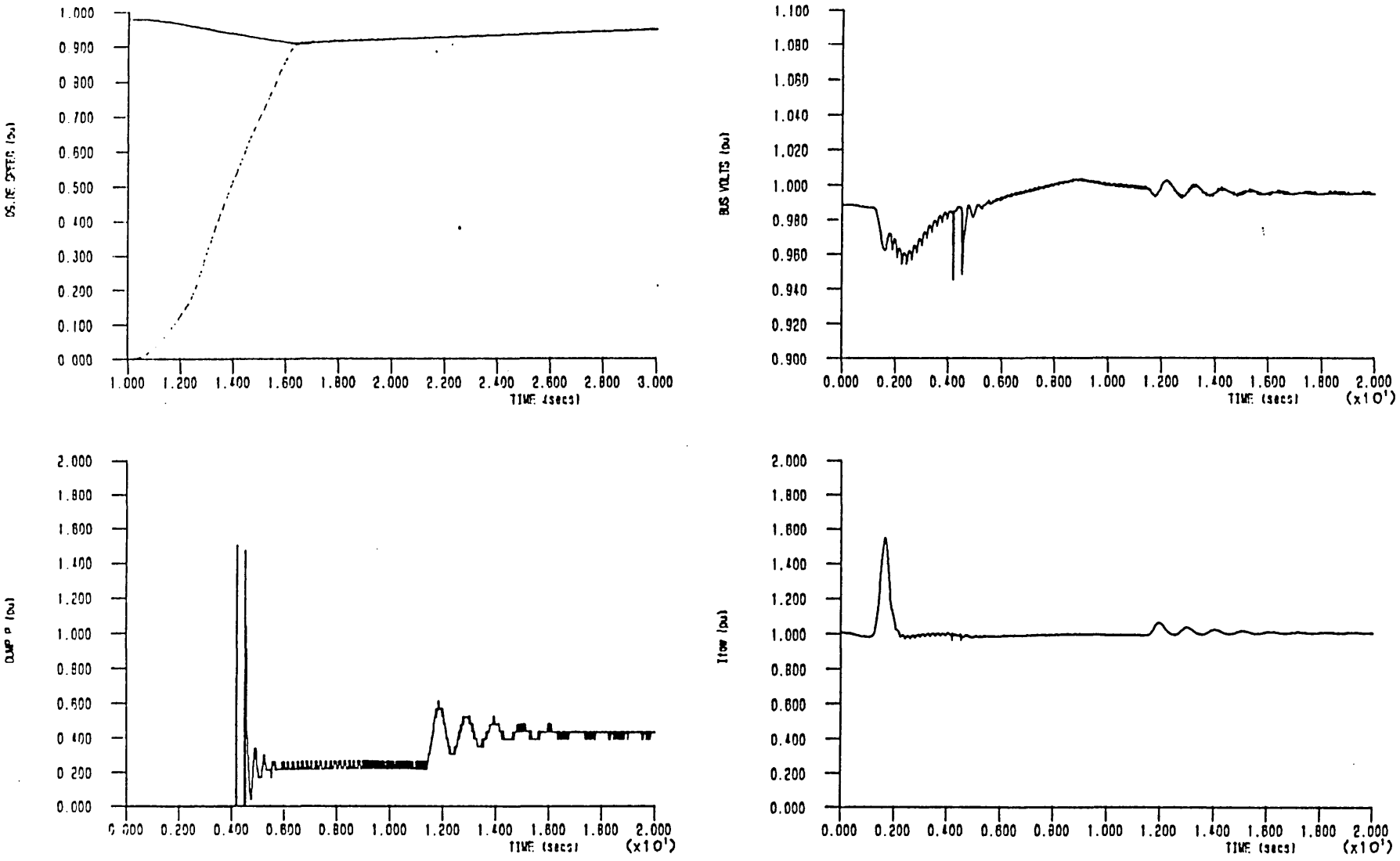

FIGURE 6.40 Contd

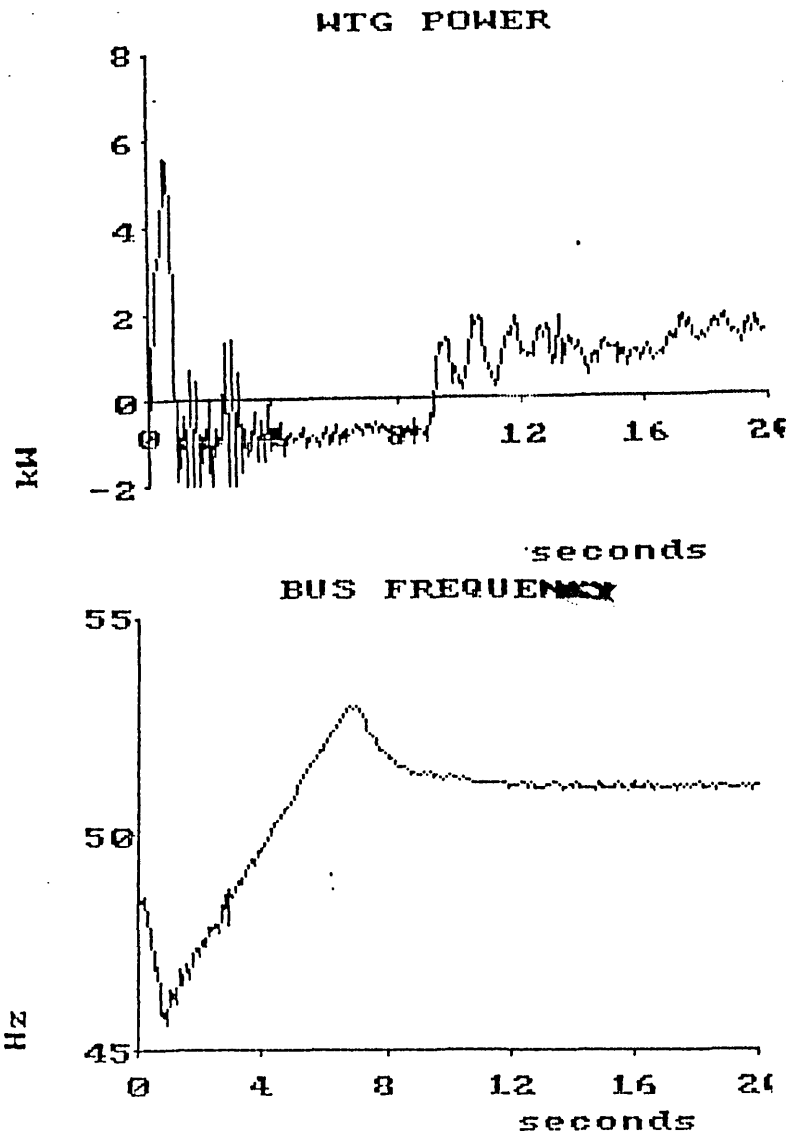

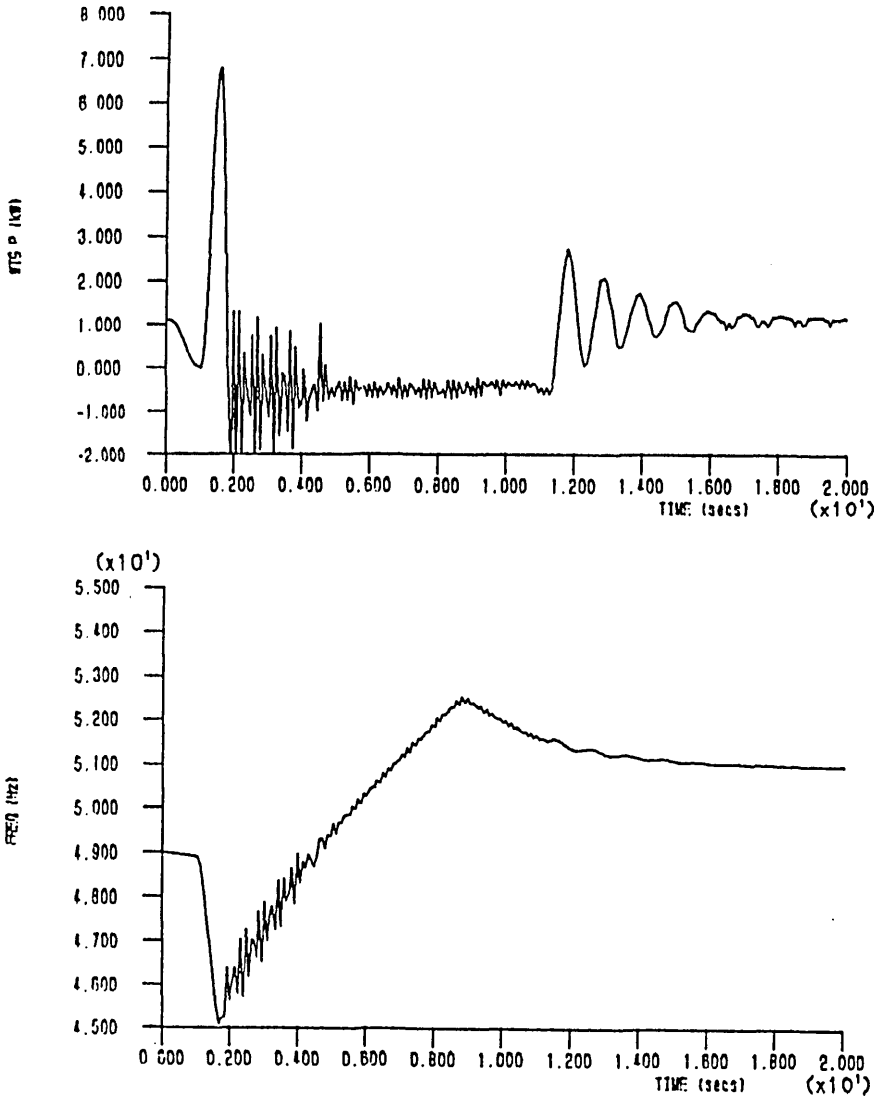

FIGURE 6.41 Wind/Diesel/Flywheel (Jfly=11.8kgm²) response following diesel "crashstart" -250 samples over 20 secs
(a) actual (b) simulated

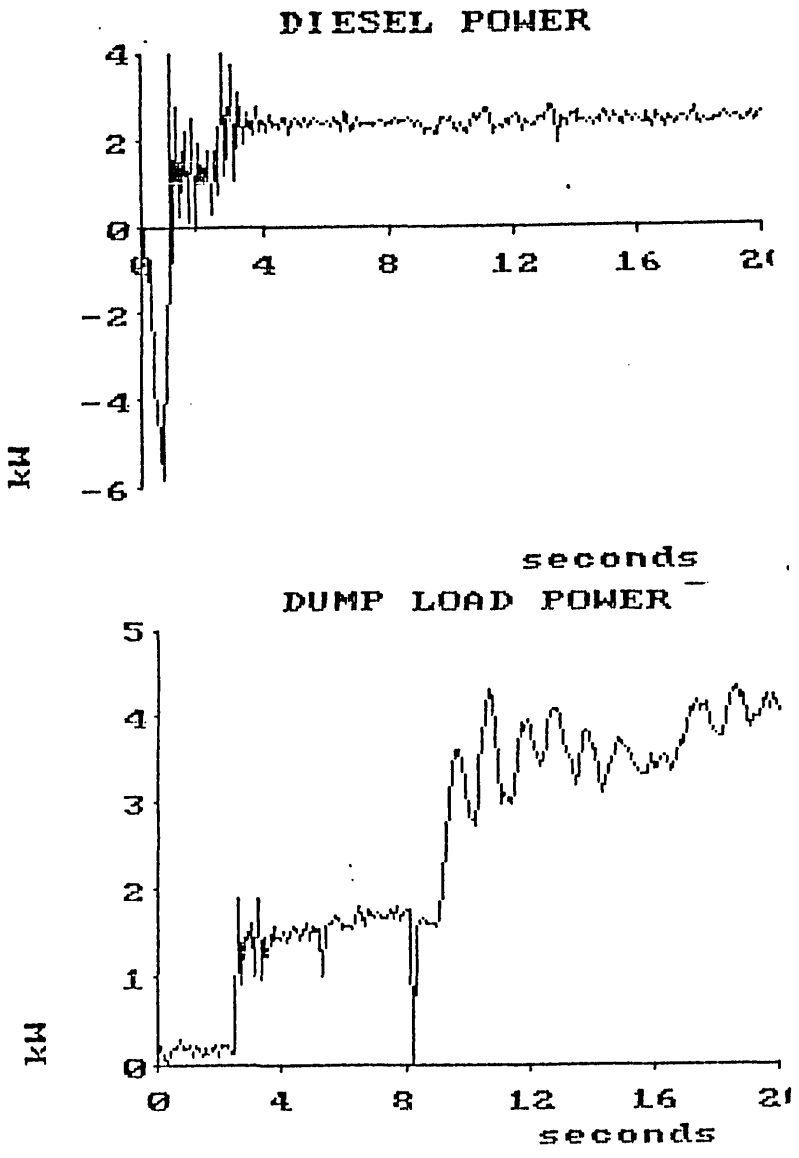

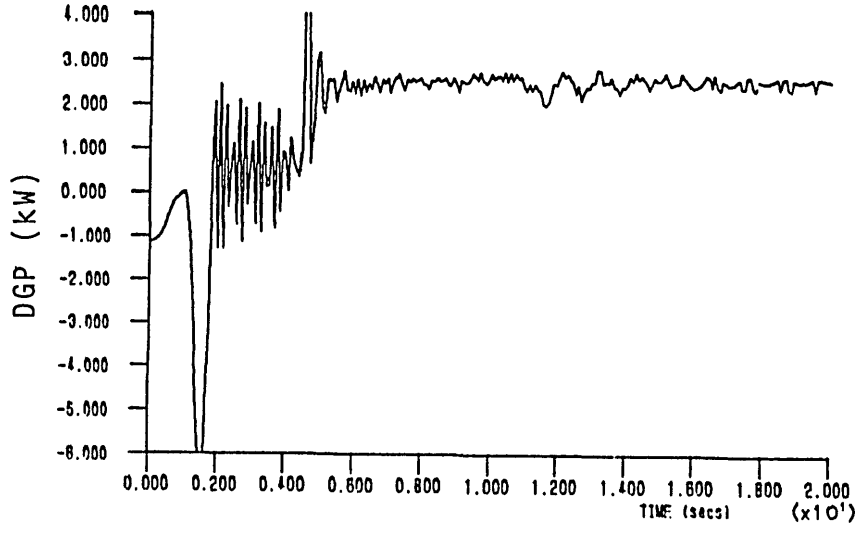

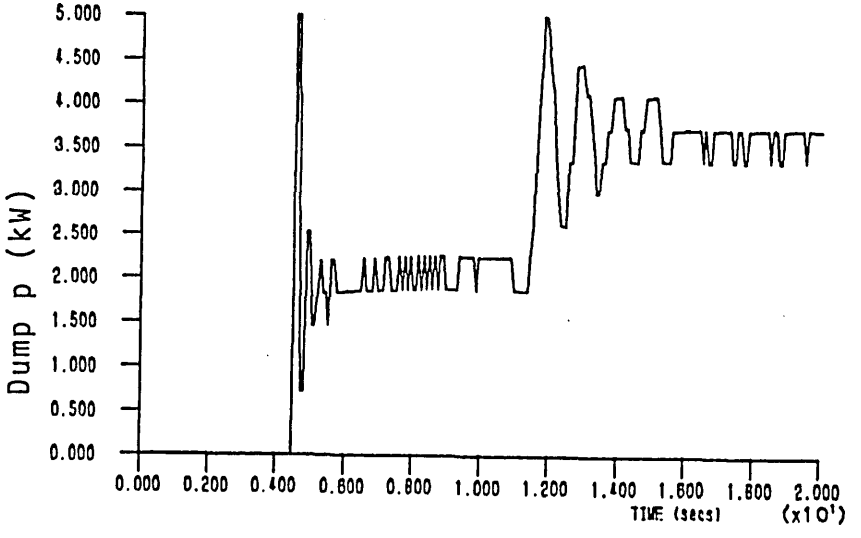

FIGURE 6.41 Contd

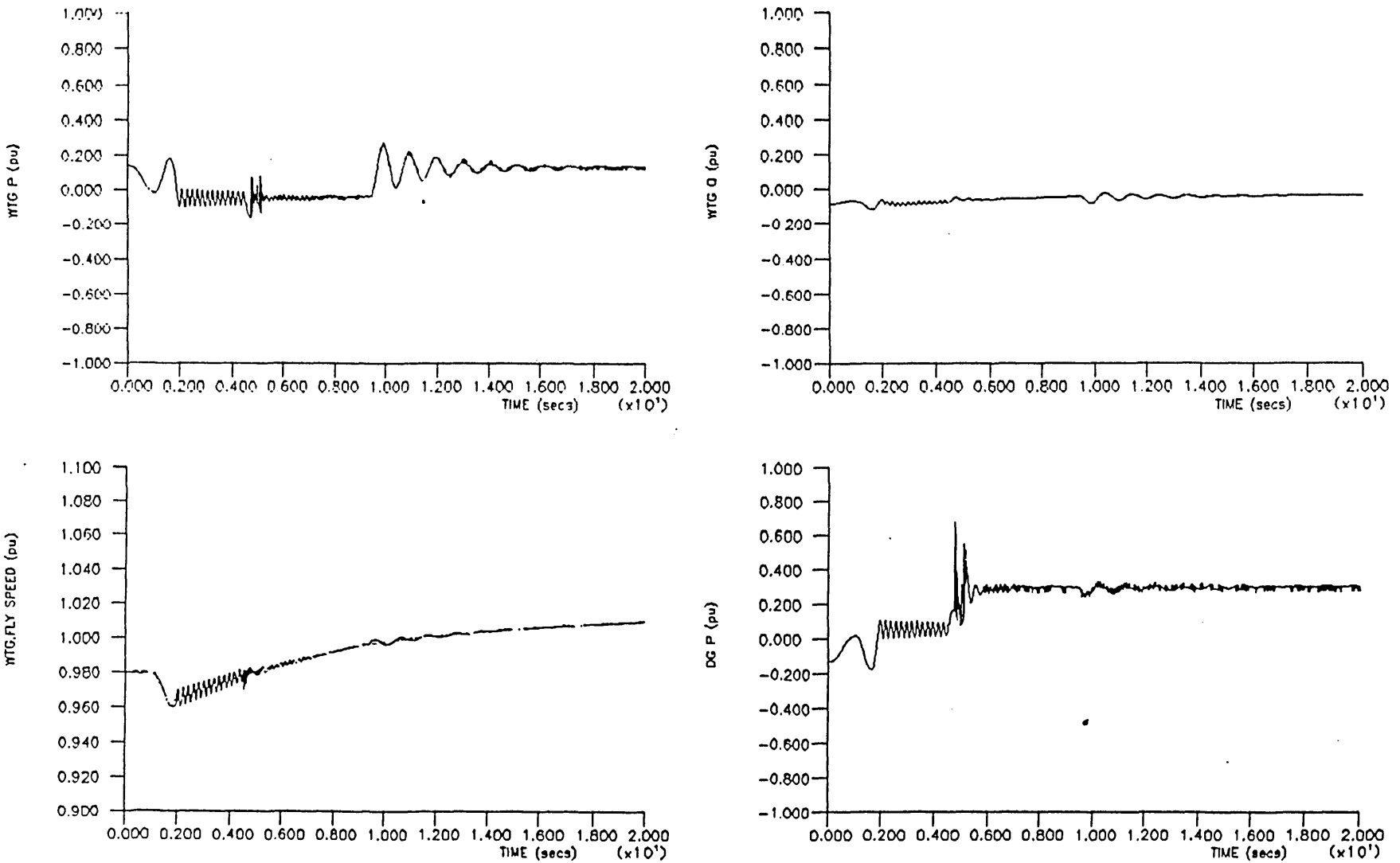

FIGURE 6.42 Wind/Diesel/Flywheel (Jfly=58kgm²) response following diesel "crashstart" - simulated

CHAPTER 7

CONCLUSIONS

7.0 Summary of Conclusions

In parallel with the development of the RAL/ICSTM wind/diesel/flywheel system, a suite of programs has been developed at Imperial College to investigate the steady-state and short-term electromechanical dynamics of that system.

The simulations were based on:

i) Park's Two-Axis representation of the electrical machine down to the transient level. Saturation models were included in both wind turbine and diesel alternators and were found to be crucial when addressing the problem of reactive power flow.

ii) The electromechanical dynamic equations were represented in state variable form and numerically integrated over two millisecond timesteps using the standard Runge Kutta fourth order method.

The simulations were used in conjunction with tests[1] on the RAL/ICSTM system to aid in the characterisation of system components. Wherever possible, the programs have been validated by direct comparison of actual and simulated results.

---

[1]Tests carried out either by or in conjunction with Dr J Bleijs and/or Dr D Infield.

Small perturbation techniques were applied to the time-stepping simulations in order to investigate small signal stability using Eigenvalue Analysis. This method was used to investigate the contribution of system components to the various oscillatory modes (Participation Matrix) and to investigate methods of system stabilisation.

The suite of linear and non-linear programs demonstrated:

1) The electrical power output of the grid connected wind turbine over the full range of windspeeds and its derating by the adjustment of the blade-pitch angle characteristic.

2) The inadequacies of the wind turbine's UPF exciter and the need for Quadrature Droop Compensation with the replacement AVR.

3) The replacement of the diesel alternator static exciter by an AVR resulted in much improved voltage regulation characteristics.

3) The wind turbine generator may be safely synchronised onto the grid without autosynchronisation equipment.

4) Both alternators demonstrated very poor damping as was shown by the mechanical decoupling of each prime-mover from the wind/diesel system:

i) Decoupling the wind turbine resulted in a very poorly damped 4.7Hz mode which was unaffected by the inclusion of a flywheel.

ii) Decoupling of the diesel engine resulted in the alternators swinging in anti-phase at a very poorly damped 8.2Hz oscillation. This mode did not occur in the wind/diesel/flywheel system.

5) The wind-excited 1Hz mode of oscillation was found to be due to insufficient mechanical damping in the wind turbine's drivetrain. The oscillation was made more severe at the higher power levels as a result of the inherent negative damping of the C_p/λ characteristic of the Wind Turbine at the higher windspeeds.

The wind/diesel system proved more susceptible to this mode in which the wind turbine swings in anti-phase to the diesel generator/engine.

The inclusion of the flywheel resulted in a mode shape in which the wind turbine swings against the diesel-flywheel. Any beneficial damping that may have been due to the diesel has therefore been lost thereby leading to a further reduction in system stability.

Increased wind turbine mechanical damping improved system stability, however, its benefit was not so great as in the grid connected arrangement.

6) Power System Stabilisation under "bang-bang" control could be used to dampen the wind-excited 1Hz mode of oscillation.

7) Frequency based dumpload control led to instabilities in both the autonomous wind turbine system and in the full system due to the sample/hold nature of the frequency transducer leading to incorrect dumpload action.

In theory, increased mechanical damping removes this mode, however, in practice, it was still evident. The performance of the wind turbine mechanical dampers may therefore be questioned.

Increased flywheel size little affected this mode.

8) Power based dumpload control with a 3.4Hz notch filter at its input allowed sufficient (P+I) controller gains to maintain the desired power setpoint and aided in system stability when active.

Derivative control was demonstrated to be unsatisfactory due to the high level of system "noise" and the stepload action of the dumpload being converted into impulses by its own controller.

9) During diesel disengagement the power setpoint of the dumpload controller was adjusted to limit the power into the alternator-flywheel. Additionally, in order to maintain an upper frequency limit an additional "speed"

(wind turbine generator or flywheel) loop was used to adjust this power setpoint. Thus, using speed instead of frequency, large gains could be used to minimise the steady-state frequency error.

10) Under the most onerous condition of a diesel "crashstart" the wind/diesel/flywheel system was able to maintain satisfactory voltage and frequency levels for both flywheel sizes.

7.1 Original Contributions

The author cites the following as his original contribution to the wind/diesel/flywheel project:

1) The development and validation of both steady-state and dynamic models of:
   i) Grid connected wind turbine.
   ii) Autonomous wind turbine supplied system.
   iii) Autonomous diesel generator supplied system.
   iv) Autonomous wind/diesel system plus flywheel storage.

2) The inclusion of the aerodynamic characteristics of the wind turbine into the electromechanical equations to allow the quantification of windspeed versus electrical power out.

3) The characterisation of system components using the simulation programs.

4) The non-linear models were used to demonstrate the dynamics of:

   i) Synchronisation of the wind turbine.

   ii) Wind excited oscillations.

   iii) The decoupling of the prime-movers.

5) An investigation to improve reactive power flows in the system using Quadrature Droop Compensation.

6) The use of perturbation techniques to study the system's small signal stability and Participation Matrices to examine a components contribution to a particular mode.

7) An investigation of methods to improve system stability culminating in the development of a Power System Stabiliser to improve the stability of the 1Hz mode.

8) An Investigation of possible control strategies for the dumpload controller under the various system configurations and transitional stages:

   i) The problem of frequency based dumpload control.

   ii) The stability limit of the system under power based dumpload control.

   iii) The maintenance of system stability after diesel disengagement.

iii) The diesel engine crashstarting onto the wind/flywheel system.

7.2 Suggested Further Work

1) The development of a transient model of an induction alternator so that a comparative study may be carried out of the advantages/disadvantages of a wind turbine with either a synchronous or an induction alternator (including forms of power factor correction equipment) in the wind/diesel/flywheel system.

2) The use of discrete time methods in the linear analysis of the system.

3) The development of more sophisticated forms of controller for the Power System Stabiliser (eg Adaptive Control).

4) A sensitivity study to reduce the complexity of the system models so that standard modular components may be used in the suite of programs.

CHAPTER 1 REFERENCES

1.1 **Marshall W** "£30 Million Wind Power Programme" CEGB Press Information ,CEGB, 23 March 1988.

1.2 **Le Gourieres D** "Wind Power Plant Theory and Design", Pergammon Press, Oxford, 1982.

1.3 **Bass J H and Twidell J W** "Wind/Diesel Power Generation - Strategies for Economic Systems", Proceedings of 8th BWEA Annual Conference (Ed Anderson and Powles), 1986.

1.4 **Lipman N H** "Autonomous Wind/Diesel Systems for Remote Applications" Wind Engineering, Vol 12 No 3, 1988.

1.5 **Cramer G** "Autonomous Electrical Power Supply Systems" Proceedings of a Workshop on wind/diesel systems, British Wind Energy Association, June 1987.

1.6 **de Bonte J A and Costa J L** "An Autonomous Wind Diesel System On the Cape Verdan Islands; Design, Testing and Practical Experiences" Proceedings of a Workshop on wind/diesel systems, British Wind Energy Association, June 1987.

1.7 **Van der Hoven I** "Power Spectrum of Horizontal Wind Speed in the Frequency Range From 0.0007 to 900 Cycles per Hour" Journal of Meteorology, Vol 14, 1957, pp 160-164.

1.8 **VOLVO Technical Journal** "Braking Energy Recovery in a Diesel Powered Bus".

1.9 "The Flywheel Electric Car", Electrical Review 209(3), February 1981.

1.10 **Bossanyi E A and Jervis B** "Compliance in Wind Turbines With Either Synchronous or Induction Generators", Proceedings of 10th British Wind Energy Conference, London, March 1988.

1.11 **Harrap M J** "Some Aspects of the Design of Hybrid Wind Diesel Systems' Proceedings of "Solar 87", ANZSES, Australia, 1987.

1.12 **Somerville W M and Stevenson W G** "Optimal Use of Wind and Diesel Generation on a Remote Scottish Island", Proceedings of the European Wind Energy Conference, Hamburg, 1984

1.13 **Linders J, Holmblad L and Andersson B** "Current Progress With the Autonomous Wind/Diesel System at Chalmers University" Proceedings of a Workshop on wind/diesel systems, British Wind Energy

Association, June 1987.

1.14 **Lundsager P** "Implementation of a 55/40kW Wind/Diesel System With Energy Storage in Cape Verde" Proceedings of a Workshop on wind/diesel systems, British Wind Energy Association, June 1987.

1.15 **Schott T, Zeidler A, Reiniger K** "Hybrid System Wind/Photovoltaic/Diesel/Battery - Theoretical and Experimental Results" Proceedings of a Workshop on wind/diesel systems, British Wind Energy Association, June 1987.

1.16 **Slack G W and Musgrove P J** "A Wind/Diesel System With Hydraulic Accumulator Energy Buffer" Proceedings of a Workshop on wind/diesel systems, British Wind Energy Association, June 1987.

1.17 **Madsen H A and Lundsager P** "The Wind/Diesel Development Programme at RISO National Laboratory" American Wind Energy Association Conference, Windpower 85, San Francisco.

1.18 **T Davies et al** "Experience with the Wind Turbine Flywheel Combination on Fair Isle", Proceedings EWEC89, July 1989, Glasgow. Peter Peregrinus, London.

1.19 **Infield D G** "An Assesment of Flywheel Energy Storage as Applied to Wind/Diesel Systems", Wind Engineering Vol 14, No 2, 1990.

1.20 **Coonick A H, Bleijs JAM and Infield D G** 'Wind/Diesel System With Flwyheel Energy Storage" Proceedings of a Workshop on wind/diesel systems, British Wind Energy Association, June 1987.

1.21 **Bass J H** "User's Guide for the Wind/Diesel Simulation Model" Energy Research Unit internal report, Rutherford Appleton Laboratory, May 1988.

1.22 **Infield D G** "Logistic Control of Wind/Diesel Systems", Course Notes from Principles of Wind Energy Conversion, Imperial College, July 1987.

1.23 **Neale M J and Eyre T S** "Piston Ring and Cylinder Liner Problems", I Mech E Conference Proceedings 1982, pp 55-63.

1.24 **Lilly C R** "Diesel Engine Reference Book', Butterworths, 1984.

1.25 **Jenkins N** "The Development and Control of an Autonomous Wind Diesel Generating System' Ph D Thesis, Imperial College, London, 1986

CHAPTER 2 REFERENCES

2.1 **CONTROLOGY Tri AVR 15R**, Technical Specification, Contrology Techniques Ltd, East Kilbride.

2.2 **CONTROLOGY Tri AVR 15E**, Technical Specification, Contrology Techniques Ltd, East Kilbride.

2.3 **Infield DG, Bleijs J, Coonick A, Bass J, White J and Harrap M** "A Wind/Diesel System Operating With Flywheel Storage", Proceedings EC Wind Energy Conference, Herning, Denmark, June 1988. Published H S Stephens and Associates, Bedford, UK.

2.4 **Jenkins N** "The Development and Control of an Autonomous Wind Diesel Generating System", Ph D Thesis, Imperial College, London, June 1986.

CHAPTER 3 REFERENCES

3.1 **White S K** "Imperial College Wind Turbine Analysis Code", internal report, January 1989.

3.2 **Infield D G**, RAL/ICSTM Internal Communication.

3.3 **Goyal M R** "Simulation of a Turbocharged Diesel Engine to Predict the Transient Response", ASME paper No 78-DGP-11 1978.

3.4 **MacDonald D C, Reece B J and Turner P J** "Turbine Generator Steady-State Reactances" Proc IEE, Vol 132, Pt C, No 3, May 1985.

3.5 **Sugiyama T, Nishiwaki T, Takeda S and Abe S** "Measurements of Synchronous Machine Parameters Under Operating Conditions" IEEE TRANS PAS, Vol PAS-101, No 4, April 1982.

3.6 **Bleijs J**, RAL/ICSTM internal communication.

3.7 **Dommel H W**, Electromagnetic Transients Program (EMTP), University of Louvain, Belgium.

3.8 **Infield D, Lipman N, Bleijs J, Freris L and Jenkins N** "Current Progress in the Development of a Wind Diesel System for Autonomous Electricity Generation" Proceedings of the Conference on Alternative Energy Systems, Coventry, September 1984. Pergamon Press, Oxford.

3.9 **Tsitsovits A J** "Dynamics and Control of Power Systems Fed From Diesel and Wind Generators", Ph D Thesis, Imperial College, September 1984.

3.10 **Jenkins N** "The Development and Control of an Autonomous Wind Diesel Generating System" Ph D Thesis, Imperial College, June 1986.

3.11 **Bleijs J**, RAL/ICSTM internal communication.

3.12 **Elgerd O I** "Electric Energy Systems Theory, An Introduction". McGraw Hill, 1982, New York .

CHAPTER 4 REFERENCES

4.1 **Hall, G and Watt, J M (eds)** "Modern Numerical Methods for Ordinary Differential Equations". Clarendon Press, Oxford 1976.

4.2 **D02EBF,** Numerical Algorithms Library (NAGFLIB) Mk 7, December 1978.

4.3 **Coonick, A H, Bleijs J A M and Infield D G** "Wind/Diesel System with Flywheel Energy Storage". Wind/Diesel Workshop, Rutherford Appleton Laboratory, June 1987.

4.4 **Anderson P M and Fouad A A,** "Power System Control and Stability" Iowa State University Press, Iowa, 1977.

4.5 **Yu Y N** "Electric Power System Dynamics" Academic Press Inc (London) Ltd, 1983.

4.6 **Moler C** "MATLAB User's Guide" Department of Computer Science, University of New Mexico, 1981.

4.7 **Smith B T, Boyle J M et Al** "EISPACK Guide", Lecture Notes in Computer Science, Vol 6, second edition, Springer-Verlag, 1976.

CHAPTER 5 REFERENCES

5.1 **Infield D G**, RAL/ICSTM Internal Communication, January 1989.

5.2 **Coonick A H, Bleijs J A M, Infield D G et al**, "Summary of the RAL/ICSTM Wind/Diesel/Flywheel Research Project", European Wind Energy Conference, Glasgow, July 1989

5.3 **Infield D G, Bleijs J A M and Coonick A H** "A Wind/Diesel System Operating with Flywheel Storage" Proceeding of the European Community Wind Energy Conference, Denmark, 1988.

5.4 **Hsu Y Y and Chen C L**, "Identification of Optimum Location for Stabiliser Applications using Participation Factors", IEE Proceedings, Vol 134, Part C, No 3, May 1987.

CHAPTER 6 REFERENCES

6.1 Bleijs J "Control Aspects of Autonomous Wind-Diesel Power Systems Incorporating Flywheel Storage", Ph D Thesis, Imperial College, June 1990.

APPENDIX 3.A

Wind Turbine Dimensional and Aerodynamic Characteristics

Number of Blades: 2

Blade Radius: 4.53m

Hub Radius: 0.133m

Blade Type: Modified GO797 Aerofoil

Nos of Blade Elements: 10

Blade Element Data:

ELEMENT	RADIUS (pu)	CHORD (m)	TWIST (deg)
1	0.05	0.000	0.0
2	0.15	0.060	20.0
3	0.25	0.049	10.0
4	0.35	0.044	8.2
5	0.45	0.040	7.5
6	0.55	0.036	7.0
7	0.65	0.031	6.5
8	0.75	0.027	6.0
9	0.85	0.022	5.5
10	0.95	0.018	5.5

Aerodynamic Characteristics

ALPHA (deg)	C_L	C_D
-9.4	0.000	0.020
-5.0	0.275	0.014
0.0	0.769	0.012
5.0	1.231	0.019
8.8	1.500	0.029
10.0	1.582	0.036
12.8	1.670	0.100
15.0	1.637	0.100
17.8	1.500	0.000
20.0	1.352	0.000

APPENDIX 3.B

Wind Turbine Mechanical and Electrical Parameters

Alternator Rating at 220V, 125rpm:	21 kVA
Wind Turbine Inertia:	170 kgm^2
Wind Turbine Losses:	0.315 kW
Mechanical Damping:	220 Nm/rad s^{-1}
Elasticity of Flexible Coupling:	10000 Nm/rad
Wind Turbine Generator Inertia:	16 kg m^2
Wind Turbine Generator Losses:	0.21 kW
WTG Direct Axis Reactance:	2.21 pu
WTG Quadrature Axis Reactance:	1.87 pu
WTG Direct Axis Transient Reactance:	1.23 pu
WTG Leakage Reactance:	1.01 pu
WTG Armature Reactance:	0.138 pu
WTG D A Transient Open Circuit	
Time Constant:	0.3 secs
Number of Poles:	48

Diesel Generator Mechanical and Electrical Parameters

Alternator Rating at 415 V, 1500 rpm:	8.5 kVA
Diesel Engine Rated Mechanical Torque:	74.0 Nm
Diesel Engine Torque Limit:	69.1 Nm
Diesel Engine Inertia:	1.39 kg m^2
Diesel Engine and DG Losses (no load):	3.3 kW
Governor Mechanical Droop:	6%
Governor Damping Coefficient:	0.95
Governor Time Constant:	0.16 secs
Time Delay of Fuel Combustion:	0.02 secs
Shaft Stiffness:	Rigid
DG Direct Axis Reactance:	1.21 pu
DG Quadrature Axis Reactance:	0.66 pu
DG Direct Axis Transient Reactance:	0.14 pu
DG Leakage Reactance:	0.05 pu
DG Armature Resistance:	0.0347 pu
DG Direct Axis Transient	
Open Circuit Time Constant:	0.7 secs
Number of Poles:	4

Flywheel Mechanical Parameters

Flywheel Inertia at 1500 rpm:	21 kg m^2
Effective Inertia at 1125rpm:	11.8 kg m^2
Typical Storage Time with 4kW Load:	6 secs
Effective Inertia at 2500 rpm:	58.3 kg m^2
Typical Storage Time with 4kW Load:	28 secs
Flywheel and Belt Drive Losses:	1.5 kW

Stepup Transformer

220/415 V Star-Delta, rated at 25kVA

Leakage Resistance (21kVA base):	0.016 pu
Leakage Reactance:	0.0223 pu
Core Loss Resistance:	60.0 pu
Magnetising Reactance:	56.0 pu

APPENDIX 3.C

Electrical Machine Per Unit Convention Used throughout the Modelling Studies

The convention assumes stator rated voltage, V_{base}, and current, I_{base}, as 1.0 per unit (pu).

The unsaturated stator reactance ,$X_{du}(\Omega)$, is defined from the synchronous machine's open-circuit and short-circuit characteristics in terms of the airgap and short-circuit current (SCC) lines.

If the field current, I_{fo}, corresponds to V_{base} on the airgap line and the field current, I_{fsc}, corresponds to I_{base} on the scc line then $X_{du}(\Omega)$ is the stator reactance assuming an internal voltage proportional to field current:

$$X_{du}(\Omega) = \frac{\text{internal voltage to give } I_{base} \text{ on scc line}}{I_{base}}$$

$$= \frac{V_{base}}{I_{base}} \frac{I_{fsc}}{I_{fo}} = Z_{base} \frac{I_{fsc}}{I_{fo}}$$

In per unit:

$$X_{du} = \frac{X_{du}(\Omega)}{Z_{base}}$$

$$X_{du} = \frac{I_{fsc}}{I_{fo}}$$

Base field current, I_{fbase}, is defined as the field current that produces the same fundamental airgap mmf as when the stator winding carries three phase currents of 1.0pu.

It is obtained from the scc using as its basis the knowledge that part of the field current, I_{fn}, is used to drive current through the stator leakage reactance, $X_l(\Omega)$. I_{fn} is obtained from the airgap line corresponding to the voltage $I_{base}X_l(\Omega)$. Thus I_{base} in the stator is equivalent to $(I_{fsc}-I_{fn})$ in the field.

Therefore the base field current is:

$$\begin{aligned} I_{fbase} &= I_{fsc} - I_{fn} \\ &= I_{fo}X_{du} - I_{fo}\frac{I_{base}X_l(\Omega)}{V_{base}} \\ &= I_{fo}(X_{du} - X_l) \end{aligned}$$

APPENDIX 3.D

TRANSIENT MODEL OF THE SALIENT POLE SYNCHRONOUS MACHINE

Under transient conditions, a salient pole synchronous machine may be represented on the rotor solely by the effect of the field winding.

Initially, assume a voltage E_q behind the Q-Axis reactance. This representation has the advantage that the phase of this voltage correctly represents the angular position of the field structure. Under transient conditions, the flux linkage ψ_f, remains substantially constant. A new fictitious internal armature voltage may be defined that is proportional to the field flux linkage and resulting from the combined effect of the field and armature currents:

$$E'_q = \omega . X_{ad} . \psi_f / (X_f + X_{ad}) \qquad (3.D.1)$$

Since both voltages are along the Q-Axis, the relationship between E_q and E'_q is:

$$E_q = E'_q + (X_q - X'_d) . I_d \qquad (3.38)$$

Applying Kirchoff's voltage law to the field winding yields:

$$V_f = R_f . I_f + p\psi_f$$

rearranging,

$$p\psi_f = V_f - R_f . I_f \qquad (3.D.2)$$

A new quantity, E_{fd}, representing the field voltage acting along the Q-Axis can be defined:

$$E_{fd} = V_f . X_{ad}/R_f \qquad (3.D.3)$$

The field induced voltage, E_I, is defined as:

$$E_I = X_{ad} . I_f \qquad (3.D.4)$$

Combining equations 3.D.1 to 3.D.4:

$$pE'_q = (E_{fd} - E_I).(\omega . R_f)/(X_f + X_{ad}) \qquad (3.D.5)$$

The transient open-circuit time constant, T'_{do} is:

$$T'_{do} = (X_f + X_{ad})/(\omega . R_f) \qquad (3.D.6)$$

Combining equations 3.D.5 and 3.D.6 results in:

$$pE'_q = (E_{fd} - E_I)/T'_{do} \qquad (3.39)$$

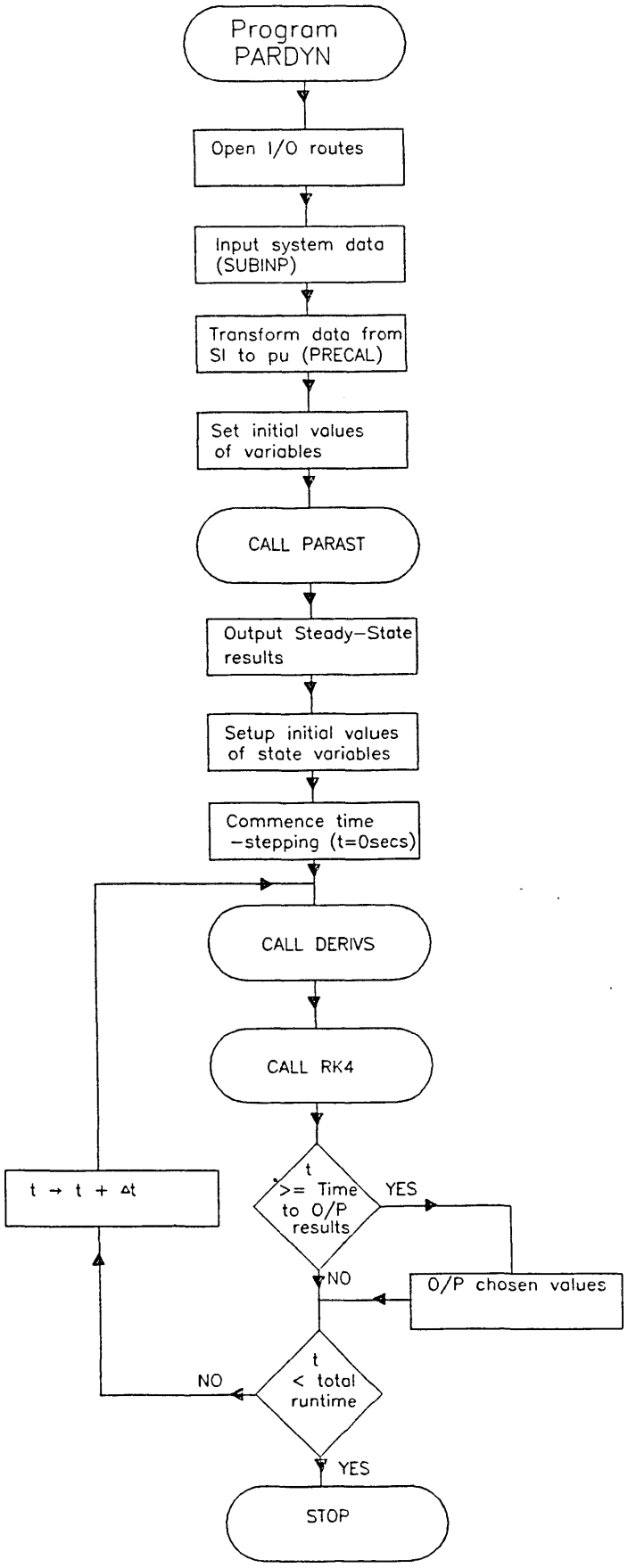

APPENDIX 4.A Flow chart of the program structure used in the dynamic simulation of the Wind/Diesel System

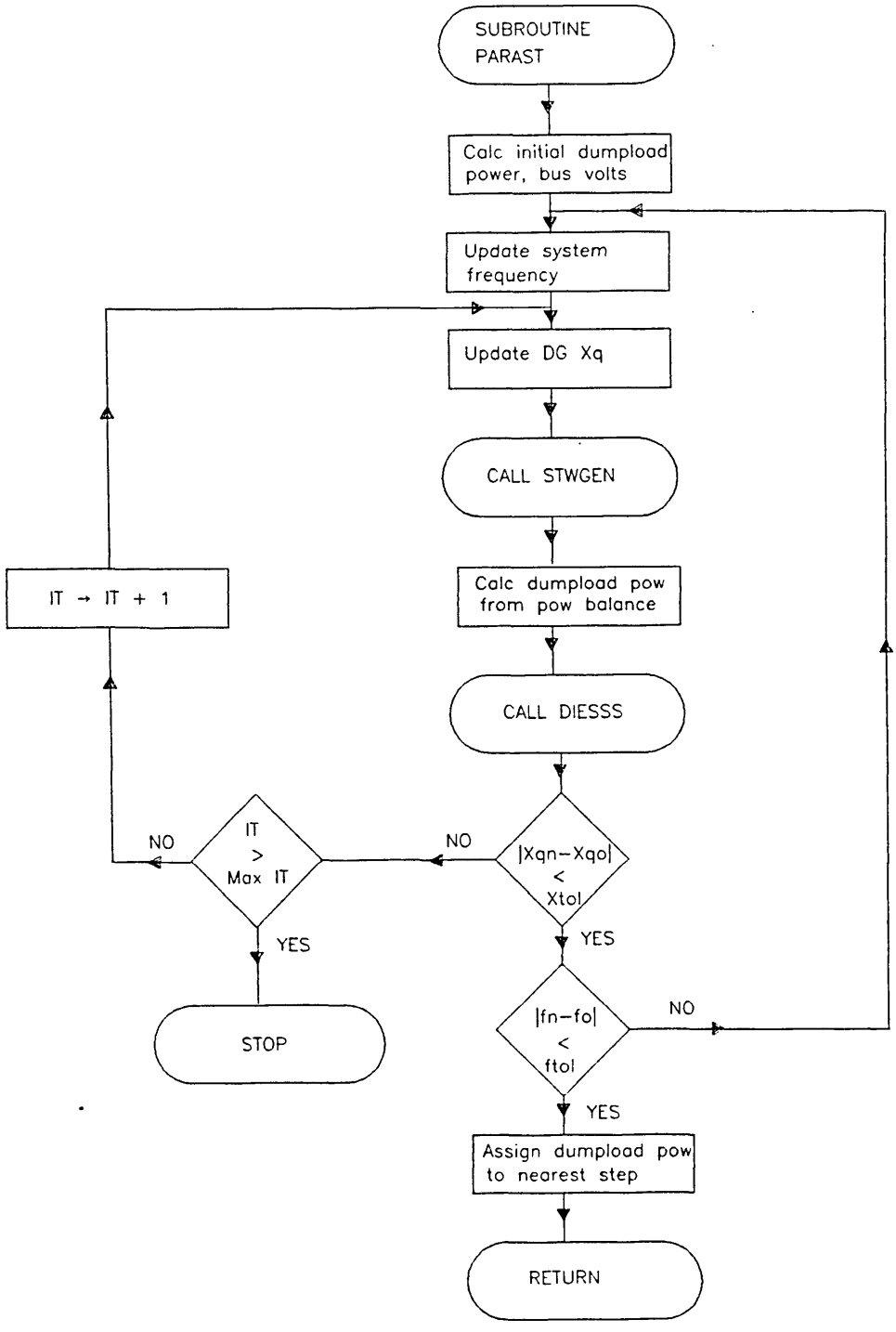

APPENDIX 4.A (contd)

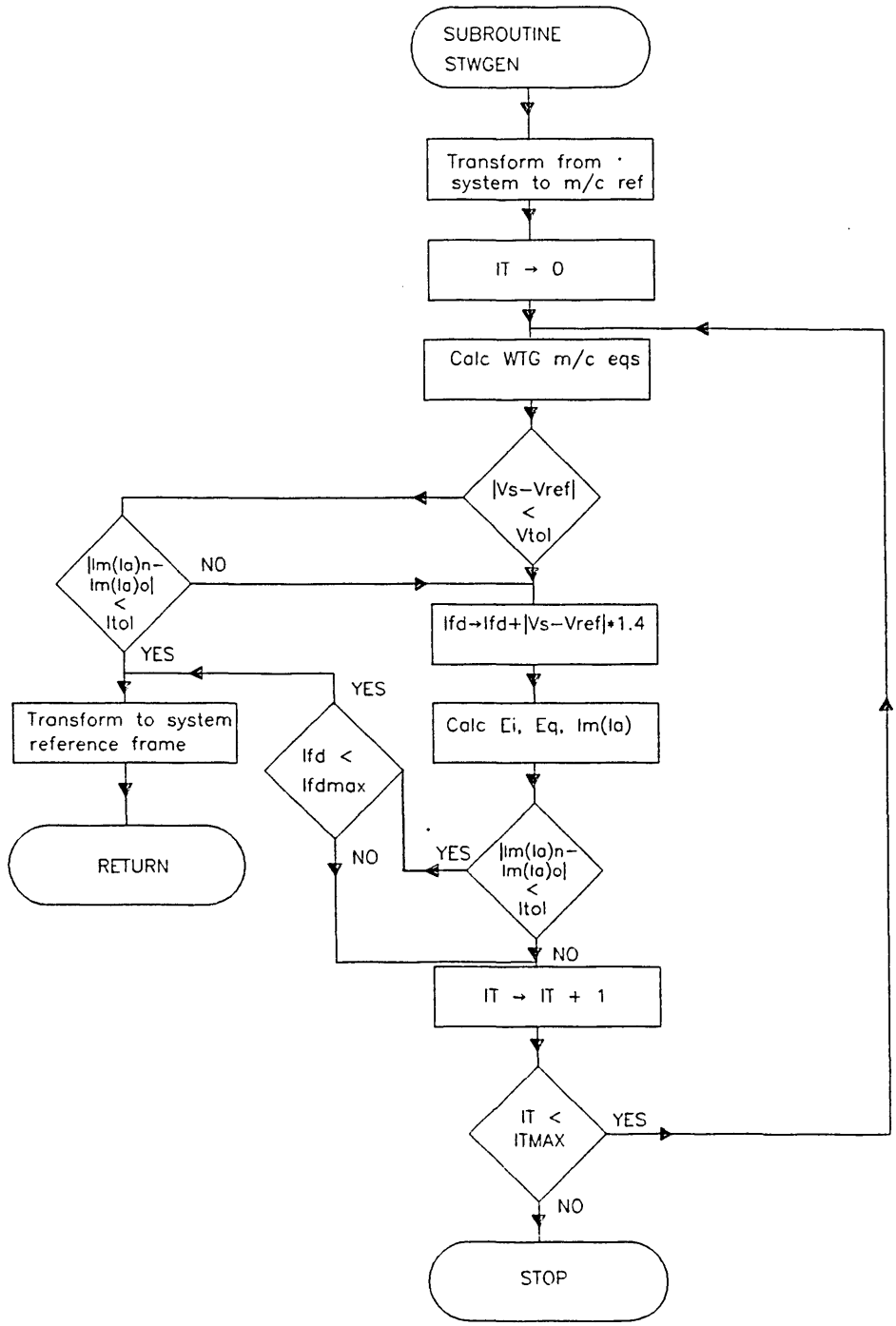

APPENDIX 4.A (contd)

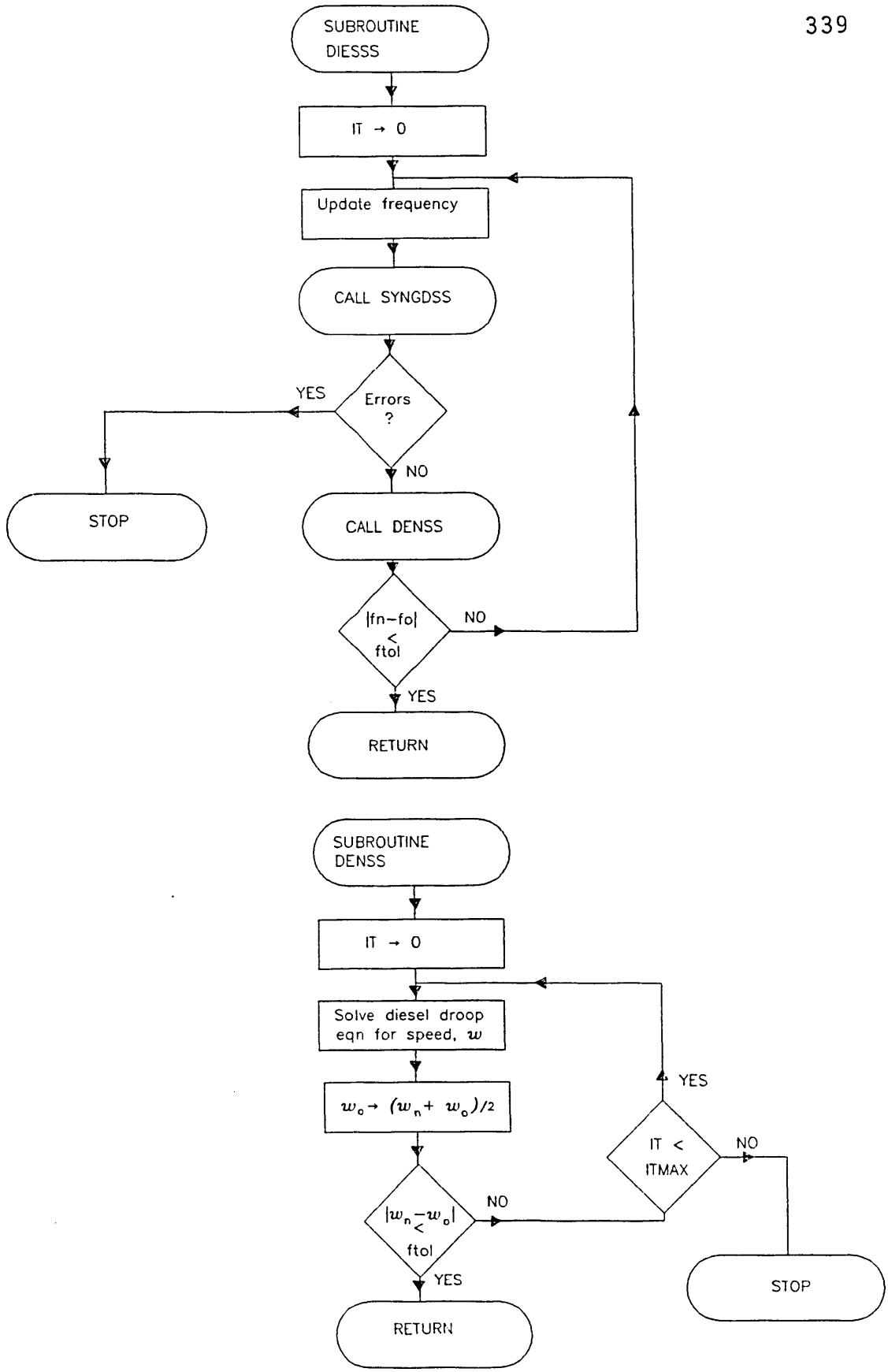

APPENDIX 4.A (contd)

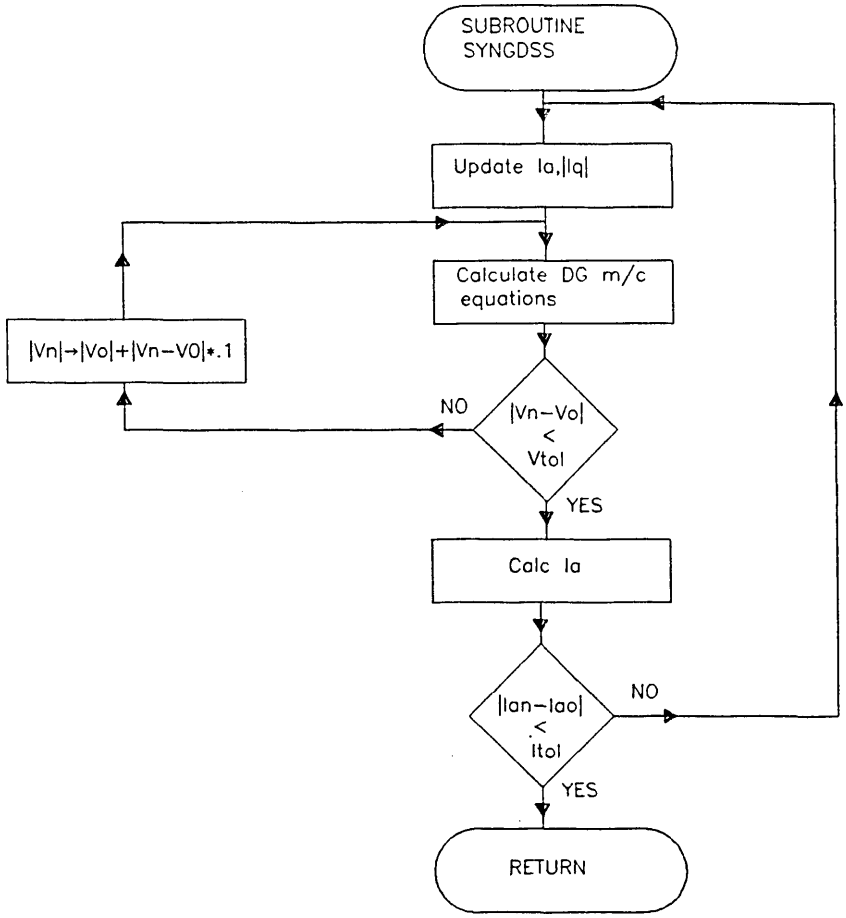

APPENDIX 4.A (contd)

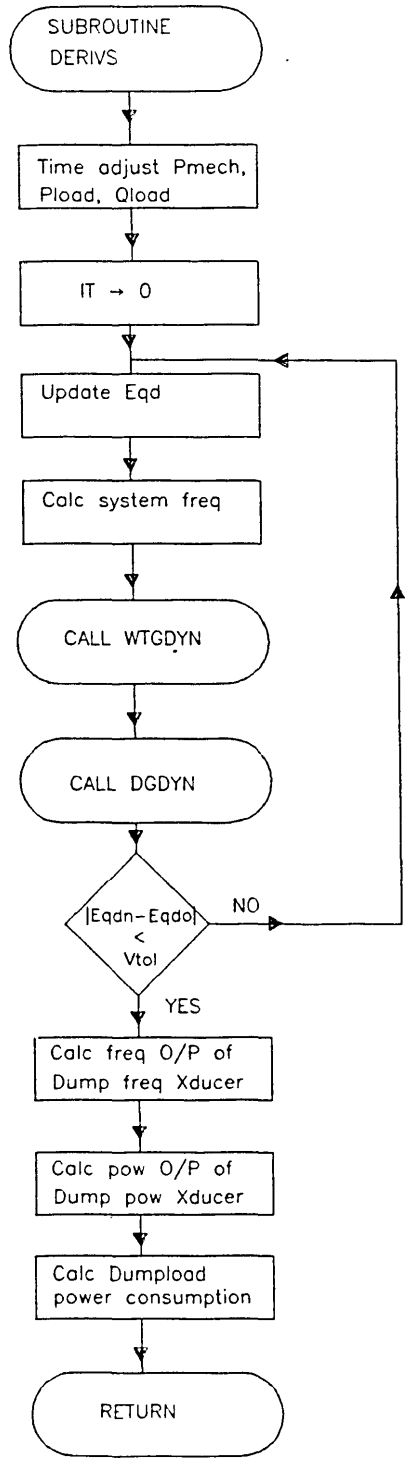

APPENDIX 4.A (contd)

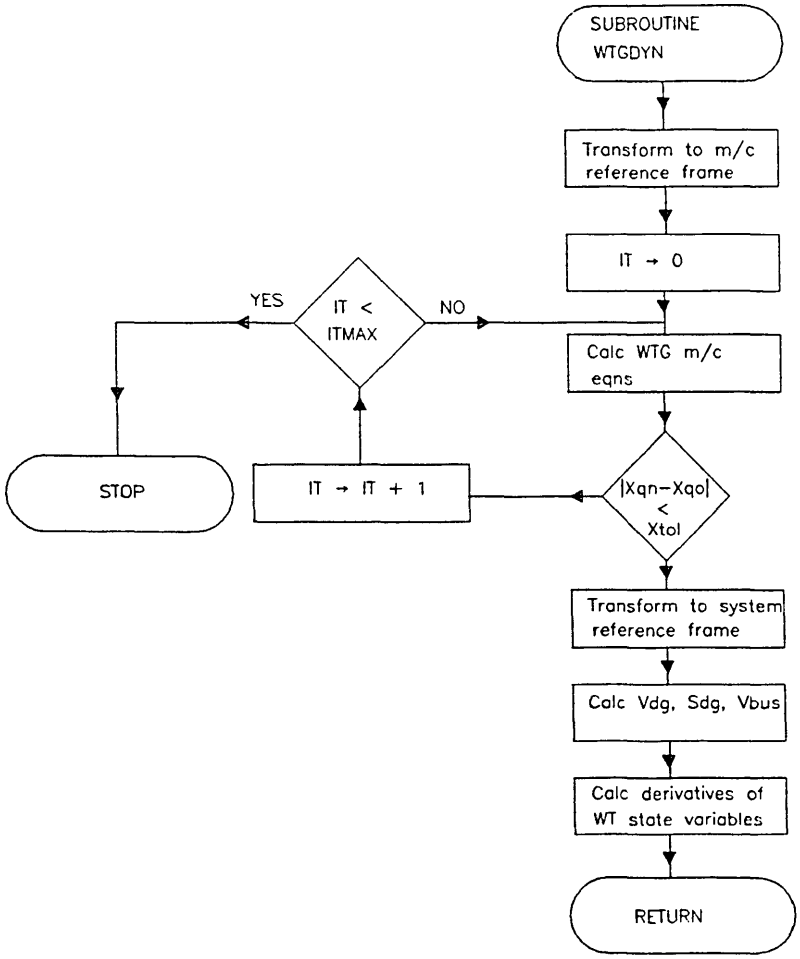

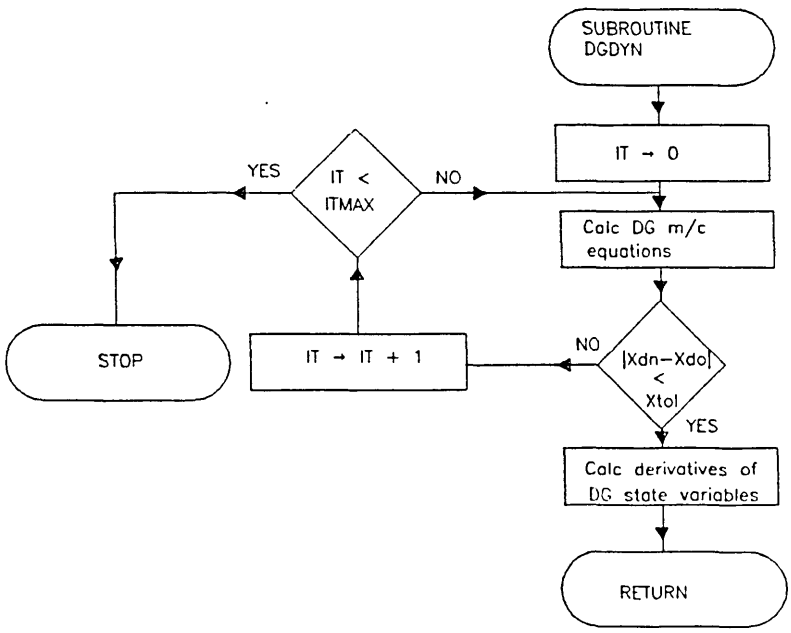

AAPENDIX 4.A (contd)

Appendix 5.A

Improved Damping of the 1Hz Mode Using the Pole Placement Technique

The state equations of a system can be represented by:

$$pX(t) = A.X(t) + B.U(t) \quad (5.A.1)$$

$$Y(t) = C.X(t) \quad (5.A.2)$$

where,

X(t) - State state vector

A,B,C - System matrices

U(t) - Control signal vector

Y(t) - Output signal vector

Transferring to its Laplace form equations 5.A.1 and 5.A.2 become:

$$sX(s) = A.X(s) + B.U(s) \quad (5.A.3)$$

$$Y(s) = C.X(s) \quad (5.A.4)$$

Matrices B and C can be obtained from the non-linear system equations via the small signal perturbation method used to produce the linearised form of the A matrix as described in Chapter 4.

Matrix B is found by perturbing Vref of the AVR and forming the matrix from:

$$B(i) = (F(i) - F0(i))/\Delta \quad (5.A.5)$$

$i = 1 \ldots n$

where,

F0(i) - Derivative of state variable prior to perturbation

F(i) - Derivative of state variable after perturbation

n - Number of state variables

Matrix C is found by perturbing each state variable and forming the matrix from:

$$C(i) = (Pw(i) - Pw0)/\Delta \qquad (5.A.6)$$

$i = 1 \ldots n$

where,

Pw0 - Wind turbine generator electrical power output prior to perturbation

Pw(i) - Wind turbine generator electrical power output after each state variable has been perturbed

The control signal U is generated by the PSS and can be expressed in the frequency domain as:

$$U(s) = H(s).Y(s) \qquad (5.A.7)$$

$$= (s.T1/(1+s.T2)).Y(s) \qquad (5.A.8)$$

Combining equations 5.A.3, 5.A.4 and 5.A.7:

$$[s.I - (A + B.H(s).C]\ X(s) = 0 \qquad (5.A.9)$$

The eigenvalues of the closed-loop system with the PSS are then the solution of the following characteristic equation:

$$|s.I - (A\ B.H(s).C)| = 0 \qquad (5.A.10)$$

Rearranging equation 5.A.10, T1 and T2 may then be computed by solving:

$$H(s) = \frac{1}{C.(s.I - A)^{-1}.B} \qquad (5.A.11)$$